Investigating the Involvement of RNA-Binding Protein ZFP36L1 in Breast Cancer Progression

Teotia, Varsha

https://doi.org/10.34737/ww3y5

Investigating the Involvement of RNA-Binding Protein ZFP36L1 in Breast Cancer Progression

Varsha Teotia

A thesis submitted in partial fulfilment of the requirements of the University of Westminster for the degree of Doctor of Philosophy

February 2024

Genome Engineering Lab

School of Life Sciences

Abstract

ZFP36L1 is an RNA-binding protein which functions as a mRNA decaying protein through binding to the adenylate-uridylate rich elements (AREs) located in the 3' untranslated region (3'UTR) of mRNAs, thereby mediating mRNA decaying. ZFP36L1 has emerged as a breast cancer driver gene, exhibiting tumour-suppressing properties. Notably, ZFP36L1 has been reported to be significantly mutated and downregulated in various tumour types. In our comprehensive study, we identified the novel role of the ZFP36L1 gene in regulating the tumorigenic traits of breast cancer, with a particular focus on hormone-positive and HER2-negative breast cancer subtypes. Furthermore, our research explored the therapeutic potential of ZFP36L1 in combination with tamoxifen, an antiestrogenic drug used as a standard treatment for the luminal breast cancer subtype. To explore functional aspects of ZFP36L1, we generated CRISPR Cas9-derived knockout of ZFP36L1 in the MCF-7 breast cancer cell line, characterised by luminal A molecular subtype. Functional assays demonstrated that the loss of ZFP36L1 in MCF-7 cells reduced the cell migration capacity and reduced cell population in the G1 phase of the cell cycle. Subsequent RNA-sequencing study and western blot analysis revealed that ZFP36L1 absence leads to upregulation of cell-cycle-related genes, including cyclin D1, CDK6 and tumour suppressor p53. Notably, cyclin D1 and CDK6 transcripts contain ARE sequences in the 3' UTR, suggesting that they could be the direct targets of ZFP36L1 in MCF-7 cells. Similarly, we observed an upregulation of several ARE-rich genes associated with cell migration and extracellular matrix in the absence of ZFP36L1 in MCF-7 cells. These findings collectively illustrated that ZFP36L1 might be crucially involved in regulating key oncogenic transcripts

encoding cell migration and extracellular matrix in MCF-7 cells. Our study also reported that ZFP36L1 depletion reduced the response of MCF-7 cells to tamoxifen, a standard drug used in endocrine therapy. Specifically, we found that while tamoxifen treatment decreased the cell migration capacity of MCF-7 cells, this effect was mitigated by the loss of ZFP36L1. Western blot analysis further confirmed that tamoxifen treatment reduced cyclin D1 expression in MCF-7 cells. Conversely, when ZFP36L1 expression was inhibited, the tamoxifen-induced reduction in cyclin D1 expression was decreased, resulting in increased cyclin D1 levels compared to tamoxifen-treated wild-type counterparts. Moreover, ZFP36L1 knockout MCF-7 cells exhibited higher IC50 values than WT MCF-7 cells. Conclusively, using molecular and transcriptomic approaches, our study convincingly demonstrates that ZFP36L1 exerts control over transcripts encoding key tumorigenic traits in MCF-7 cells and highlights the potential of synergistically combining ZFP36L1 with tamoxifen, offering potential treatment opportunities for hormone-positive breast cancer subtypes.

Acknowledgements

First, I would like to express my gratitude to God for giving me this opportunity, and I feel incredibly grateful and blessed as I write this acknowledgement. I would like to give my sincere thanks to my supervisors, Dr Kalpana Surendranath and Dr John Murphy. I want to wholeheartedly thank Dr Kalpana for giving me this opportunity. I am deeply grateful for her perpetual approachability, invaluable guidance, mentorship, passion for science and commitment to excellence, which have been a constant source of inspiration throughout my PhD journey. I want to extend my heartful gratitude to Dr John Murphy for his continuous encouragement, profound knowledge and mentorship, which has been extremely helpful in shaping my research. I sincerely appreciate the collaborative spirit of both of my supervisors in facilitating the progression of my research and am sincerely thankful for their kindness, patience, and constant support, even during the lowest times of my PhD journey. I would like to thank the University of Westminster for providing me with a scholarship to pursue my PhD studies.

I have been so lucky to meet such amazing colleagues during my PhD journey. Special thanks to Ahmed Sidali for his unstoppable laughter comments and for providing expertise on my work; you have always been an amazing friend. Thanks to Nahida for the never-ending conversations, and none gone unappreciated. Finally, thanks to Khalid for always cheering me up as a big brother and always offering a helping hand; I wish we had spent more time as lab mates!

I would like to thank my family, my mum and dad, and especially my brother, Siddharth, for his endless love, support and motivation to make it through. I would like to give my heartful thanks to my sister, Parul and my brother-in-law, Puneet, for giving me love

and support throughout my PhD and a place to call home, miles away from home. Finally, I would like to give big thanks to my boyfriend and now husband, Jignesh, for being “the technical guy” for me, patiently listening to my countless problems and being my unwavering rock. I am truly grateful to you for consistently supporting me in every possible way. I am thankful to be surrounded by so many supportive and loving people.

Author Declaration

I declare that all the work presented in this thesis was carried out following the guidelines and regulations of the University of Westminster. I declare that all the material presented in this thesis is original and is my own work unless otherwise acknowledged or referenced.

Contents

List of Figures

List of Tables

Chapter 1: Introduction

1.1 An Introduction to Breast Cancer

Breast cancer is a heterogeneous molecular disease; this malignancy has emerged as the leading cause of cancer-related deaths in women worldwide. Recent statistical data highlights breast cancer as the most frequently diagnosed cancer, outnumbering lung cancer (Sung et al., 2021). In recent years, there has been a significant evolution in breast cancer treatments, driven by a deeper understanding of the disease's heterogeneity. This has led to a pronounced shift in focus towards biologically targeted therapies. The two major treatment regimens followed in breast cancer management are locoregional treatment and systemic therapy. Surgery is still considered for initial treatment for women diagnosed with early-stage tumours, regardless of tumour grade, histology or the patient's age (Burstein et al., 2021). However, molecular and histological characteristics are crucial in determining the treatment regimen for breast cancer patients. The "tumours classification" approach confers a simplification of the multiple molecular alterations exhibited by breast tumours. In 2000, the molecular subtype classification reported by Perou and Sorlie group (Perou et al., 2000; Sorlie et al., 2001) became the most widely utilised system, providing the most valuable biological information about breast cancer. Breast cancer was distinguished into four intrinsic subtypes, including luminal A and luminal B (expressing the oestrogen receptor (ER)), basal-like and human epidermal growth factor receptor 2 (HER2)-enriched (without ER expression). This classification has created a paradigm shift in breast cancer treatment, making biology-centred approaches as the driving principle for modern therapies. With the increasing global burden of breast cancer, the demand for better clinical management of the disease has resulted in increased treatment efficacy at the early and later stages of the disease, reflecting a growing understanding of breast cancer biology. The multifaceted nature of risk factors associated with breast

cancer underscores the importance of further research to inform the development of multimodal treatment approaches and the emergence of novel therapeutic drugs.

1.1.1 Breast cancer epidemiology

A survey study performed using GLOBOSCAN 2020 database reported that breast cancer was the most diagnosed cancer in women, surpassing lung cancer in 2020 (Sung et al., 2021). An estimated new number of breast cancer cases is approximately 2.3 million, accounting for 11.7% of all cancer cases. The countries that showed the highest incidence rates (>80 per 100,000 females) were marked in Australia/New Zealand, Western Europe, Northern America and Northern Europe and the lowest rates (<40 per 100,000 females) in Central America, Eastern and Middle Africa, and South-Central Asia. This global burden, targeting the female population, is increasing by 3.1% annually and will continue in upcoming years, expected to be approximately 3 million cases per year in 2040 (Arnold et al., 2022). There is a disparity among the incidence of breast cancer cases found all over the globe, where a higher incidence rate is found in high-income regions, including North America, Australia, and New Zealand, than lower-income regions, including Eastern Asia and Middle Africa. The variations are more pronounced in mortality rates. Mortality statistics have revealed that close to half of the percentages of deaths globally occurred in Eastern, South Central and South-Eastern Asia combined, followed by North America and Western Europe, ranked as 5th and 6th in terms of the number of deaths (Arnold et al., 2022). The pattern observed in death cases differs from that in breast cancer incidence rates, where breast cancer survivors are significantly lower in low- and middle-income countries than in high-income countries. For example, Africa shared 8.3% of all global incidences in 2020 while contributing 12.5% of all global deaths, which is considerably higher than incidence rates (Arnold et al., 2022). These patterns correlate with the risk

factors and the availability and utility of screening facilities. Furthermore, the mortality rates also differ within the breast cancer subtype, where HER2-positive breast cancer is associated with a higher death rate, followed by TNBC, luminal A and B subtypes (Ren et al., 2019).

1.1.2 Breast Cancer associated risk factors

The incidence and mortality rates correlate with age, where the cases incline sharply at age 40 and peak at 60. Women in developing countries are more susceptible to breast cancer at a relatively young age than their Western counterparts (Agarwal et al., 2007). Recent studies have illustrated that the proportion of young patients (<35 years) ranges from 25% in developing Asian countries to 10% in developed countries (Agarwal et al., 2007). Ethnicity is another risk factor that impacts the mortality rate of breast cancer (Chlebowski et al., 2005). For example, African and African American women populations have shown a disproportionately higher incidence of triple-negative breast cancer, an aggressive type of breast cancer. In addition, this group is associated with a poor survival rate irrespective of uniform treatment and controlled stage of disease, tumour characteristics and other breast cancer risk factors (Chlebowski et al., 2005; Iqbal et al., 2015).

Hormonal and reproductive-associated risk factors influence breast tumour development (Horn et al., 2013; Dall and Brit, 2017). Early menarche and late menopause are associated with increased breast cancer risk, as illustrated in Figure 1.1. This demographic is particularly susceptible to developing oestrogen receptor-positive and lobular carcinomas, indicating that prolonged reproductive years and the influence of oestrogen and progesterone could increase the vulnerability of developing breast cancer. However, studies have shown that increased exposure to oestrogen

during pregnancy decreases breast cancer risk (MacMahon et al., 1970; Horn et al., 2013), suggesting that the timing and the age at which hormone exposure occurs play a crucial role in determining breast cancer risks (Dall and Britt, 2017).

Other lifestyle factors significantly influencing the risk of developing breast cancer are obesity, alcohol consumption and smoking (Danaei et al., 2005; Chen et al., 2011) (Figure 1.1). Studies have shown that these modifiable risk factors account for 20% of breast cancers globally (Danaei et al., 2005). For instance, it is estimated that consuming 3-6 glasses of wine per week is associated with a 10% increase in breast cancer risk in both premenopausal and postmenopausal women (Chen et al., 2011). Furthermore, obesity has negatively affected survival, particularly in women with Asian ancestry (Bandera et al., 2015). Compared to general adiposity, central obesity attributes higher risk in African-American women when measured by body mass index (Bandera et al., 2015). In support of the relationship between smoking and breast cancer, studies have indicated that women who smoke longer prior to their first pregnancy are at higher risk compared to comparative years of smoking post-pregnancy (Bandera et al., 2015). All these modifiable risk factors provide an opportunity to reduce the disease burden by following a healthy lifestyle. It is evident that involving exercise and weight loss in their lifestyle may benefit women, particularly women with high BMI and breast density, a crucial risk factor for breast cancer. Studies have also shown that postmenopausal Asian women with high BMI (≥5.0) are more likely to be at higher risk of developing breast cancer compared to ones that have stable BMI (described as a difference of ±2.5 in BMI). Furthermore, within the postmenopausal population, the population with body mass index (BMI) ≥20 and with high (≥6.5) glycated haemoglobin (HbA1c) are at increased risk compared to those with low (<5.5) glycated haemoglobin (Suzuki et al., 2017). Thus, raising awareness

among women about these risk factors and encouraging them to avoid the lifestyle that promotes these risk factors could be beneficial in reducing the growing global burden of breast cancer.

1.1.3 Genetic predisposition

A family history of breast cancer influences the risk of developing the disease (Brewer et al., 2017). Having a first-degree relative with breast cancer increases the risk by two-fold or higher in women, and the risk is higher with increasing numbers of relatives and younger relatives (Brewer et al., 2017). Mutations in two high-penetrance breast cancer-related genes, BRCA1 and BRCA2, found on chromosomes 17q21 and 13q13, respectively, contribute to most familial breast cancer. In patients with a hereditary predisposition, the average cumulative risk of developing breast cancer is 72% for *BRCA1* and 69% for *BRCA2* by the age of 80 (Kuchenbaecker et al., 2017). More than 2000 mutations and rearrangements in *BRCA* genes have been known; however, few occur predominantly, for example, 185delAG and 5382insC in BRCA1 and BRCA2 genes (Karami and Mehdipour, 2013). Apart from these two genes, other high penetrant genetic susceptibility genes that are determined include *p53, PTEN, STK11/LKB1* and *CDH1,* while others like *ATM, CHECK2, BRIP1*, and *PALB2* are considered as moderate penetrant genetic susceptibility genes (Kuusisto et al., 2011) (Figure 1.1).

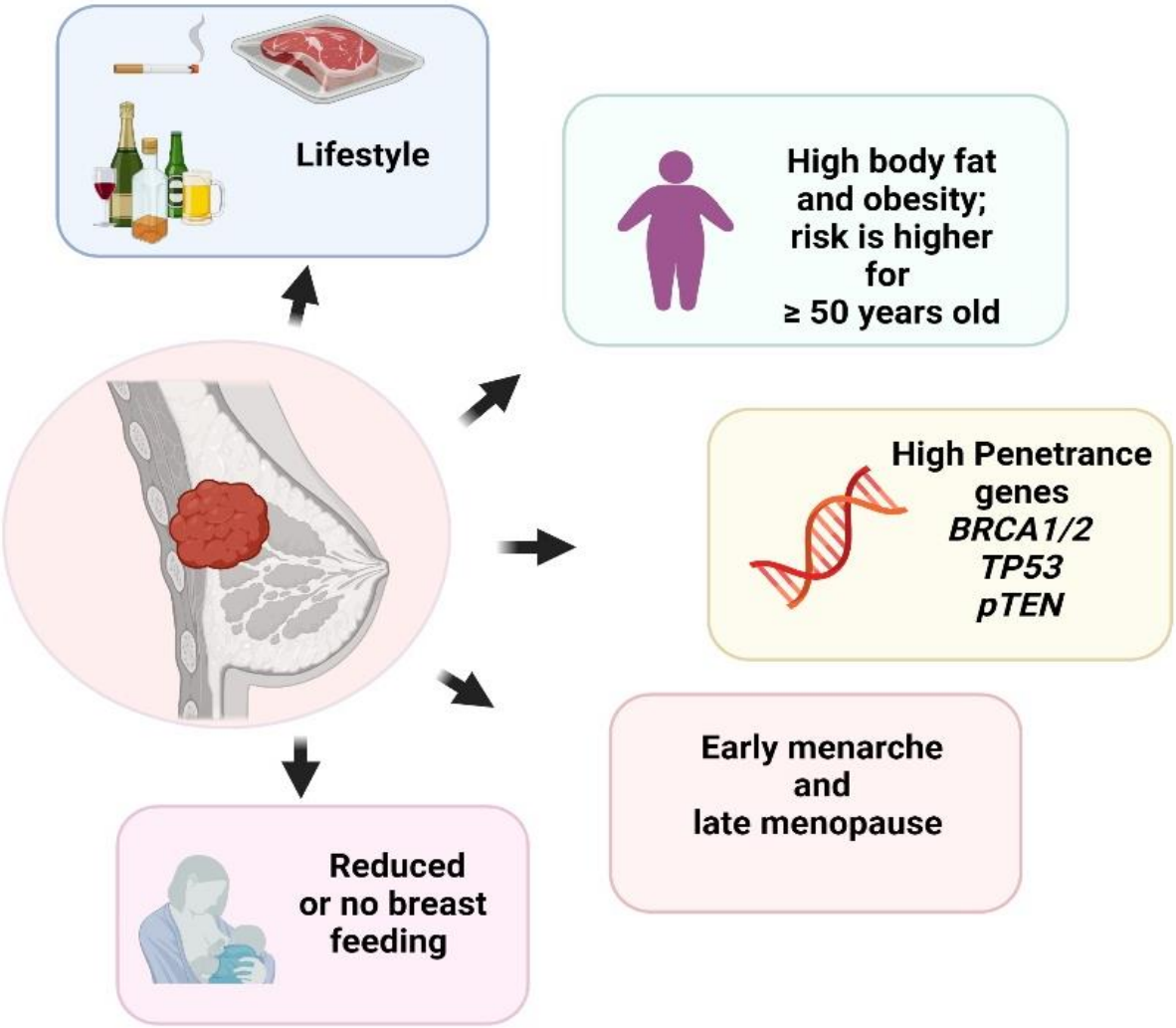

Figure 1.1: Outline of the risk factors associated with breast cancer, including lifestyle factors, high body fat ratio, obesity, hormonal and reproductive associated factors, and mutations in high-penetrance genes. Figure prepared with Biorender.com.

1.1.4 Breast Cancer and its Classification

Several efforts have been made to characterise breast cancer into distinct groups based on clinical, molecular, and morphological attributes (Weigelt et al., 2008; Cardiff and Borowsky, 2014). Over the last two decades, scientists have been exploring the molecular data extracted from advanced techniques, including gene expression profiling, comparative genomic hybridisation, sanger sequencing and next-generation sequencing to improve breast cancer classification, developing prognostic and predictive subgroups with the aim of individualised therapeutic techniques (Weigelt et al., 2008; Cardiff and Borowsky, 2014; Pankotai-Bodó et al., 2024).

Based on the histological outcome, breast cancer is classified into in-situ carcinoma and invasive carcinoma (Malhotra et al., 2010). The former, in-situ carcinoma, is further subclassified as ductal carcinoma in situ (DCIS; more common) or lobular carcinoma in situ (LCIS; less common). Invasive carcinoma is further subdivided into infiltrating ductal (IDC), invasive lobular, ductal/lobular, mucinous (colloid), tubular, medullary and papillary carcinomas, in which IDC is the most frequently occurring carcinomas owing to 70-80% of all invasive carcinomas (Li, Uribe and Daling, 2005; Malhotra et al., 2010).

In 2000, a landmark study by the Perou and Sorlie group distinguished breast cancer into distinctive subtypes based on the cDNA microarrays (Perou et al., 2000; Sørlie et al., 2001). These subtypes represent characteristic differences in the gene expression patterns or “molecular portraits”. Based on the expression of oestrogen (ER), progesterone (PR), and human epidermal growth factor receptor 2 (HER2), ‘the four intrinsic subtypes of breast cancer’ were identified, including luminal-like, basal-like, HER-2 enriched and normal breast-like (Perou et al., 2000; Sørlie et al., 2001). Luminal-like was further subdivided into Luminal A type and Luminal B type. The

distribution of ER-positive and ER-negative tumours into distinct entities was an important implication of this study, as these entities significantly differ in incidence, risk factors, prognosis, and treatment response. The differences and characteristics of these subtypes are summarised in Table 1.1.

Table 1.1 The features of the intrinsic molecular subtypes of breast cancer.

Intrinsic Subtype	**Luminal A**	**Luminal B**	**HER-2 enriched**	**Basal-Like**
ER/PR/HER-2 Status	ER+, PR+, HER2–	ER+, PR+/-, HER-/+	ER-, PR-, HER+	ER-, PR-, HER-
Frequency	50-60%	10-20%	10-15%	10-20%
Histological grade	Low	High	High	High
Site of Recurrence	Axillary lymph nodes, Bone, Brain, Lung	Bone, Lung, Liver	Brain, Bone, Lung	Lung, Central nervous system, Lymph nodes
Treatment	Hormone Therapy	Hormone therapy, chemotherapy, anti-HER2 if HER2+	Anti-HER2, chemotherapy	Chemotherapy

1.1.4.1 Luminal Tumours

The luminal group accounts for the most common cancer subtype, where Luminal A represents the majority (50-60%) (Raica et al., 2008). The expression of the genes associated with the ER transcription factor distinguishes the Luminal tumours. Depending on the expression of hormone receptors, Luminal A is identified as a tumour with ER positivity, and/or PR positivity and HER2 negativity (ER+, PR+, HER2-); Luminal B is recognised as a tumour with ER positivity, and/or PR positivity and/or HER2 positivity (ER+, PR+/-, and HER2+/-). These genes are typically expressed in the luminal epithelium lining the mammary ducts; hence, they are named luminal tumours. A low histological grade, a good prognosis, a low rate of proliferation (low Ki-67), high survival and a significantly lower relapse rate than other subtypes are the characteristics of the Luminal A subtype (Raica et al., 2008; Kennecke et al., 2010).

In comparison, Luminal B is a more aggressive subtype with high histological and tumour grade and with increased expression of proliferation marker Ki-67, which mainly differentiates Luminal B from Luminal A (Raica et al., 2008). Patients with Luminal A tumour exhibit the highest expression of GATA3, which is associated with the better prognosis and survival (Yoon et al., 2010). Moreover, with the Luminal A subtype, the relapse rate is significantly lower (27.8%) than other subtypes, with a longer survival rate of the median of 2.2 years (Kennecke et al., 2010). On the other hand, Luminal B tumour has a worse prognosis than Luminal A, with a relapse rate of 1.6 years (Kennecke et al., 2010). Bone is the most common site of recurrence for both the luminal tumours; however, for Luminal B tumours, the preferential recurrence site is the lungs (Wu et al., 2016). Luminal A and B patients are treated and respond well to hormonal therapy (tamoxifen and aromatase inhibitor); Luminal B responds better to neoadjuvant chemotherapy as represented by the pathological complete

response (pCR) of 17% in Luminal B tumours compared to 7% in Luminal A (Eroles et al., 2012).

1.1.4.2 HER-2 Tumours

HER-2 type tumours are distinguished with the high expression of the HER2 gene and HER-2 associated pathways, including Ras/MAPK (Mitogen-activated protein kinases) or PI3/AKT pathways (Phosphoinositide 3-kinase/ Protein kinase B) (Harbeck et al., 2019). These pathways are related to increased cell proliferation and survival, contributing to this subtype's highly proliferative and aggressive nature (Harbeck et al., 2019). This cancer subtype is highly proliferative; 75% have a high histological grade, and more than 40% are associated with p53 mutations. Clinically, patients with the HER-2 subtype have a poor prognosis; however, the HER-2 subgroup is more sensitive and responds better than those luminal A and B tumours in the neoadjuvant studies (Bernard et al., 2009). The brain is the most common site of recurrence in this subtype (Wu et al., 2016).

1.1.4.3 Basal-Like Tumours

Clinically recognised as triple-negative breast cancer, this subtype does not exhibit ER, PR and HER-2 expression (ER-, PR-, HER-), the three critical receptors in breast cancer (Bosch et al., 2010). Representing 10-20% of all breast tumours, this subtype often expresses normal breast myoepithelial cell gene characteristics, including high molecular weight cytokeratin CK5 and CK17, P-cadherin, caveolin 1 and 2, CD44 and increased expression of proliferative-related genes, including MYC, CDK6, CCNE1 genes (Bosch et al., 2010). Basal-like tumours express cytokeratin genes, including CK8/18 and CK19, overlapping with the characteristics of luminal-like tumours; however, the expression is significantly lower in the basal-like subtype. The relevant feature of this subtype is high histological grade, altered DNA repairs such as deletion of BRCA 2, PTEN, MDM2, high p53 mutations (Harbeck et al., 2019), poor prognosis

and high frequency of lymph node affectation (Bosch et al., 2010). In addition, compared to luminal tumours, this subtype displays a better response to chemotherapy (36% pCR); however, this subtype has a high relapse rate in the first three years, and the predominant site for the metastatic relapse are visceral organs, including lung, central nervous system, and lymph nodes (Kennecke et al., 2010). Immunohistochemically, the specifically identified markers of this subtype are ER, PGR, HER2, EGFR and CK5/6 (Nielsen et al., 2004).

In 2007, a newly recognised intrinsic subtype, the ‘Claudin-low’ subtype, emerged, which was hierarchically clustered close to the basal-like subtype as both shared vital characteristics, such as low HER 2 expression and luminal gene cluster (Herschkowitz et al., 2007; Prat et al., 2010). However, unlike the basal-like subtype, this group displays over-expression of 40 immune response-related genes. This subtype is marked by the reduced gene expression associated with tight junctions and intercellular adhesion, including claudin-3, -4, -7, cingulin, occludin, and E-cadherin, hence named as Claudin-low (Prat et al., 2010). With a poor prognosis, this subtype exhibits an insufficient response to neoadjuvant chemotherapy, demonstrating characteristics between basal and luminal tumours (Prat et al., 2010).

1.1.4.4 Normal breast-like tumours

This subtype of tumours, accounting for 5-10% of all tumours, is poorly differentiated and categorised alongside fibroadenomas and normal breast samples (Yersal and Barutca, 2014). They are classified as triple negative because they lack expression of ER, PR, and HER-2; however, this subtype has not been considered basal-type since it doesn't express CK5 and EGFR. Studies have suggested that this subtype might be a pseudo-existence resulting from high contamination with normal tissue during microarray analysis (Yersal and Barutca, 2014).

1.1.5 Breast Cancer Treatment

Breast cancer treatment strategies depend on the clinical tumour subtypes and their associated clinical outcomes (Harbeck et al., 2019). The therapeutic regimen for a breast cancer patient is decided with the goal of achieving a curative outcome, and often, the treatment decisions are made collaboratively in a multidisciplinary setting (Harbeck et al., 2019). The treatment strategies for a breast cancer patient include locoregional approaches (surgery and radiation therapy) and systemic therapy approaches. The systematic therapy approaches involve endocrine therapy for hormone receptor-positive subtypes, anti-HER2 for HER2-positive subtypes, poly (ADP-ribose) polymerase inhibitors for *BRCA* mutation carriers and a recent advancement, immunotherapy (Harbeck et al., 2019).

1.1.5.1 Locoregional therapies

In early breast cancer treatment, irrespective of the molecular subtype, locoregional therapies involve surgical tumour removal. This proves beneficial in either staging the axillary tumour burden or removing the affected axillary lymph nodes (Margenthaler and Ollila, 2016). In the past decade, breast conservation has replaced mastectomy as the primary surgical goal. Depending on the factors, such as tumour size, tumour-to-breast size relationship, tumour biology, comorbidities and patient choice, surgery is considered the first or second step after initial systemic therapy (Margenthaler and Ollila, 2016). In addition to advanced oncoplastic techniques, neoadjuvant systemic therapies have proven to be advantageous for breast-conserving surgery to reduce the size of tumours prior to the surgical procedure (Haloua et al., 2013).

The inclusion of radiation therapy after surgery has positive outcomes in both disease-free and overall survival in early breast cancer patients, mainly when there is an involvement of lymph nodes and breast conservation surgery (Bartelink et al., 2015).

In most cases, radiation therapy following surgery leads to approximately 75% reductions in locoregional recurrences with a dose-effect relationship (Bartelink et al., 2015). This improvement can be attributed to removing any residual tumour cells (McGale et al., 2014) and potentially activating an abscopal effect (Jatoi, Benson and Kunkler, 2018), leading to decreased recurrences within the treated region. However, the overall advantages concerning any recurrences, including distant metastases, depend on the complex interaction with the risk factors of the primary tumour and the effectiveness of the adjuvant systemic therapy (Poortmans, 2014). Radiation therapy, along with other treatments, can be beneficial in alleviating symptoms from distant metastases, including bone, brain, and soft tissue (Phillips, Jeffree and Khasraw, 2017). A personalised and multidisciplinary approach should be considered while scheduling doses and fractionation, considering the patient's remaining life expectancy and the severity of the lesions (Phillips, Jeffree and Khasraw, 2017). The use of radiation therapy in treating metastatic disease has spurred exciting possibilities for new research in the field of immunotherapy. Several translational and clinical studies are currently examining the effects of combining immune checkpoint blockade strategies and adoptive immunotherapies with radiation treatment to boost the cancer cell-killing mechanism (Bernier, 2016).

1.1.5.2 Systemic therapies

For patients with luminal early breast cancer (all ER+ and/or PR+), post-surgery adjuvant endocrine therapy is the standard treatment for at least 5 years, and tamoxifen is the common drug option for premenopausal and postmenopausal patients (Francis et al., 2018). The high-risk premenopausal patients receiving additional adjuvant chemotherapy may benefit from adding ovarian suppression with a gonadotropin-releasing hormone (GnRH) analogue, which improves disease-free

survival (DFS) and overall survival (OS) as compared to tamoxifen alone (Francis et al., 2018). In postmenopausal with luminal early breast cancer, tamoxifen and aromatase inhibitors are considered as the first option or in sequential use. The inclusion of aromatase inhibitors in adjuvant endocrine therapy has shown a reduction in the recurrence rate compared with tamoxifen (Bradley et al., 2015). However, there is not much variation in the influence on overall survival (Bradley et al., 2015). ER-positive breast cancers are often associated with late recurrences, which can occur from 5 to 20 years post-surgery, determined by the primary tumour, nodal status, and histological grade. Multiple clinical trial studies, as reviewed by (Hong and Xu, 2022), demonstrated that extended adjuvant endocrine therapy for more than 5 years reduces the recurrence risk in patients at high relapse risk, for example, node-positive or high genomic score (Tjan-Heijnen et al., 2017). Several clinical trials are investigating CDK4/6 inhibitors, such as palbociclib and ribociclib, which block the cell cycle combined with endocrine therapy in hormone receptor-positive, HER2-negative metastatic breast cancer. These clinical trials have evidenced substantial enhancements in response rates, progression-free survival (PFS), and, in certain cases, overall survival (OS) with CDK4/6 inhibitors (Goetz et al., 2017; Hortobagyi et al., 2016; Turner et al., 2018). Apart from CDK4/6 inhibitors (palbociclib, ribociclib and abemaciclib), mechanistic target of rapamycin (mTOR) inhibitors (everolimus) has been studied and approved to delay or overcome endocrine resistance in the ER-positive, HER2-negative metastatic breast cancer. The use of everolimus in combination with exemestane, a steroidal endocrine therapy drug, has been shown to improve the PFS but not OS in patients who experience progression during or after treatment with non-steroidal aromatase inhibitors (Piccart et al., 2014).

The use of adjuvant chemotherapy is recommended for luminal-positive, HER2-negative patients when the individual risk of recurrence is estimated at >10% over 10 years. Currently, several western countries utilise first-generation assays such as OncotypeDx (Sparano et al., 2018) and MammaPrint (Cardoso et al., 2016) to predict the early relapse risk and late recurrences, and thereby, the need for neoadjuvant or adjuvant chemotherapy for early breast cancer patients. The standard regimen for adjuvant chemotherapy includes sequential taxane with or without anthracyclines. Compared to increasing conventional dose, increasing dose-dense administration of chemotherapy has proven beneficial in improving 10-year breast cancer-related mortality (Gray et al., 2019).

HER2-positive early breast cancer patients are given neoadjuvant chemotherapy with anti-HER2 therapy as standard care, where trastuzumab and pertuzumab are the commonly used dual HER2-blockade in combination with the chemotherapy (Cortazar et al., 2014). This treatment combination has shown an improved rate of pCR, which correlates with improved long-term outcomes (DFS and overall survival) (Gianni et al., 2016; Cortazar et al., 2014). Involvement of pertuzumab and trastuzumab with chemotherapy in the adjuvant setting has been found to significantly improve the rate of invasive disease-free survival (IDFS) in patients with operable HER2-positive breast cancer, particularly those with node-positive disease (Minckwitz et al., 2017). This treatment regimen is also preferred for patients with HER2-positive advanced breast cancer as first-line options, where commonly used chemotherapeutic drugs include docetaxel, paclitaxel, nab-paclitaxel, vinorelbine or capecitabine. Trastuzumab emtansine (T-DM1), along with chemotherapy drugs, usually capecitabine, vinorelbine or taxane, is preferred as a second-line option (Giordano et al., 2018). In addition, other chemotherapeutic drugs used in combination with T-DM1 as a second-line

option include eribulin, liposomal anthracyclines, platinum, and gemcitabine (Giordano et al., 2018).

In triple-negative breast cancer (TNBC), particularly stage II or III tumours, chemotherapy is preferred, typically involving dose-dense anthracycline and taxane-based regimens (Nitz et al., 2019). Anthracycline-free chemotherapy can be taken into account for stage I triple-negative cancer patients (Nitz et al., 2019). Adding platinum compound in neoadjuvant settings can show increased pCR, independent of BRCA status (Hahnen et al., 2017). For non-pCR TNBC patients, adding additional adjuvant chemotherapy, such as capecitabine therapy, is effective in prolonging DFS and overall survival, as demonstrated by a CREATE-X clinical study (Masuda et al., 2017). For BRCA-associated advanced TNBC, the involvement of PARP inhibitors, such as olaparib or talazoparib, has also proven effective, showing increased PFS and improved quality of life compared to monochemotherapy (Litton et al., 2018). Figure 1.2 summarises all the therapeutic strategies based on the different molecular subtypes and tumour burden.

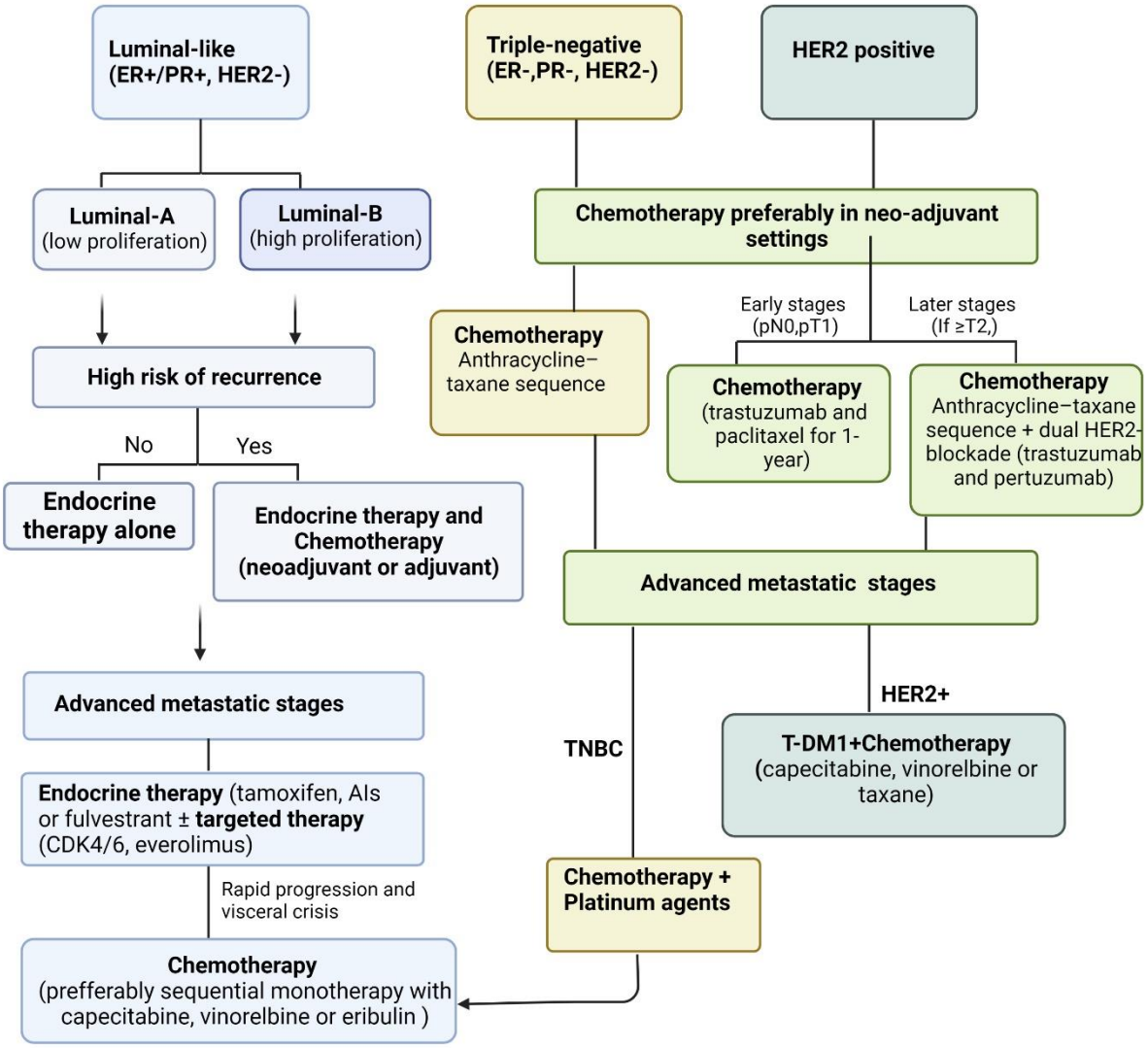

Figure 1.2: Schematic representation of systemic treatment strategy for breast cancer patients based on tumour burden and molecular subtype. All patients with luminal-like subtypes receive adjuvant therapy, whereas patients with high-risk of recurrence are also recommended chemotherapy. Patients in advance metastatic stage with this subtype are recommended targeted therapy, including CDK4/6 inhibitors or mTOR inhibitors, with endocrine therapy. In cases where chemotherapy is required, sequential monotherapy is recommended. For HER2-positive and triple-negative breast cancer patients (TNBC), chemotherapy in neoadjuvant settings is recommended, followed by surgery. For HER2-positive patients, anti-HER2 therapy is also combined with chemotherapy as a standard care. This combination is also recommended as a first-line treatment for advanced-stage HER2-positive breast cancer treatment, followed by trastuzumab emtansine (T-DM1) with chemotherapy as a second-line option for HER2-positive patients. For patients with TNBC disease, chemotherapy is the standard treatment, and for patients in the advanced stage with

TNBC subtype, adding platinum agents with chemotherapy is preferred. Additionally, monotherapy is also recommended for TNBC metastatic disease. Figure prepared with Biorender.com and adapted from Harbeck et al., 2019.

1.2 Introduction to RNA binding protein, ZFP36L1

1.2.1 The origin of the ZFP36L1 family

RNA binding protein ZFP36L1 (also known as TIS11b or BRF1) is a tristetraprolin (TTP) family member that belongs to the family containing the CCCH class of tandem zinc finger proteins (Sanduja, Blanco and Dixon, 2011). Identified initially as TPA (12-O-tetradecannoylphorbol-13-acetate) inducible sequence-11 (TIS11), the identification of three proline repeats in the primary sequence of this protein led to the description of its name as tristetraprolin (TTP) (Taylor et al., 1991; Sanduja, Blanco and Dixon, 2011). Concurrent with the discovery of TTP, two additional cDNA sequences commonly called BRF (butyrate response factor) -1 and 2 were identified, which displayed a 70% amino acid similarity with TTP within the region of two tandem zinc-finger (Cys3His) domains (Varnum et al., 1991). Subsequently, these descriptions were followed by the ZFP36 sequence and its chromosomal locations in humans (Taylor et al., 1991). The TTP family has been universally acknowledged as the ZFP36 family, consisting of four mammalian members, as outlined in Table 1.2. These members include ZFP36 (also known as TTP, Nup475, GOS24, TIS11), ZFP36L1 (also known as TIS11b, Berg36, ERF1, BRF1), *ZFP36L2* (also known as BRF2, ERF2, TIS11D). The fourth member, zfp36l3*,* is expressed only in placental tissues and yolk sacs of rodents (Blackshear et al., 2005).

Table 1.2 Overview of ZFP36L1 gene family members.

Gene	Alternative Names	Species	Chromosomal Location	Proteins (KDa)
ZFP36	TTP, TIS11, NUP475, GOS24	Human	19q13.1	34
		Mouse	7qA3	33.6
		Rat	1q21	33.7
ZFP36L1	TIS11b, Berg36, ERF1, BRF1	Human	14q24.1	36.3
		Mouse	12qC3	36.4
		Rat	6q24	36.4
ZFP36L2	TIS11d, BRF2, ERF2	Human	2p21	51
		Mouse	17qE4	50
		Rat	6q12	50
Zfp36l3	AY661338, RGD1559581	Mouse	XqA5	72.3
		Rat	Xq36	72.2

1.2.2 ZFP36 family acts as a post-transcriptional regulator of gene expression

ZFP36 family functions as a post-transcriptional regulator of mRNAs that contains Adenylate-Uridylate (AU)-rich elements (AREs) located in the 3' untranslated region (UTR) of the mRNA transcript. The initial link that identified the ZFP36 family as an mRNA decaying factor was found when a study reported that ZFP36 inhibits the expression of TNF-α through its binding to the ARE present in the TNF-α mRNA transcript (Carballo, Lai and Blackshear, 1998). Since then, several studies have documented that all three members of this family mediate the expression of several ARE-rich mRNAs, including those that encode proteins related to development, cell

differentiation, tumorigenesis, the inflammatory response and apoptosis (Sanduja et al., 2012).

The presence of two conserved tandem zinc finger domains of CCCH-type (Cys-Cys-Cys-His) are the defining characteristics shared between ZFP36 family members (Lai, Kennington and Blackshear, 2002). These two zinc finger domains act as a type of trans-acting factor which binds to cis-acting mRNA structural components, particularly AREs, located in 3' untranslated regions (UTR). The CCCH residues play a crucial role in binding to AU-rich elements and establishing the function of the ZFP36 family as an mRNA-decaying protein (Lai, Kennington and Blackshear, 2002). Within each of the two zinc finger domains (ZFDs), there are 64 amino acids organised in a distinct CX8CX5CX3H sequence, where 'X' represents variable amino acids and the CCCH residues are positioned in a specific arrangement. An 18-amino acid linker separates these two ZFDs, and preceding both ZFDs are two conserved motifs, RYKTEL and KYKTEL (as shown in Figure 1.3) (Lai et al. 2000; Ciais, Cherradi and Feige, 2012). Studies have shown that a single mutation of the amino acid (cysteine to arginine) in one of the zinc finger motifs could hinder mRNA binding and destabilisation activity (Lai, Kennington and Blackshear, 2002). These findings illustrated that the conserved ZFD sequences highly influence the binding capability of ZFP36 members with their target mRNAs.

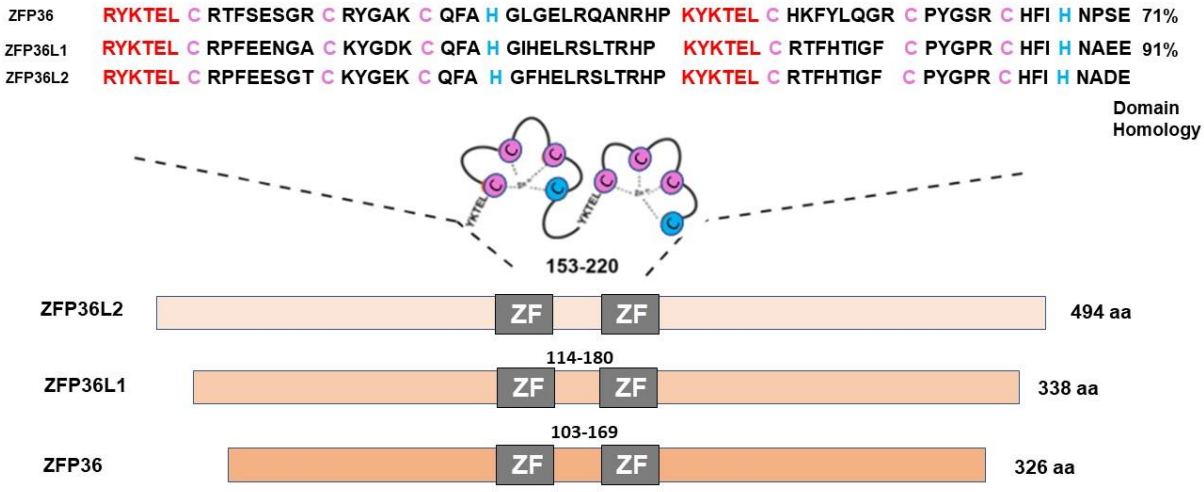

Figure 1.3: Similarities in the zinc finger protein domains of ZFP36 family members. The two zinc finger domains in each ZFP36L1 family member have a high sequence homology characterised by CCCH type, which is preceded by an R/K-YKTEL motif. The zinc finger domain between ZFP36 and ZFP36L1 shares 71% sequence identity, while between ZFP36L2 and ZFP36L1 shares 91% sequence identity. Figure adapted from Ciais, Cherradi and Feige, 2012 and prepared with BioRender.com.

1.2.3 The ZFP36 family and action of mechanism in post-transcriptional regulation

ZFP36 family-mediated post-transcriptional gene regulation initiates with the binding of CCCH-type zinc finger motifs to AREs in 3'UTR of mRNA, where AREs are typically comprised of multiple copies of "AUUUA" motifs (Blackshear, 2002). Subsequentially, this binding event serves as a platform for recruiting other mRNA decaying components through direct or indirect interactions, resulting in poly(A) tail shortening, decapping and degradation of target mRNA. For poly(A) tail shortening, the mammalian cell adopts one of the three complexes for processing mRNA deadenylation: Ccr4/Caf1/Not (Ccr4-Not) complex, the poly A-specific ribonuclease (PARN) complex, and the Pan2/Pan3 complex. Notably, studies have shown that

ZFP36 and ZFP36L1 can directly promote deadenylation through the Ccr4-Not complex, as evidenced by co-immunoprecipitation experiments (Lykke-Andersen and Wagner, 2005). In contrast, a different research study revealed that ZFP36 and ZFP36L1 could enhance deadenylation via the PARN complex. However, no direct correlation was found between the two, implying that there may be an indirect interaction involving other proteins (Lai, Kennington and Blackshear, 2003).

The deadenylation process often results in rapid decay of the mRNA body, which is carried out through two pathways adopted by ZFP36 family members in mammalian cells. One of the pathways known as 5′-3′ decay pathway involves the recruitment of decapping enzymes Dcp1 and Dcp2 and degradation by 5′-3′ XRN1 exonuclease. All these enzymes are accumulated in small cytoplasmic foci known as processing bodies (P-bodies). Under cellular stress, ZFP36 and ZFP36L1 localised to stress granules, which interact with P-bodies to facilitate mRNA degradation, as shown by immunofluorescence microscopy (Kedersha et al., 2005; Murata et al., 2005). Moreover, ZFP36 and ZFP36L1 also colocalise ARE-mRNAs to P-bodies for mRNA degradation (Franks and Lykke-Andersen, 2007) and interact with several P-body components, such as Dcp1a, Dcp2, and Hedls, along with the 5′-3′ exonuclease Xrn1, to promote degradation through 5′-3′ decay pathway (Lykke-Andersen and Wagner, 2005; Fenger-Grøn et al., 2005; Hau et al., 2007)

An alternative pathway is known as the 3′-5′ decay exosome-dependent pathway, where multiprotein complexes of exonucleases, including RNase-specific subunits Rrp44 and Rrp6, are required to facilitate the degradation of mRNAs. ZFP36 family members have demonstrated that they also interact with the components of the exosome pathway, Rrp44 and Rrp6 (Hau et al., 2007; Chen et al., 2001), and are required for 3′-5′ decay (Houseley, LaCava and Tollervey, 2006). The ZFP36 family

promote ARE-mRNA degradation through both mechanisms, exosomes and P-bodies (Figure 1.4). Although it remains uncertain which mechanism is preferentially employed over the other, most research studies suggest that the 5'-3' decay pathway is primarily dominant in most mRNA decay cases, including ARE-dependent mRNA decay (Brooks and Blackshear, 2013).

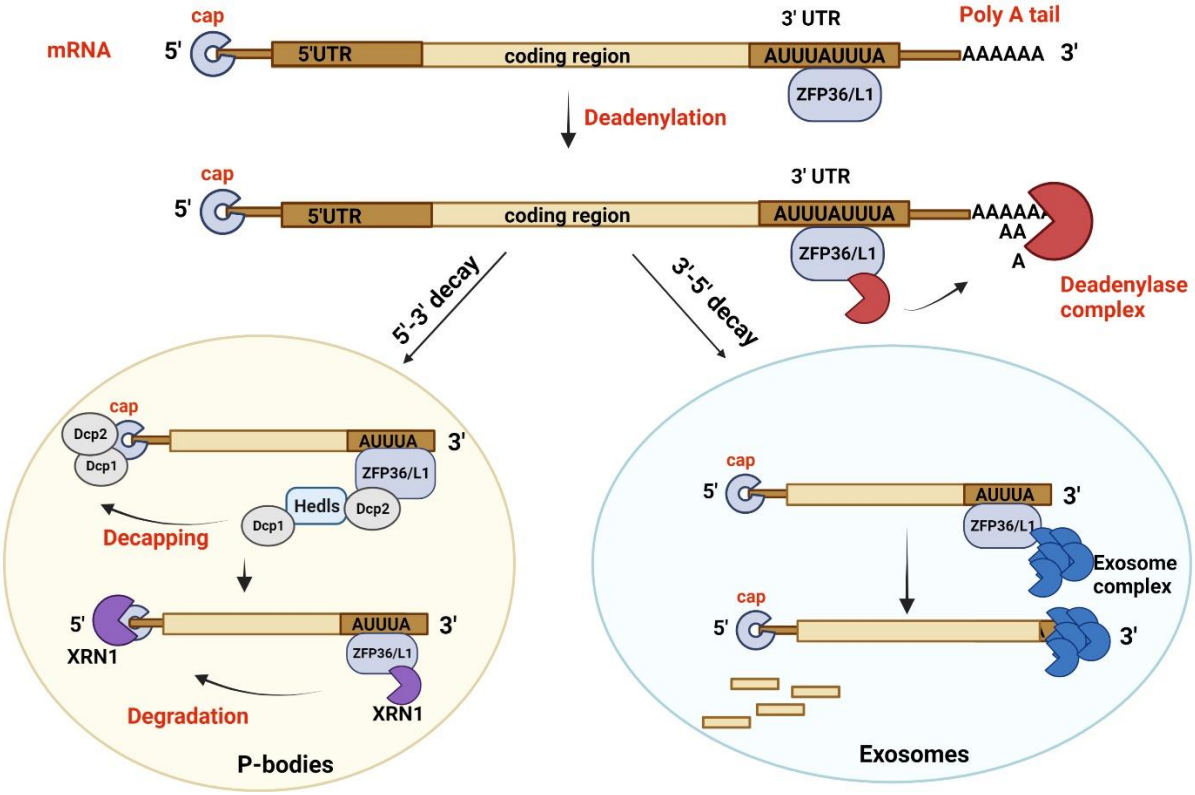

Figure 1.4: The mechanism employed by the ZFP36 family to degrade ARE-mRNAs. ZFP36L1 binds to the AU-rich sequence in the 3'UTR region of mRNA, which is subsequentially followed by deadenylation and poly-A tail removal by PARN or CCR4/NOT complex. Degradation occurs through 5'-3' decay in P-bodies or 3'-5' decay pathways. 5'-3' decay pathway involves decapping enzymes (Dcp1a, Dcp2, and Hedls) and degradation by XRN1 exonuclease. 3'-5' decay pathways involve interaction of exosome complex with ZFP36L1, leading to decaying of mRNA in 3'-5' direction. Figure adapted from Sanduja, Blanco and Dixon, 2010, and prepared with biorender.com.

1.2.4 Posttranslational modification controls expression and function of the ZFP36L1 family

Numerous studies have provided compelling evidence that the expression of the ZFP36 family is modulated post-translationally by extensive phosphorylation at serine and tyrosine residues (Brooks and Blackshear, 2013; Rataj et al., 2016; Clark and Dean, 2016). ZFP36L1 harbours 49 out of 338 phosphorylation sites, and ZFP36 family members, including ZFP36L1, are directly modulated by various protein kinases, such as p38-MAPK2-activated protein kinase 2 (MK2), c-Jun N-terminal kinases (JNK), protein kinase A (PKA) and protein kinase B (PKB) (Brooks and Blackshear, 2013; Rataj et al., 2016; Clark and Dean, 2016). In response to extracellular stimuli, these kinases directly or indirectly interact and phosphorylate ZFP36L1 family members at the serine and threonine residues, attenuating the mRNA decaying function of the ZFP36L1 family. Many studies have highlighted that ZFP36 family members play a key role in p38 MAPK and downstream kinases MK2-mediated regulation of inflammatory responses. The regulation of targeted mRNAs through post-translational modification, such as phosphorylation, is the most extensively studied and understood for the ZFP36 protein (Chrestensen et al., 2004; Stoecklin et al., 2004). For instance, during lipopolysaccharide (LPS)-induced inflammatory response, binding of LPS to toll-like receptor 4 (TLR4) triggers activation of p38 MAPK pathway, which leads to MK2-mediated phosphorylation of ZFP36 at S60 and S186 in humans (Chrestensen et al., 2004) and S52 and S178 in mice (Stoecklin et al., 2004). Phosphorylation of ZFP36 promotes its binding to 14-3-3 protein, a regulatory protein that recognises phosphorylated serine and threonine residues (Munier, Ottmann and Perry, 2021). This binding results in the stabilisation and subsequent inactivation of ZFP36 protein, which increases the TNF-α mRNA levels, one of the known targets of ZFP36 protein (Makita, Takatori and Nakajima, 2021; Stoecklin et al., 2004;

Chrestensen et al., 2004). Furthermore, the mutational substitution of these phosphorylation sites to alanine in ZFP36 protein prevented MK2-mediated stabilisation of TNF-α mRNA (Stoecklin et al., 2004).

Similarly, phosphorylation of ZFP36L1 by MK2 at S92, S203, and S54 facilitates its binding to 14−3-3 protein, leading to its stabilisation and inhibition of mRNA decaying activity (Maitra et al., 2008). According to Rataj et al. (2016), two target residues, S54 and S334, are phosphorylated by PKA, enhancing the ZFP36L1 protein stability and mRNA turnover. Similarly, protein kinase PKB also phosphorylates ZFP36L1 at S92 and S203 serine residues, resulting in its binding to 14-3-3 protein and stabilisation of ZFP36L1 protein while preventing the execution of mRNA decaying activity of ZFP36L1 (Benjamin et al., 2006).

Major phosphorylation sites do not significantly overlap within the ZFP36 family; in some scenarios, the phosphorylatable sites are not always conserved. For example, ZFP36 exhibits proline-rich domains between residues 80 and 90 that are significantly phosphorylated and are not found in ZFP36L1 and ZFP36L2. In other scenarios, surrounding residues may affect the potential phosphorylation sites conserved within the family (Clark and Dean, 2016). For example, serine 220, present in ZFP36, is followed by a proline residue. In contrast, equivalent serine residue, when followed by alanine or serine in ZFP36L1 or ZFP36L2, reduced the probability of phosphorylation by proline-directed kinases (Clark and Dean, 2016). While few phosphorylation sites, such as serine 52, are specific to ZFP36, certain phosphorylation sites are specific to ZFP36 and ZFP36L1, such as Ser-54 and Ser-92 of ZFP36L1 and at Ser-57 and Ser-127 of ZFP36L2. The phosphorylation sites might differ within the proteins, but they might retain the same function by phosphorylation. For example, phosphorylation of ZFP36L1 at Ser-92 and Ser-203 and ZFP36 at Ser-52 and Ser-178 (Benjamin et al.,

2006; Stoecklin et al., 2004) results in the increased stability of both the proteins via recruitment of 14-3-3 proteins and decreased mRNA-destabilising activity. These findings suggest that these proteins might have evolutionary diverged in terms of the location of novel phosphorylation sites; however, the basic mechanism of regulation by phosphorylation remains the same (Clark and Dean, 2016).

1.2.5 Cell-type specific role of ZFP36 family

The ZFP36 family members demonstrate remarkable similarities in the ZFDs in the binding affinity to RNA molecules, and they also employ identical mechanisms to govern the degradation of their specific targets (Sanduja, Blanco and Dixon, 2010). Moreover, these proteins share a similar regulation mechanism by phosphorylation and can function redundantly, causing overlap in targeted mRNAs (Vogel et al., 2016; Hodson et al., 2010; Suk et al., 2018). However, despite all these similarities, these proteins exhibit distinct physiological specificity. For example, the disruption of each of the three genes in mice led to different phenotypes. ZFP36 deficiency results in an early onset of severe inflammatory phenotype (Taylor et al., 1996), ZFP36L1 deficiency in mice led to embryonic lethality due to placental dysfunction (Stumpo et al., 2004), and ZFP36L2 gene disruptions caused perinatal mortality due to defective haematopoiesis (Stumpo et al., 2009). Furthermore, the ZFP36 family displays significant variations in their transcriptomic and protein expression levels in normal human tissues and different cancer cell lines (Carrick and Blackshear, 2007; Brennan et al., 2009). This variability also extends to different breast cancer cell lines, where all three members showed remarkable heterogeneity in the cDNA expression levels (Carrick and Blackshear, 2007). A parallel trend is also observed in data obtained from the Expression Atlas, European Molecular Biology Laboratory - European Bioinformatics Institute (EMBL-EBI) database, where RNA transcript expression levels

among the ZFP36 family vary significantly in various breast cancer cell lines (Figure1.5).

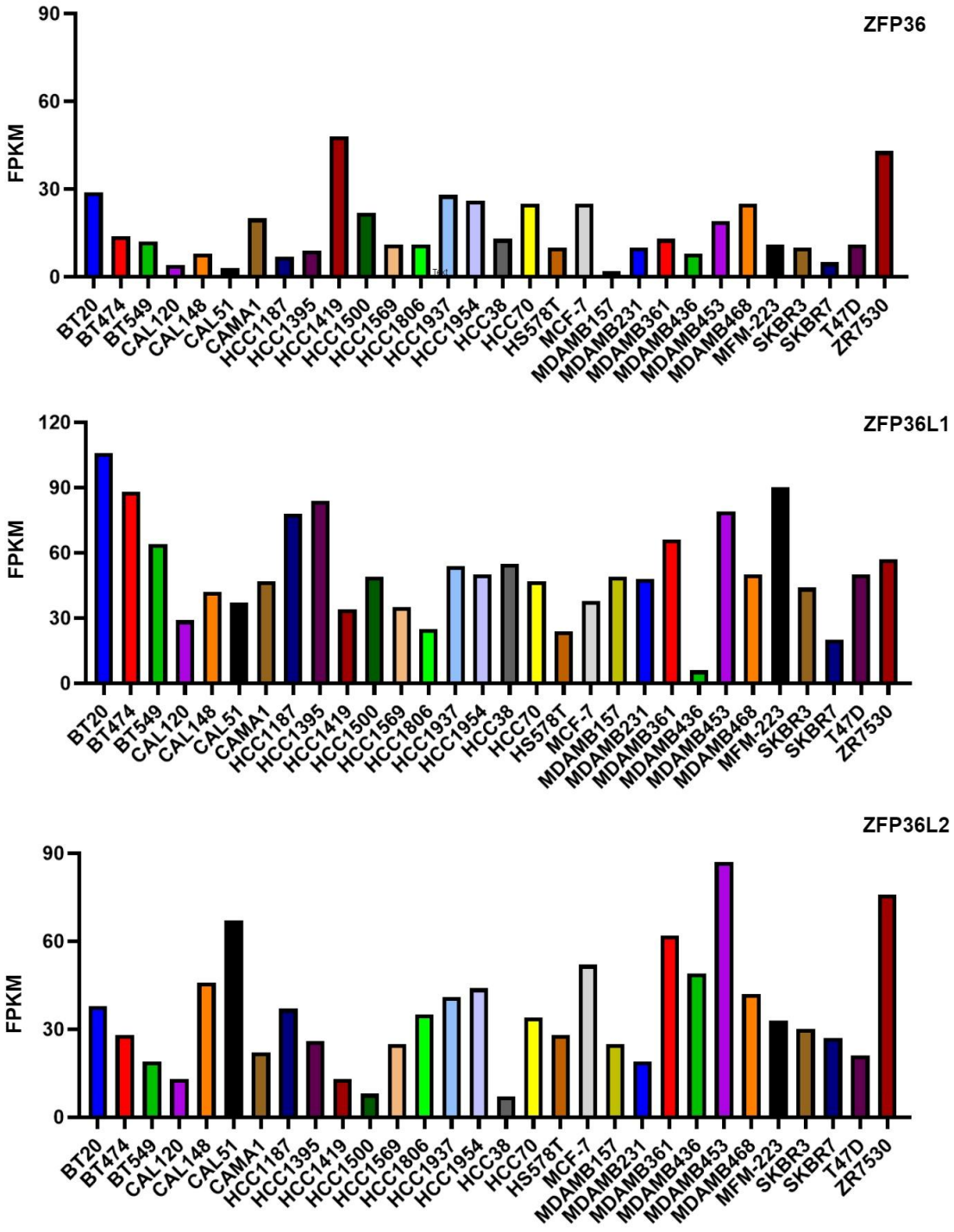

Figure 1.5: Variations in mRNA expression levels of ZFP36 family members across distinct breast cancer cell lines (n=30). The RNA transcript expression levels (quantified in FPKM, Fragments Per Kilobase of transcript per Million mapped reads) of all three ZFP36 family members vary significantly in different breast cancer cell lines. The RNA transcript levels of

ZFP36 are consistently lower relative to ZFP36L1 and ZFP36L2 across all breast cancer cell lines. These graphs are constructed using data extracted from the Expression atlas, EMBL-EBI (https://www.ebi.ac.uk/gxa).

Inhibition of ZFP36 expression led to phenotypic alterations in various tumours in a cell-type-specific manner. For example, suppression of ZFP36 destabilised VEGF mRNA in the cervical adenocarcinoma cell line, Hela, and the mouse embryonic fibroblast cell line, MEF. Contrastingly, reduced expression of ZFP36 did not affect VEGF mRNA levels in prostate tumours, indicating that the correlation between VEGF mRNAs and ZFP36 is abrogated (Brennan et al., 2009). Many studies have also reported the cell-specific role of ZFP36L1 and ZFP36L2. For instance, few studies have reported that suppression of ZFP36L1 expression results in diminished apoptosis and increased cell survival (Lee et al., 2005; Martínez-Calle et al., 2019). Conversely, other studies have demonstrated that the absence of ZFP36L1 expression reduced proliferation and survival (Vogel et al., 2016). Recently, a study conducted by the Kaehler group found that the loss of ZFP36L1 leads to decreased proliferation of chronic myeloid leukaemia (CML) cells in vitro, which challenges the conventional role of ZFP36L1 as a tumour suppressor gene in hematologic malignancies, emphasising that the function of ZFP36L1 is influenced by the cellular context (Kaehler et al., 2021). Researchers have attempted to understand the mechanisms that contribute to the underlying cellular specificity and target selection of these proteins. The presence or absence of mRNA secondary structure could influence the binding of ZFDs to its optimum “UUAUUUAUU” target sequence and it was evident that the secondary structure in mRNA was absent while binding to zinc fingers of ZFP36L2 (Hudson et al., 2004). Another factor could be interference with other RNA-binding proteins. For example, HuR interrupts the binding of ZFP36, leading to the suppression of its mRNA

decaying activity (Mukherjee et al., 2014; Tiedje et al., 2012). The other possible factors could be the subcellular location of the ZFP36 family member proteins as well as their target mRNA, post-transcriptional modifications of the ZFP36 family member proteins, the stoichiometry ratios of available protein and mRNAs, and protein-protein interactions that might affect RNA binding (Wells, Perera and Blackshear, 2017). These factors contributing to the cell-specific function of the ZFP36 family proteins have not been studied much. However, understanding the mechanism that underlies the target selection and specificity of the ZFP36 family is crucial to understanding the role of the ZFP36 family in controlling gene expression.

1.2.6 The ZFP36 family regulates AU-rich genes related to tumorigenesis

According to estimates, around 16% of the genes responsible for coding human protein contain at least one consensus motif of an ARE in their 3'UTR (Gruber et al., 2011), and approximately 8% of mammalian transcripts are potential targets of ARE-binding proteins, including ZFP36 family proteins (Baou, Norton and Murphy, 2011). The ZFP36 family members are involved in the post-transcriptional regulation of several genes that contain AREs in the 3'UTR of mRNA transcript. Initially, the ZFP36 family were identified as proteins that regulate the genes associated with inflammatory cytokines; however, their role as tumour-suppressive genes has only emerged in the past decade. Multiple studies have highlighted that ZFP36 family proteins are aberrantly expressed in various tumours, and their loss is often associated with the overexpression of ARE-mRNAs that are involved in various hallmarks of cancer, as reviewed in (Khabar, 2017; Saini, Chen and Patial, 2020) and summarised in Figure 1.6.

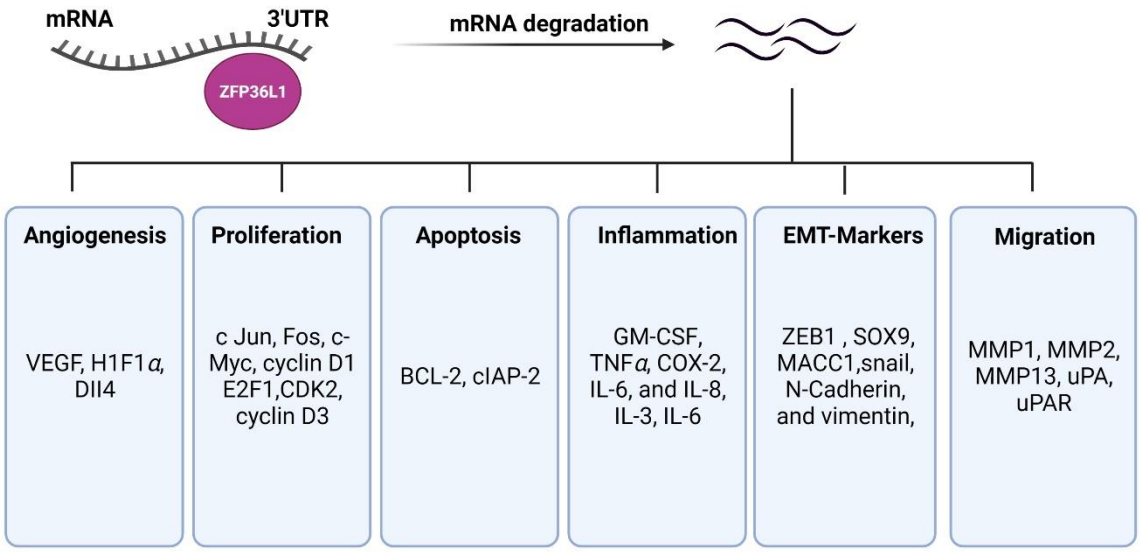

Figure 1.6: The ZFP36L1 family is involved in destabilising multiple ARE-containing mRNAs associated with different hallmarks of cancer, including proliferation, angiogenesis, apoptosis, inflammation, EMT-markers and migration, prepared with biorender.com.

ZFP36 governs the expression of several ARE-containing key cell cycle regulators, including c-Myc, cyclin D1 and E2F1 (Marderosian et al., 2006). Another example of a ZFP36-mediated cell cycle regulator is c-JUN. ZFP36 inhibits c-Jun expression by blocking nuclear factor kappa-light-chain-enhancer of activated B cells (NF-κB) p65 nuclear translocation, leading to increased expression of Wee1, which regulates cell cycle transition from S to G2 phase (Xu et al., 2015). Studies have shown that ZFP36 functions within the nucleus as a transcriptional coregulator. It interacts with nuclear hormone receptors and histone deacetylases, specifically HDAC1s, at the promoter region of ERα target genes. This interaction is crucial in regulating cell proliferation and the development of oestrogen-dependent tumours in breast cancer (Barrios-García et al., 2014). Similarly, ZFP36L1 is also reported to be negatively regulating multiple cell-cycle-related proteins, including CDK2, cyclin D3, c-myc, E2F1, and cyclin

D1, at a post-transcriptional level (Loh et al., 2020). Upregulated expression of these cell-cycle regulators is frequently associated with high-grade tumours, tumour recurrence, and poorer overall survival in different tumours (reviewed in Otto and Sicinski, 2017). In bladder and breast cancer cell lines, it has been observed that upregulation of ZFP36L1 leads to a decrease in cell proliferation and migration, whereas downregulation of ZFP36L1 enhances cell growth (Loh et al., 2020).

Research has indicated that ZFP36L1 and ZFP36L2 function redundantly in tumour suppression in various types of cancer. In bladder and breast cancer cell lines, it has been observed that upregulation of ZFP36L1 leads to a decrease in cell proliferation and migration, whereas downregulation of ZFP36L1 enhances cell growth (Loh et al., 2020). Simultaneous deletion of both ZFP36L1 and ZFP36L2 in mouse thymocytes resulted in the onset of T-cell acute lymphoblastic leukaemia (T-ALL) through stabilisation of an oncogenic transcriptional regulator, Notch 1 (Hodson et al., 2010). Moreover, forced expression of ZFP36L1 and ZFP36L2 has been shown to inhibit cell proliferation by inhibiting cyclin D expression in three human colorectal cancer cell lines, indicating that these proteins exhibit tumour suppressive roles in colorectal cancer (Suk et al., 2018). The abnormal hypermethylation in the second exon of ZFP36L1 in myelofibrosis results in its reduced expression, consequently increasing the expression of its target mRNA, resulting in diminished apoptotic activity in leukaemia cells. These findings revealed that ZFP36L1 can serve as a potent tumour suppressor gene that is subjected to epigenetic regulation (Martínez-Calle et al., 2019).

Numerous studies have revealed that the ZFP36 family, including ZFP36L1, is considerably mutated and under-expressed in various types of cancer, such as breast, bladder, and colon (Brennan et al., 2009; Loh et al., 2019; Nik-Zainal et al. 2016; Rataj

et al., 2019). The ZFP36 mRNA levels analysis with tumour grade in breast cancer patients showed a consistent negative correlation, where advanced tumours were typically associated with weaker ZFP36 expression. In addition, a reduced expression of ZFP36 was also observed at protein levels among a small cohort of breast tumour patients (Brennan et al., 2009). ZFP36L1 is suppressed in multiple aggressive breast cancer cell lines, including MDA-MB-231, 4T1, and MDA-MB-453, as well as in breast cancer tumour tissues (Rataj et al., 2019). The ZFP36L1 protein is extensively mutated in several types of cancer. From the 25 studies displayed on the breast tumours in the cBioPortal database, a total of 68 mutations were identified in the ZFP36L1 protein. Among these, there are 15 missense mutations, 45 truncating mutations, 6 inframe deletions, and 2 splice and fusion mutations. Notably, the N-terminal and zinc finger domains of the ZFP36L1 protein are the most frequently mutated region and mutations leading to truncation of the ZFP36L1 protein are the most prevalent type of mutations found in breast cancer patients (Figure 1.7, shown in blue). (cBioPortal for Cancer Genomics). These findings highlighted that the truncated form of ZFP36L1 could be potentially associated with the development of tumorigenic properties of breast cancer.

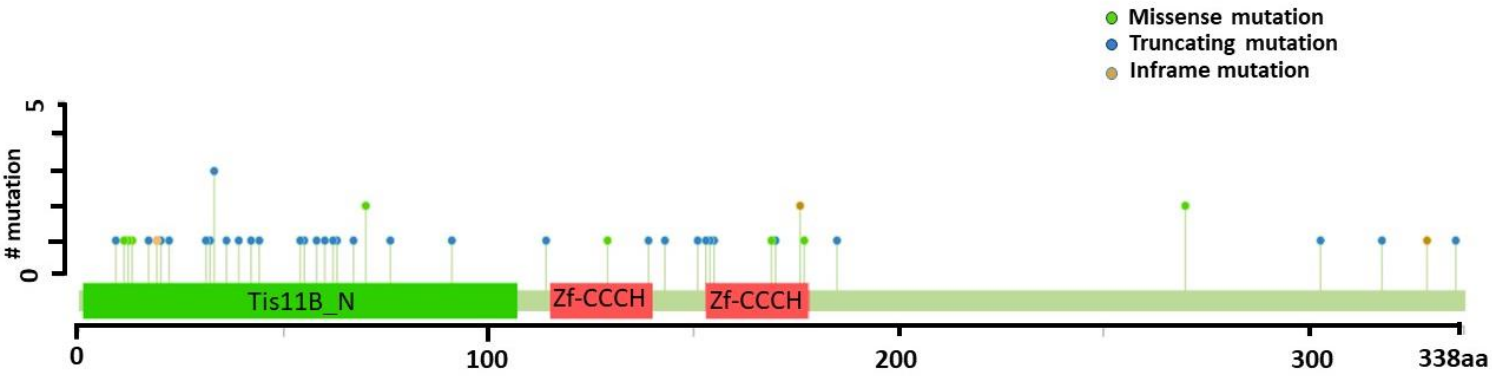

Figure 1.7: The mutations associated with ZFP36L1 protein in breast cancer patients. The data was extracted from breast cancer studies querying 11632 samples from 10851 patients (cBioPortal for Cancer Genomics).

ZFP36L1 has also been stated as a master regulator of angiogenesis. A study conducted by Planel et al., 2010 showed that administering a ZFP36L1 fusion protein through a single intratumoral injection resulted in the reduction of VEGF, acidic FGF, TNFα, IL-1α, and IL-6 expression levels and decreased tumour growth (Planel et al., 2010). Another gene associated with angiogenesis called delta-like-4 (DII4) is also targeted by ZFP36L1, as found by Desroches-Castan et al. in 2011. Their study showed that when ZFP36L1 is downregulated, DII4 mRNA and protein levels increase in endothelial cells exposed to hypoxic conditions. Both ZFP36 and ZFP36L1 have been proven to regulate HIF1α, an integral gene responsible for driving the adaptive response of cells to hypoxic conditions (Chamboredon et al., 2011; Loh et al., 2020). The ZFP36 family also participates in controlling the epithelial-mesenchymal transition and apoptosis. The genes such as ZEB1 (zinc finger E-box binding homeobox 1), SOX9 (sex-determining region Y box 9), and MACC1 (metastasis-associated in colon cancer 1), which are the key regulators of the EMT process, are directly controlled by ZFP36 in colorectal cancer (Montorsi et al., 2016). Forced expression of ZFP36 in MDA-MB-231 breast cancer cells decreased cell migration and destabilised transcripts of three critical regulators of invasion and metastasis, including Matrix Metalloproteinase-1 (MMP1), urokinase-type Plasminogen Activator (uPA), and urokinase-type Plasminogen Activator Receptor (uPAR) (Al-Souhibani et al., 2010). *In vivo* and *in-vitro* expression of a derivative of *ZP36L1* in MDA-MB-231 breast cancer cells, exhibiting N-terminal domain deletion and serine-to-aspartate substitution at position 334, reduced the expression of EMT markers, including snail, N-Cadherin, and vimentin (Rataj et al., 2019). Moreover, *in-vivo* treatment with ZP36L1 derivative reduced the expression levels of major mediators of cancer-associated inflammation and invasion such as Fractalkine (CX3CL1), monocyte chemoattractant protein 1

(MCP-1/CCL2), nephroblastoma overexpressed (NOV/CCN3), stromal-derived factor 1 (SDF-1/CXCL12) and tissue inhibitor of metalloprotease 1 (TIMP-1). In malignant B cells, ZFP36L1 is implicated in the downregulation of BCL2 mRNA, a pro-survival protein, showing its role in the induction of apoptosis (Zekavati et al., 2014). Another study illustrated that the cellular inhibitor of apoptosis protein -2 (cIAP2) is targeted by ZFP36L1 in human head and neck squamous cell carcinoma (HNSCC) cell lines. Increased ZFP36L1 expression enhanced the cisplatin sensitivity of HNSCC cell lines by lowering cIAP2 expression, which results in increased activity of Caspase-3 and cisplatin-induced apoptosis (Lee et al., 2005). The role of the ZFP36 family, including ZFP36L1, has been well-characterised as an inflammatory/immune regulator (Zekavati et al., 2014) as they target an extensive overlapping repertoire of key cytokines via degrading their mRNA transcripts. ZFP36L1 has been shown to regulate granulocyte-macrophage colony-stimulating factor (GMCSF) and interleukin-3 (IL-3). In addition, some targets of ZFP36, including GM-CSF, TNF, COX-2, IL-6, and IL-8, are also targeted and controlled by ZFP36L1 (Loh et al., 2019). Thus, dysregulation of ARE-binding proteins, including the ZFP36 family, is considered a critical factor in the progression of tumorigenesis (Wang et al., 2016).

1.3 Aims of Study

The increasing recognition of breast cancer's heterogeneous nature has prompted a more comprehensive characterisation of genes within distinct breast cancer subtypes. Given the emerging link suggesting ZFP36L1 as a driver gene in breast cancer (Nik-Zainal et al. 2016), this study aims to investigate the novel role of ZFP36L1 in breast cancer, specifically in hormone-positive and HER-2-negative breast cancer subtypes. Our primary focus is to understand how ZFP36L1 influences the oncogenic traits in these subtypes, independently and in combination with tamoxifen, a standard

treatment for luminal breast cancer subtypes. Furthermore, we aim to identify key downstream molecular targets and pathways regulated by ZFP36L1 that may contribute to tumorigenesis. By elucidating ZFP36L1's function in this context, this study explores the potential of ZFP36L1, alone and in combination with other existing therapies, in refining and developing more effective breast cancer therapeutic regimens.

The primary objectives of this study are as follows:

1) **Generating a *ZFP36L1 KO* Model:** Creating a ZFP36L1 knockout (KO) model in MCF-7 breast cancer cells using the CRISPR-Cas9 gene editing methodology. This model served as the foundation for exploring the functions of the ZFP36L1 gene in breast cancer progression.
2) **Investigating Chemosensitivity:** Assessing the effect of ZFP36L1 KO on the chemosensitivity of MCF-7 cells in combination with endocrine therapeutic drugs commonly used for hormone-positive breast cancers, such as tamoxifen and palbociclib.
3) **RNA Sequencing Analysis:** Conducting RNA sequencing analysis to elucidate the impact of ZFP36L1 absence on the transcriptomic profile of MCF-7 cells. This analysis aims to unveil the differentially expressed key biological and molecular pathways in the absence of the ZFP36L1 gene and identify potential targets of the ZFP36L1 gene in MCF-7 cells that may contribute to breast cancer progression.
4) **Cell-Specific Role Exploration:** Investigating the cell-specific role of the ZFP36L1 gene by utilising the ZFP36L1 KO model in the MCF-7 breast cancer cell line and ZFP36L1 truncated model in the HCT116 colorectal cancer cell line. This dual-cell model approach provides insights not only into the potential

role of the ZFP36L1 gene in breast cancer but also in colorectal cancer progression.

Overall, the study aims to shed light on the multifaceted role of ZFP36L1 in breast cancer, from its impact on chemosensitivity to its involvement in key molecular pathways, expanding the scope of its potential as a therapeutic target in breast cancer treatment.

Chapter 2: Materials and Methods

2.1 Breast Cancer Cell Line

This study is facilitated using the breast cancer cell line MCF-7 cells that were kindly provided by Dr Kanagaraj Radhakrishnan, the Francis Crick Institute. MCF-7 cells were cultured in complete Dulbecco-modified Eagle's Medium (DMEM; Gibco # 11965092) supplemented with 10% fetal bovine serum (FBS; Sigma-Aldrich, #F-9665) and 1% penicillin-streptomycin (P/S) antibiotic (ThermoFisher Scientific, #11548876). Genotypes of both cell lines have been confirmed by short tandem repeat (STR) profiling (Appendix A, Table A1). HCT-116 colorectal cancer cells were also utilised in this study and grown using similar conditions mentioned for MCF-7 cell lines

2.1.1 Routine Cell Culturing and Maintenance

MCF-7 cells were grown and maintained in a T-25 flask for routine culturing, and the cells were passaged at 70-80% confluency in a Laminar hood under aseptic conditions. Following removing the medium from the flasks, cells were washed with 5 mL phosphate-buffered saline (PBS) to remove residual media. To detach cells, 1-2 mL 0.05% Trypsin-EDTA (Gibco, #25300054) was added to the flask and incubated at 37^{o}C for 5-10 minutes, and cells were observed under a light microscope to check and ensure the detachment of the cells. Trypsinisation of cells was neutralised by adding 5mL of complete media and mixed well by pipetting up and down. The cell suspension was added in a 15 mL conical tube for centrifugation at 189 x g for 5 minutes. Cell pellets were resuspended in media depending on the split ratio and added to the next T-25 flask containing 6-8mL media. Cells were maintained in a humidified incubator at 37^{o}C and 5% CO2. Similar conditions were utilised for routine cell culturing and maintenance of HCT 116 cell lines.

2.1.2 Cell Counting and Viability

Cells were counted for the experiments that required defined seeding density. Cells were counted using a haemocytometer. To assess cell viability, cell pellets were suspended in an equal ratio (1:1) with the Trypan blue (ThermoFisher Scientific, #15250061). Only the live cells, the unstained ones, were counted using a haemocytometer under a light microscope.

2.1.3 Freezing and Cell Storage

Early passaged cells were frozen in liquid nitrogen and stored in a -80^{o}C freezer to use as per requirement. For freezing cells, cells were collected as described in section 2.1.1. The collected pellet of cells (~1-2 million cells) was mixed with 1 ml Bambanker, a serum-free cell freezing medium (Fischer Scientific, # 13109155) and stored in a 2 mL cryovial in -80^{o}C freezer.

2.2 Designing CRISPR tools for targeting the ZFP36L1 gene in MCF-7 cell line

2.2.1 Designing of guide RNAs targeting ZFP36L1 gene

The human ZFP36L1 gene transcript was retrieved from Ensembl (transcript ID: ENST00000439696.2). The online software Benchling (https://benchling.com) designed a list of guide RNAs from the first 250 base pairs of exon-2 of the ZFP36L1 gene. As Exon 1 of the ZFP36L1 gene codes only for 19 amino acids of the gene, it was not considered the first choice for designing guide RNAs. Three guide RNAs were selected from the list provided by Benchling with the highest on-target specificity to the PAM site, as shown in Table 2.1. Further, these guide RNAs were modified for cloning into plasmid pSpCas9(BB)-2A-Puro V2.0 (PX459) (Addgene, #62988) (Appendix A, Figure A1).

Table 2.1 Selected guide for targeting ZFP36L1 gene.

Guide RNAs	Sequence	PAM	On-target Score
Guide 1	5’ CAGCTCCGTCTTGTAGCGGC 3’	TGG	90
Guide 2	5’ TGTCTCGCGAGCTCAGAGCG 3’	GGG	93
Guide 3	5’ GTCTCGCGAGCTCAGAGCGG 3’	GGG	89

All the modifications were carried out (as shown in Table 2.2) to facilitate the cloning of guide oligos to the plasmid vector PX459, including 5’- 3’ BbsI overhangs (CACC; blue) for ligation at the BbsI restriction sites on the plasmid and guanine (G) nucleotide (red) to initiate transcription by the U6 promoter. The reverse complementary strand is also appended with a 3’ - 5’ sgRNA scaffold overhang (CAAA; green). Eurofins synthesised and provided the modified guide RNAs and their complementary sequence.

Table 2.2 Modified guide RNA oligos with the complementary sequence and BbSI overhangs.

Guide RNAs	Modified Sequence
Guide 1	5’ CACCG CAGCTCCGTCTTGTAGCGGC 3’ 3’ C GTCGAGGCAGAACATCGCCG CAAA 5’
Guide 2	5’ CACCG TGTCTCGCGAGCTCAGAGCG 3’ 3’ C ACAGAGCGCTCGAGTCTCGC CAAA 5’
Guide 3	5’ CACCG GTCTCGCGAGCTCAGAGCGG 3’ C CAGAGCGCTCGAGTCTCGCC CAAA 5’

2.2.2 Annealing of guide oligos

The guide oligos received from Eurofins were phosphorylated and annealed together following the protocol by Ran et al., 2013. To summarise, 1µl of each forward and reverse guide oligos was mixed with 1 µl of 10x T4 DNA ligase buffer (NEB, #B0202S), 1 µl of T4 Polynucleotide Kinase Enzyme (NEB, #M0201S) and 6 µl RNase-free water (ThermoFisher Scientific, #AM9906), followed by incubation at 95oC for 5 minutes on a heating block. The reaction was left to cool down at room temperature until reaching 25oC. The annealed oligos were diluted with RNAase-free water at a 1:100 ratio (oligo: RNase-free H2O) for ligation.

2.2.3 Restriction digestion of pSpCas9(BB)-2A-Puro (PX459) plasmid

The PX459 plasmid vector was digested at the BbsI restriction site to clone the annealed guide oligos. The reaction mixture for the vector digestion was prepared by mixing 3µg of PX459, 5 µl of 10x CutSmart Buffer (NEB, #B7204S), 10 units of BbsI restriction enzyme (NEB, #R0539S), making it upto 50 µl of the reaction mixture by adding the remaining volume of RNase-free water. This reaction mixture was incubated at 37˚C for 30 minutes. The shrimp alkaline phosphatase (SAP) (NEB Cat# M0371S) treatment was given to the BbsI digested PX459 plasmid for dephosphorylation of 5’ ends of digested vector by incubating at 37˚C for 30 minutes.

2.2.4 Ligation of annealed oligos into BbsI digested pSpCas9(BB)-2A-Puro (PX459) plasmid

The digested and dephosphorylated PX459 plasmid vector is run on a 0.8% agarose gel, which is excised and purified using a gel extraction kit (Qiagen, # 28706). The diluted annealed oligos were ligated into digested PX459 vector at a molar ratio of 6:1 (oligos: plasmid using 1unit of T4 DNA ligase (NEB# M0202) incubated overnight in a

water bath at 16˚C. Following the overnight incubation, the reaction mixture is incubated at 65˚C for 5 min to inactivate the T4 DNA ligase enzyme.

Transformation of the mixture containing ligated plasmid was performed using One Shot TOP10 Chemically Competent E. coli (Invitrogen, #C404010) according to the manufacturer's instructions. In brief, 50 µl of competent E. coli cells were gently mixed with 5 µl of the overnight ligated mixture and incubated on ice for 30 min. The mixture was given a heat shock for 20 seconds, followed by an ice shock for 2 minutes and briefly spun to collect all the reaction mixture. 950 µl of pre-warmed SOC medium (ThermoFisher Scientific, #15544034) is added to the incubated cells and incubated at 37˚C in a shaker (180rpm) for 1 hour. Subsequently, the transformation mixture was plated on pre-warmed Luria broth agar plates (Invitrogen, #22700025) containing ampicillin of concentration (100µg/ml). The agar plates were incubated overnight at 37˚C. Following overnight incubation, well-isolated individual bacterial colonies were selected and subjected to colony PCR to screen the bacterial colonies containing ligated plasmids with guide RNAs.

2.2.5 Colony PCR screening of bacterial colonies containing sgRNA-pSpCas9(BB)

Bacterial colonies were screened by colony PCR to assess the successful ligation of gRNA oligos into the pSpCas9(BB) plasmid. The cells from individual bacterial colonies were resuspended into the PCR tube, and a reaction mixture of 20 µl was prepared for colony PCR. The reaction mixture contained the following components: 0.5 µl of U6 promoter (5' GAGGGCCTATTTCCCATGATTCC 3') in pSpCas9(BB) plasmid as the forward primer, 0.5 µl of reverse complementary sequence corresponding to guide RNA was used as reverse primers (guide 1: 5' GCCGCTACAAGACGG 3'; guide 2: 5' CGCTCTGAGCTCGCG 3'; CCGCTCTGAGCTCGC, 0.125 µl of Taq DNA polymerase, 0.5 µl of 10 mM dNTPs,

2 µl of 10x PCR buffer. Lastly, RNAase free-water was added to the mixture to complete the 20 µl reaction mixture. PCR was performed in a Bio-Rad thermocycler using the following thermocycling conditions:

95°C for 5 min (Initial denaturation), followed by 25 cycles of

a. 95°C for 1 min (Denaturation)

b. 50°C for 30 secs (Annealing)

c. 72°C for 20 secs (Extension), and final extension at 72°C for 5 minutes

After PCR, the amplified products were run on the 1% agarose gel by electrophoresis and visualised using a UVI doc gel documentation system. The selected colonies with positive results showing amplicons of approximately 260 base pairs were picked using a sterile pipette tip and inoculated into 5ml LB medium (Invitrogen, #12795027) containing 100µg/ml ampicillin. The tubes containing inoculated colonies are incubated overnight at 37°C in a shaker with constant agitation at 200 rpm. The next day, bacterial pellets were isolated and purified using the QIAprep Spin Miniprep Kit (Qiagen, #27104) following the manufacturer's protocol. Purified plasmid DNA samples were sequenced by Sanger sequencing to confirm the insertion of 20 base pairs guide RNA in the plasmid vector with the correct orientation. Sanger sequencing is facilitated by employing a U6 polymerase forward primer (5'-GAGGGCCTATTTCCCATGATTCC-3') provided by GENEWIZ, UK. The DNA sequence provided by Sanger sequencing was aligned with the pSpCas9(BB) plasmid backbone (Addgene) to check for the 20 bp insertion of the gRNAs between the U6 promoter and sgRNA scaffold. After confirmation of successful gRNA cloning into PX459, plasmids were amplified using a plasmid midi kit (QIAGEN, #12143) according to the manufacturer's protocol.

2.2.6 Lipid mediated delivery of sgRNA ligated pSpCas9(BB) plasmid in the MCF-7 cell line

To introduce the reconstructed PX459 plasmid, cationic lipid-mediated transfection was performed using lipofectamine 3000 (Invitrogen). Approximately 0.40 x 10^6 MCF-7 cells were seeded in a 6-well culture plate in culture media with no antibiotics. After 24 hours, cells were transfected with the plasmid DNA using Lipofectamine 3000 reagent (Invitrogen# L3000001). To summarise, 5 µg of plasmid DNA was diluted in 250 µl of reduced serum media (Opti-MEM, Gibco 31985062) and 10 µl of p3000 buffer reagent. In addition, 5 µl of lipofectamine 3000 transfection reagent was diluted in 125 µl of reduced serum media. After dilution, 125 µl of plasmid DNA and transfection reagent were mixed and incubated at room temperature for 15 minutes. The prepared reaction mixture was added to the cells. As a negative control, a well was transfected with the plasmid no guide RNA (empty vector). The following day, the transfected medium was replenished with the fresh medium for 24 hours, followed by puromycin selection starting with 2 µg/ml concentration. Post 24-hour, puromycin-containing media was replenished with a complete medium and grown until the 6-well plate got 60-70% confluent with the transfected cells. The same transfection procedure was followed to introduce ZFP36L1-specific guide RNA in HCT 116 cells.

2.3 Screening and validation of CRISPR-mediated ZFP36L1 monoclones

2.3.1 Extraction of Genomic DNA

DNA extraction was performed using the Qiagen QiaAmp DNA mini kit (#51304) according to the manufacturer's instructions. Cells were harvested, washed with PBS and resuspended in 200 µl of PBS. Cells were mixed with 20 µl of proteinase K and 4 µl of RNase A and incubated at room temperature for 5 min. Buffer AL (200 µl) was added to cells, vortexed for 15 secs, and then incubated at 56˚C for 10 min. After

spinning, molecular-grade ethanol (200 µl) was added, vortexed for 15 secs, then transferred to QIAmp Mini spin columns and centrifuged at 14,000 rpm for 1 min. Spin columns were washed with 500 µl AW1 Buffer and 500 µl AW2 Buffer and spun at 14,000 rpm for 3 min. After an empty spin, genomic DNA was eluted with 100µl of RNase-free water. The quality of genomic DNA was checked and measured using a Nanodrop (ND-1000, ThermoFisher, UK). The genomic DNA was also run on 1% agarose gel for 45 min at 100 V, and an image was captured using a UVIdoc gel documentation system.

2.3.2 PCR screening of ZFP36L1 targeted monoclones

PCR screening was performed to assess the genome editing within the targeted region of the ZFP36L1 gene. Exon 2 of the ZFP36L1 gene was amplified at position 40-489 using the primers shown in Table 2.3. The ZFP36L1 exon 2 sequence showing amplified region with the primers is shown in the appendix (Figure A2). The primers were synthesised and provided by Eurofins. For amplifying the targeted region, a total of 50 µl reaction mixture was prepared, and the components used to amplify the targeted region were as follows: 2 µl of forward primer (40 forward primer) and 2 µl of reverse primer (489 reverse primer) (Eurofins) (Table 2.3), 25 µl of 2x Taq Red mix (Bioline, 25043), and 5 µl of DNA template. Lastly, RNAase free-water was added to the mixture to complete the 50 µl reaction mixture.

Table 2.3 Primer sequences utilised to screen ZFP36L1 targeted monoclones.

Primers	Sequence	Target (ZFP36L1 gene)
40 Forward Primer	CTGCTGGACAGAAAGGCAGT	Exon 2; Bp 40
489 Reverse Primer	ATCCACAACGCTGAAGAGCGC	Exon 2; Bp 489

PCR was performed in a Bio-Rad thermocycler using the following thermocycling conditions:

95˚C for 1 min (Initial denaturation), followed by 25 cycles of

a. 95˚C for 15 sec (Denaturation)

b. 60˚C for 15 secs (Annealing)

c. 72˚C for 10 secs (Extension) and final extension at 72˚C for 5 minutes.

Following PCR amplification, DNA amplicons were run on 1.5% agarose gel at 100 volts for 45 minutes. PCR samples were purified using a PCR purification kit (Qiagen #28104) following the manufacturer's instructions.

2.3.3 Immunoblotting to analyse the protein expression of ZFP36L1 targeted monoclones

Cells were harvested and lysed by resuspending in the RIPA buffer which contains 50 mM Tris-HCl (pH 8.0), 150 mM NaCl, 0.1% Triton X-100, 0.5% sodium deoxycholate, 0.1% sodium dodecyl sulphate (SDS), 1 mM sodium orthovanadate, 1 mM NaF, and a protease inhibitors cocktail tablet (EDTA-free; Roche, #1183617001). The cells were then sonicated for 15 seconds; cellular debris was removed by centrifugation at 16,000 g for 20 min at 4˚C, and the supernatant containing extracted protein was collected.

The Bradford method was utilised to quantify the protein concentration (Biorad, # 5000002), and absorbance was measured at 595 nm. To denature total protein

extracts, they were incubated at 95^0C for 5 minutes in 4X SDS sample loading buffer (0.2 M Tris-HCl, 0.4M DTT, 277 mM SDS, 6 mM Bromophenol blue, and 4.3 M Glycerol). The equivalent amount of denatured samples, along with a pre-stained protein marker (Thermofisher scientific #26619), were loaded onto NuPAGE 10% Bis-tris protein gels (Invitrogen, #NP0301) and run in MOPS SDS running buffer (Invitrogen# NP0001) using the XCell Sure Lock Mini-Cell System at 150V for 1 hour. The separated proteins were transferred to a Hybond-P PVDF membrane (Merck, #IPVH00010) using a transfer buffer (25 mM Tris, 190 mM Glycine and 20% Methanol) in a wet tank blotting system (Biorad) for 90 min at 100V at 4˚C. Following the transfer of proteins, the membrane was stained with Ponceau S (Sigma, #P3504) to check for protein transfer quality and washed twice with TBST [20 mM Tris-HCl (pH 7.5), 150 mM NaCl, 0.1% (v/v) Tween-20]. Blocking of the membrane was carried out with 5% non-fat dry milk in TBST for 1 hour. The membrane was incubated overnight with the primary antibody in 5% non-fat dry milk/TBST at 4˚C in a cold room. The following day, the membrane was washed four times with TBST and incubated with the horseradish peroxidase coupled (HRP) secondary antibody in 5% non-fat dry milk /TBST for 1 hr at room temperature. The membrane is washed four times with TBST after secondary antibody incubation. Detection of bands was achieved using western sure chemiluminescence reagent (LI-COR), and imaging was done using a UVP BioSpectrum imaging system. The primary and secondary antibodies used for analysing the protein expression of ZFP36L1 edited monoclones are listed in Table 2.4.

Table 2.4 List of primary and secondary antibodies used in immunoblotting.

Antibodies	Host	Dilution	Supplier
BRF1/BRF2 (ZFP36L1/ZFP36L2) Polyclonal antibody	Rabbit	1:1000 in 5% BSA/TBST	Cell Signalling (2119)
β-actin monoclonal antibody	Mouse	1:1000 in 5% nonfat milk/TBST	Thermofisher (AM4302)
Anti-Rabbit-HRP (secondary antibody)	Goat	1:5000 in 5% nonfat milk/TBST	Thermofisher (31460)
Anti-Mouse-HRP (secondary antibody)	Goat	1:5000 in 5% nonfat milk/TBST	Cell Signalling (7076)

2.3.4 Verifying ZFP36L1 edited monoclones by deep amplicon sequencing (NGS)

Genomic DNA was isolated from the ZFP36L1 edited monoclones as elaborated in section 2.3.1, and PCR amplified as described in section 2.3.2. The PCR amplicons from the edited clones and empty vector control were sequenced through NGS analysis (Genewiz, UK). NGS sequencing generated paired-end reads, which were analysed using an online software tool CRISPResso2 (Clement et al., 2019) to assess genome editing outcomes.

2.4 Functional and cytotoxic assay

2.4.1 Growth Curve Analysis

Cell viability was assessed using 3-(4,5-dimethylthiazol-2-yl)-2, 5-diphenyltetrazolium bromide (MTT) (Sigma, #M5655). WT MCF-7 and *ZFP36L1 KO* clones were seeded at a density of 4x 10^3 cells in a 100 µl medium in a 96-well plate. All the cell lines were seeded in triplicates, and in total, 5 plates were seeded, where one plate was analysed

for each day. MTT dye at 0.5 mg/ml concentration was added to each well in the 96-well plate. Following 4-hour incubation (+37°C, 5-6.5% CO_2), purple formazan crystals were dissolved by adding 100 µl of DMSO solubilisation solution to each well. The absorbance of the plate was measured after a 1-hour incubation at 570 nm and 600 nm using the SPECTROstar nano microplate reader (BMG Labtech, United Kingdom). Each day of the procedure was repeated and counted as day 1 to day 5, with the day of seeding labelled as day 0. Following the MTT protocol assay provided by Sigma, all the absorbance values of the samples measured at 550 nm were subtracted from the samples measured at 690 nm to assess the proliferation. The mean from the triplicate values was calculated and plotted using the GraphPad prism software.

2.4.2 Dose-response curve

WT MCF-7 and *ZFP36L1 KO* clones were seeded at a density of 1.5 x 10^3 cells in a 100 µl medium in a 96-well plate, where all cell lines were seeded in triplicates. After 48 hours, the cells were treated with the appropriate drug where the drug concentration ranged from 500 µM- 5nM for the tamoxifen drug and 500 µM - 1µM for the palbociclib drug. Following 48-hour drug treatment, cell viability was measured using MTT dye following the procedure discussed in section 2.4.1. To construct a dose response curve, drug doses were converted into the log form, and the absorbance values were normalised into the percentage cell viability using the following formula:

$$\% \text{ Cell viability} = \frac{A1 - A2}{A3 - A2} \times 100$$

where A1 = absorbance of treated samples

A2 = absorbance value of the control sample (cells treated with DMSO only)

A3 = absorbance value of the untreated samples

The normalised cell viability values were plotted using a non-linear regression curve graph. The experiment was performed three independent times, with triplicate samples taken each time.

2.4.3 Cell cycle analysis

To perform cell cycle analysis, 4 x 10^5 cells were seeded in 6 cm cell culture dishes incubated at 37^{o}C at 5% CO2. The following day, cells were either untreated or treated with drugs for 48 hours. Following 48 hours of drug incubation, cells were harvested and washed twice with PBS and centrifuged at 1500 rpm for 5 minutes at 4^{o}C. After removing the supernatant, the cells collected by centrifugation were fixed with 5mL of ice-cold 70% ethanol added slowly while stirring gently. Following fixation, the cells were stored overnight at -20^{o}C. The next day, the fixative was removed from the cells and washed twice with PBS. On the day of FACS analysis, the fixed cells were stained with 500 µl FxCycle PI/RNase staining solution (Invitrogen, #F10797) following the manufacturer's instructions. After an hour of incubation, cells were analysed with the BD X-20 flow cytometer and data was analysed using FlowJo online software. The experiment was repeated three times independently.

2.4.4 Wound-healing scratch assay

For scratch assay analysis, cells were seeded in 6-well plates and grown until the cells reached confluency. A scratch in the cell monolayer was made across the width of every well using a P200 pipette tip. The drug was added to the well immediately after the scratch was made for the drug-treated samples. Wells were imaged using the EVOS imaging system (#AMF5000, Thermo Fisher) immediately after the scratch (considered as day 0) and 24 hours post scratch (considered as day 1). The images were analysed using Image J software, where the area of the scratch was measured.

The experiment was performed three independent times, with triplicate samples taken each time. The percentage of the wound closure was calculated using the formula:

$$\% \text{ Wound closure} = \frac{\text{Area of the scratch on Day 1}}{\text{Area of the scratch on Day 0}} \times 100$$

2.4.5 Colony formation assay

For colony formation analysis, the cells were seeded in triplicates in 6-well plates at a density of $5x10^3$ cells. After 48 hours of seeding, the cells were treated with the appropriate drugs for 24 hours, followed by a replacement with a fresh medium. Following 10-12 days of incubation, the cells were with PBS and fixed in methanol for 5 min. After removing the fixing reagent, cells were stained with crystal violet solution (Sigma) for 15 min and washed with distilled water twice to remove the stain completely. The wells were photographed with an EVOS imaging system, and cells were counted manually, counting colonies with more than 50 cells. The experiment was repeated three times independently.

2.4.6 Apoptosis assay

FITC Annexin V apoptosis detection kit with PI (Biolegend, #640914) was used. Cells were seeded at a density of $5x10^5$ in a 6-well plate. The next day, cells were treated with the drug and incubated for 48 hours. Post 48-hour incubation, cells were washed twice with PBS and resuspended in Annexin V binding buffer at a concentration of $1X10^7$ cells/ml. Cells were stained with 5 µl of FITC Annexin V and 10 µl of PI solution. Cells were vortexed and incubated in the dark for 30 min on ice. Three types of controls were used in the experiment: unstained cells, cells stained with only PI, and cells stained with only Annexin V. Apoptosis in each condition were analysed using flow

cytometry BD X-20 flow cytometer, and data was analysed using FlowJo online software. The experiment was repeated three times independently.

2.4.7 Western blot analysis

Cells were seeded at a density of 1 x 10^6 in 10cm dishes. The following day, cells were treated with the drugs and incubated for 48 hours. Post 48-hours incubation, cells were harvested and lysed by resuspending in the RIPA buffer and immunoblotting was performed as discussed in section 2.3.3. The protein expression of several genes tested in MCF-7 cells is listed in Table 2.5.

Table 2.5 List of primary and secondary antibodies used in western blotting.

Antibodies	Host	Dilution	Supplier
p53 Polyclonal antibody	Rabbit	1:1000 in 5% BSA/TBST	Cell Signalling (9282S)
β-actin monoclonal antibody	Mouse	1:1000 in 5% BSA/TBST	Cell Signalling (3700S)
CyclinD1 monoclonal antibody	Mouse	1:1000 in 5% non-fat/TBST	Thermofisher (AM29)
Anti-Rabbit-HRP (secondary antibody)	Goat	1:5000 in 5% nonfat milk/TBST	Thermofisher (31460)
Anti-Mouse-HRP (secondary antibody)	Goat	1:5000 in 5% nonfat milk/TBST	Cell Signalling (7076)

2.4.8 Statistical Analysis

Unless otherwise stated, plotting and statistical analysis of the experimental data was performed using the GraphPad Prism 9 software. All the experimental data is represented as the mean ± standard deviation, and statistical significance was determined using unpaired t-tests.

2.5 RNA extraction using RNeasy plus mini kit, Qiagen

Total RNA was extracted from 70-80% confluent cells from a T-75 flask using RNeasy plus mini kit from Qiagen, following the manufacturer's protocol. Cells were harvested, washed with PBS and centrifuged at 300 x g for 5 minutes. Buffer RLT Plus containing β-mercaptoethanol was added to disrupt the centrifuged pellet and vortexed to homogenise the lysate. The lysate was passed through the genomic DNA (gDNA) eliminator spin column provided in the kit to remove the genomic DNA in the lysate. 70% ethanol (Sigma-Aldrich, #E7023) is added to the lysate collected from the gDNA eliminator, mixed well, and transferred to the RNeasy spin column placed in a 2 ml collection tube. The spin column was centrifuged for 15 s at ≥8000 x g (≥10,000 rpm). After every wash, the spin column membrane is washed with buffer RW1 and RBE and centrifuged for 15 s at ≥8000 x g (≥10,000 rpm). An additional centrifuge at full speed is given to remove any carryover from buffers. Lastly, RNA is eluted from the spin column with RNase-free water, centrifuging for 1 minute at ≥8000 x g (≥10,000 rpm). Eluted RNA is stored at -20^{o}C.

To assess the quality of eluted RNA, RNA concentration (ng/uL) is measured using a Nanodrop spectrophotometer (ND-2000, ThermoFisher, UK) and high-quality RNA showing absorbance ratios of 260/280 nm (~1.8-2.0) and 260/230 nm (~1.8-2.0) were used for further experiments. Gel-electrophoresis was also used to test the quality of RNA. Eluted RNA was run on a 1% agarose gel using tris-base, boric acid, and EDTA (TBE buffer) for 15 min at 150 V. An image was captured using a UVI doc gel documentation system.

2.6 RNA Sequencing and Bioinformatic Analysis

For the RNA sequencing and bioinformatic analysis, extracted RNA was shipped to Novogene. The bioinformatics analysis comprised several steps, including cDNA library preparation, quality assessment, aligning the reads with the reference genome, normalisation of read counts and extensive enrichment analysis. To commence the bioinformatic analysis, the cDNA library was prepared following RNA fragmentation. Novogene employed high-throughput sequencing platforms, like Illumina, to generate raw reads stored in FASTAQ format. Rigorous quality assessment procedures were executed to eliminate the low-quality reads and provide filtered reads. Subsequently, filtered reads were aligned to the reference genome using HISAT2 software (Kim et al., 2019). The human genome version GRCH 38.p13 from Ensembl was utilised as a reference genome. The alignment results were provided in a BAM file format. The quantification of gene expression levels was performed in fragments per kilobase of transcript sequence per million base pairs sequenced (FPKM) using the Cufflinks assembler. Further quantified reads were normalised using DESeq2 R software (Love, Huber and Anders, 2014). Gene Ontology (GO) enrichment analysis and Kyoto Encyclopedia of Genes and Genomes (KEGG) pathway enrichment analysis were conducted to gain insights into the biological significance of differentially expressed genes using Cluster Profiler software (Yu et al., 2012). All these expression analyses are based on the read counts of gene expression levels calculated by estimating FPKM. (Eswaran et al., 2012).

Chapter 3: Generation of ZFP36L1 knockout breast cancer model using the CRISPR- Cas9 gene editing system

3.1 Introduction to CRISPR-Cas9 System

The development of custom-designed nucleases has revolutionised genetic engineering. These programmable site-specific nucleases have enabled researchers to directly manipulate any gene of interest efficiently and precisely, commonly called "genome editing". In the past decade, among all customised nucleases, including zinc-finger nucleases (ZFN), transcription activator-like effector nucleases (TALENs), clustered regularly interspaced short palindromic repeats (CRISPR)/CRISPR-associated (Cas) system has gained significant attention in inducing targeted genomic alterations because it allows more cost-effective, efficient and flexible in disease modelling and gene therapy (Cong et al., 2013, Pellagatti et al., 2015, Alagoz and Kherad, 2020, Cai and Yang, 2014). Researchers have adapted the bacterial defence mechanism into a user-friendly laboratory device for studying genotypes related to diseases. Currently, it is a widely utilised method in a diverse range of animal and cellular models (*in-vivo and in-vitro)* to silence, mutate, repress/interfere with or activate targeted genes (Cong et al., 2013; Brabetz et al., 2017; Platt et al., 2014). As a tool, genetic engineering has great clinical potential in cell-based therapeutics (Saudemont, Jespers and Clay, 2018), and several ongoing clinical trial studies are currently employing gene editing technologies to explore the potential future applications of these customised nucleases, as reviewed in (Ashmore-Harris and Fruhwirth, 2020).

The CRISPR system, adapted from bacteria and archaea, serves as an adaptive immune system that fights against bacteriophage's genetic material (Cong et al., 2013). Among three major types of CRISPR-Cas system, the type II CRISPR-Cas9 system has been widely studied, re-engineered and applied for genome editing in a eukaryotic system. Originating from *Streptococcus pyogenes*, this type II CRISPR-

Cas9 system requires Cas9 protein along with two RNA components, i.e., short CRISPR RNAs (crRNAs) and trans-activating RNA (tracrRNA). The short segments of viral DNA sequences, also known as protospacers, are integrated into an array of repeated elements, transcribed and processed into short CRISPR RNAs (crRNA). The crRNA binds with trans-activating RNA (tracrRNA), forming a tracrRNA:crRNA duplex, which guides Cas9 nuclease to mediate sequence-specific cleavage and destruction of invading viral DNA. The crRNA-tracrRNA complex comprises a single-strand sgRNA with two segments: a duplex RNA structure at the 3′ end to bind Cas9 and a guide sequence at the 5′ end to bind the target DNA sequence (Jinek et al., 2012). To facilitate the DNA target site recognition, the Cas9 nuclease requires a three base pairs sequence known as a protospacer-adjacent motif (PAM) located adjacent to the 3' end of the DNA target site. The presence of a PAM site is crucial for ensuring that the Cas9 target can effectively bind to the target site and initiate the cleavage process (Sternberg et al., 2014). Following double-strand breaks (DSBs), the cell starts fixing these DSBs by two intrinsic DNA repair mechanisms: non-homologous end-joining (NHEJ) and homology-directed repair (HDR). In the NHEJ repair system, DSB repair occurs without using a DNA homologous template, which leads to random indels in the gene sequence. HDR-mediated repairing occurs by utilising a DNA homologous template that leads to precise DNA repair of the mutation (Jinek et al., 2012). Scientists are routinely using the type II CRISPR-Cas9 system to edit the genome of the mammalian system by simply designing 20 nucleotide guide sequences of sgRNA complementary to the target DNA sequence. This customisable 20 base pairs nucleotide sequence is the segment of crRNA that also contains an additional sequence complementary to the tracrRNA. Together, sgRNA and Cas9 are simple and powerful tools to manipulate and edit any DNA target of interest.

Adapted from Ran et al., 2013, we have used a simple and straightforward plasmid-based approach to edit our gene of interest. As listed here, this protocol is outlined in 5 steps (shown in Figure 3.1):

1. Identification of the ZFP36L1 target site and designing the ZFP36L1 specific sgRNA sequence using a bioinformatics tool.

2. Cloning of ZFP36L1 guide RNA sequence in pSpCas9(BB)-2A-Puro plasmid that expresses both chimeric CRISPR RNA- auxiliary trans-activating crRNA (cRNA-tracrRNA). The gRNA scaffold present at BbsI sites in the pSpCas9(BB)-2A-Puro plasmid enables cloning of ZFP36L1-specific gRNAs into pSpCas9(BB)-2A-Puro plasmid at the target region.

3. Introduction of ZFP36L1 sgRNA expressing pSpCas9(BB)-2A-Puro plasmid in MCF-7 cells by lipid-mediated transfection followed by puromycin selection of transfected cells.

4. Isolation and expansion of single-cell clones from heterogeneous ZFP36L1 edited population to achieve homozygous edited cell population.

5. Knockout verification of monoclones by various strategies such as western blot, PCR, and high throughput sequencing.

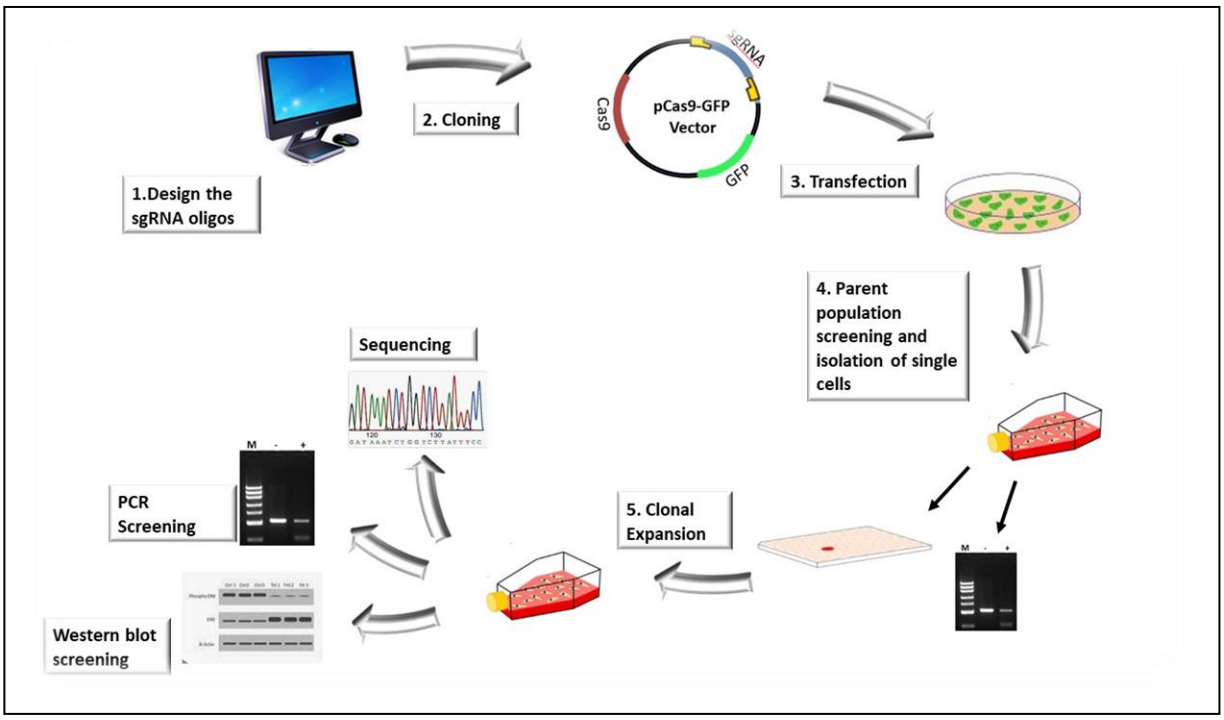

Figure 3.1: The schematic outline of CRISPR workflow. The figure represents all the stages of successfully editing a gene using a plasmid-based approach. The procedure involves: 1. Designing and constructing guide (sgRNA) oligos, 2. Performing cloning to insert sgRNA oligos into the plasmid, 3. Lipid-mediated transfection of the plasmid into the cell line, 4. Parent population screening and isolation of single cell clones, 5. Clonal expansion and editing verification by PCR screening, western blot, and NGS sequencing techniques.

3.2 CRISPR-Cas9 methodology to generate ZFP36L1 knockout MCF-7 cell model system

3.2.1 Designing guide oligos targeting ZFP36L1 using Benchling webtool

The ZFP36L1 gene, located on the reverse strand of chromosome 14q24 (Ensembl ID: ENSG00000185650), consists of 2 exons, translated into a protein length of 338 amino acids (aa). The exon 2 of this gene encodes for 316 amino acids in size, accounting for most of the translated sequence of ZFP36L1 protein. Notably, exon 2 is responsible for encoding highly conserved zinc finger domains that play a crucial role in the mRNA binding function of this gene. Therefore, we aimed to target exon 2 of this gene to abolish the expression of this protein and used exon 2 to design guide

RNAs using the Benchling tool (http://www.benchling.com/). Benchling offers an easy-to-use graphical user interface for creating CRISPR experiments. Benchling provided a list of guides targeting the ZFP36L1 gene, where guide RNAs (sgRNAs) were scored based on the specificity of PAM target sites. Three guides with high on-target scores were selected from the list for Cas9-mediated editing (Table 3.1). To ensure the accuracy of the designed guides, the ZFP36L1 sequence was cross-referenced from Benchling with Ensembl (Ensembl transcript ID: ENST00000439696.3; Ensembl Genome Browser).

Table 3.1 List of selected ZFP36L1 gene-specific guides from the Benchling webtool.

Guides List	Sequence	PAM	On-target score
Guide 1	CAGCTCCGTCTTGTAGCGGC	TGG	93
Guide 2	TGTCTCGCGAGCTCAGAGCG	GGG	90
Guide 3	GTCTCGCGAGCTCAGAGCGG	GGG	89

3.2.2 Reconstruction of pSpCas9(BB)-2A-Puro plasmid targeting ZFP36L1 gene

Gene disruptions at a specific target site require the co-expression of the nuclease Cas9 and the desired sgRNA target within the cell. Strategies frequently deployed for this purpose include delivering plasmid-based CRISPR-Cas9 system (either encoding Cas9 and guide RNA in one vector or two different vectors separately), delivering Cas9 mRNA and guide RNA mixture, and delivering Cas9 protein and guide RNA mixture into the cell (Liu et al., 2017). An all-in-one plasmid system approach was chosen for this gene-editing system, which is the most straightforward and convenient strategy and exhibits fewer off-target effects than other approaches (Liu et al., 2017). The selected guides RNAs were cloned separately in the plasmid pSpCas9(BB)-2A-Puro

(Addgene, #62988) (Appendix A, Figure A1) that encodes for both *Streptococcus pyogenes* Cas9 (hSpCas9) and the chimeric CRISPR RNA- auxiliary trans-activating crRNA (cRNA-tracrRNA) duplex. It also contains a gRNA scaffold that enables the cloning of designed gRNAs at the BbsI restriction enzyme site. The plasmid containing cloned sgRNA targeting ZFP36L1 was transformed into DH5α competent *E.coli* bacterial cells. Bacterial cell colonies obtained were screened by colony PCR and sequence verified by Sanger sequencing to ensure the gRNA insertion in pSpCas9 (BB) plasmid (Appendix B, Figure B1).

3.2.3 Lipid-mediated delivery of reconstructed pSpCas9(BB)-2A-Puro plasmid system in the MCF-7 cell line

Studies have shown that transient transfection of the all-in-one vector may be optimal for achieving a single gene knockout, which can be introduced in the cell by transfection or transduction (Giuliano et al., 2019). Cationic lipid-mediated transfection delivered reconstructed ZFP36L1sgRNA-PX459 plasmids in MCF-7 cells utilising lipofectamine 3000. Many studies have evidenced the growing trend of multiplex genome editing, highlighting the importance of multiplexed strategies in increasing the efficiencies of genetic editing (McCarty et al., 2020; Joberty et al., 2020; Hsieh-Feng and Yang, 2020). To increase the possibility of knocking out the target gene, we hypothesised that using a guide strategy targeting the proximity of exon 2 of the ZFP36L1 gene will show a synergistic effect, leading to high indel rates. Since all three guides targeting ZFP36L1 were cloned individually in pSpCas9(BB)-2A-Puro plasmid, all types of the plasmids expressing different guide RNAs were pooled in two different combinations, (guide1 and guide2) and (guide1 and guide3), to transfect MCF-7 cells in a 6-well dish utilising lipofectamine. The well-transfected with the pSpCas9(BB)-2A-Puro plasmid without any guide RNA sequence (empty vector) was considered as the

negative control. Since pSpCas9(BB)-2A-Puro plasmid encodes for the puromycin resistance gene, transfected cells were selected with a 2 µg/ml puromycin concentration. After 24 hours, the puromycin-containing medium was replenished with the fresh medium and further grown for a week in a medium containing 10% FBS and 1% PEST. To determine the gene editing at the targeted region, puromycin-selected cell populations were screened by PCR. These puromycin-selected edited cells, containing heterogeneous cell populations, were subjected to limiting dilution to generate a monoclonal cell population. With the limiting dilution, monoclones were generated from a single cell to achieve a homogeneous edited cell population, showing uniform protein expression (Figure 3.2).

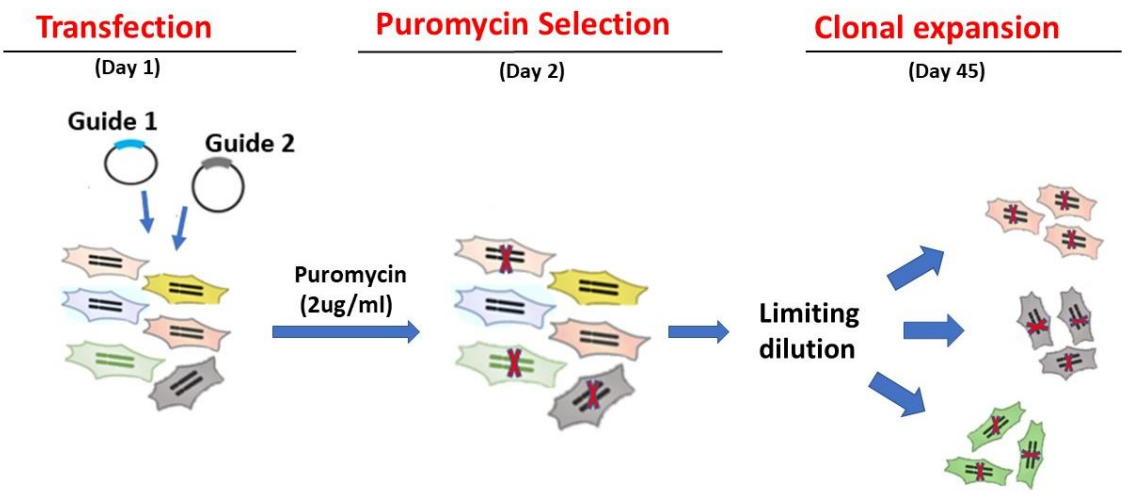

Figure 3.2: Overview and timeline of ZFP36L1 monoclones generation. MCF-7 cells were transfected with the ZFP36L1 guide RNAs and selected with 2 µg/ml puromycin concentration. After limiting dilution, the edited cells were expanded and grown from a single cell to achieve a homogeneous edited cell population. Figure adapted from Ran et al., 2013.

3.3 Validation of CRISPR Cas9-mediated gene editing in MCF-7 cells

Several techniques were implemented to screen and validate the edited cell population at different stages. First, PCR screening of the monoclones, generated by limiting dilution, was performed to analyse the editing outcomes. Second, the western blot analysis was performed to determine the effect of editing on ZFP36L1 protein expression. Third, based on PCR and western blot results, a few monoclones were selected for NGS sequencing to determine the indel profile at the targeted region.

3.3.1 Genomic PCR screening of the monoclones to determine the editing outcomes at the targeted region

To screen multiple monoclones, genomic DNA was extracted from the monoclones (as discussed in section 2.3.1) to perform genomic PCR screening. The primers utilised for PCR screening covered 449 base pairs region, which included the area targeted by ZFP36L1 specific guide RNAs (Appendix A, Figure A2). To analyse the CRISPR-mediated editing outcomes, we compared the PCR-amplified region of monoclones with unedited MCF-7 cells expressing wild-type ZFP36L1. PCR amplification, visualised on a gel, showed significant differences in the DNA fragments of monoclones compared to unedited MCF-7 cells. Multiple monoclones showed distinct DNA fragments running at a lower position (lower than 449 bp) than unedited WT control (Figure 3.3; clones 1, 3, 4, 5, 10, 12 and 13), indicating that the deletion of base pairs occurred at the CRISPR-Cas9 targeted site. On the other hand, a few monoclones showed DNA fragments running at 449 bp position and lower than 449 bp (Figure 3.3; clones 7 and 9), indicating a heterogenous edited population. Very few monoclones showed DNA fragments running at the same position as WT unedited MCF-7 cells (450 bp) (Figure 3.3; clones 2 and 8), indicating a possibility of an

unedited population. However, these clones cannot be ruled out as there could be smaller insertions or deletions, which cannot be detected by PCR amplification. Only clone 14 showed multiple DNA fragments above and below 449 base pairs, indicating heterozygous mutations at the targeted site.

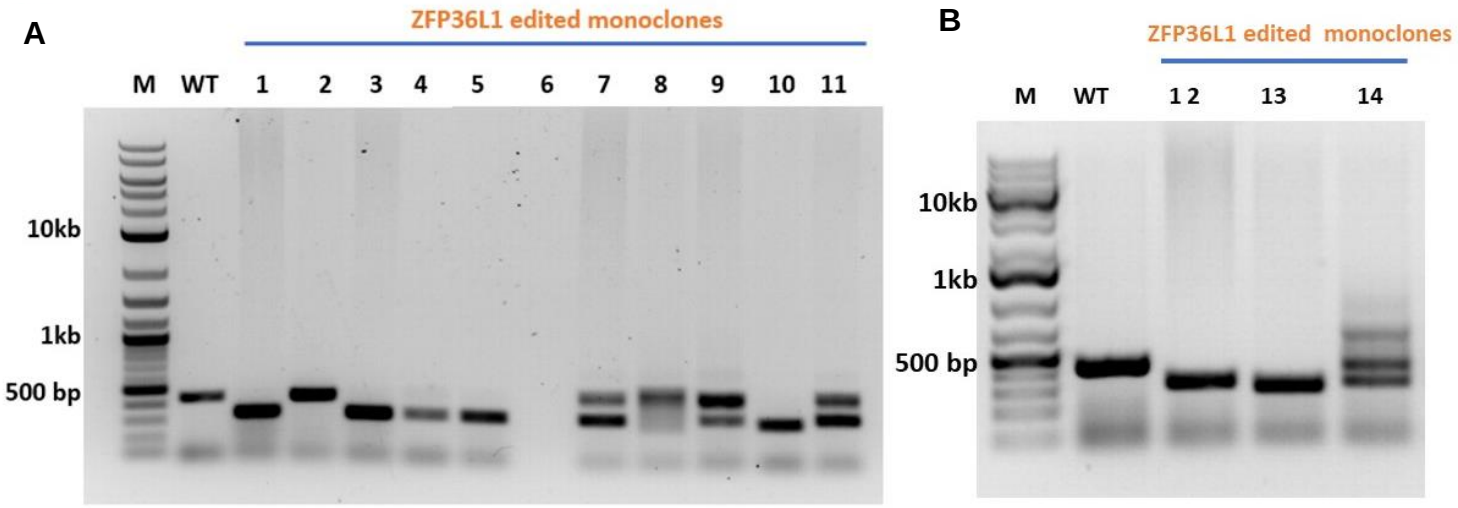

Figure 3.3: Agarose gel electrophoresis of exon 2 target site on ZFP36L1. Monoclones were screened by PCR amplifying the ZFP36L1 sequence encompassing the targeted region (449 base pairs) in MCF-7 cells. 1% agarose gel was utilised for the electrophoresis of PCR-amplified monoclones. Wild-type MCF-7 cells (WT) generated DNA fragments of (~450) base pairs in size. Multiple monoclones demonstrated homozygous deletion (1,3,4,5,10,12,13), producing shorter DNA fragments (< 450 bp), whereas few of the monoclones exhibited multiple bands, showing heterozygous mutation (7,9,11,14). In addition, only a few monoclones were running at the same position as the WT clone (2,8). Marker M is a 10kb DNA ladder.

3.3.2 Western blot analysis to determine ZFP36L1 protein expression in monoclones

Western blot screening was performed to examine whether indels created at the targeted region resulted in any ablation in the ZFP36L1 protein expression. The total cellular protein extracts were prepared and analysed by western blotting using a polyclonal antibody against ZFP36L1 and ZFP36L2 (discussed in section 2.3.3). The

PCR results aligned with the western-blot results as we observed that the monoclones representing DNA fragments running lower than 449 base pairs on agarose gel also demonstrated reduced ZFP36L1 protein levels on the western blot (Appendix B, Figure B2).

From Figure 3.3 B, the monoclones 12, 13, and 14 (referred to as B4, F7, and D3, respectively from here onwards) showed a complete loss of ZFP36L1 protein expression on the western blot (Figure 3.4), which was probed using the polyclonal antibody that detects protein expression of both ZFP36L1 and ZFP36L2. The β-Actin was used as a loading control to ensure all the clones had an equal loading. Together, PCR and western blot results demonstrated that CRISPR Cas9 gene editing generated indels at the targeted region, leading to successful knockout of the ZFP36L1 protein in MCF-7 clones. Further, NGS analysis was performed to investigate and characterise the nature of insertions and deletions generated in these three clones.

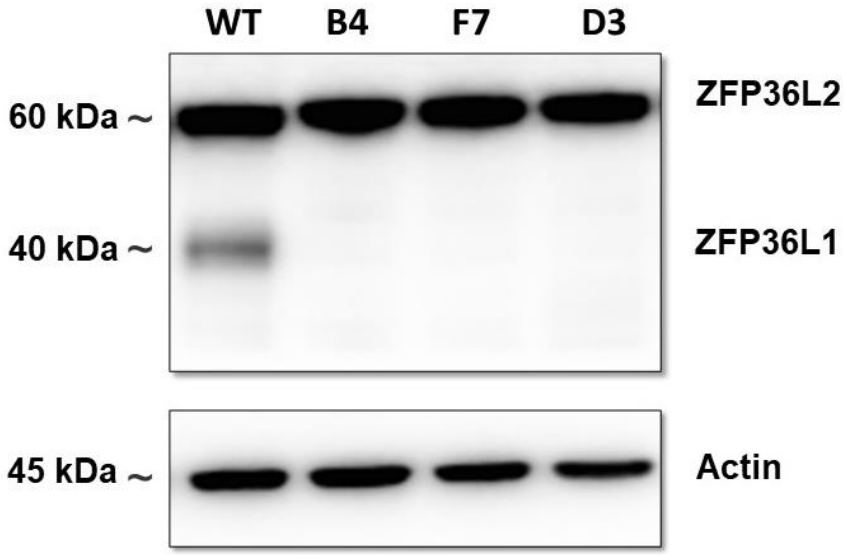

Figure 3.4: Represents the protein expression of ZFP36L1, ZFP36L2 and β-Actin in selected monoclones (B4, F7 and D3). The absence of ZFP36L1 protein expression in MCF-7 cells is confirmed by western blot in all three clones, where WT showed regular expression of ZFP36L1 in MCF-7 cells. The band observed at 60 kDa corresponds to ZFP36L2, 40 kDa corresponds to ZFP36L1, and 45 kDa corresponds to β-Actin.

3.3.3 NGS analysis to analyse the nature of editing of ZFP36L1 knockout monoclones

After PCR and western blot confirmed CRISPR-mediated knockout of the ZFP36L1 gene, amplicon deep sequencing (NGS) analysis was performed to determine the nature of editing in the selected three clones (B4, F7, D3). WT-MCF-7 cells transfected with an empty vector were used as a control. Genomic DNA was extracted from the selected samples and PCR-amplified, and the amplicons proceeded through NGS sequencing (Genewiz). The generated amplicon reads were interpreted and quantified using the bioinformatic web tool CRISPRESSO (Clement et al., 2019), where the ZFP36L1 reference sequence (Ensembl Id: ENST00000439696.2) was utilised to align amplicon reads produced by amplicon sequencing. NGS analysis demonstrated that all three clones vary regarding the type of editing in the sequence targeted by

ZFP36L1 guide RNA, where clones B4 and F7 showed deletion of 108 and 130 base pairs, respectively, and D3 showed one base pair insertion. Although PCR results also showed insertion in the D3 clone, we could not detect it by ampliseq sequencing as only an amplicon length of 500 base pairs was selected for NGS analysis. Table 3.2 outlines the nature of editing in all three clones provided by the NGS analysis using the CRISPRESSO web tool. Clone F7 showed approximately 100% gene editing with 130 base pairs deletion (Figure 3.5 A); clone B4 also showed approximately 99% gene editing with 108 base pairs deletion and 1% varying base pairs insertion (Figure 3.5 B); and clone D3 showed approximately 70% deletion, with one base pair insertion in 26% of the cell population (Figure 3.5 C). The NGS analysis results of WT-MCF-7 cells transfected with an empty vector (EV) used as a control are shown in (Appendix B, Figure B3).

Table 3.2 NGS analysis details provided by the CRISPRESSO tool.

Monoclones	Read aligned with reference sequence (%)	Editing Frequency (%)	Deletion (%)	Deletion (bp)	Insertion (%)
Clone F7	50	99.98	99.60	130	0
Clone B4	12	99.97	98.13	108	0.31 (1 bp) 0.28 (4bp)
Clone D3	46	26.37	72.7		24.8 (1 bp)

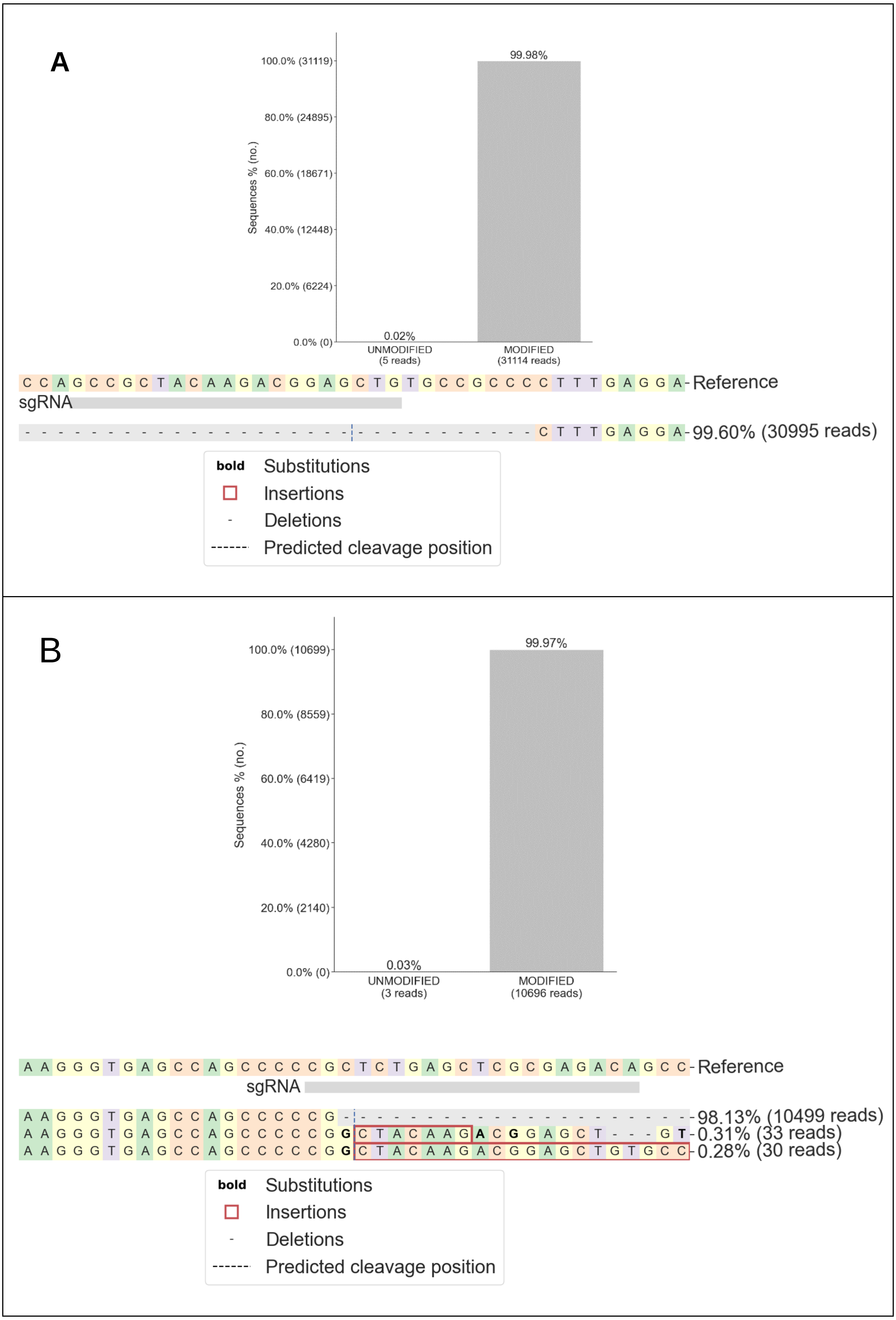

A
100.0% (31119)
80.0% (24895)
60.0% (18671)
40.0% (12448)
20.0% (6224)
0.0% (0)
Sequences % (no.)
99.98%
0.02%
UNMODIFIED
(5 reads)
MODIFIED
(31114 reads)
C C A G C C G C T A C A A G A C G G A G C T G T G C C G C C C C T T T G A G G A
Reference
sgRNA
C T T T G A G G A
99.60% (30995 reads)
bold Substitutions
Insertions
Deletions
Predicted cleavage position
B
100.0% (10699)
80.0% (8559)
60.0% (6419)
40.0% (4280)
20.0% (2140)
0.0% (0)
Sequences % (no.)
99.97%
0.03%
UNMODIFIED
(3 reads)
MODIFIED
(10696 reads)
A A G G G T G A G C C A G C C C C C G C T C T G A G C T C G C G A G A C A G C C
Reference
sgRNA
A A G G G T G A G C C A G C C C C C G
98.13% (10499 reads)
A A G G G T G A G C C A G C C C C C G G C T A C A A G A C G G A G C T - - - G T
0.31% (33 reads)
A A G G G T G A G C C A G C C C C C G G C T A C A A G A C G G A G C T G T G C C
0.28% (30 reads)
bold Substitutions
Insertions
Deletions
Predicted cleavage position

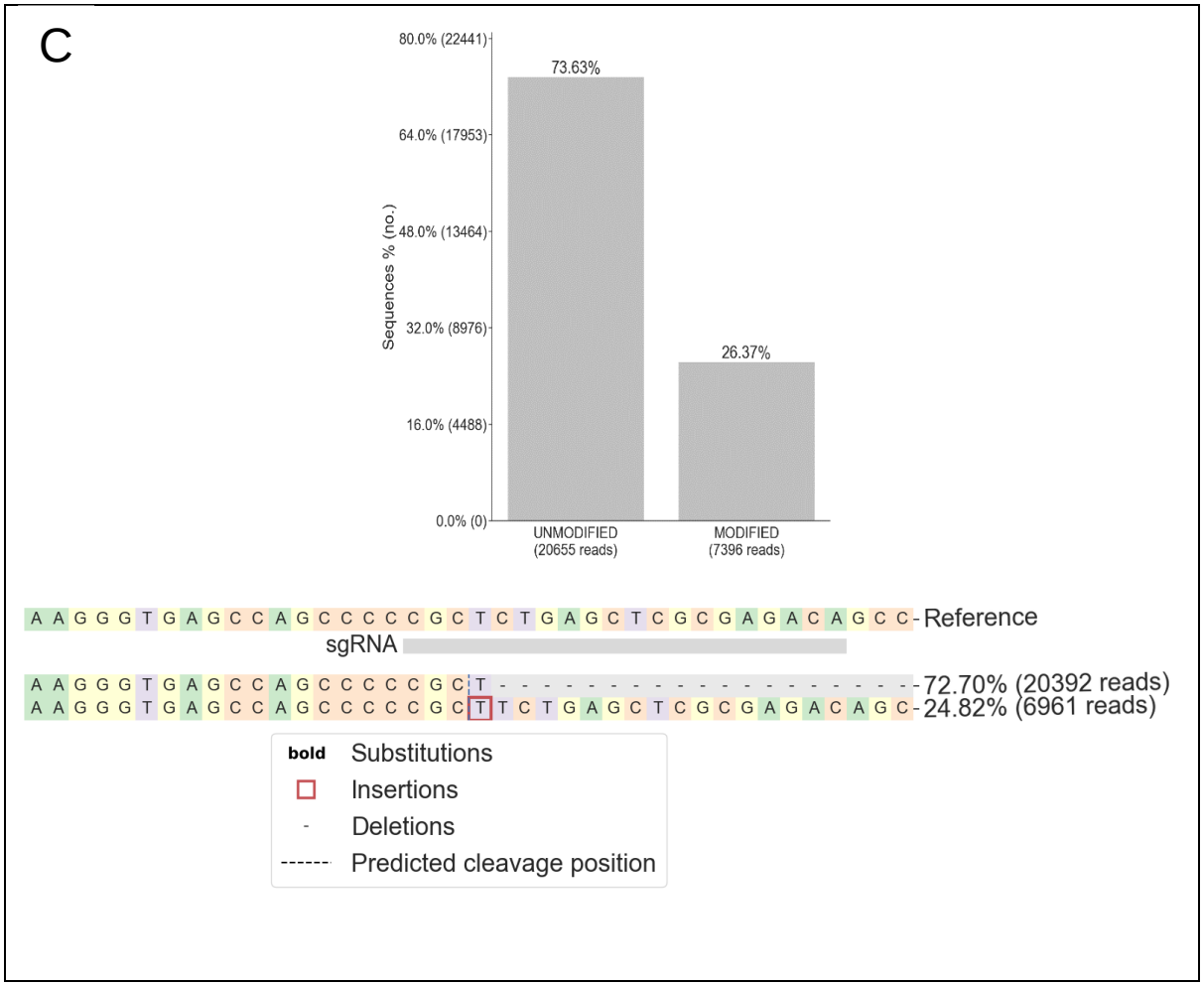

Figure 3.5: Amplicon deep sequencing analysis of CRISPR Cas9 mediated editing of ZFP36L1. Reads provided by NGS sequencing were analysed using the CRISPRESSO web tool. A, B, and C (top) demonstrate the histogram of the percentage of the modified cell population (represented by reads) in clones F7, B4, and D3. The bottom of each section (A, B and C) represents the allele frequency table around the ZFP36L1 target site in clones F7, B4, and D3, respectively. The allele frequency table represents the nature of editing induced in all three clones.

3.4 Discussion

The identification of the CRISPR system has significantly advanced gene-editing technologies and displayed immense clinical potential in medicine, genetics, embryology, and pathology. Not only has it simplified the detection of therapeutic targets, but it has also improved the screening of therapeutic targets for genetic diseases. Unlike other nucleases, such as ZFN and TALEN, which demand cumbersome designing of an engineered protein, CRISPR requires only designing a customisable short 20 nucleotides guide RNA sequence to target any specific region of DNA. Notably, in comparison, CRISPR Cas9 has shown significant advantages in terms of efficiency, versatility, and practicality. In this study, the CRISPR Cas9 system was adapted to abolish the expression of the ZFP36L1 protein in the MCF-7 cell line. We have utilised a plasmid-based method to introduce CRISPR-Cas9 plasmid in the cell to mediate editing of the ZFP36L1 gene in the MCF-7 cells. Using multiple guide RNAs strategy proved beneficial for the successful knockout of the ZFP36L1 with high editing efficiency (Joberty et al., 2020). Moreover, all the guide RNAs associated with high scores regarding specificity to the target sequence were selected using an online benchling tool to avoid the possibility of any off-target effects (Clement et al., 2019). Through multidimensional approaches, we enhanced specificity to the target site while minimising the possibility of off-target effects and increased editing efficiency by using the multiple guide RNAs approach.

In this study, targeting within the initial sequences of exon 2 of the ZFP36L1 gene proved advantageous in disrupting the early coding region and functional zinc finger domains of this protein. Verification of the editing outcomes was performed at several levels using different techniques. First, ZFP36L1 expression was verified at the genomic level with PCR screening of multiple monoclones, amplifying the targeted

ZFP36L1 region. Interpretations of PCR results demonstrated the first line of evidence of possible CRISPR/Cas9-mediated editing, where we predominantly observed deletions in the ZFP36L1 sequence in various monoclones. Secondly, the editing outcomes at the translational level were verified by western blot, which corroborated with the PCR results. Compared to unedited MCF-7 cells, most of the CRISPR-Cas9 edited monoclones demonstrated truncation in ZFP36L1 protein length, whereas few monoclones exhibited heterogenous editing, showing both truncated and full-length proteins. A small proportion of monoclones showed no protein expression, indicating complete ablation of ZFP36L1 protein (Appendix B, Figure 2).

Selected clones B4, F7, and D3, which exhibited no ZFP36L1 protein expression, were further investigated by amplicon deep sequencing analysis (NGS). Lastly, NGS sequencing analysis confirmed the nature of editing in all three clones. The reads generated by amplicon sequencing analysis were aligned with the ZFP36L1 amplicon sequence (reference sequence), which was utilised to amplify the clones prior to sequencing (Appendix B, Figure B4). For clones F7 and D3, around 50% of the generated reads were aligned with the reference sequence. In contrast, only 10% of the reads were aligned with the reference sequence in clone B4. 99% of the cell population exhibited deletion of 130 base pairs, which corresponded to the frameshift mutation in the F7 clone, disrupting the open reading frame of ZFP36L1 and, thereby, complete abrogation of ZFP36L1 protein. Clone B4 displayed the deletion of 108 base pairs in 98% of the cell population, which does not correspond to the frameshift mutations. However, only 12% of reads were aligned in the B4 clone, which accounts for the deletion of 108 base pairs. Thus, we relied on the western blot results, which showed complete abrogation of ZFP36L1 protein expression in the B4 clone. Clone D3 showed heterogenous editing, showing both one base pair insertion in

approximately 27% of the cell population and multiple types of deletion leading to a frameshift mutation and no protein expression of ZFP36L1 protein in MCF-7 cells, as shown by western blot results.

To comprehensively investigate the functional consequences of ZFP36L1 loss in MCF-7 cells, we have employed these three CRISPR-edited ZFP36L1 clones (B4, F7, and D3), demonstrating complete knockout of ZFP36L1 protein in MCF-7 cells. Since each of these three clones possesses a distinct type of editing, this multi-clone approach has strengthened and improved the reliability of this study by reducing the influence of potential off-target effects from the CRISPR Cas9 editing and ensuring that the observed phenotypic changes are primarily due to the specific loss of ZFP36L1. To summarise, we have successfully utilised CRISPR-Cas9 editing to generate ZFP36L1 KO clones in MCF-7 cells and investigate the functional role of ZFP36L1 in breast tumorigenesis.

Chapter 4: Evaluating the Impact of ZFP36L1 Depletion on the Responsiveness of MCF-7 Cells to Tamoxifen

4.1 Introduction

Breast cancer treatment strategies depend on the distinct clinical tumour subtypes and their associated clinical outcomes. The current treatment modalities include locoregional approaches, such as surgery and radiation therapy, and systemic therapy approaches, such as endocrine therapy, chemotherapy, targeted therapy, and immunotherapy (Costa et al., 2020). Currently, in the case of ER+ breast cancer patients, endocrine therapy is the preferred regimen in both early and advanced disease. Endocrine therapy mainly involves the combination of two or more drugs that can directly block the oestrogen receptors of cancer cells, such as selective oestrogen receptor modulators (SERMs), or can block the key enzyme in the biosynthesis of oestrogens, such as aromatase inhibitors (AIs) (Lloyd et al*.,* 2022; Corti et al., 2023).

Tamoxifen drug is the most extensively used SERM in endocrine therapy and is often recommended as an adjuvant treatment option for pre- and postmenopausal patients to reduce recurrence risk and enhance overall survival (Lloyd et al*.,* 2022; Komm and Mirkin, 2014). Orally administered tamoxifen is metabolised by the liver into active metabolites, such as 4-hydroxytamoxifen (4HT), which competes with the endogenous oestrogen hormone 17*β*-estradiol (E2) for binding to intracellular oestrogen receptors, oestrogen receptor alpha (ERα) and beta (ERβ) (Sfogliarini et al., 2022). Depending on the interaction with the tissue-specific transcriptional coregulators, tamoxifen can act as an ER agonist or antagonist of oestrogen signalling (Sfogliarini et al., 2022). Clinically, in ER*α*-positive breast cancers, tamoxifen is used as an antagonist of oestrogen signalling in mammary epithelial cells. The binding of tamoxifen to oestrogen receptors disrupts its interaction with coactivators, downregulating transcriptional activity and proliferation in breast tumours (Lloyd et al*.,* 2022; Sfogliarini

et al., 2022). On the other hand, it provides secondary ER*α*-agonist effects in bone, preventing osteoporosis (Komm and Mirkin, 2014).

Alternatively, AIs such as anastrozole, letrozole and exemestane are also considered for adjuvant therapy in managing early localised breast cancer. However, for the specific tumour that exhibits resistance or becomes resistant to endocrine therapy, the combination of additional drugs is also considered with SERMs or AIs, including cyclin-dependent kinase 4/6 inhibitors (palbociclib) and mammalian target of rapamycin (mTOR) inhibitors (everolimus) (Corti et al., 2023; Costa et al., 2020). Thus, combining existing drugs or new drug targets is an established way to optimise treatment, especially in handling treatment resistance.

The role of ZFP36L1 family members is well established in regulating tumorigenesis-related mRNAs; however, the therapeutic potential of these proteins, particularly ZFP36L1, in combination with other conventional chemotherapeutic drugs is only explored by very few studies (Lee et al., 2005; Kehler et al., 2021). In this study, for the first time, we investigated the therapeutic potential of ZFP36L1 as a treatment, alone and in combination with endocrine therapy drugs, which are currently used for treating luminal-like subtypes, including tamoxifen and palbociclib. Several cytotoxic assays were conducted, including MTT, wound-healing, clonogenic, and apoptosis on WT and *ZFP36L1 KO* MCF-7 cell lines to determine how ZFP36L1 loss affects the chemosensitivity of MCF-7 cells. Furthermore, we evaluated the therapeutic potential of ZFP36L1 in combination with tamoxifen and palbociclib each to observe the impact of ZFP36L1 loss in MCF-7 cells. We aimed to determine the potential synergistic effects of ZFP36L1 with endocrine therapeutic drugs (tamoxifen and palbociclib) for treating luminal-like molecular subtype breast cancer. This study is divided into two chapters; in this chapter, we examined the effect of ZFP36L1 loss, specifically in the

combination of tamoxifen drug, whereas, in the next chapter, we will determine the impact of ZFP36L1 loss in combination with palbociclib drug in MCF-7 cell line.

4.2 Results

4.2.1. ZFP36L1 absence decreased sensitivity of MCF-7 cells to tamoxifen

To examine the growth-inhibitory effects of tamoxifen drugs on MCF-7 cells, cell viability was measured using an MTT assay at different drug concentrations, ranging from 500 µM-1 nM (Appendix C, Table C1) after 48 hours of drug treatment. The IC_{50} value was determined from the dose-response inhibition curve for the WT MCF-7 cells and all three clones of *ZFP36L1 KO* cells, as shown in Figure 4.1 and Table 4.1. The calculated IC_{50} values for the tamoxifen drug were found to be significantly increased for all three *ZFP36L1 KO* clones compared to WT MCF-7 cells. These results illustrated that the loss of ZFP36L1 showed a decrease in sensitivity to tamoxifen, suggesting that loss of ZFP36L1 increased resistance of MCF-7 cells towards endocrine therapy.

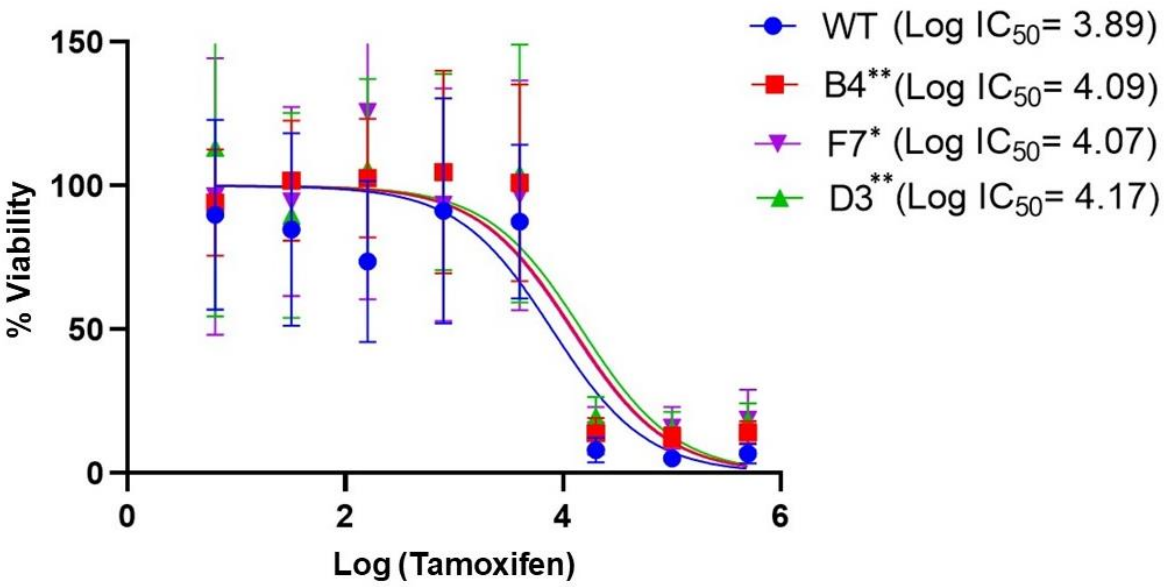

Figure 4.1: The dose-response inhibition curves for the WT MCF-7 cells and *ZFP36L1 KO* clones (B4, F7 and D3) following a 48-hour treatment with tamoxifen. The x-axis represents the concentration of tamoxifen in log form, and the y-axis represents the percentage viability of cells. Results represented here are the average of triplicate wells and represent the findings from three separate and independent experiments. The error bars represent the standard error of the values obtained from triplicate experiments. Statistical analyses were performed by paired t-test. * $p < 0.05$, ** $p < 0.005$.

Table 4.1 IC_{50} values for tamoxifen in WT and ZFP36L1 depleted MCF-7 cells.

Cell line	Log IC_{50}	IC_{50} value (μM)
WT	3.89	7.9
B4	4.09	12.4
F7	4.07	11.9
D3	4.17	14.8

4.2.2 ZFP36L1 loss does not impact the proliferation rates of MCF-7 cells

We observed the impact of ZFP36L1 depletion on the growth of MCF-7 cells by tracking cell proliferation for five days (120 hours), measuring at 24-hour intervals, using MTT dye. As a result, no significant difference was observed in the cell proliferation of WT MCF-7 and three clones of *ZFP36L1 KO* MCF-7 cells (B4, F7, D3), as shown in Figure 4.2.

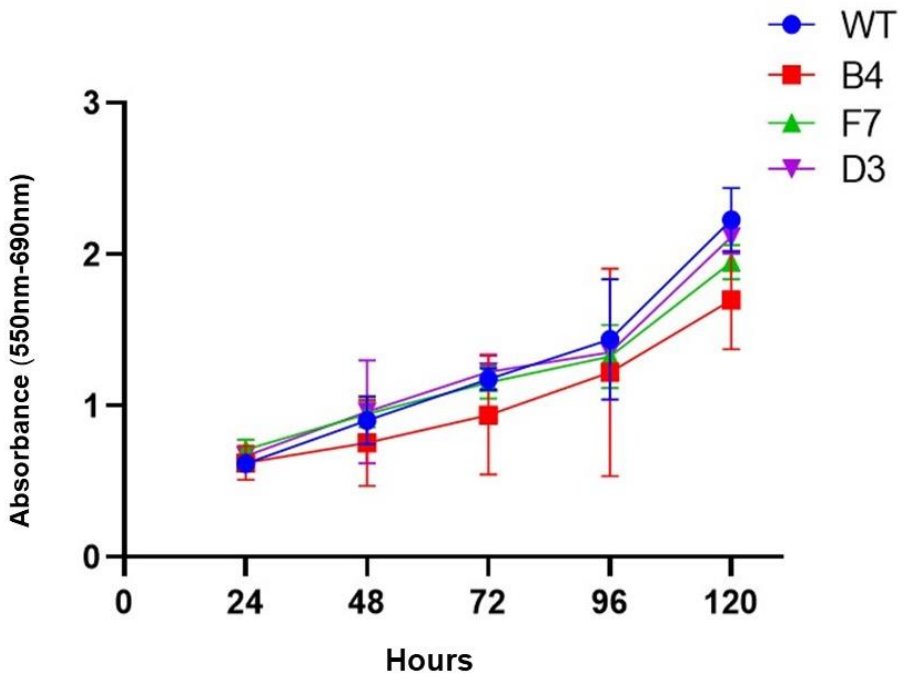

Figure 4.2: The growth curves of both WT MCF-7 cells and *ZFP36L1 KO* clones were monitored at 24-hour intervals over a span of five days. The results presented here are the averages obtained from triplicate wells and are representative of the findings from three separate and independent experiments. The error bars represent the standard error of the values obtained from triplicate experiments. Statistical analyses were performed by unpaired t-test. * $p < 0.05$, ** $p < 0.005$.

Furthermore, FACS analysis after propidium iodide (PI) staining was also performed to assess the *ZFP36L1 KO* effect on the cell cycle analysis. The cell cycle analysis results showed that all three *ZFP36L1 KO* clones significantly decreased the percentage of cells in the G1 phase, suggesting that ZFP36L1 is involved in controlling cell cycle regulation during the G1 phase of the cell cycle (Figure 4.3).

A

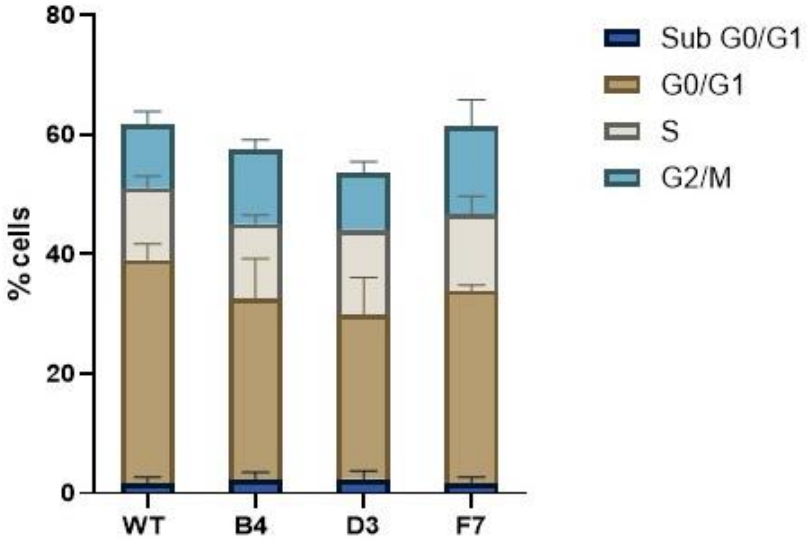

B

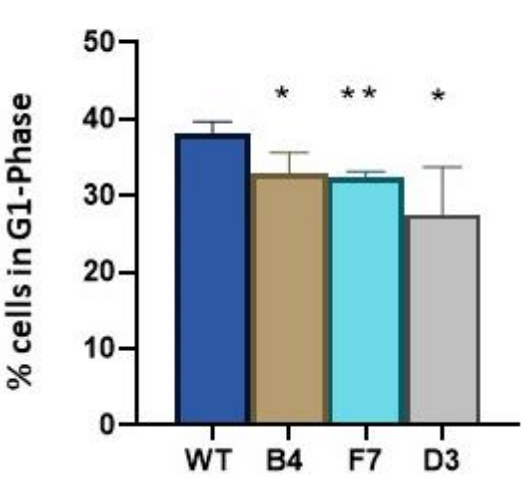

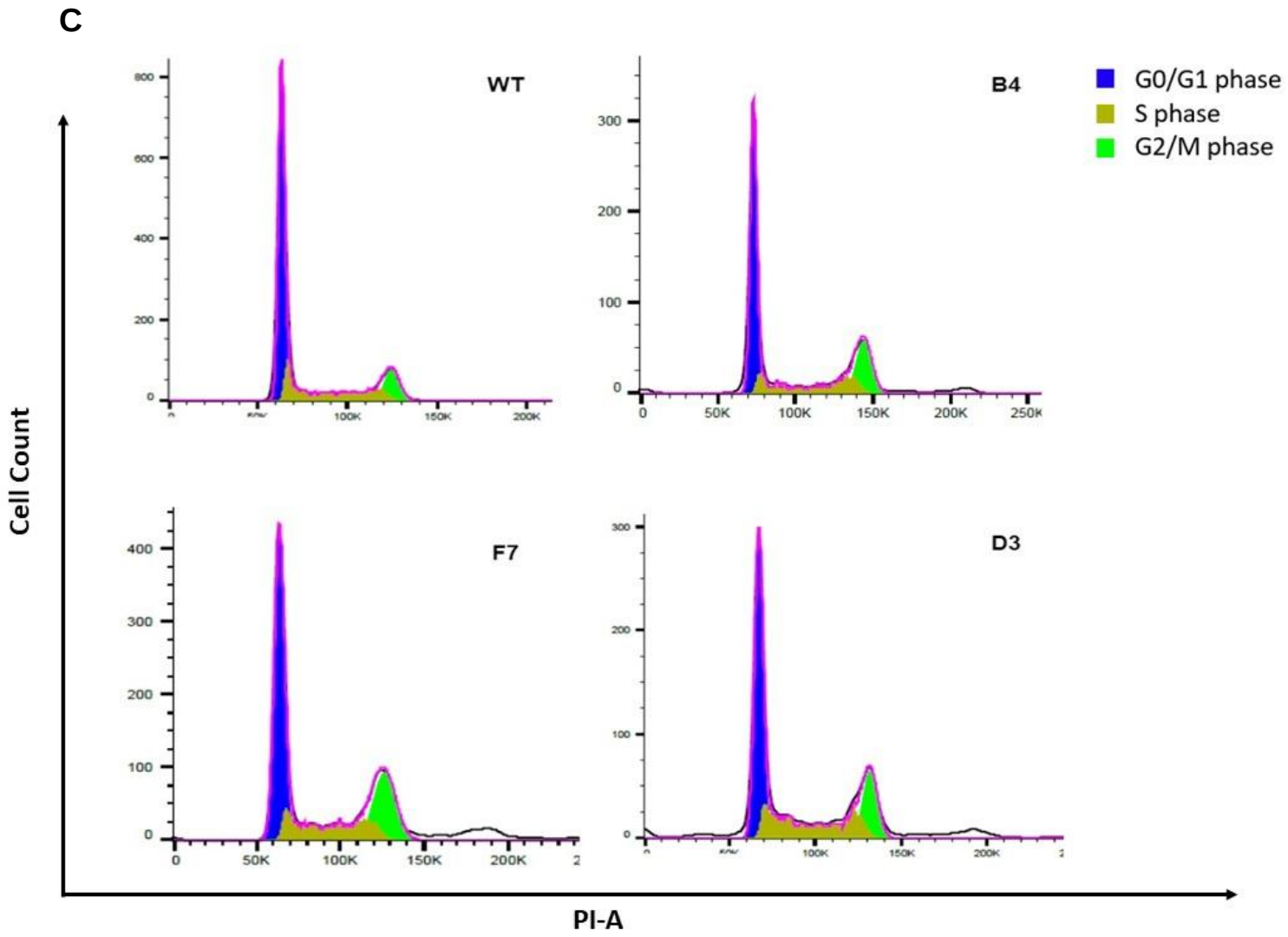

Figure 4.3: Cell cycle analysis through flow cytometry of PI-stained MCF-7 cells. **A** represents the graph quantifying the percentage of cells in each cell cycle phase (sub-G0/G1, G0/G1, S, and G2/M) in both untreated WT MCF-7 cells and the *ZFP36L1 KO* clones. **B** represents the graph quantifying the percentage of cells specifically in the G0/G1 phase of the cell cycle, demonstrating a reduced G0/G1 population in *ZFP36L1 KO* clones compared to WT MCF-7 cells. These findings represent averages from three independent experiments, with error bars indicating standard errors calculated from triplicate measurements. Statistical analyses were performed by unpaired t-test (* $p < 0.05$, ** $p < 0.00$). **C** displays representative histograms showing cell cycle distribution in the PI-stained MCF-7 cells, including WT MCF-7 cells and the *ZFP36L1 KO* clones. The blue, yellow and green area represents the cell population in the G0/G1 phase, S phase, and G2/M phase, respectively. The images were generated using FlowJo software.

4.2.3 ZFP36L1 loss does not impact cell cycle distribution in tamoxifen-treated MCF-7 cells

Cell cycle analysis was executed to examine the effect of ZFP36L1 loss on the cell cycle distribution of MCF-7 cells after tamoxifen treatment. FACS analysis was performed after the cells were treated with tamoxifen for 48 hours at 4 μM and 16 μM concentrations (Figure 4.4). FACS analysis revealed that, in comparison with untreated cells (Figure 4.3), 16 μM tamoxifen treatment resulted in an increase in the cell population in the G0/G1 and G2/M phases, along with a decrease in the S-phase of the cell cycle in all the examined cell lines (Figure 4.4 B and D), which included WT MCF-7 and three *ZFP36L1 KO* MCF-7 cell clones (B4, F7, D3). However, no significant difference was observed between WT MCF-7 cells and *ZFP36L1 KO* MCF-7 clones during any phase of the cell cycle.

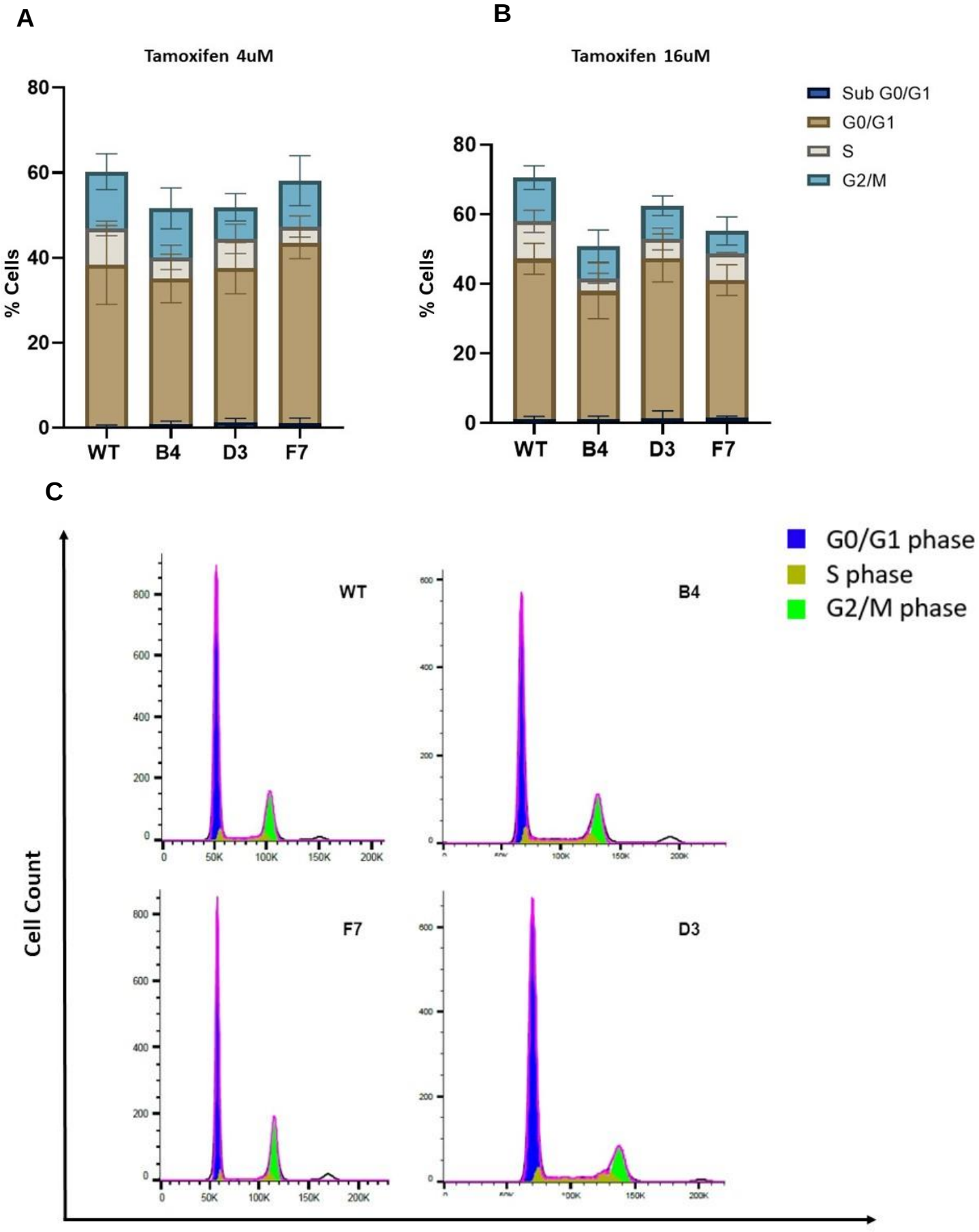
A
Tamoxifen 4uM
% Cells
80
60
40
20
0
WT
B4
D3
F7
B
Tamoxifen 16uM
% Cells
80
60
40
20
0
WT
B4
D3
F7
Sub G0/G1
G0/G1
S
G2/M
C
G0/G1 phase
S phase
G2/M phase
Cell Count
WT
B4
F7
D3
800
600
400
200
0
0
50K
100K
150K
200K

D

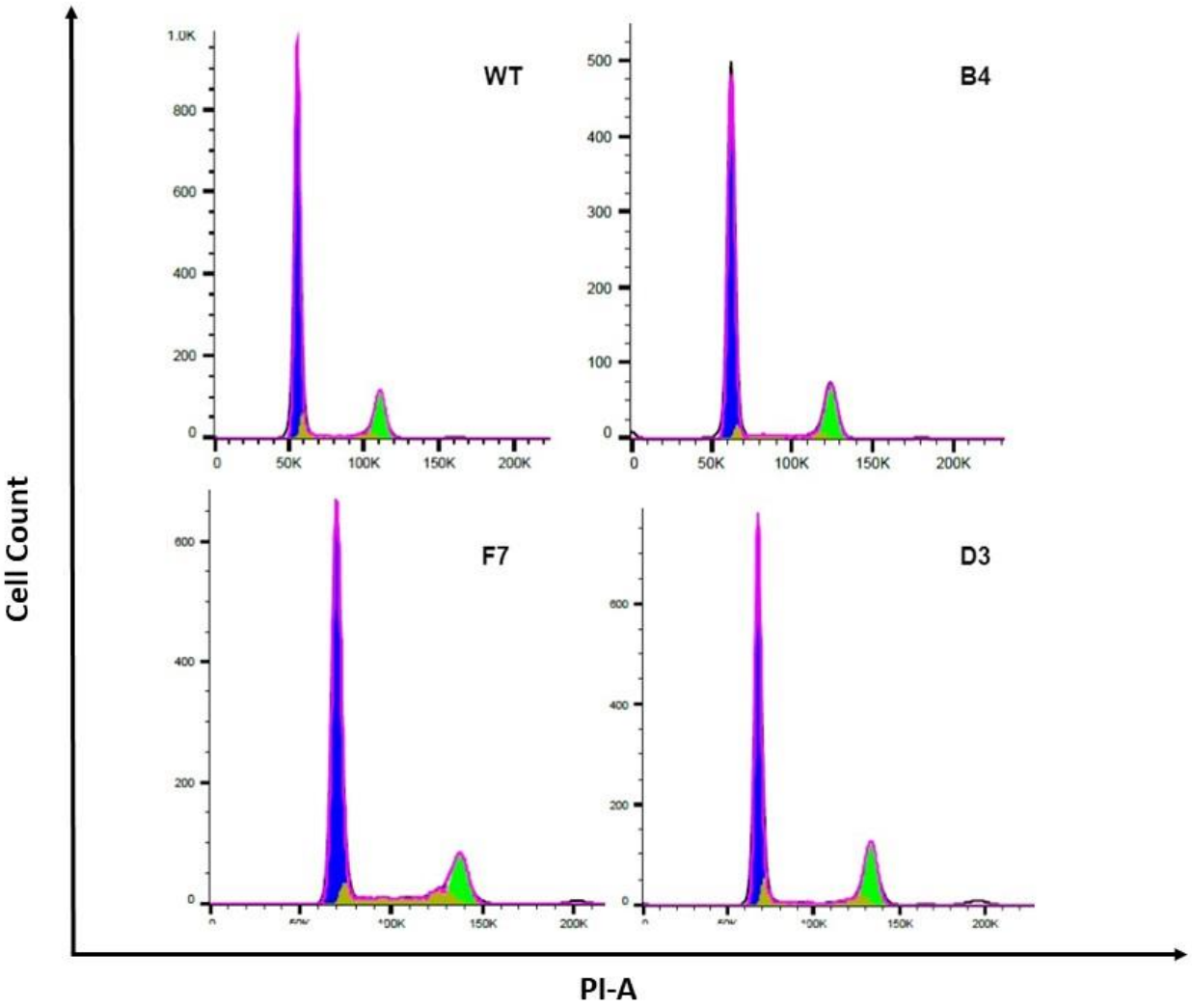

Figure 4.4: Cell cycle analysis through flow cytometry of PI-stained MCF-7 cells following tamoxifen treatment at 4 µM **(A)** and 16 µM **(B)** concentrations**. A** illustrates the graph quantifying the percentage of cells in each stage of the cell cycle (sub-G0/G1, G0/G1, S, and G2/M) following tamoxifen treatment at 4 µM. **B** illustrates the graph quantifying the percentage of cells in each stage of the cell cycle (sub-G0/G1, G0/G1, S, and G2/M) following tamoxifen treatment at 16 µM. The results presented here are the averages obtained from three separate and independent experiments. The error bars represent the standard error of the values obtained from triplicate experiments. Statistical analyses were performed by unpaired t-test. * $p < 0.05$, ** $p < 0.00$. **C** and **D** are the histograms showing the representative images of cell cycle distribution in the PI-stained MCF-7 cells after treatment with 4 µM and 16 µM, respectively. The blue, yellow and green area represents the cell population in the Go/G1 phase, S phase, and G2/M phase, respectively. The images were generated using FlowJo software.

4.2.4 Absence of ZFP36L1 reduces wound healing capability of MCF-7 cells

A wound-healing scratch assay was conducted to determine the migration capability of MCF-7 cells in the absence of ZFP36L1 expression. All the examined cell lines were scratched and incubated for 24 hours to assess the healing capability of MCF-7 cells. WT MCF-7 cells recovered the wound approximately 80%, whereas all three clones of *ZFP36L1 KO* MCF-7 cells showed significantly delayed healing compared to WT MCF-7 cells, covering only 50-60% of the wound area (Figure 4.5).

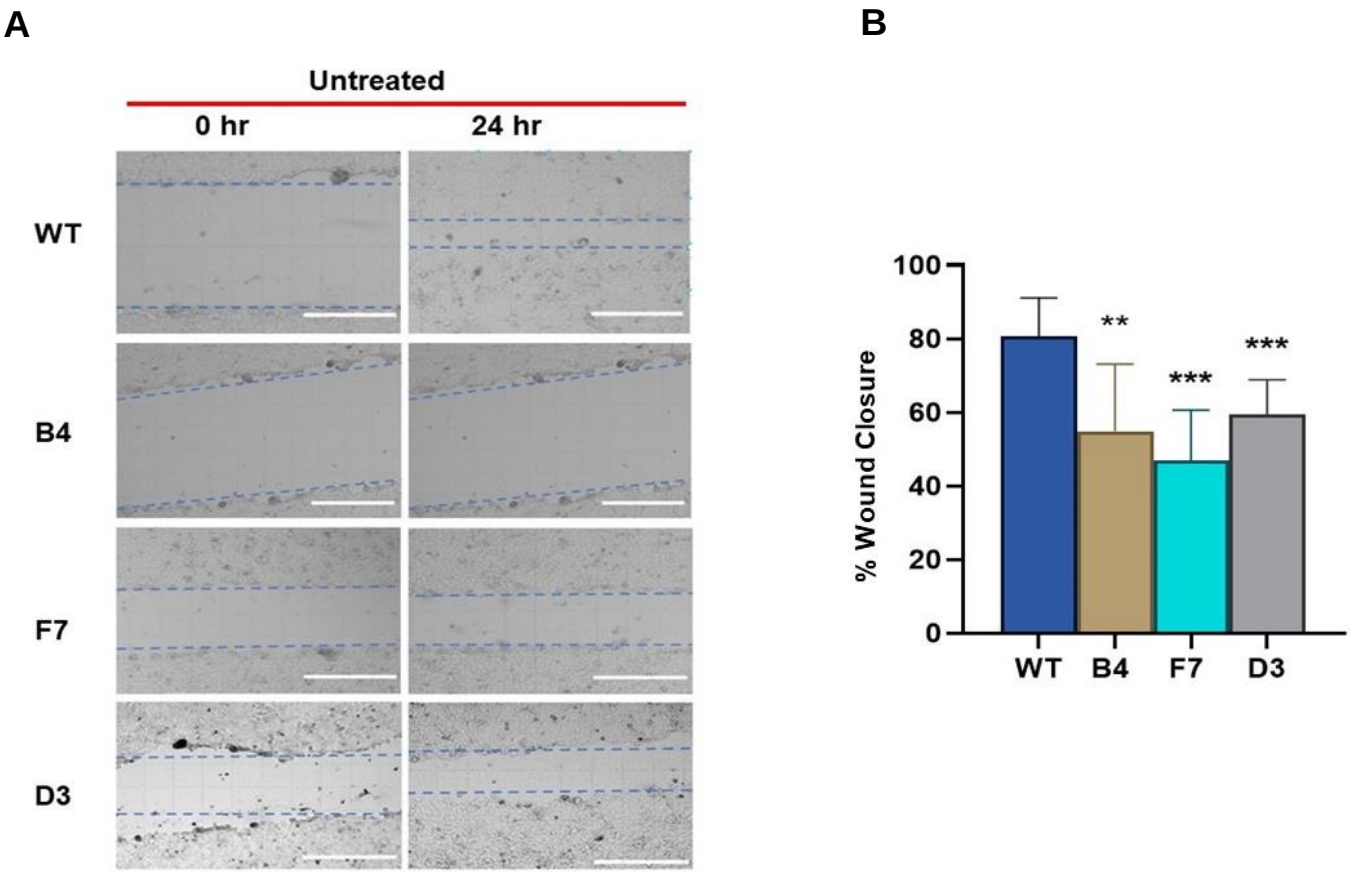

Figure 4.5: Wound-healing scratch assay. **A** shows the representative images from the wound healing assay of MCF-7 cells**. B** represents the graph quantifying the percentage of the wound healing capacity of WT MCF-7 cells and *ZFP36L1 KO* MCF-7 cells (Scale bar, 250 µm). The results represent the average of triplicate wells and represent three independent experiments. The error bars represent the standard error of the values obtained from triplicate experiments. Statistical analyses were performed by unpaired t-test. * $p < 0.05$, ** $p < 0.005$, *** $p < 0.0005$.

4.2.5 The effect of tamoxifen on the wound healing capacity reduced in ZFP36L1-depleted MCF-7 cells

Furthermore, wound healing capacity was also determined in the presence of tamoxifen at concentrations 4 μM and 16 μM for all the examined MCF-7 cell lines. Compared to untreated cells, the wound healing ability of WT MCF-7 cells was reduced by 10-15% with the increasing concentration of tamoxifen treatment. However, *ZFP36L1 KO* MCF-7 clones remained unaffected by the increasing concentration of tamoxifen, suggesting that the absence of ZFP36L1 reduces the sensitivity of MCF-7 cells to the tamoxifen cytotoxic effects (Figure 4.6).

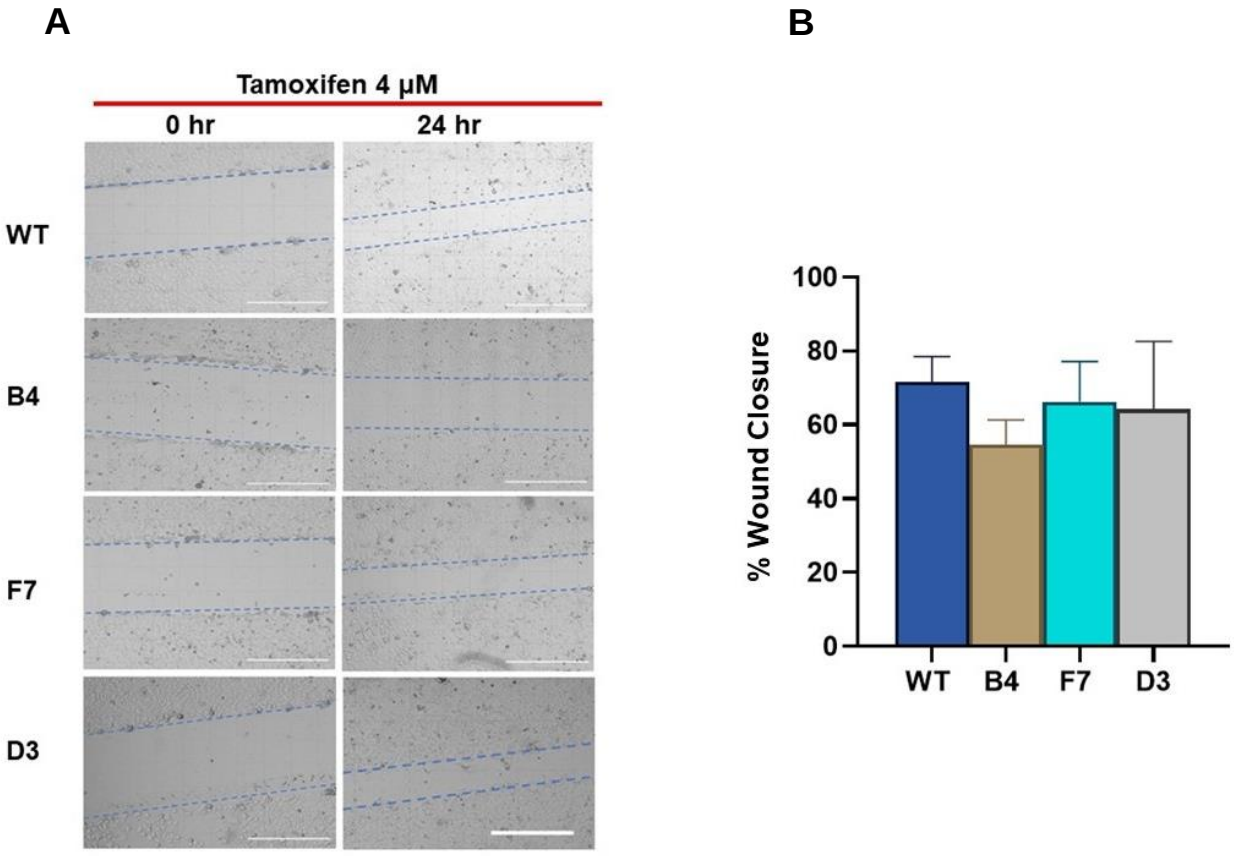

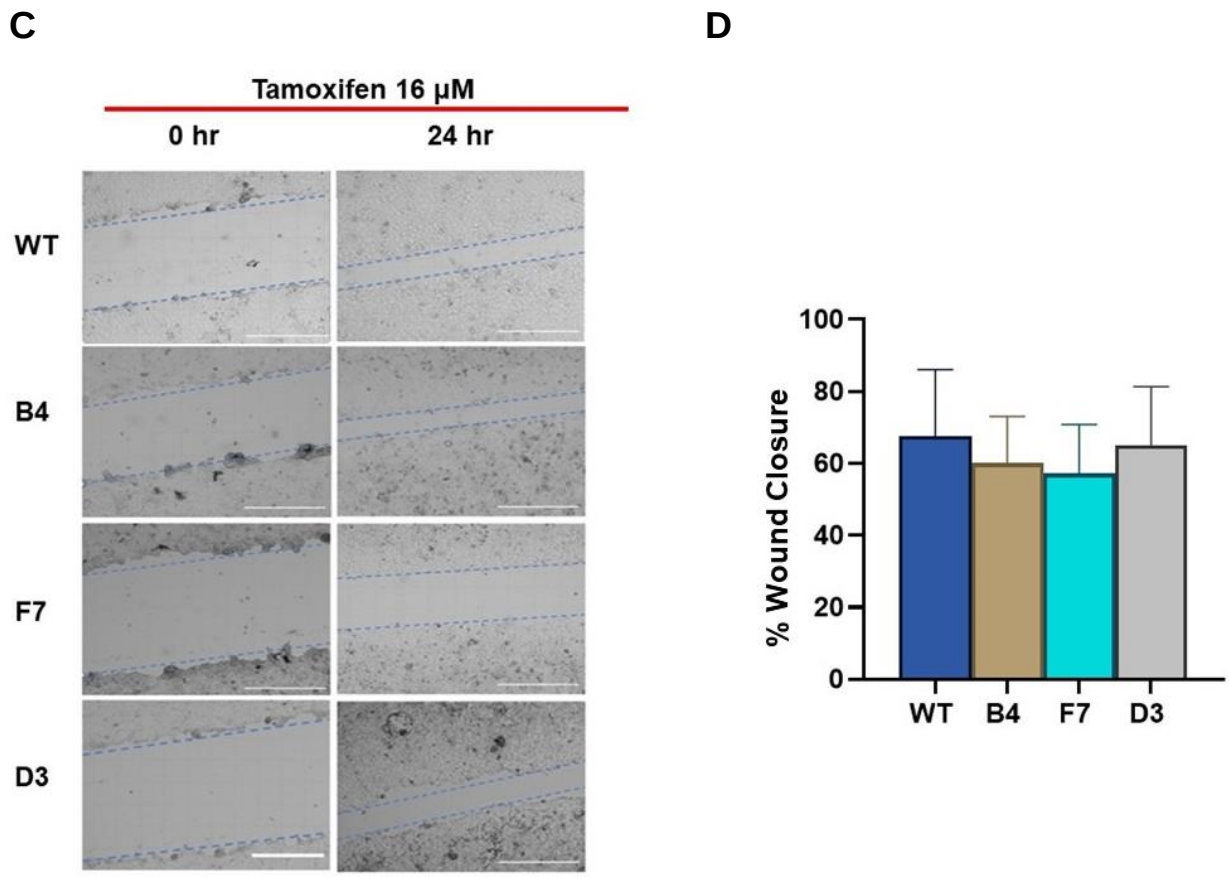

Figure 4.6: Wound-healing scratch assay following tamoxifen treatment. **A** and **C** are representative images from the wound healing assay of MCF-7 cells treated with tamoxifen at 4 µM and 16 µM concentrations, respectively**. B** and **D** are the graphs quantifying the percentage of the wound closure of WT MCF-7 cells and *ZFP36L1 KO* MCF-7 cells when treated with tamoxifen at concentrations of 4 µM and 16 µM, respectively. Scale bar, 250 µm. The results represented here are the average of triplicate wells performed at three independent times. The error bars represent the standard error of the values obtained from triplicate experiments. Statistical analyses were performed by unpaired t-test. * $p < 0.05$, ** $p < 0.005$.

4.2.6 Absence of ZFP36L1 does not alter the clonogenic potential of MCF-7 cells

Cell colony formation assay was conducted to evaluate the impact of ZFP36L1 depletion on the clonogenic capacity of MCF-7 cells. The clonogenic potential of *ZFP36L1 KO* clones was found to be equivalent to WT-MCF-7 cells, except for the D3 clone, suggesting that ZFP36L1 does not influence the clonogenic potential of MCF-7 cells (Figure 4.7 A and C). Furthermore, we conducted a cell colony assay following exposure to two different concentrations of tamoxifen: 4 µM and 16 µM. Remarkably, no colonies were detected after treatment with 16 µM tamoxifen. However, when all cell lines were exposed to 4 µM tamoxifen, we observed the formation of colonies, albeit with a consistent reduction in the numbers of colonies across all the cell lines (Figure 4.7 B and C). Similar to untreated cells, only the D3 clone significantly reduced the number of colonies compared to treated WT MCF-7 cells. Thus, no difference was observed in the clonogenic potential of tamoxifen-treated WT-MCF-7 cells and *ZFP36L1 KO* clones.

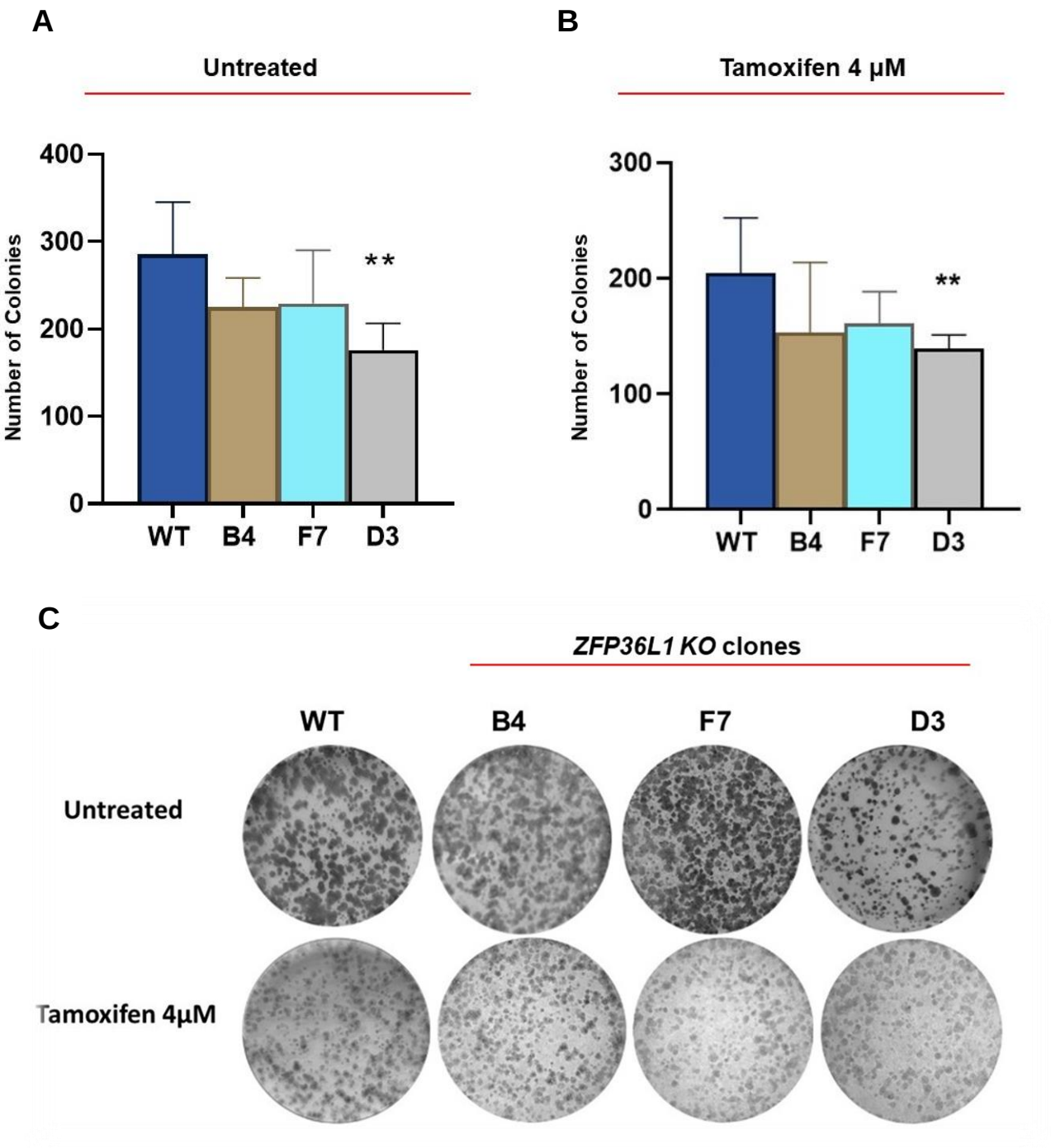

Figure 4.7: Cell colony formation assay. **A** represents the graph quantifying the number of colonies formed in WT MCF-7 cells and *ZFP36L1 KO* clones. **B** represents the graph quantifying the number of colonies formed in WT MCF-7 cells and *ZFP36L1 KO* clones after tamoxifen treatment at 4 µM concentration. **C** shows representative images of the colonies formed in all the examined cell lines in a 6-well plate. The results represent the average of triplicate wells and represent three independent experiments. The error bars represent the standard error of the values obtained from triplicate experiments. Statistical analyses were performed by unpaired t-test. * $p < 0.05$, ** $p < 0.005$.

4.2.7 Absence of ZFP36L1 does not induce apoptosis in MCF-7 cells

Flow cytometric analysis was performed to evaluate the impact of ZFP36L1 depletion on MCF-7 cell apoptosis. All the examined cell lines were subjected to flow cytometric analysis after Annexin V and PI staining (Appendix C, Figure C1). FACS analysis interpretation showed that all the cell lines, including WT MCF-7 and *ZFP36L1 KO* MCF-7 clones, showed a higher percentage of cell population as live (Annexin V-, PI−), followed by early (Annexin V+, PI−) and late (Annexin V-, PI+) apoptosis. The lowest percentage of the cell population was found in the apoptotic stage (Annexin V+, PI+). Notably, all the cell lines, including WT MCF-7 cells and *ZFP36L1 KO* MCF-7 clones, showed equivalent distributions of cells in all stages without any drug treatment (Figure 4.8 A). We also examined the apoptosis induced in the cell lines when treated with tamoxifen at 4 μM and 16 μM concentrations. In conclusion, the increase observed in the early and late apoptotic cell population in *ZFP36L1 KO* clones after tamoxifen treatment was insignificant (Figures 4.8 B and C).

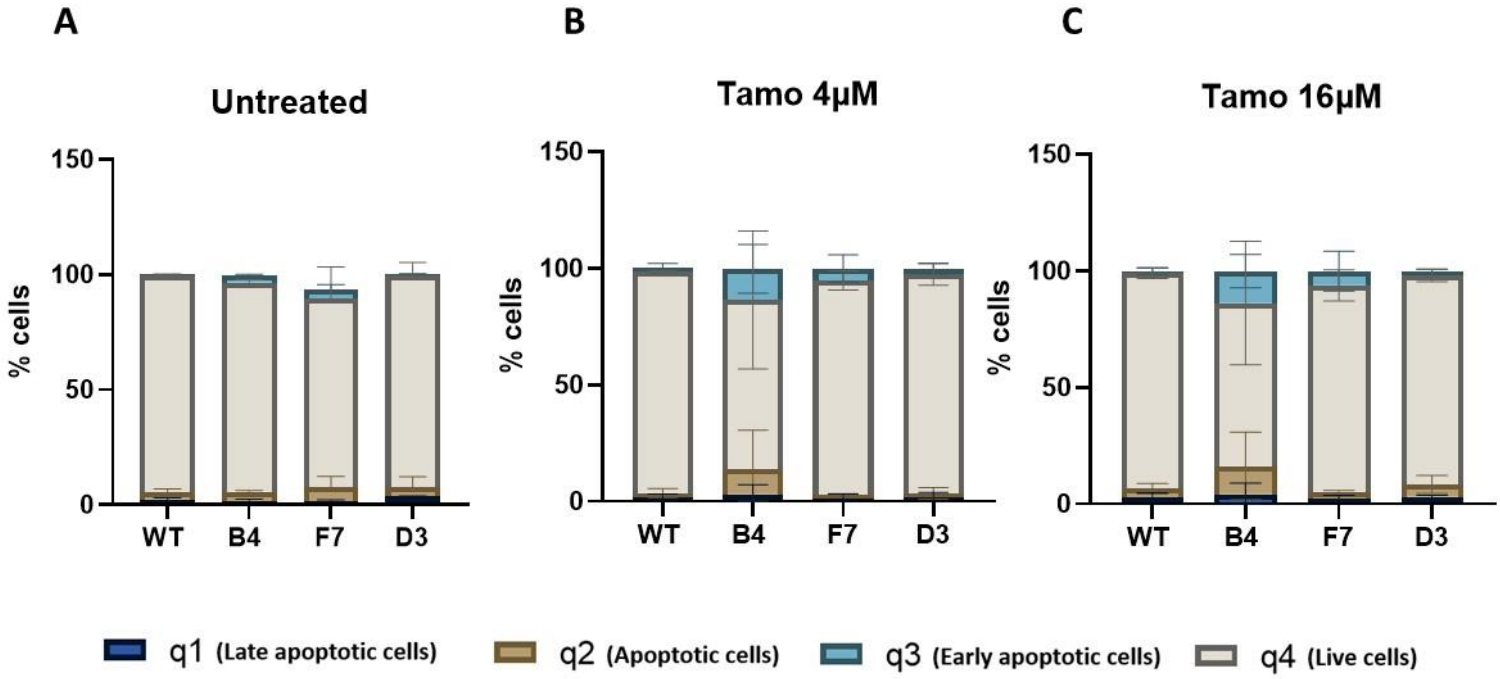

Figure 4.8: Apoptosis assay evaluated by FACS analysis after Annexin V and PI staining. **A, B** and **C** represent the graphs quantifying the percentage of apoptotic cells in the WT MCF-7 cells and *ZFP36L1 KO* clones when untreated, 4 μM tamoxifen treatment, and 16 μM tamoxifen treatment, respectively. Q1 represents late apoptotic cells, q2 represents the apoptotic cells, q3 represents the early apoptotic cells, and q4 represents the live cells. The results represent the average of three independent experiments. The error bars represent the standard error of the values obtained from triplicate experiments. Statistical analyses were performed by unpaired t-test. * $p < 0.05$, ** $p < 0.005$, *** $p < 0.0005$.

4.2.8 ZFP36L1 absence reduces tamoxifen's effect on cyclin D expression in MCF-7 cells

Consistent with the findings of Suk et al., 2018, we found that the suppression of ZFP36L1 expression in MCF-7 cells increased the cyclin D expression. However, after exposure to tamoxifen at concentrations of 4 μM and 16 μM for 48 hours, all the MCF-7 cell lines showed a reduction in the cyclin D expression compared to untreated cells. These findings suggest that tamoxifen is effectively exerting an anti-estrogenic effect on MCF-7 treated cells. However, tamoxifen treatment at 16 μM showed an increase

in the cyclin D expression in *ZFP36L1 KO* clones (F7 and D3) compared to WT MCF-7 cells, indicating that the absence of ZFP36L1 could decrease the anti-estrogenic effect of tamoxifen in MCF-7 cells.

Furthermore, we found an increase in the protein expression of a tumour suppressor gene, *TP53*, in the *ZFP36L1* KO clones (B4 and F7), as compared to WT MCF-7 cells, suggesting that ZFP36L1 is involved in regulating the expression of *TP53* gene in MCF-7 cells. Exposure to tamoxifen at 4 µM decreased TP53 protein expression in all the cell lines, and 16 µM tamoxifen exposure showed an increase in the TP53 protein expression. However, the results across all the cell lines were inconsistent, and no definitive conclusions could be drawn from these results (Figure 4.9).

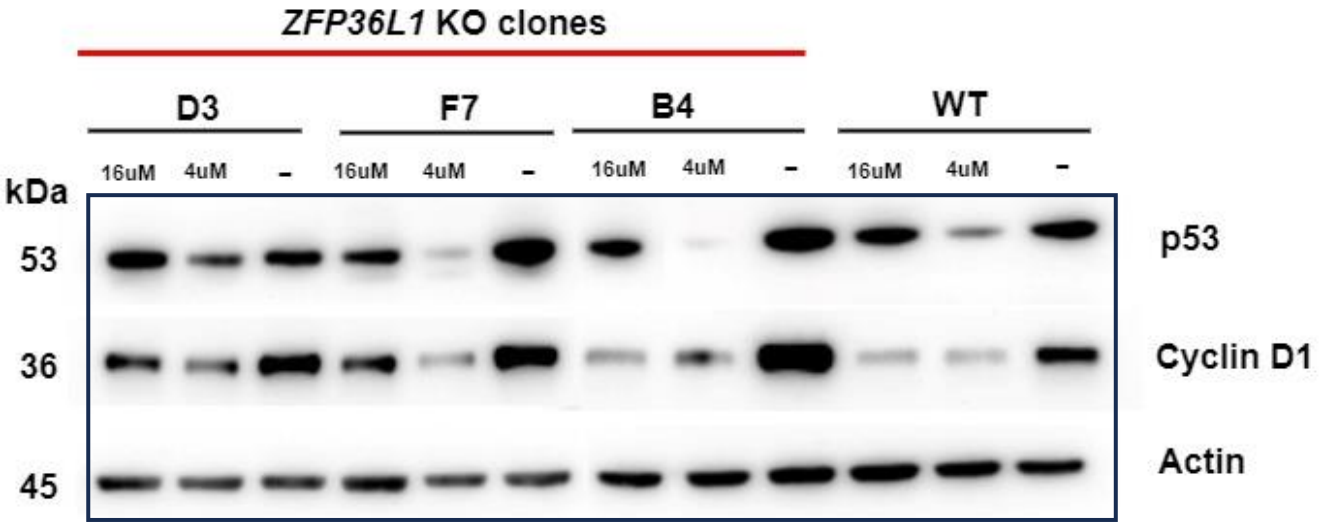

Figure 4.9: The western blot analysis of targets of ZFP36L1. The western blot image illustrates the protein expression levels of TP53 and cyclin D1 in WT MCF-7 cells and *ZFP36L1 KO* clones under two conditions: untreated (-) and following 48 hours of tamoxifen treatment at concentrations of 4 µM and 16 µM. In untreated cells, *ZFP36L1 KO* clones demonstrated increased TP53 and cyclin D1 protein expression levels compared to WT MCF-7 cells. Under 16 µM tamoxifen treatment, *ZFP36L1 KO* clones displayed increased cyclin D1 expression relative to WT MCF-7 cells, illustrating a reduction in the tamoxifen impact associated with the loss of ZFP36L1 in MCF-7 cells. β-Actin was used as a loading control.

4.3 Discussion

In this chapter, we explored the ZFP36L1 gene functions in breast tumour progression and found that ZFP36L1 displays a multifaceted role in the MCF-7 cell line. Here, we have extensively studied the impact of ZFP36L1 loss on various oncogenic traits which promote tumour development in MCF-7 cells. Using the ZFP36L1 knockout cell models (B4, F7 and D3), we carried out several *in-vitro* functional assays, such as the MTT assay, wound healing scratch assay, apoptotic assay, and cell colony formation assay to examine how the absence of ZFP36L1 affects the known hallmarks of cancer (Hanahan and Weinberg, 2011). Furthermore, by employing these functional assays, we demonstrated that depletion of ZFP36L1 in MCF-7 cells decreased the sensitivity of MCF-7 cells towards tamoxifen, a standard drug used in endocrine therapy.

Previous studies have reported that ZFP36L1 serves as a negative post-transcriptional regulator of several cell-cycle-associated genes and controls cell-cycle progression (Galloway et al., 2016; Vogel et al., 2016; Loh et al., 2020). In this study, cell cycle analysis showed that the loss of ZFP36L1 resulted in a significant decrease in the G1-phase cell population in MCF-7 cells. In support of this, western blot analysis showed increased protein expression levels of Cyclin D1, and RNA-sequencing results showed upregulated *CDK6* mRNA levels in *ZFP36L1 KO* MCF-7 clones. *CyclinD1* and *CDK6* regulate the G1 to S phase progression in the cell cycle, and both exhibit ARE sequences in the 3'UTR of their mRNA. Together, these results suggested that ZFP36L1 directly mediate the mRNA levels of the cell-cycle-associated genes that control the cell cycle transition from G1 to S phase in MCF-7 cells. Additionally, we found that loss of ZFP36L1 increased the tumour suppressor gene *TP53* gene expression in MCF-7 cells. These results contrast with the findings of Suk et al. 2018, which illustrated that the ZFP36L1 overexpression enhanced the *TP53* expression in

colorectal cancer cell lines. Although the *TP53* gene does not have an ARE sequence in its 3'UTR region, it can be inferred that ZFP36L1 indirectly controls the *TP53* gene expression, depending on the cellular context. Despite the upregulation of the *TP53* gene in *ZFP36L1* KO MCF-7 clones, no changes were observed in the proliferation, clonogenicity and apoptosis in MCF-7 cells. Within this study, it remains unclear why the upregulation of *TP53* or *CyclinD1* in the absence of ZFP36L1 does not affect the proliferation rate of MCF-7 cells. It is possible that the upregulation of *TP53* led to an increase in the *p21* levels, which further blocked the CDK4/6 activity (Sobhani et al., 2019). Other key cell cycle-related proteins that contain ARE sequences, such as CDK2, cyclin D3, p21, and E2F1, have also been identified as the targets of ZFP36L1 in bladder cancer (Loh et al., 2020; Kaehler et al., 2021). Further investigation into the expression levels of these proteins in ZFP36L1-deficient MCF-7 cells could lead to a better understanding of ZFP36L1 involvement in MCF-7 cell cycle progression. Overall, the lack of ZFP36L1 does not affect the growth rate, clonogenicity, or apoptosis in MCF-7 cells.

Conversely, wound healing scratch assay indicated that the loss of ZFP36L1 induced a significant reduction in the healing capability of MCF-7 cells. These results contradict the Rataj et al., 2019 study, where they showed that the forced expression of *ZP36L1* derivative in breast cancer cell lines reduced migration and expression of EMT markers. These results suggested that ZFP36L1 might have a cell migration-promoting effect in MCF-7 cells. Although, in this study, we observed that loss of ZFP36L1 in MCF-7 cells is associated with tumour-suppressing properties, reduced migration in ZFP36L1 depleted cells have also demonstrated the tumour-promoting effect of this gene, suggesting the opposing roles of ZFP36L1 in regulating tumorigenesis in MCF-7 cells. Congruently, a study conducted by Yuan et al., 2022

also demonstrated the conflicting roles of ZFP36L1 in regulating the progression of muscle-invasive breast cancer, where high expression of ZFP36L1 promoted the invasiveness and suppressed the self-renewal of bladder cancer cells. Thus, ZFP36L1 can exhibit opposing and context-dependent roles in regulating tumour progression. In conclusion, ZFP36L1 might have a critical function in controlling the mRNA levels of migration and invasion-related genes in breast cancer. Later, in Chapter 6, we further discussed the potential targets of the ZFP36L1 gene involved in migration and invasion in MCF-7 cells.

Approximately 40% of oestrogen-positive breast cancer cases treated with tamoxifen do not respond or exhibit only a partial response to adjuvant endocrine therapy. Moreover, the recurrence of the disease 20 years after the commencement of adjuvant endocrine therapy following primary surgery is relatively common (Richman and Dowsett, 2018). Here, we provided several experimental findings which suggest that ZFP36L1 depletion decreased the sensitivity of MCF-7 cells toward the tamoxifen drug. The dose-response curve showed that loss of ZFP36L1 reduced the sensitivity of MCF-7 cells towards tamoxifen drug, as we observed that *ZFP36L1 KO* MCF-7 clones have higher IC50 values than WT MCF-7 cells. The wound healing scratch assay illustrated another compelling piece of evidence. We noticed that *ZFP36L1 KO* MCF-7 clones are ineffective to the increasing concentration of tamoxifen treatment, whereas WT-MCF-7 cells showed a 10-20% reduction in wound healing capability when exposed to higher levels of tamoxifen. Consistent with these findings, western blot analysis showed that the 16 μM tamoxifen exposure resulted in a rise in cyclin D1 protein expression levels in the *ZFP36L1 KO* clones compared to the WT MCF-7 cells, reducing the anti-estrogenic impact of tamoxifen in MCF-7 cells. These findings indicated that the ZFP36L1 depletion could potentially reduce the sensitivity of MCF-

7 cells towards endocrine therapy. To further substantiate these observations and translate them into clinical practice, an in-depth exploration of ZFP36L1's role in tamoxifen-resistant MCF-7 cells could be considered in future research. Immunohistochemistry (IHC) staining performed by Loh and colleagues showed that ZFP36L1 expression was consistently reduced in breast invasive ductal carcinoma and associated with worse survival in patients with breast cancer (Loh et al., 2020). Furthermore, conducting a comprehensive analysis of the correlation between ZFP36L1 expression levels and crucial clinical outcomes, such as disease-free survival, overall survival, and distant metastases survival, in the cohort of tamoxifen-resistant ER+ breast cancer patients can provide invaluable insights into the clinical advantages and intricacies of ZFP36L1 involvement with tamoxifen therapy. In conclusion, the potential synergy between ZFP36L1 and tamoxifen therapy offers an exciting avenue for future research and clinical application in ER/PR+ breast cancer treatment.

Chapter 5: Evaluating the Impact of ZFP36L1 Depletion on the Responsiveness of MCF-7 Cells to Palbociclib

5.1 Introduction

Endocrine therapy (ET) is the preferred treatment option for most women with metastatic hormone-positive and HER2-negative (ER/PR+, HER2-) breast cancer patients. In the past decade, new targeted therapies, mainly cyclin-dependent kinase 4/6 inhibitors (palbociclib) and mammalian target of rapamycin (mTOR) inhibitors (everolimus), have been introduced in combination with ET. The complementary effects of these drugs have proven beneficial in overcoming the primary or acquired resistance and significantly improved progression-free survival and overall survival in metastatic breast cancer patients (Goetz et al., 2017; Hortobagyi et al., 2016). In the last chapter, experimental data showed that the loss of ZFP36L1 decreased the sensitivity of MCF-7 cells toward the tamoxifen drug. To the best of our knowledge, for the first time, we identified a new synergistic role of the ZFP36L1 gene in combination with the tamoxifen drug for treating ER/PR+, HER2- breast cancer patients. Continuing from the previous chapter, we conducted experiments to investigate whether the loss of the ZFP36L1 gene impacts the effectiveness of the palbociclib drug in the MCF-7 cell line. All the cytotoxic assays were performed on WT MCF-7 cells and *ZFP36L1 KO* clones after 48-hour treatment with palbociclib, including MTT assay, wound-healing scratch assay, cell cycle analysis and clonogenic assay to assess the impact on ZFP36L1 depletion on MCF-7 cells in the presence of palbociclib drug.

5.2 Results

5.2.1 ZFP36L1 loss decreased the sensitivity of MCF-7 cells to palbociclib

To examine the growth inhibitory effects of the palbociclib drug on MCF-7 cells, cell viability was measured using an MTT assay at different drug concentrations, ranging from 500 µM-1 µM, after 48 hours of drug treatment (Appendix C, Table C2). The IC_{50}

values were determined from the dose-response inhibition curve for the WT MCF-7 cells and all three clones of *ZFP36L1 KO* cells, as shown in Table 5.1 and Figure 5.1. The calculated IC_{50} values for palbociclib drug for three *ZFP36L1 KO* clones do not differ much from the IC_{50} values of WT MCF-7 cells. These results suggested that the loss of ZFP36L1 does not alter the sensitivity of MCF-7 cells to the palbociclib drug.

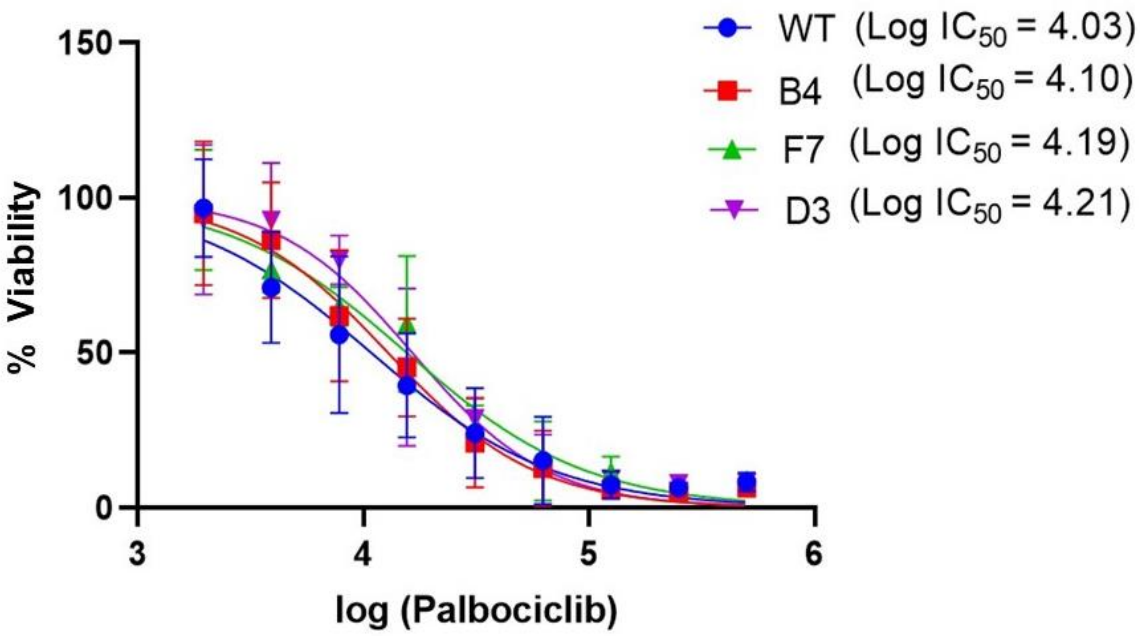

Figure 5.1: The dose-response inhibition curves for the WT MCF-7 cells and *ZFP36L1 KO* cells (B4, F7 and D3) following a 48-hour treatment with palbociclib. The x-axis represents the concentration of palbociclib in log form, and the y-axis represents the percentage viability of cells. Results represented here are the average of triplicate wells and represent the findings from three separate and independent experiments. The error bars represent the standard error of the values obtained from triplicate experiments. Statistical analyses were performed by paired t-test. * $p < 0.05$.

Table 5.1 IC_{50} values for palbociclib in WT and ZFP36L1 depleted MCF-7 cells.

Cell lines	Log IC50	IC_{50} value (μM)
WT	4.03	10.8
B4	4.10	12.8
F7	4.19	15.4
D3	4.21	16.4

5.2.2 Loss of ZFP36L1 does not interfere with cell cycle distribution in palbociclib-treated MCF-7 cells

To assess the effect of palbociclib treatment on the cell cycle distribution of MCF-7 cells, FACS analysis was conducted after 48 hours of palbociclib treatment. The cells were stained with propidium iodide (PI) and analysed using flow cytometry (Figure 5.2, C). After palbociclib treatment, all the cell lines showed an overall increase in the percentage of cell population in the sub-G0/G1 and G0/G1 phases compared to untreated cells. Concomitantly, there was a decrease in the S-phase cell population compared to untreated cell lines. However, in all the cell cycle phases, no significant difference was detected between the palbociclib-treated WT MCF-7 cells and *ZFP36L1 KO* MCF-7 clones (Figure 5.2, A and B).

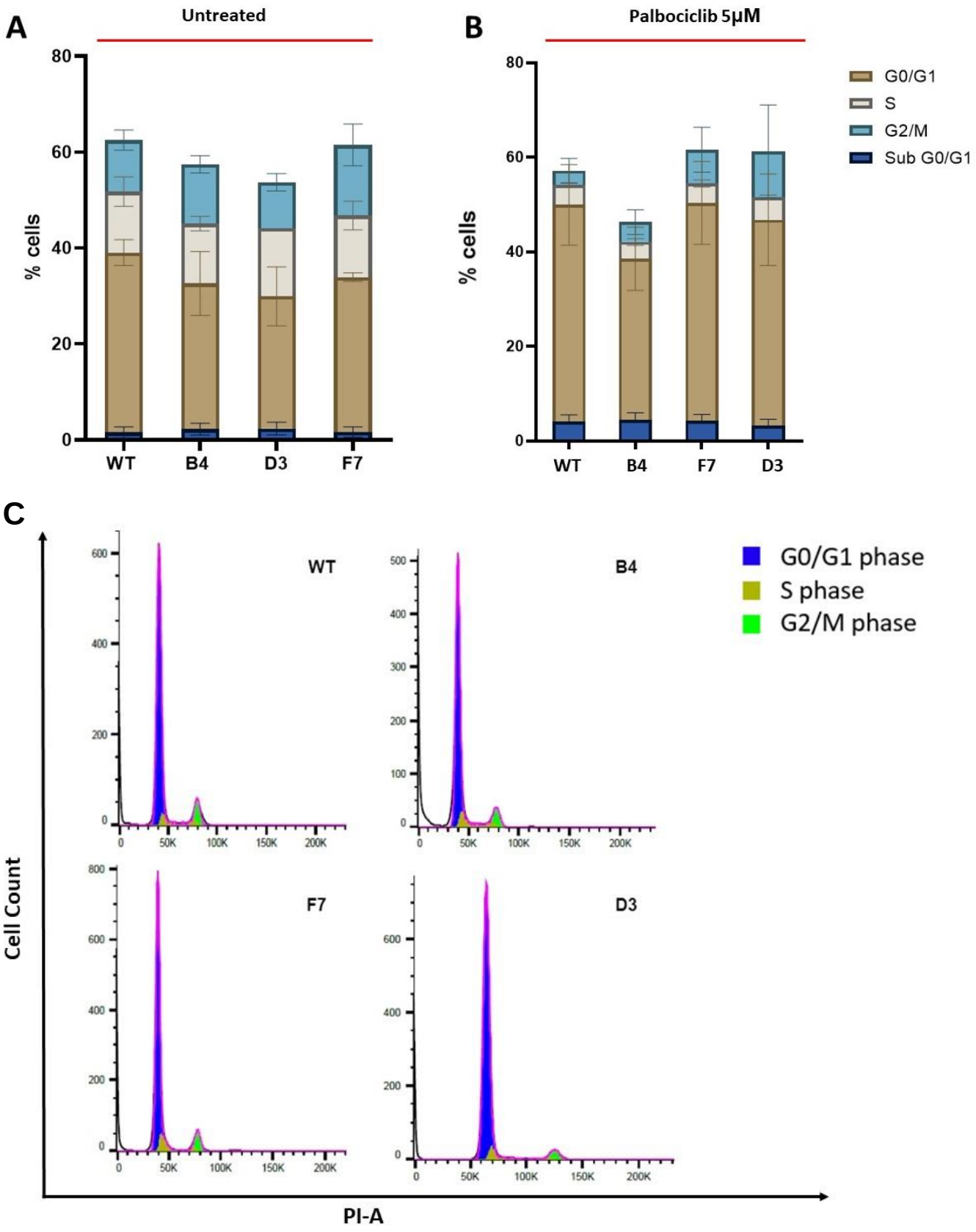

Figure 5.2: Cell cycle analysis through flow cytometry of PI-stained MCF-7 cells under two conditions: **(A)** untreated and **(B)** when treated with palbociclib at 5 µM concentration. **A** and **B** represent the graphs quantifying the percentage of cells in the sub-G0/G1, G0/G1 phase, S

phase, and G2/M phase of the cell cycle in WT MCF-7 cells and the *ZFP36L1* KO clones. The results presented here are the averages obtained from three separate and independent experiments. The error bars represent the standard error of the values obtained from triplicate experiments. Statistical analyses were performed by unpaired t-test. * $p < 0.05$, ** $p < 0.00$. **C** represents the histograms showing the representative images of cell cycle distribution in the PI-stained MCF-7 cells after treatment with 5 μM palbociclib. The blue, yellow and green area represents the cell population in the G0/G1 phase, S phase, and G2/M phase, respectively. The images were generated using FlowJo software.

5.2.3 ZFP36L1 absence does not interfere with palbociclib effect on MCF-7 cell's wound healing capacity

The wound healing capability was determined after treatment with palbociclib at 5 μM and 10 μM concentrations for all the MCF-7 cell lines. The results showed that as the dosage of palbociclib treatment increased, the wound healing capability of all examined cell lines decreased by 10% to 15%. Notably, this reduction was uniform for both WT MCF-7 and *ZFP36L1 KO* MCF-7 clones, indicating that ZFP36L1 depletion does not influence the impact of palbociclib on wound healing capability of MCF-7 cells (Figures 5.3 A, B, C and D).

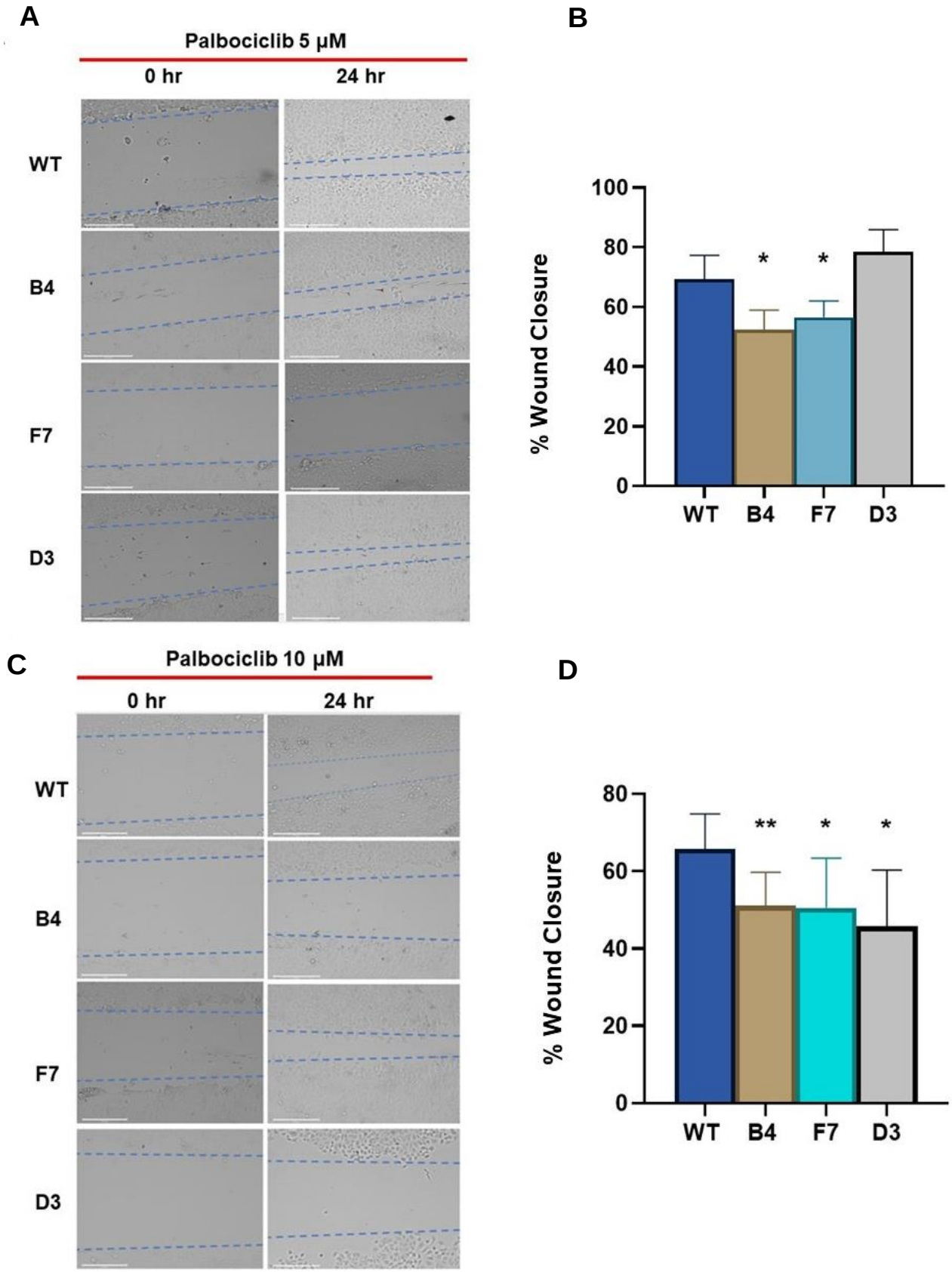

Figure 5.3: Wound healing scratch assay. **A** and **C** are representative images from the wound healing assay of MCF-7 cells treated with palbociclib at 5 µM and 10 µM concentrations,

respectively**. B** and **D** are the graphs quantifying the percentage of wound closure in WT MCF-7 cells and *ZFP36L1 KO* MCF-7 cells when treated with palbociclib at concentrations 5 μM and 10 μM, respectively. Scale bar, 250 μm. The results represented here are the average of triplicate wells performed at three independent times. The error bars represent the standard error of the values obtained from triplicate experiments. Statistical analyses were performed by unpaired t-test. * $p < 0.05$, ** $p < 0.005$.

5.2.4 ZFP36L1 depletion does not alter the palbociclib effect on the clonogenic potential of MCF-7 cells

Cell colony formation assay was conducted to evaluate the impact of ZFP36L1 depletion on the clonogenic capacity of MCF-7 cells in the presence of the palbociclib drug. The cell colony assay was performed after exposure to palbociclib at a concentration of 5 μM (Figure 5.4 C). Compared to untreated colonies (Figure 5.4 A), exposure to the palbociclib drug reduced the number and size of the colonies in all the examined cell lines (Figure 5.4 B). However, the number of colonies in treated *ZFP36L1 KO* clones was found to be equivalent to treated WT-MCF-7 cells, suggesting that ZFP36L1 does not influence the clonogenic potential of MCF-7 cells in the presence of the palbociclib drug.

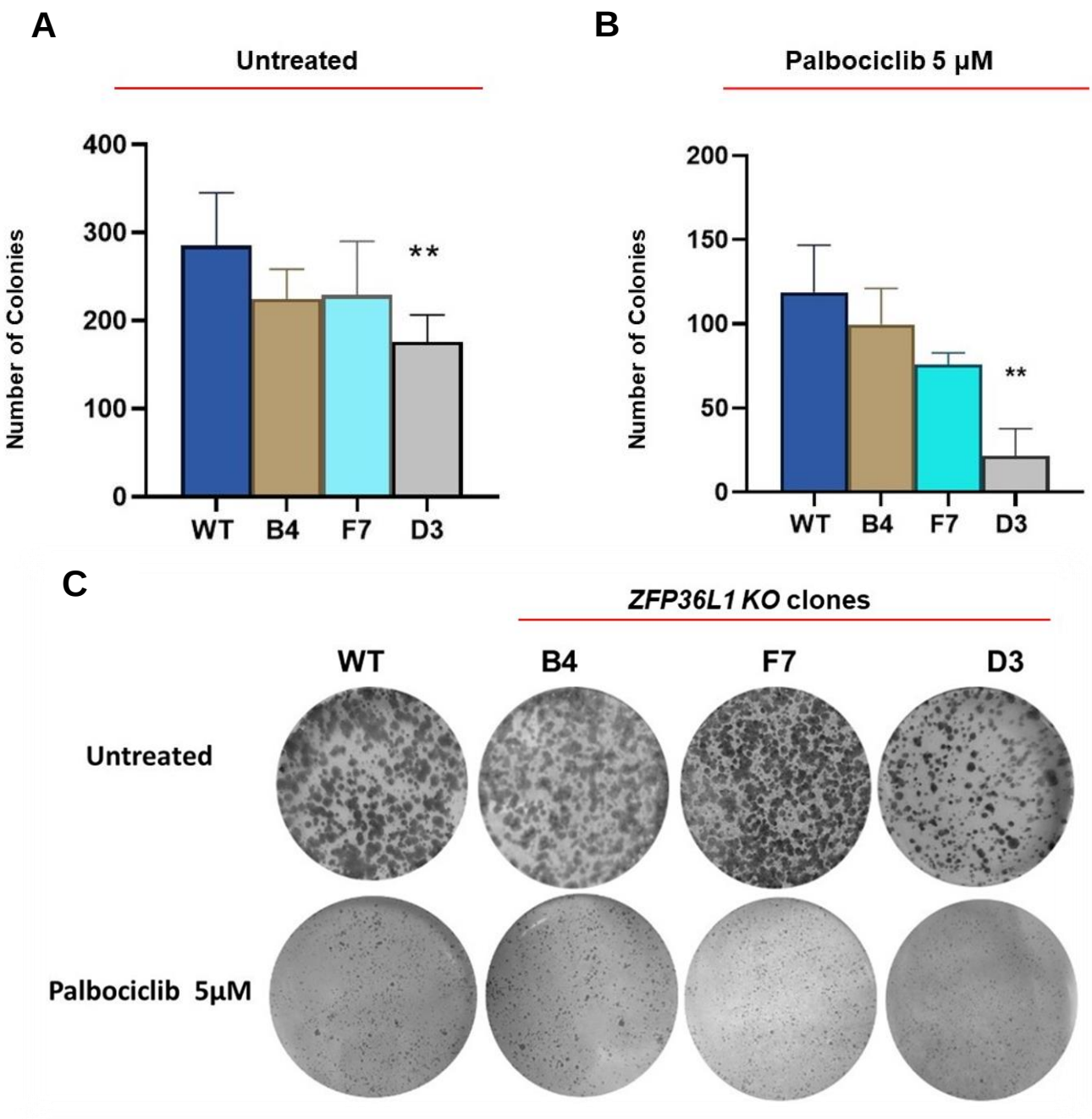

Figure 5.4: Cell colony formation analysis. **A** represents the graph quantifying the number of colonies formed in WT MCF-7 cells and *ZFP36L1 KO* clones. **B** represents the graph quantifying the number of colonies formed in WT MCF-7 cells and *ZFP36L1 KO* clones after palbociclib treatment at 5 µM concentration. **C** shows representative images of the colonies formed in all the examined MCF-7 cell lines in a 6-well plate. The results represent the average of triplicate wells and represent three independent experiments. The error bars represent the standard error of the values obtained from triplicate experiments. Statistical analyses were performed by unpaired t-test. * $p < 0.05$, ** $p < 0.005$.

5.2.5 ZFP36L1 absence enhances the palbociclib effect on cyclin D expression in MCF-7 cells

Consistent with the previous results discussed in the last chapter (section 4.2.8), western blot analysis indicated elevated cyclin D1 and TP53 protein levels in *ZFP36L1 KO* clones compared to WT MCF-7 cells (Figure 5.5). Moreover, a 48-hour exposure to palbociclib treatment (5 μM) does not affect the cyclin D1 and TP53 expression in any of the examined cell lines, including WT and *ZFP36L1 KO* clones. These findings suggested that the absence of ZFP36L1 does not interfere with the impact of the palbociclib drug on MCF-7 cells.

MCM-7, a key subunit of heteromeric MCM helicase, has a significant role in tumour formation and progression and is considered a biomarker in various human malignancies (Toyokawa et al., 2011; Ren et al., 2006). By western blot analysis, we found that the MCM-7 protein levels are increased in the *ZFP36L1 KO* clones compared to WT MCF-7 cells. In addition, when treated with palbociclib, MCM-7 protein expression levels did not differ and were similar in all the examined cell lines. These results suggested that ZFP36L1 might be involved in DNA replication initiation and maintenance in MCF-7 cells (Figure 5.5).

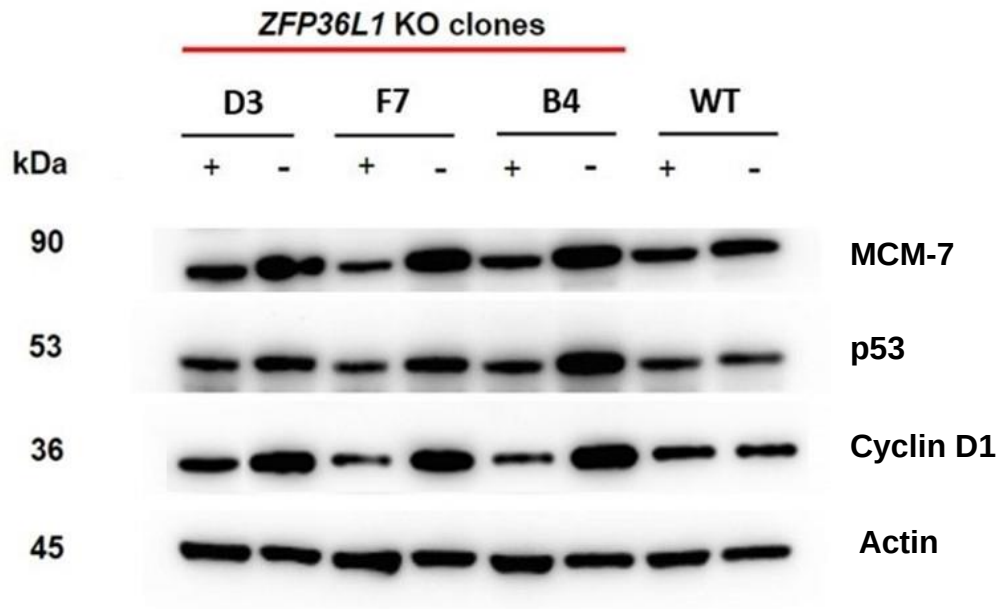

Figure 5.5: The western blot analysis of targets of ZFP36L1. The western blot image demonstrates the protein expression levels of MCM-7, p53 and Cyclin D1 in WT MCF-7 cells and *ZFP36L1 KO* clones under two conditions: untreated (-) and following 48 hours of palbociclib treatment at 5 μM concentration (+). In untreated cells, *ZFP36L1 KO* clones demonstrated increased expression levels of p53, cyclin D1 and MCM-7 protein as compared to WT MCF-7 cells. Under 5 μM palbociclib treatment, the protein levels of MCM-7, p53 and Cyclin D1 are comparable between *ZFP36L1 KO* clones and WT MCF-7 cells. β-Actin was used as a loading control.

5.3 Discussion

The clinical application of CDK4/6 inhibitors, such as palbociclib, has significantly benefitted ER/PR-positive metastatic breast cancer patients. Nevertheless, it is important to acknowledge that CDK4/6 inhibitors, while capable of substantially delaying disease progression, do not entirely prevent the emergence of primary or acquired resistance to endocrine therapy, which remains a persistent challenge in the field (Huang et al., 2022).

Building upon the findings from the previous chapter, we explored the therapeutic potential of ZFP36L1 in combination with palbociclib in MCF-7 cells. We conducted several *in-vitro* functional assays, such as the MTT assay, wound healing scratch assay, and cell colony formation assay, to determine whether the impact of palbociclib in MCF-7 cells differs due to ZFP36L1 depletion.

In the last chapter, the wound healing scratch assay revealed that MCF-7 cells lacking ZFP36L1 exhibited a significantly diminished capability for cell migration compared to wild-type (WT) MCF-7 cells. This trend persisted when we subjected *ZFP36L1 KO* MCF-7 clones to palbociclib treatment at a concentration of 10 μM. However, palbociclib treatment led to a uniform reduction of 10-15% across all cell lines compared to untreated cells, suggesting that ZFP36L1 depletion does not impact palbociclib's ability to inhibit cell migration in MCF-7 cells. Similar to these results, other cytotoxic assays, including dose-response curve, proliferation, and colony formation, also revealed that the effects of palbociclib were indistinguishable between WT-MCF-7 and *ZFP36L1 KO* MCF-7 clones. These findings suggested that ZFP36L1 absence does not influence the palbociclib effects in MCF-7 cells.

Consistent with the previous chapter, our findings indicated that the loss of ZFP36L1 increases cyclin D1 and the TP53 protein expression levels in untreated MCF-7 cells. Furthermore, we have observed an upregulation in the expression of mini-chromosome maintenance complex (MCM-7) protein, a crucial subunit of the heteromeric MCM helicase, upon depletion of ZFP36L1. Notably, while the *MCM-7* gene lacks ARE sequences in its mRNA, this phenomenon may be attributed to a positive correlation between *cyclin D1* and *MCM-7* expression (Qu et al., 2017). These findings suggest an indirect involvement of ZFP36L1 in maintaining essential components of DNA replication in MCF-7 cells. RNA-immunoprecipitation assay also

demonstrated that ZFP36L1 also interacts with other heteromeric MCM helicase subunits containing ARE-rich sequences, including *MCM-6* and *MCM-2* (Loh et al., 2020). In support of these results, mass-spectroscopy-based proteomic analysis conducted in our laboratory has also demonstrated interactions between ZFP36L1 and multiple DNA helicase proteins, RNA helicase proteins, and Mismatch repair proteins (Sidali, A., 2023). These experimental data underscore the potential role of ZFP36L1 in regulating crucial elements of DNA replication in MCF-7 cells, thus opening new avenues for investigating ZFP36L1's function in DNA damage and replication within the context of breast cancer.

Following 48 hours of exposure to palbociclib, the cyclin D1, TP53 and MCM-7 protein expression levels were similar in the WT MCF-7 cells and *ZFP36L1 KO* clones. Moreover, FACS analysis results demonstrated cell cycle arrest in the sub-G0/G1 and G1 phase in all the examined cell lines cells following 48-hour palbociclib treatment at 5 μM concentration. However, the response was consistent between both WT MCF-7 cells and *ZFP36L1 KO* clones, suggesting that the absence of the ZFP36L1 gene does not alter palbociclib effects on MCF-7 cell cycle progression. Although 5 μM palbociclib treatment did not reduce cyclin D1 protein levels in MCF-7 cells, further investigation into the impact of higher concentrations of palbociclib on cell cycle-related proteins in ZFP36L1-depleted MCF-7 cells can enhance the strength and reliability of our observations.

Palbocilib-resistant tumour cells can continue cell cycle progression by bypassing CDK4/6 inhibition and upregulation or amplification of other cell cycle-related proteins, including cyclin E1, p16, E2F, CDK6 (Gomatou et al., 2021). Furthermore, the upregulation of cyclin E1-CDK2/cyclin E2-CDK2 is also a possible mechanism to circumvent CDK4/6 inhibition and developing palbociclib resistance in tumour cells

(Gomatou et al., 2021). Since *CDK2* and *E2F1* transcripts contain AU-rich pentamers in the 3'UTR and have been reported as the targets of ZFP36L1 (Loh et al., 2020), investigation of the expression levels of these proteins in ZFP36L1 depleted MCF-7 cells in the presence of palbociclib may provide deeper insights into the mechanistic involvement of ZFP36L1 to palbociclib resistance in MCF-7 cells. In conclusion, ZFP36L1 depletion does not influence palbociclib mediated effect on MCF-7 cells and requires further investigation to confirm these results.

Chapter 6: Identifying ZFP36L1's targets in MCF-7 cells through transcriptomic profiling

6.1 Introduction

In recent decades, quantifying the mRNA population through transcriptome analysis has been a common and routinely used phenotyping method. Compared to classic microarrays, high-throughput RNA sequencing offers the study of novel transcripts with better resolution, a better range of detection and fewer technical variabilities (Finotello and Di Camillo, 2015). Thus, RNA sequencing has become the preferred method of studying transcriptomic analysis and has opened the possibility of evaluating global dynamic changes in gene expression for specific biological processes. High-throughput RNA sequencing, commonly termed RNA-Seq, is a method of mapping sequenced complementary DNA (cDNA) fragments. These sequenced fragments generate reads, which are aligned to a standard reference genome. The number of reads that align with a particular gene is then used to determine its level of expression (Wang, Gerstein and Snyder, 2009).

The exploratory application of RNA-Seq is diverse. It has been utilised to reveal the functions of novel transcript species that are not translated, such as long non-coding RNA, miRNA, and siRNA, involved in regulating RNA stability, protein translation, or the modulation of chromatin states (Kim et al., 2010). For example, enhancer RNA, which has a role in epigenetic gene regulation, has been identified and studied using RNA sequencing (Robertson et al., 2010). Moreover, RNA sequencing has proved beneficial in identifying allele-specific expression, disease-associated single nucleotide polymorphisms (SNPs), and gene fusions, highlighting its potential to increase our understanding of disease causal variants in cancer (Maher et al., 2009; Conde et al., 2013).

RNA binding proteins are the critical effectors of gene expressions; they form extensive regulatory networks and are involved in post-transcriptional targeting of mRNA localisation, stability, and translation that helps maintain cellular haemostasis (Gebauer et al., 2021). Mechanistically, ZFP36L1 directly interacts with the ARE-rich sequences of mRNA transcripts and is involved in post-transcriptionally maintaining targeted gene expression. In this study, we performed a comprehensive RNA sequencing study to better understand ZFP36L1-regulated gene expression in the MCF-7 breast cancer cell line. This chapter aims to reveal the unknown key biological and molecular pathways regulated by the ZFP36L1 gene that could be mechanistically involved in tumorigenesis in MCF-7 breast cancer cells. The objective of this chapter is to understand and compare the transcriptomic profiling of MCF-7 cells with and without the expression of ZFP36L1 obtained through RNA sequencing analysis. This transcriptomic analysis study will help us to delineate the effect of ZFP36L1 knockout on the global gene expression profiles of MCF-7 cells and identify the genes that might be potential targets of the ZFP36L1 gene.

Biological replicates are crucial in determining the reliability, robustness and statistical power of RNA sequencing analysis (McIntyre et al., 2011; Marioni et al., 2008). Consequently, experimental designing plays a crucial role in RNA sequencing, considering the sensitivity and specificity of the experiment. We performed this study with 3 biological replicates of each group, which were pivotal to reducing the technical artefacts and achieving accurate and reproducible results. The 3 biological replicates of WT MCF-7 cells were named WT group, and 3 biological replicates of *ZFP36L1* KO MCF-7 cells (clone B4, F7 and D3) were named KO group. The total RNA extracted from all 6 samples (3 WT and 3 *KO*) were sent to Novogene for further RNA Seq analysis utilising a user-friendly workflow pipeline outlined in Figure 6.1.

This study can be effectively summarized into two main sections: Experimental Biology and Computational Biology. The Experimental Biology segment encompasses processes such as RNA extraction, fragmentation, and cDNA library preparation, and the Computational Biology aspect comprises six distinct steps, as discussed in detail here:

1. High-throughput sequencing platforms like Illumina served as a starting material for computational bioinformatic analysis. Illumina platforms performed paired-end RNA sequencing, and the obtained raw reads were stored in FASTAQ format files containing sequences of reads.
2. Quality assessment was performed to ensure a coherent result. The infiltration process involved removing the low-quality reads, including reads containing adaptor contamination and uncertain or low-quality nucleotides (base quality less than 5).
3. Aligning the reads with the reference genome allowed us to determine the original location of the reads. Novogene performed alignment using HISAT2 software, a fast spliced aligner (Kim et al., 2019). The human genome version GRCH 38.p13 from Ensembl was utilised as a reference genome. The mapping results were provided in a BAM file format.
4. To predict their novelty, the Cufflinks assembler counted the number of alignments mapped to each gene and compared them to the reference transcripts. The read counts were measured in fragments per kilobase of transcripts sequence per million base pairs sequenced (FPKM), a standard method for estimating gene expression levels (Trapnell et al., 2010). Read counts were proportional to the gene expression level, length, and sequencing depth.

5. Novogene adapted DESeq2 R software (Love, Huber and Anders, 2014), a statistical method based on the negative binomial distribution, to normalise the read counts. The normalisation was mainly done to avoid any bias due to sequencing depth. The differentially expressed genes were screened using the common empirical value |log2(Fold Change)| ≥ 1, where fold change is the ratio of gene expression level between the *ZFP36L1 KO* group and the WT control group. To prevent false positive results, the p-value was calibrated and termed as the Padj value using Benjamini and Hochberg's approach.
6. Extensive enrichment analysis of differentially expressed genes (DEGs) was performed using different system biology analyses, which include Gene Ontology (GO) enrichment analysis and Kyoto Encyclopedia of Genes and Genomes (KEGG) pathway enrichment analysis to identify the altered genes and pathways. Novogene used the Cluster Profiler software (Yu et al., 2012) for enrichment analysis, including GO Enrichment and KEGG database Enrichment analysis. All these expression analyses are based on the read counts of gene expression levels calculated by estimating FPKM. (Eswaran et al., 2012).

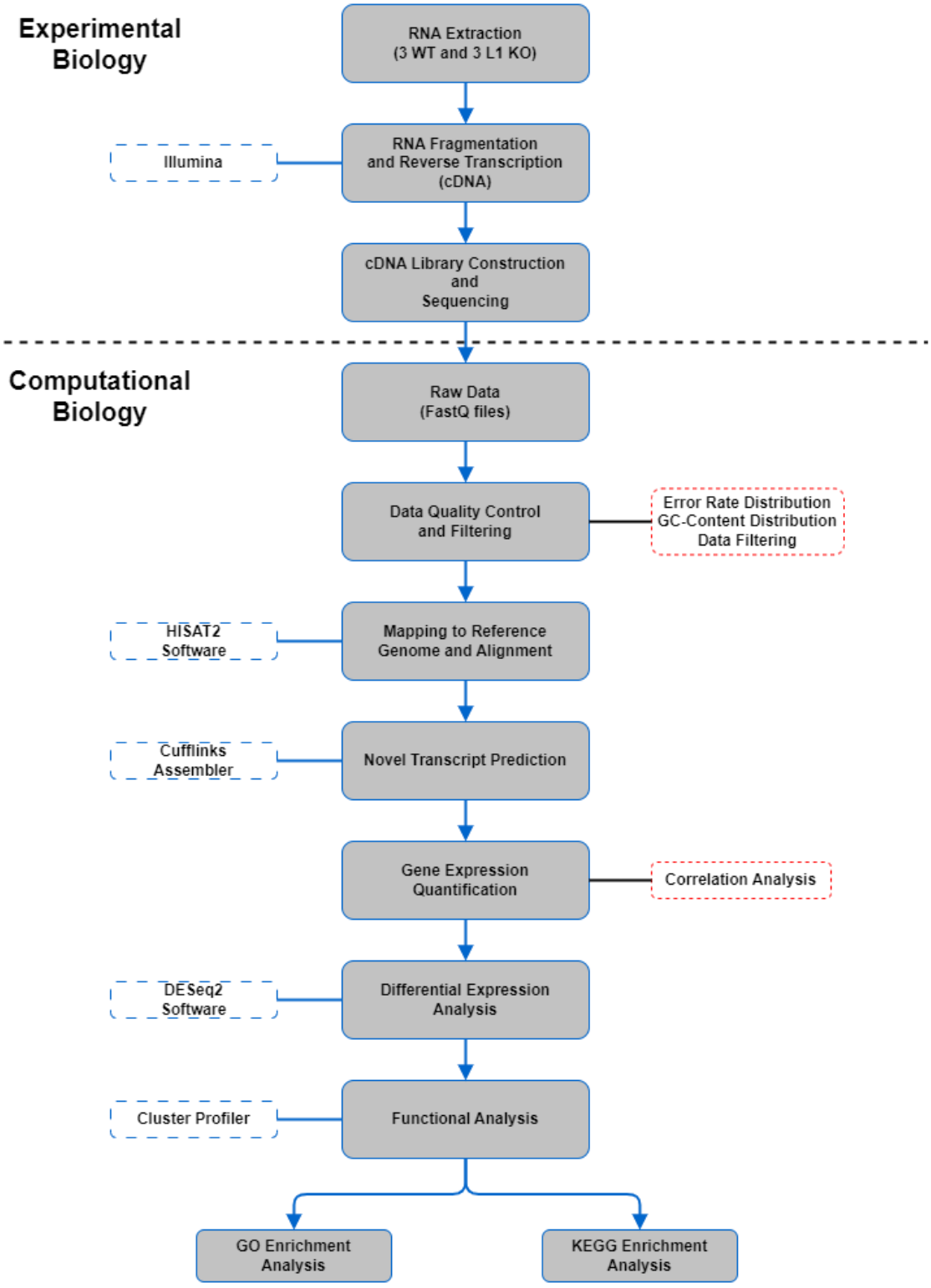

Figure 6.1: A representative workflow of a standard bioinformatic analysis for RNA sequencing comprising experimental and computational work. The RNA was extracted, fragmented, and converted into cDNA by random priming. The cDNA was transformed into a molecular library for sequencing by high-throughput sequencing platforms like Illumina. The

sequenced reads (raw data) were stored in FASTAQ formats. High-quality data was acquired by filtering data through different ways, including removing low-quality reads or base adaptors. Filtered sequenced reads were mapped to the reference genome using HISAT2 software, and the data was provided in BAM file format. The assembled alignment novelty prediction was made by counting the number of alignments mapped to each gene performed by the cufflinks assembler and compared to the reference transcripts. Gene expression was normalised and quantified using the DESeq2 program, and the quantified values were used extensively to assess several analyses, such as correlation analysis, differential gene expression and other functional analyses using cluster profiler software.

6.2 Results

6.2.1 Identification of differentially expressed genes in *ZFP36L1 KO* MCF-7 cell line

Among the WT and KO groups in MCF-7 cells, a total of 849 genes were identified to be differentially expressed, where 267 genes were significantly upregulated, and 582 genes were significantly downregulated (Figure 6.2). These gene expression changes, associated with the *ZFP36L1 KO*, were statistically significant with adjusted p-value < 0.05 and log 2-fold change of >1. Since the ZFP36L1 gene modulates mRNA levels in target genes by destabilising their mRNA, we mainly focused on the differentially upregulated genes found in RNA sequencing data. Within the significantly upregulated genes, we explored the genes containing AU-rich elements (AUUUA pentamers) in the 3'UTR in the mRNA sequence, which could be the direct target of the ZFP36L1 gene (Appendix D, Table D1). Of the 267 significant upregulated genes, 84 genes harbour AU-rich sequence in the 3' UTR of their mRNA transcript. We utilised an AU-rich element database (Bakheet, Hitti and Khabar, 2018) to list these 84 genes.

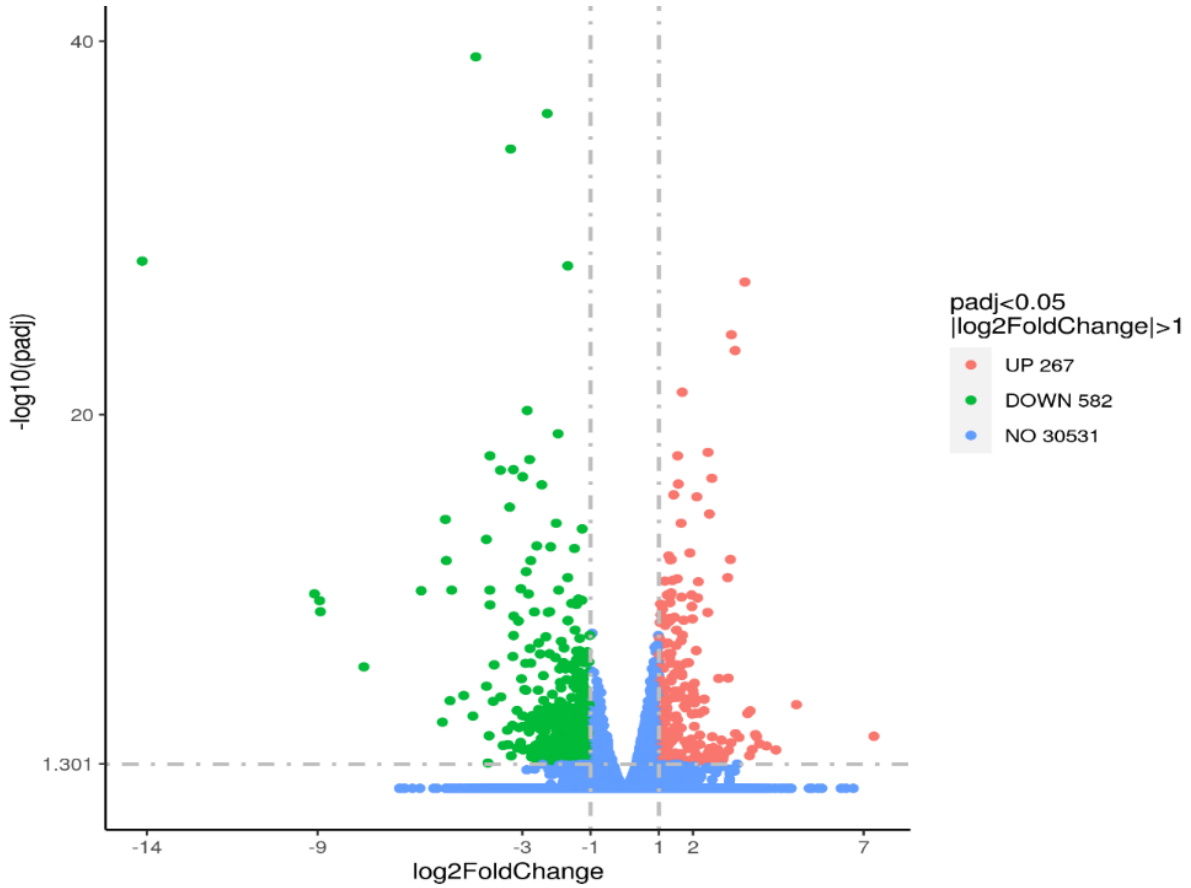

Figure 6.2: Represents the volcano plot of differentially expressed genes in MCF-7 cells among the WT vs. KO group. The X-axis represents the fold change of genes, and the y-axis represents the statistically significant degree of changes in gene expression levels. The smaller the padj-value, the bigger is -log10 (padj-value), and the more significant the difference. Genes are represented by the points where blue points represent genes that have no significant difference in gene expression levels, the red points represent significantly upregulated differential expression genes, and green dots represent downregulated differential expression genes. The blue dashed line indicates the threshold line for differential gene screening criteria. (Figure source: Novogene).

6.2.2 Functional annotation and enrichment analysis of DEGs in *ZFP36L1 KO* MCF-7 cell line

Gene Ontology (GO) classification and enrichment analysis were performed according to three main ontologies: biological process (BP), cellular component (CC), and molecular function (MF). The GO classification with a Padj value ≤ 0.05 was considered to be significantly enriched. In total, 36 GO terms were found enriched for the significant upregulated DEGs, where 24 GO terms belonged to the BP category,

10 GO terms belonged to the CC category, and 2 GO terms belonged to the MF category. The GO terms associated with the higher number of DEGs containing AU-rich elements are represented in the histogram (Figure 6.3). Most of the AU-rich upregulated genes were involved in enriched GO terms such as synapse organisation, aminoglycan biosynthetic process, cellular extravasation, proteoglycan biosynthetic process, monovalent inorganic anion homeostasis and regulation of heterotypic cell-cell adhesion.

Further, the list of all other upregulated GO-enriched terms and their corresponding AU-rich upregulated genes are listed in Appendix D (Table D2). For the significantly downregulated genes, 65 enriched GO terms were obtained, where 39 enriched GO terms belonged to the BP category, 16 to the CC category, and 8 to the MF category. The most significant GO terms in all three main ontologies for downregulated DEGs are represented in the histogram (Figure 6.4). The downregulated DEGs involved in these enriched GO terms are listed in Appendix D (Table D4).

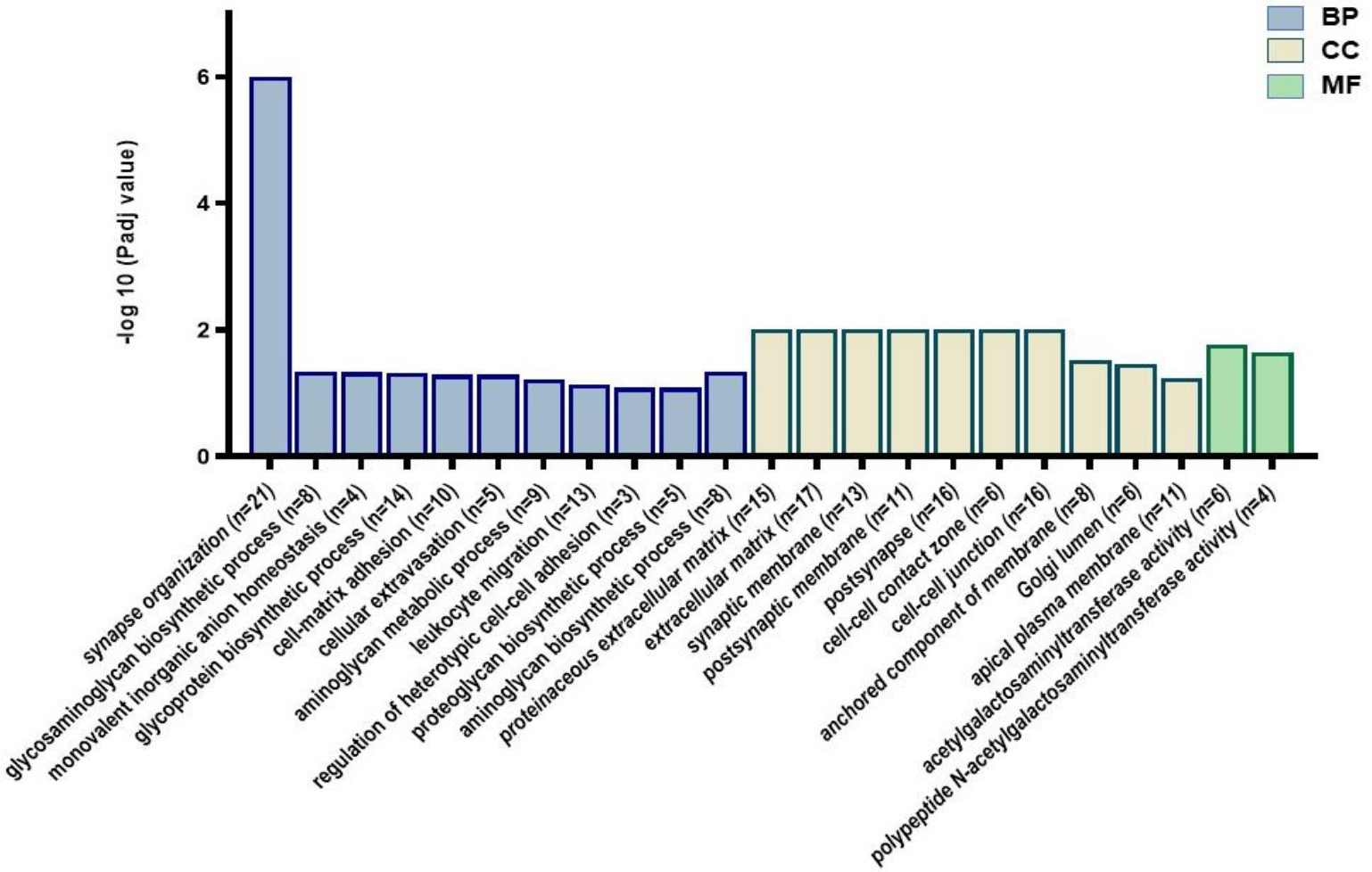

Figure 6.3: Histogram plot representing the significantly enriched GO terms for upregulated DEGs. The y-axis represents the statistically significant degree of changes in gene expression levels. The smaller the padj-value, the bigger -log10 (padj-value) and the more significant the difference. The x-axis represents the enriched GO terms, and n represents the number of upregulated DEGs involved in the corresponding GO terms.

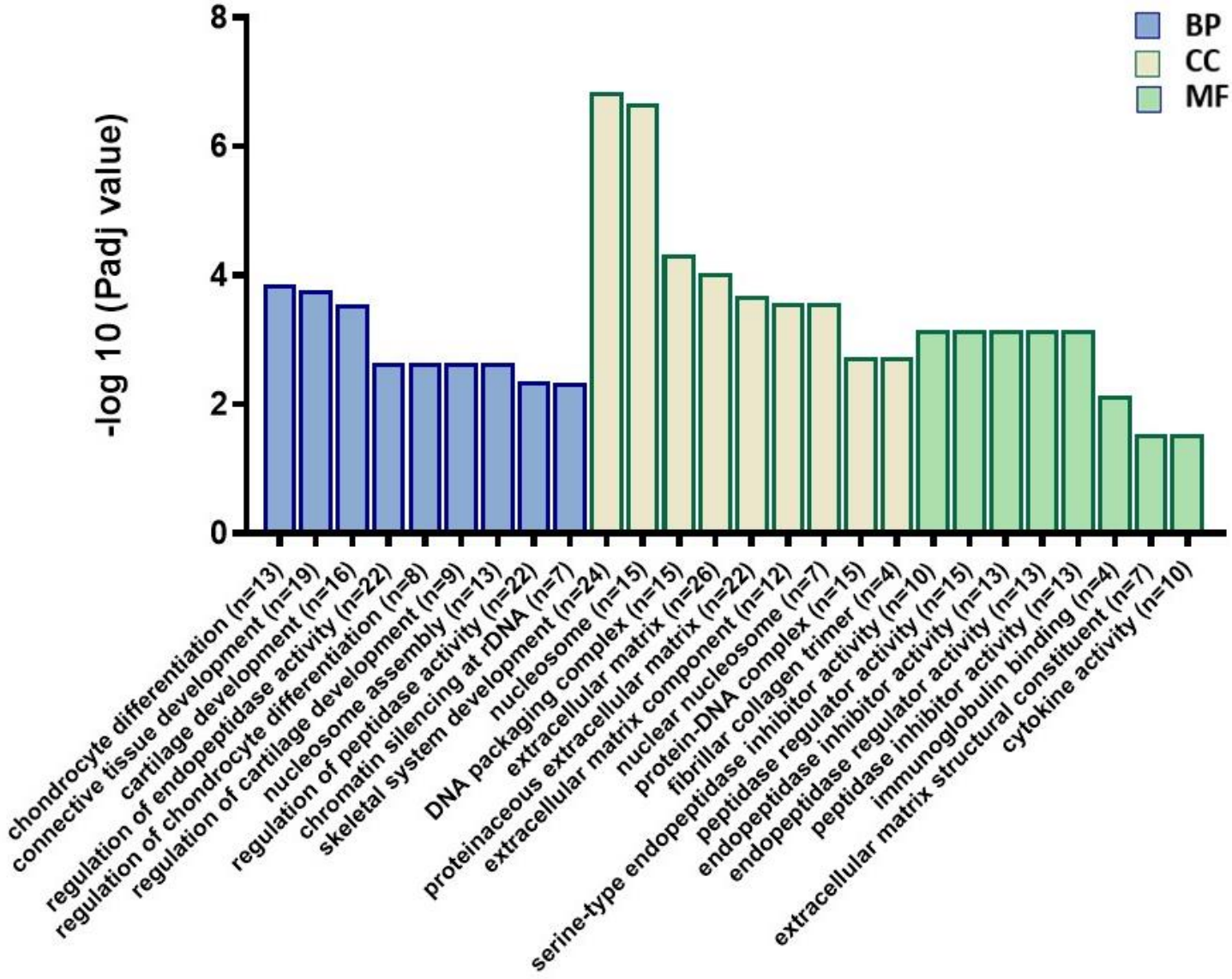

Figure 6.4: Histogram plot representing the significantly enriched GO terms for downregulated DEGs. The y-axis represents the statistically significant degree of changes in gene expression levels. The smaller the padj-value, the bigger -log10 (padj-value) and the more significant the difference. The x-axis represents the enriched GO terms, and n represents the number of downregulated DEGs involved in the corresponding GO terms.

Furthermore, differentially expressed genes were mapped to KEGG pathways to explore the activated molecular networks and biological pathways without the ZFP36L1 protein in MCF-7 cells. The KEGG pathway enrichment analysis related to upregulated DEGs revealed that six pathways are significantly enriched, which are

represented in the histogram in Figure 6.5. Most AU-rich DEGs associated with upregulated KEGG pathways are involved in the cytokine-cytokine receptor interaction pathway. All the upregulated DEGs associated with enriched KEGG pathways are listed in Appendix D (Table D3). Within the KEGG pathways related to the downregulated DEGs, 6 pathways were found to be significantly enriched, which are represented in the histogram in Figure 6.6.

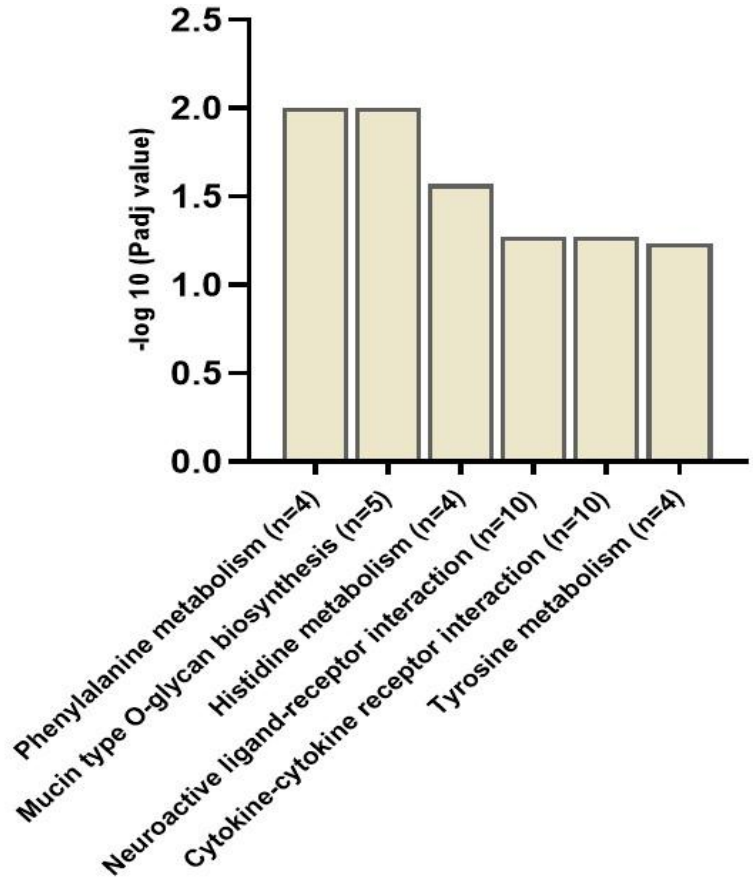

Figure 6.5: Histogram plot representing the significant upregulated enriched KEGG pathways with corrected p-value ≤ 0.05. The X-axis represents the enriched pathways, where n represents the number of downregulated DEGs associated with that pathway. The Y-axis represents the statistically significant degree of changes in the KEGG pathway where the smaller is the corrected padj-value, the bigger is -log10 (padj-value), and the more significant is the difference.

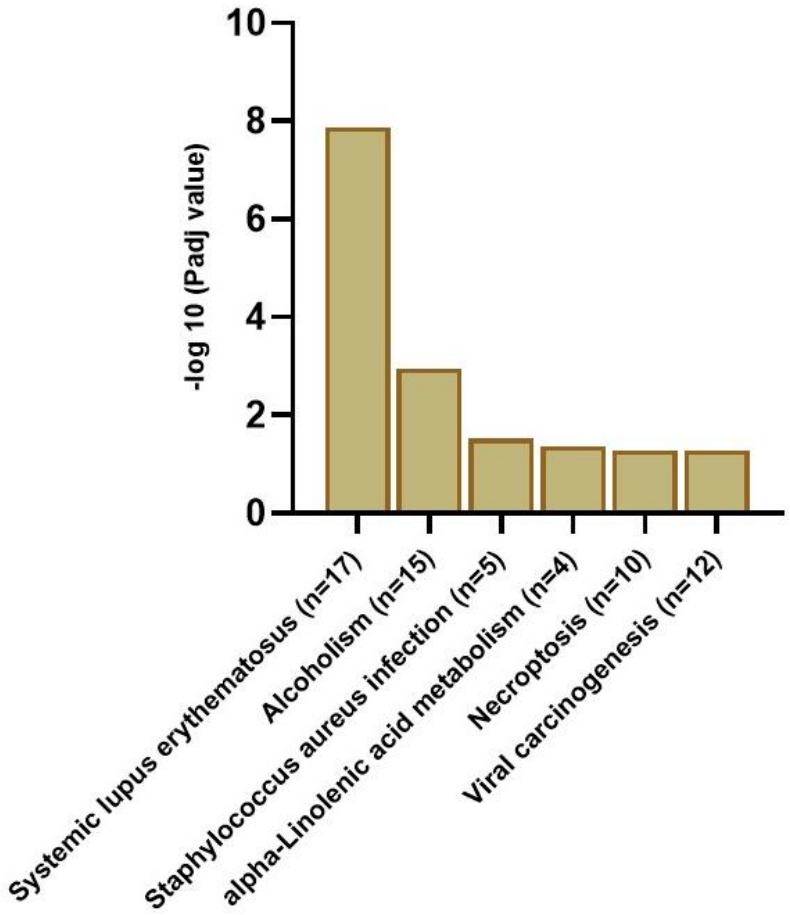

Figure 6.6: Histogram plot representing the significant downregulated enriched KEGG pathways with corrected p-value ≤ 0.05. The X-axis represents the enriched downregulated pathways, where n represents the number of downregulated DEGs associated with that pathway. The Y-axis represents the statistically significant degree of changes in the KEGG pathway where the smaller is the corrected padj-value, the bigger is -log10 (padj-value), and the more significant is the difference.

6.3 Discussion

In the past decades, the advancement and evolution of sequencing and array technologies have given us significant knowledge of breast cancer. These technologies have allowed scientists to acquire valuable information and identify genetic alterations involved in the progression of cancer. The traditional microarray technique has been surpassed by RNA-sequencing technology, which is now widely

adopted in both research and clinical laboratories to study transcriptomic analysis. The comprehensive knowledge of the transcriptome aids in unravelling the functional components of the genome and understanding the underlying mechanisms of several pathological conditions, including cancer (Wang, Gerstein and Snyder, 2009). In this chapter, through the analysis of transcriptomic profiling of MCF-7 cells, we aim to delineate the molecular pathways that could be potentially modulated by the ZFP36L1 gene and involved in promoting tumorigenesis in MCF-7 cells.

RNA sequencing analysis revealed that 267 genes were identified as significantly upregulated, and 562 genes were significantly downregulated in the *ZFP36L1 KO* group. We utilised an AU-rich element database (Bakheet, Hitti and Khabar, 2018) to generate a list of the 84 significantly upregulated DEGs harbouring AU-rich sequence in the 3' UTR of their mRNA transcript (Appendix D, Table D1). The GO-term enrichment analysis showed that lack of ZFP36L1 led to the upregulation of several transcripts involved in synapse organisation, cell-matrix adhesion, regulation of heterotypic cell-cell adhesion, cell-cell contact zone, and cell-cell junction, as depicted in Figure 6.3. It is evident from these findings that suppressing ZFP36L1 expression resulted in transcriptional changes linked to neuronal functions, cell adhesion and mobility. Moreover, considering that a majority of upregulated DEGs involved in these enriched GO terms are AU-rich genes containing at least 1 or 2 pentamers motifs in the 3'UTR of their mRNA transcripts (Appendix D, Table D2), these results strongly suggest that the ZFP36L1 could be functionally involved in regulating the AU-rich DEGs associated with cell migration. These outcomes were in-line with the wound-healing assay results, where the absence of ZFP36L1 showed a significant reduction in the wound-healing capability of MCF-7 cells.

Among all the upregulated GO terms, the DEGs involved in synapse organisation were maximum and demonstrated the highest level of statistical significance in this study. According to the quick GO term, EMBL-EBI database (www.ebi.ac.uk/QuickGO), the GO term synapse organisation is defined as a biological process which is involved in the assembly, arrangement of constituent parts, or disassembly of a synapse, the junction between a neuron and a target. In this study, within the upregulated DEGs related to the synapse organisation, several DEGs, including *CLSTN2, NRCAM, PCDH, SEMA3E,* and *ADGRL3*, belonging to cell adhesion molecules, are known to play crucial roles in cell adhesion and interaction, particularly in cell-cell neural connections (Wu and Maniatis, 1999; Morishita and Yagi, 2007; Tamagnone and Rehman, 2013; Sakurai, 2012). Other upregulated DEGs, such as *TIAM1* and *DOCK10*, regulate cytoskeleton organisation, promoting cell-migration invasion and metastasis in breast tumours (Minard et al., 2004; Westcott et al., 2015). While these DEGs are typically involved in neuronal functions, their association with cell migration and invasion in tumour cells is well-documented. These findings suggest a potential role of ZFP36L1 in modulating the transcriptomic expression of cell-adhesion molecules, thereby influencing cell migration and invasion in MCF-7 cells.

Moreover, inhibiting ZFP36L1 expression induced significant upregulation of several GO terms and KEGG pathways associated with glycosylation-related pathways. These GO terms include proteoglycan biosynthetic process, glycosaminoglycan biosynthetic process, glycosaminoglycan metabolic process, acetylglucosaminyl transferase activity, polypeptide N-acetylgalactosaminyl transferase activity. Glycosylation is fundamentally involved in several processes promoting tumourigenesis, such as signalling, invasion, angiogenesis and metastasis (Carvalho, Reis and Pinho, 2016; Lin and Lubman, 2024). Alterations in glycan-related structures

are frequently observed at the early stages of malignancy, where glycosylation molecules undergo profound modifications and play a driving force behind malignant cell transformations and metastasis of tumour cells (Kolbl, Andergassen and Jeschke, 2015; Potapenko et al., 2015).

Additionally, several DEGs associated with extracellular matrix were found to be significantly enriched in both upregulated and downregulated GO terms, including cell-matrix adhesion, regulation of heterotypic cell-cell adhesion, cell-cell contact zone, and cell-cell junction, proteinaceous extracellular matrix, extracellular matrix components, and extracellular matrix. The role of ECM is well-known for regulating the tumour microenvironment (Closset et al., 2023; Pally and Naba, 2024). ECM also serves as a critical component of the breast tumour microenvironment, potentially acting as the initial barrier against breast tumour cell invasion and metastasis (Pally and Naba, 2024). However, tumour cells often hijack and exploit the ECM to manipulate the microenvironment, resulting in altered composition, structure, and biomechanical properties. For e.g. one of the key ECM components, collagen, which serves as a scaffold to provide physical support, is often substantially elevated in malignant tumour cells, resulting in increased cross-linking (Yu et al., 2023). The dysregulated expression of ECM-associated genes in tumour cells strongly correlates with increased lymphangiogenesis, inflammation and angiogenesis (Yu et al., 2023). Additionally, during tumorigenesis, ECM serves as a niche for cancer stem cells (CSCs) and disseminated cancer cells (DCCs), impacting cancer dormancy (Poltavets et al., 2018; Sistigu et al., 2020; Li et al., 2016). Thus, loss of ZFP36L1, resulting in differential expression of ECM-related genes in MCF-7 cells, could be a critical factor in promoting immune cell evasion, angiogenesis, cancer cell migration, and metastasis in hormone-positive breast tumours.

The upregulated AU-rich DEGs associated with these GO terms, such as *CSGALNACT1, HS3ST5, TIAM1, CEMIP, VCAN, CHSY3, CD44* and *BMPR1B* are often documented as deregulated and deranged in several tumours, correlating with poor prognosis and aggressive behaviour in breast cancer patients (Dong et al., 2021; Du et al., 2012; Li et al., 2016). Furthermore, using the cBioPortal database (cBioPortal for Cancer Genomics), we found that few of the upregulated AU-rich DEGs, including *VCAN, PCLO and UTRN*, are also associated with the high frequency of mutations (2.2%, 3.3% and 3.2%, respectively, Appendix D, Table D1) in breast cancer. These results aligned with the previous literature where an RNA-pulldown and RNA sequencing analysis conducted by Loh et al. in 2020 validated that *VCAN and UTRN* are the direct downstream targets of ZFP36L1. Furthermore, other genes identified as a direct downstream target of the ZFP36L1 in the Loh et al. 2020 study were also found to be significantly upregulated in the *ZFP36L1 KO* group. These genes include *ASPH, ATP1B1, CASK, CSGALNACT1, GALNT7, KDELC2, MAFF, MAOA, PAQR8, PLAT, RAPGEF5, SOX2, TNF, TTC28 and XPR1.* The mutation frequencies associated with these genes in breast cancer are listed in Appendix D (Table D1), where *CASK* and *TTC28* exhibit high mutation frequency in breast cancer among other upregulated genes. Based on these findings, it can be proposed that ZFP36L1 might be directly involved in regulating several key EMT-related markers affecting cell-cell adhesion and, hence, tumour-cell migration, invasion and metastasis in ER/PR+ breast cancer cell line. However, further experimental studies, such as q-PCR and western-blot analysis, will be required to validate these research outcomes, providing deeper insights into the ZFP36L1-mediated regulation of migration and metastasis in the MCF-7 cell line.

In this RNA transcriptomic analysis, GO, and KEGG pathways revealed that loss of ZFP36L1 in MCF-7 cells resulted in the differential expression of several genes, which have potential roles in promoting cell migration, angiogenesis, invasion, and metastasis, the key hallmarks of breast tumorigenesis. Based on these findings, it can be hypothesised that ZFP36L1 could also be potentially involved in regulating the transcriptomic expression of epithelial-mesenchymal transition (EMT)-related markers, thereby influencing cell-cell adhesion and tumour cell migration and metastasis in estrogen/progesterone receptor-positive breast cancer. However, further experimental validation, such as qPCR and western blot analysis, is warranted to confirm these findings and provide deeper insights into the mechanisms underlying ZFP36L1-mediated regulation of migration and metastasis in the MCF-7 cell line.

Chapter 7: Deciphering cell-specific functions of the ZFP36L1 through RNA transcriptomic profiling

7.1 Introduction

In the first chapter of this thesis, we have discussed in detail the cell-specific role of the ZFP36 family (Section 1.2.5). Despite sharing striking biochemical similarities, such as comparable zinc finger domains, similar RNA molecule-binding affinities, and identical decay mechanisms for their respective targets, these members exhibit specificities in selecting their RNA targets. While several studies have examined the specific targets of ZFP36 family proteins in hematologic malignancies (Galloway et al., 2016; Vogel et al., 2016), the specific RNA targets of ZFP36L1 and ZFP36L2 across diverse cell types and tissues under different experimental conditions remain largely unexplored. In cases where these proteins coexist within the same cell type, such as in normal tissues and human cell lines, the question of target selection and specificity becomes considerably more complex and intricate. In this chapter, our objective is to investigate the cell-type-specific function of the ZFP36L1 gene within two distinct cellular contexts: the MCF-7 breast cancer cell line and the HCT116 colorectal cancer cell line. We hypothesised that ZFP36L1 targets a diverse range of mRNAs, and therefore, the absence of the protein is anticipated to result in the enrichment of distinct sets of differentially expressed genes (DEGs) in each of these cell lines. In both HCT116 and MCF-7 cell lines, the ablation of ZFP36L1 protein expression was achieved using CRISPR Cas9 technology. As discussed in Chapter 3, we created *ZFP36L1* knock-out models in the MCF-7 cell line. Following the CRISPR Cas9 methodology as described in Chapter 3, we generated the truncated version of the ZFP36L1 protein in HCT-116 colorectal cancer cell lines (named as *Δ ZFP36L1* HCT116). The combination of guides 1 and 2 specific to ZFP36L1 induced CRISPR Cas9 mediated editing in HCT116 cells (Appendix A, Figure A2). The truncation induced in the ZFP36L1 gene in the HCT 116 cell line was verified through western

blot and NGS analysis (Appendix E, Figure E1 and E2). The RNA sequencing analysis was performed with the following set of samples in both cell lines:

1) MCF-7 cell line (6 samples): 3 WT MCF-7 and 3 *ZFP36L1 KO* MCF-7 samples.

2) HCT 116 cell line (2 Samples): WT HCT-116 and *ZFP36L1* truncated HCT 116 samples.

Following the methodology discussed in Chapter 6, Novogene provided the RNA sequencing and bioinformatic analysis for both MCF-7 and HCT-116 cell lines. Since the ZFP36L1 gene functions in destabilising its target mRNA, we mainly focussed on the upregulated DEGs in both cell lines harbouring the dysfunctional ZFP36L1 gene. Further, Gene ontology (GO) and Kyoto Encyclopaedia of Genes and Genomes (KEGG) analysis of upregulated DEGs were performed to identify the specific enriched pathways involved in both the cell lines lacking functional ZFP36L1 gene. Since we already have discussed RNA sequencing results and bioinformatic analysis in the MCF-7 cell line in the last chapter (Chapter 6), this chapter will more elaborately analyse the results of transcriptomic profiling of the HCT-116 cell line in the presence of *Δ ZFP36L1* gene. Furthermore, we will explore the differences in the enriched GO terms in both cell lines harbouring the dysfunctional ZFP36L1 gene to identify the distinct molecular and biological terms enriched in both cell lines and, thus, to determine the cell type-specific role of the ZFP36L1 gene.

7.2 Results

7.2.1 Identification of differentially expressed genes in *Δ ZFP36L1* HCT116 cell line

In the HCT 116 cell lines, 2 samples were utilised for RNA sequencing analysis, which included the WT HCT-116 cell line and Δ *ZFP36L1* HCT-116 cell line, containing truncated ZFP36L1 protein. Among the WT HCT-116 and *Δ ZFP36L1* HCT-116 cell

lines, 104 genes were differentially expressed, where 93 genes were found to be upregulated, and 11 genes were found to be downregulated. These gene expression changes, associated with the truncated ZFP36L1, were statistically significant with an adjusted p-value < 0.05 and log 2-fold change of >1. Within the upregulated genes found in *ZFP36L1 KO* MCF-7 and *Δ ZFP36L1* HCT116 cell lines, only three genes, including *CCL28, IGSF11, and OAS1,* were found to be common in both cell lines.

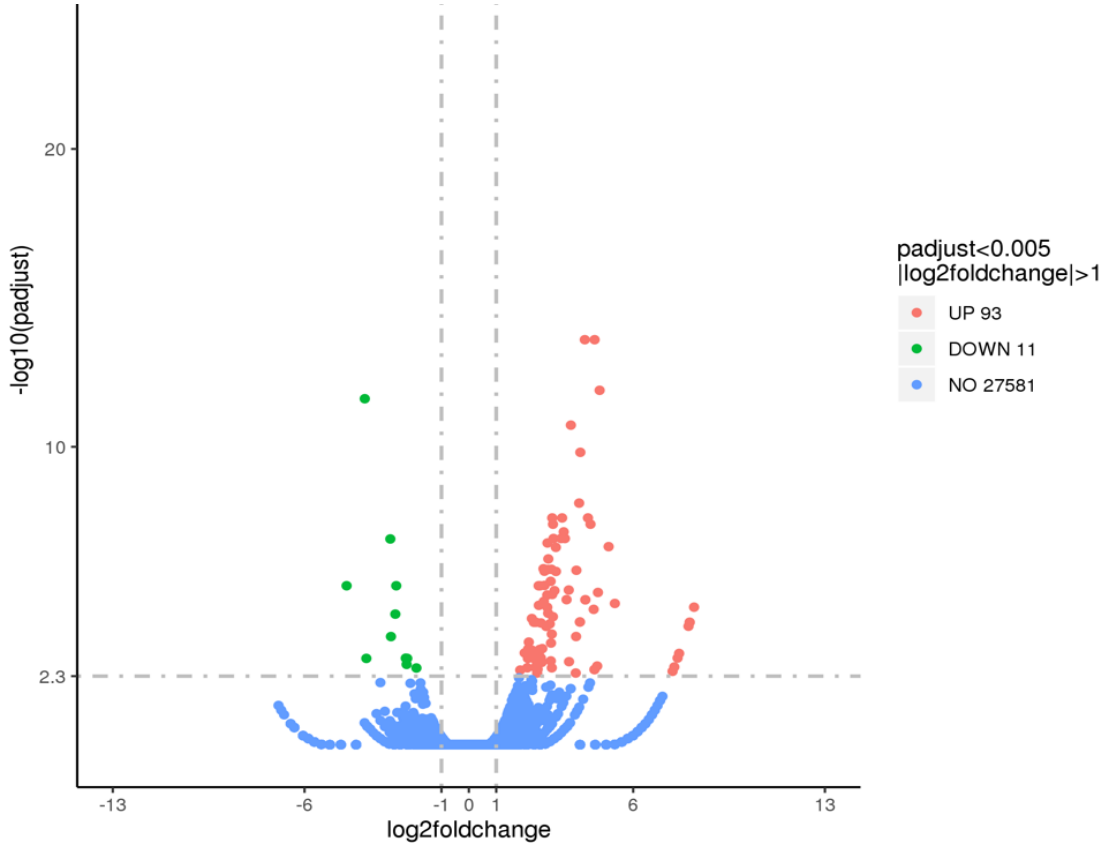

Figure 7.1: Represents the volcano plot of differentially expressed genes in HCT-116 cells among WT and Δ ZFP36L1 cell lines. The X-axis represents the fold change of genes, and the y-axis represents the statistically significant degree of changes in gene expression levels. The smaller the corrected p-value, the bigger the -log10 (corrected p-value) and the more significant the difference. Genes are represented by the points where blue points represent no significant difference, the red dot represents significantly upregulated differential expression genes, and the green dots represent downregulated differential expression genes. (Figure source: Novogene).

7.2.2 Functional annotation and enrichment analysis of DEGs in HCT-116 cell line

As described in the last chapter, Gene Ontology (GO) classification and enrichment analysis were performed according to three main ontologies: biological process (BP), cellular component (CC), and molecular function (MF). The GO classification with a Padj value ≤ 0.05 was considered to be significantly enriched. In the *Δ ZFP36L1* HCT-116 cell line, 43 GO terms were found enriched for the significantly upregulated DEGs, where 36 GO terms belonged to the BP category, and 7 GO terms belonged to the CC category. However, no GO term in the molecular Function (MF) category showed significant enrichment. The GO terms associated with the higher number of DEGs containing AU-rich elements are represented in the histogram (Figure 7.2). Most GO terms related to the BP category are involved in epithelial cell proliferation, endothelium development, negative regulation of cell-cell adhesion, and negative regulation of cell development. Analysis of the DEGs enriched in the CC category demonstrated that most GO terms are crucial in ion transportation and membrane signalling through the cell membrane. The list of all significantly GO-enriched terms and their corresponding AU-rich upregulated genes are listed in Appendix E (Table E1). The significantly upregulated AU-rich DEGs were selected and listed using an AU-rich element database (Bakheet, Hitti and Khabar, 2018).

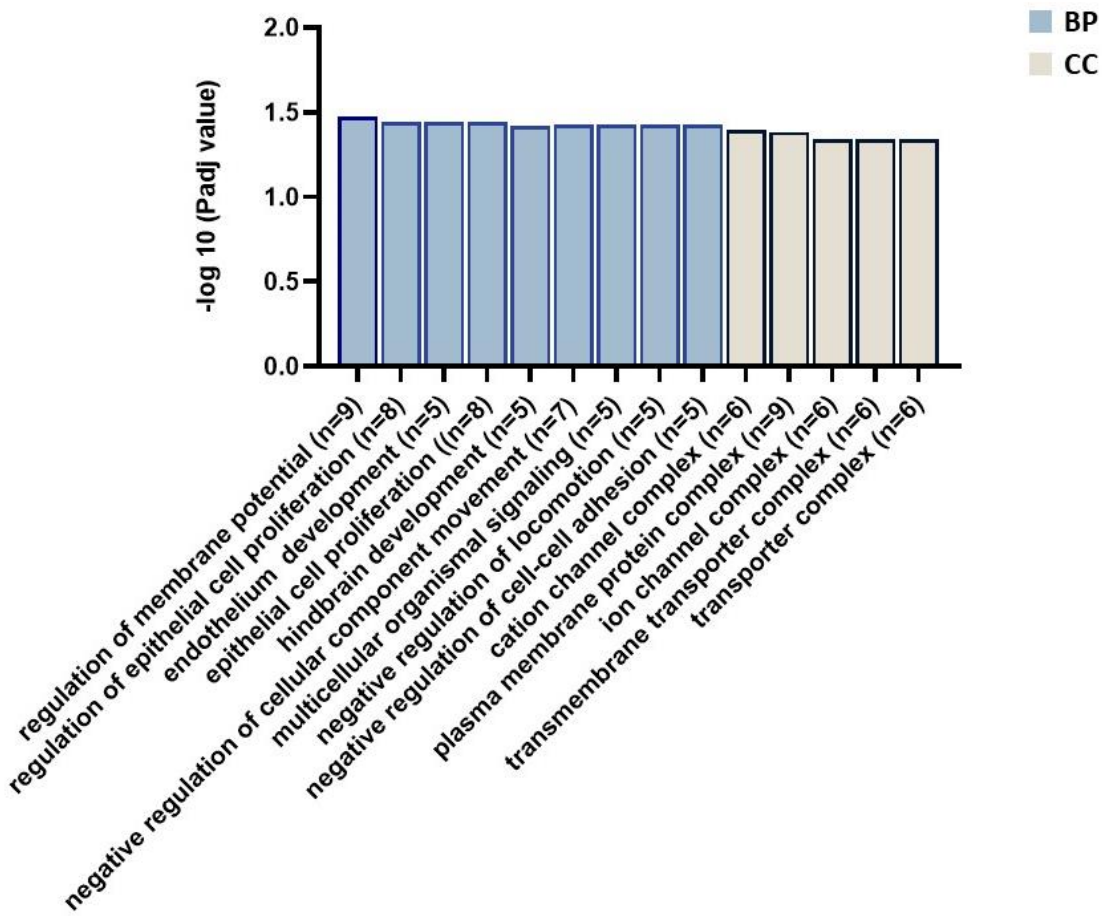

Figure 7.2: Histogram plot representing the significantly enriched GO terms for upregulated DEGs in HCT-116 cells. The y-axis represents the statistically significant degree of changes in gene expression levels where the smaller the padj-value, the bigger is the -log10 (padj-value) and the more significant is the difference. The x-axis represents the enriched GO terms, and n represents the number of upregulated DEGs involved in the corresponding GO terms.

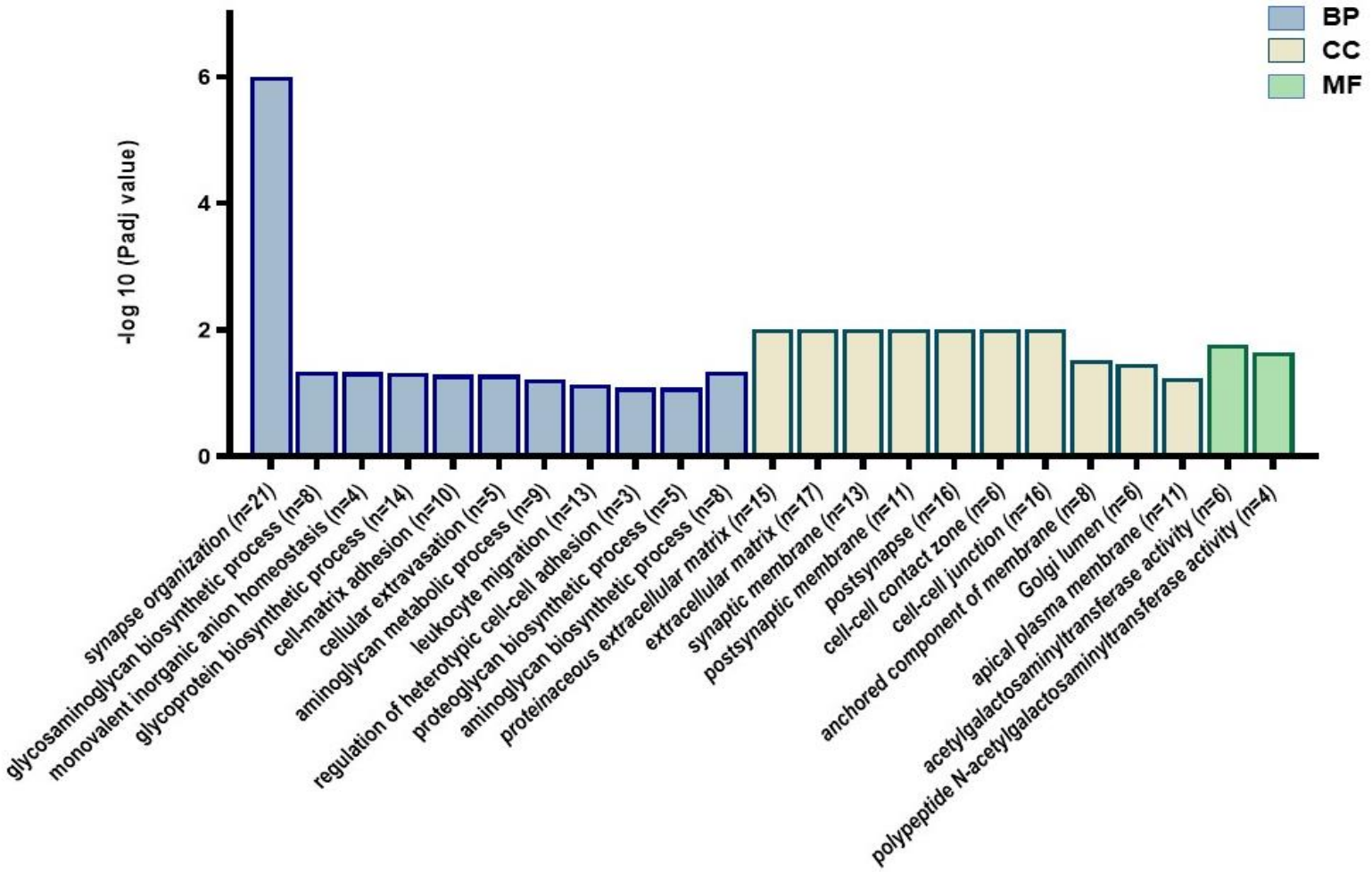

Figure 7.3: Histogram plot representing the significantly enriched GO terms for upregulated DEGs in MCF-7 cells. The y-axis represents the statistically significant degree of changes in gene expression levels. The smaller the padj-value, the bigger is -log10 (padj-value) and the more significant the difference. The x-axis represents the enriched GO terms, and n represents the number of upregulated DEGs involved in the corresponding GO terms.

Table 7.1 List of significant GO-enriched terms associated with upregulated DEGs and AU-rich upregulated DEGs in MCF-7 and HCT116 cell lines.

MCF-7 Cell line			
GO	**Description**	**Gene Names**	**AU-rich gene names**
BP	Cell-matrix adhesion	LYPD3/CD44/CDK6/SEMA3E/CCL28/CASK/TIAM1/UTRN/VEGFC/NEXMIF	CD44/CDK6/CASK/TIAM1/UTRN/VEGFC
BP	Cellular extravasation	GCNT1/CCL28/IL1R1/PTGER4/TNF	GCNT1/IL1R1/PTGER4/TNF
BP	Regulation of cell-matrix adhesion	CDK6/SEMA3E/CCL28/CASK/UTRN/VEGFC/NEXMIF	CDK6/CASK/UTRN/VEGFC
BP	Regulation of heterotypic cell-cell adhesion	CD44/GCNT2/TNF	CD44/TNF
CC	Cell-cell contact zone	ATP1B1/PCDH9/TIAM1/ANK3/FGF13/CDH2	ATP1B1/PCDH9/TIAM1/
CC	Cell-cell junction	ATP1B1/PCDH9/AMTN/ABCC2/POF1B/OXTR/CASK/TIAM1/ANK3/FGF13/AKR1B1/TMEM47/FGFR4/CGNL1/CDH2/ADGRL3	ATP1B1/PCDH9/ABCC2/POF1B/CASK/TIAM1/TMEM47/ADGRL3
HCT-116 Cell line			
BP	Epithelial cell proliferation	TACSTD2/AKT3/WNT7A/PTN/NOG/CCL2/CEACAM1/ATOH8	WNT7A/CCL2/CEACAM1
BP	Regulation of epithelial cell proliferation	TACSTD2/AKT3/WNT7A/PTN/NOG/CCL2/CEACAM1/ATOH8	WNT7A/CCL2/CEACAM1
BP	Negative regulation of cellular component movement	TACSTD2/CCL28/PTN/IL1RN/NOG/CCL2/LDLRAD4	CCL2/LDLRAD4
BP	Negative regulation of locomotion	TACSTD2/CCL28//NOG/CCL2/LDLRAD4	CCL2/LDLRAD4
BP	Negative regulation of cell-cell adhesion	VTCN1/LGALS9/CCL28/IL1RN/CEACAM1	CEACAM1

7.3 Discussion

In this chapter, we focused on investigating the cell type-specific role of the ZFP36L1 using two different cell line model systems, MCF-7 breast cancer cell line and HCT116 colorectal cancer cell line, where both cell lines contain dysfunctional ZFP36L1 protein. We aimed to identify the specific targets of ZFP36L1 in MCF-7 and HCT116 cell lines using RNA sequencing technology. Through RNA sequencing and bioinformatic analysis, we identified the significantly upregulated DEGs in the absence of ZFP36L1 in both cell lines. Furthermore, we also analysed and compared the significantly enriched GO terms to identify the ZFP36L1-mediated functions in both cell lines.

Through analysis of the upregulated DEGs in both MCF-7 and HCT116 cell lines, we found that the inhibition of the ZFP36L1 gene led to the enrichment of distinct sets of DEGs, in which only three DEGs, including *CCL28, IGSF11, and OAS1* were found to be common in both cell lines. These findings demonstrated the divergence in the genes targeted by the ZFP36L1 in MCF-7 and HCT-116 cell lines. As there was no significant enrichment in the HCT116 cell lines according to KEGG pathways, our focus shifted towards a comparison of significantly enriched GO terms in both cell lines. This analytical approach provided us with a means to explore the divergent biological functions of ZFP36L1 within these two cell lines.

In the *Δ ZFP36L1* HCT-116 cell line, several GO terms related to proliferation and migration were found to be significantly enriched, including regulation of epithelial cell proliferation, epithelial cell proliferation, and negative regulation of cell-cell adhesion. (Figure 7.2). Conversely, in the MCF-7 cell line, inhibition of ZFP36L1 resulted in the upregulation of GO terms inhibiting cell migration and mobility, including cell-matrix

adhesion, cell-cell contact zone cell-cell junction and neuronal organisation (Figure 7.3). Previous studies have shown that overexpression of ZFP36L1 leads to the suppression of proliferation, cell-cycle progression and migration in multiple cancer cell lines (Rataj et al., 2019; Loh et al., 2020). Here, we found that silencing of ZFP36L1 was associated with the upregulation of DEGs involved in cell migration in both cell lines and proliferation in HCT-116 cell lines. However, the GO terms and associated DEGs involved in proliferation and migration are entirely different in both cell lines. In the HCT 116 cell line, the upregulated AU-rich DEGs involved with proliferation and migration included *WNT7A, PTN, CCL2, SLC26A9, CEACAM1,* and *LDLRAD4.* The upregulation of these genes might result in increased proliferation and migration in the HCT116 cell line (Table 7.1). On the other hand, in MCF-7 cell lines, the upregulated AU-rich DEGs involved with migration included CD44, CDK6, CASK, TIAM1, UTRN, VEGFC, GCNT1, IL1R1, PTGER4, TNF, ATP1B1, PCDH9 and CASK (Table 7.1). The upregulation of these genes might reduce cell migration in the MCF-7 cell line. These results demonstrated that the loss of ZFP36L1 protein function led to the upregulation of diverse biological pathways in MCF-7 and HCT116 cell lines, highlighting the opposing roles of the ZFP36L1 gene in both cell lines. Furthermore, various GO terms associated with ions transportation and membrane signalling, including cation channel complex, plasma membrane protein complex, ion channel complex and transmembrane transporter complex, were only found enriched in the *Δ ZFP36L1* HCT-116 cell line (Figure 7.2). Similarly, various GO terms associated with regulating and maintaining extracellular matrix were found enriched mostly in the MCF-7 cell line (Figure 7.3). Thus, it is evident that the function of ZFP36L1 varies depending on the cell type.

Although this study demonstrated the cell type-specific role of the ZFP36L1 gene, there were a few limitations associated with this study. The first one is that the size of the samples used in the RNA sequencing study in HCT116 cell lines was relatively small compared to the MCF-7 cell lines. Secondly, the CRISPR-Cas9 gene editing led to the different modifications of the ZFP36L1 gene in both cell lines, where we obtained a complete knockout of ZFP36L1 in the MCF-7 cell line and a truncated model of the ZFP36L1 protein in the HCT 116 cell line. However, in both cases, the zinc finger domain of the ZFP36L1 protein was disrupted, which plays a crucial role in the functioning of ZFP36L1 as an mRNA-decaying protein. In summary, our research has provided a proof-of-concept that ZFP36L1 is involved in modulating distinct and diverse sets of genes across different cell types, contributing to understanding the multifaceted roles of ZFP36L1, which are contingent on the specific cellular context. In HCT 116 cell lines, the truncation of ZFP36L1 led to the upregulation of pro-tumorigenic traits, establishing convincing evidence for further investigations into the precise involvement of ZFP36L1 in the progression of colorectal cancer.

Chapter 8: Overall Discussion, Future Work and Conclusions

8.1 Discussion

Over the past decades, numerous studies have investigated the role of ZFP36L1 in tumorigenesis across various types of cancer. ZFP36L1 is often epigenetically silenced, mutated and downregulated in multiple tumours (Martinez-Calle., 2019; Loh et al., 2020; Rataj et al., 2019; Priestley et al., 2019). Remarkably, the study conducted by Nik-Zainal et al. in 2016 highlighted ZFP36L1 as a novel breast cancer driver gene, which prompted our interest in investigating the function of this gene in breast cancer progression. In this study, we utilised an integrated molecular and transcriptomic approach to explore how ZFP36L1 contributes to tumour progression in the MCF-7 cell line. Furthermore, we aim to unveil the molecular mechanisms and biological pathways governed by ZFP36L1 in breast tumorigenesis.

In this study, we identified a previously unappreciated role of ZFP36L1 in enhancing the sensitivity of MCF-7 cells towards tamoxifen, a standard drug utilised in endocrine therapy. This research provided several lines of evidence demonstrating that loss of ZFP36L1 can reduce the impact of tamoxifen in the MCF-7 cell line. We observed that MCF-7 cells lacking ZFP36L1 exhibited higher cell viability than wild-type treated MCF-7 cells. Wound healing scratch assay showed that tamoxifen treatment reduced the healing capability of MCF-7 cells. However, this effect was less pronounced in the ZFP36L1-depleted MCF-7 cells. Notably, the anti-estrogenic effect of tamoxifen decreased in ZFP36L1-depleted MCF-7 cells, resulting in elevated cyclin D1 protein levels compared to tamoxifen-treated wild-type cells. All these research outcomes have shed light on the synergistic combination of ZFP36L1 with tamoxifen, suggesting that assessing the status of ZFP36L1 could potentially lead to improved therapeutic options for ER/PR+ breast cancer patients when combined with tamoxifen.

Additionally, the study postulated that ZFP36L1 might be critically involved in regulating several tumorigenic traits in the MCF-7 cellular model. The research findings discussed in Chapter 4, including wound healing scratch assay, demonstrated that ZFP36L1 depletion in MCF-7 cells could significantly decrease cell migration capability and increase cyclin D1 and TP53 protein expression levels in MCF-7 cells. Furthermore, transcriptomic analysis revealed that ZFP36L1 loss resulted in significant upregulation of several transcriptomic signatures involved in cell adhesion, extracellular matrix, and glycosylation. Given that ZFP36L1 exerts a negative regulatory effect on the post-transcriptional expression of several ARE-rich genes, we anticipated that the absence of ZFP36L1 would increase the expression of its target genes. Within the upregulated DEGs, we selected and generated a list of upregulated ARE-containing genes that could be the potential downstream targets of ZFP36L1 in the MCF-7 cell line. Notably, numerous GO terms and KEGG pathways associated with upregulated AU-rich DEGs were involved in cell adhesion, cell mobility, extracellular matrix and glycosylation pathways. These results indicated that ZFP36L1 could be directly modulating the expression of several genes encoding for migration and distant metastases, which collectively lead to the microenvironment conducive to tumourigenesis.

Previous literature has extensively reported an inverse correlation between ZFP36L1 and cell-cycle-related proteins (Galloway et al., 2016; Vogel et al., 2016; Loh et al., 2020). This evidence underscores the critical function of ZFP36L1 in negatively regulating the expression of several important cell-cycle-related proteins containing ARE sequences. Supporting these results, integrated investigation through western blot and RNA-sequencing analysis revealed that ZFP36L1 depletion increased protein expression levels of Cyclin D1 and upregulated *CDK6* mRNA levels in MCF-7 cells.

CyclinD1 and *CDK6* regulate the G1 to S phase progression in the cell cycle, and both exhibit ARE sequences in the 3'UTR of their mRNA. Taken together, these results suggested that ZFP36L1 acts as a direct mediator of multiple cell-cycle-associated genes that control the cell cycle transition from G1 to S phase in MCF-7 cells. Furthermore, contrasting to the findings of Suk et al. 2018, the loss of ZFP36L1 increased the TP53 protein levels, a tumour suppressor gene, suggesting that ZFP36L1 could be indirectly involved in meditating TP53 expression, given that *TP53* does not contain ARE-sequences in its mRNA. Depletion of ZFP36L1 increased protein expression levels of MCM-7, which lacks ARE-sequences. ZFP36L1 also mediates other subunits of the heteromeric MCM helicase containing ARE-sequences, including *MCM-6* and *MCM-2.* These experimental data underscore the potential role of ZFP36L1 in regulating the crucial elements of DNA replication in MCF-7 cells, thus opening new avenues for investigating ZFP36L1's function in DNA damage and replication within the context of breast cancer.

Recently, few studies have discussed the emerging roles of the ZFP36L1 gene as ambiguous (Kaehler et al., 2021; Yuan et al., 2022), which was previously established as a tumour-suppressing gene in various malignancies (Martinez-Calle., 2019; Loh et al., 2020, Rataj et al., 2019). In this study, we found that ZFP36L1 behaves in a contrasting and ambiguous way in breast tumorigenesis. Consistent with the Yuan et al., 2022 study, our research findings demonstrated that the ZFP36L1 depletion in MCF-7 upregulated the expression levels of cell-cycle-related genes, including *cyclinD1* and *CDK6* and decreased the sensitivity of MCF-7 cells toward tamoxifen, exhibiting tumour suppressing properties. Conversely, ZFP36L1 depletion in MCF-7 cells significantly reduced cell migration in the MCF-7 cell line, indicating tumour-promoting effects. These findings suggest that the role of the ZFP36L1 in breast

tumorigenesis is complex, and it may exhibit both tumour-suppressing and tumour-promoting properties depending on the specific aspects of breast tumorigenesis being considered. Further, these research outcomes highlight further in-depth investigation to understand its role in breast cancer development and progression.

8.2 Prospects for Future Studies

Our study has established a clear link between the absence of ZFP36L1 and reduced responsiveness to tamoxifen in MCF-7 cells. To reinforce these findings and potentially apply them in clinical settings, a thorough investigation of ZFP36L1*'s* role in tamoxifen-resistant MCF-7 cells could be considered in future research. Further studies into the intricate role played by ZFP36L1 protein in tamoxifen-resistant MCF-7 cells will enhance the robustness and improve the overall reliability of the existing research outcomes. Since tamoxifen resistance in hormone-positive breast cancer remains a persistent challenge in clinical practice, it underscores the importance of expanding our understanding of the underlying molecular mechanisms leading to tamoxifen resistance.

Subsequently, evaluating ZFP36L1 expression levels within a cohort of tamoxifen-resistant ER+ breast cancer patients will be a potential step in gaining deeper insights into the association between ZFP36L1 expression and tamoxifen resistance. However, this should not be viewed in isolation; it should be complemented by a comprehensive analysis of its correlation with clinical outcomes, including disease-free survival, overall survival, and distant metastases survival. Such an integrated approach is essential to shed light on the clinical benefits that ZFP36L1 may confer in the context of tamoxifen resistance. Furthermore, addressing questions such as: Does upregulation of ZFP36L1 signify a potential biomarker for treatment response or

prognosis? Does its downregulation hint at a pathway to overcome tamoxifen resistance? Finding solutions to these queries will serve to bridge the gap between basic research and tangible clinical applications.

8.3 Conclusion

Considering the ambiguous and opposing role played by the ZFP36L1 gene, it would be challenging to clearly define ZFP36L1 as a tumour-suppressing or tumour-promoting gene. However, the work presented in this thesis has comprehensively investigated the involvement of ZFP36L1 in the tumour progression in the MCF-7 cell line and contributed to understanding the multifaceted role of ZFP36L1 in breast tumour progression. Moreover, this study has brought to the attention the potential of ZFP36L1 as a therapeutic target in combination with tamoxifen, which can be further extended and investigated in future research.

Appendices

Appendix A

Table A1 STR profiling of MCF-7 and HCT 116 cells provided by Eurofins.

Sample Code	MCF-7 Cell line	HCT116 Cell line
D8S1179	9,10,13,14	10,11,12,13,14,15
D21S11	30,30	29,30
D7S820	8,9	11,12
CSF1PO	10,10	7,10,11
D3S1358	16,16	12,13,17,18,19
TH01	6,6	8,9
D13S317	11,11	10,12,13
D16S539	11,12,13,	10,11,12,13,14
D2S1338	21,23	15,16
D19S433	13,14	12,13
vWA	14,15	17,21,22,23
TPOX	9,12	8,9
D18S51	14,14	16,17,18
AMEL	X,X	X,Y
D5S818	11,12	10,11
FGA	23,25	18,19.2,22,23,24

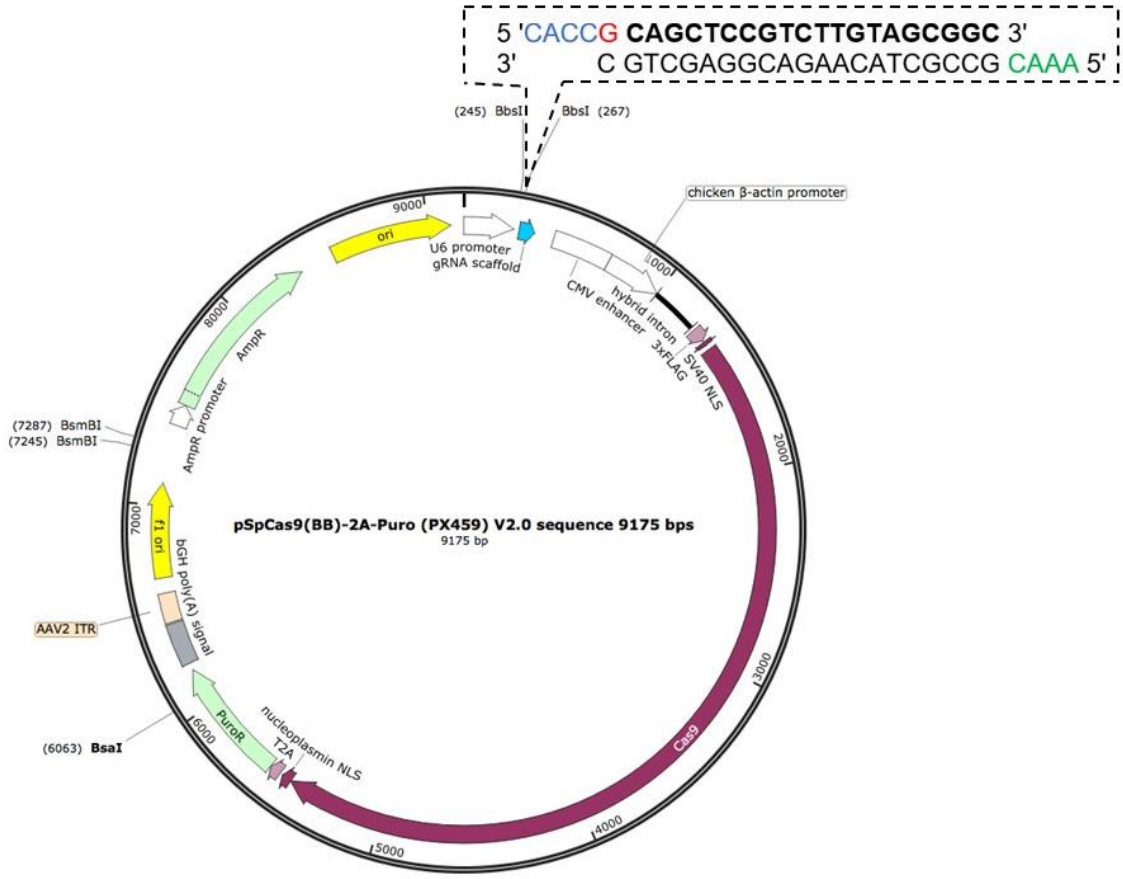

Figure A1: Schematic representation of single guide RNA cloning into pSpCas9(BB)-2A-Puro (PX459) plasmid. pSpCas9(BB)-2A-Puro (PX459) plasmid consist of a Cas9-expression cassette and sgRNA scaffold. BbsI restriction sites near the sgRNA scaffold represent the region used for cloning the designed gRNA oligos. Selectable markers, ampicillin and puromycin, aided in the selection of transformed bacterial and transfected mammalian cells, respectively, due to the presence of an ampicillin and puromycin-resistant gene in pSpCas9(BB)-2A-Puro (PX459) plasmid. Image adapted from Addgene.

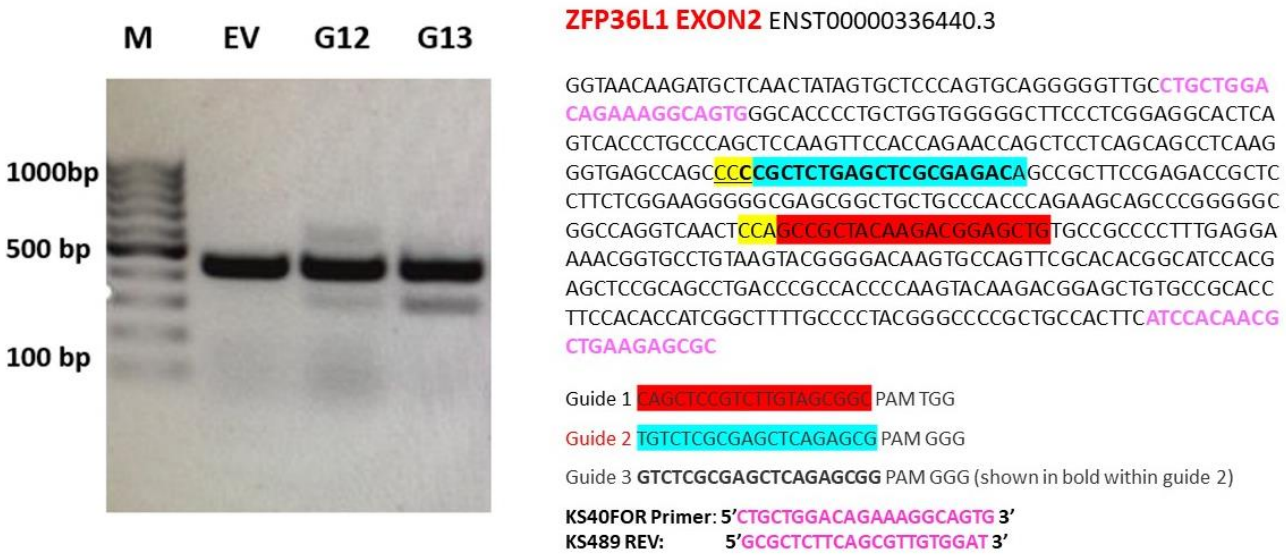

Figure A2: PCR amplification of ZFP36L1 gene, with amplicon length of 449 base pairs, in MCF-7 cells to assess gene editing. On the left side, a gel image is shown, representing the cell pools transfected with empty vectors without sgRNAs (EV), a combination of guide1 and guide 2 (G12), and a combination of guide1 and guide 3 (G13), and marker (M). Exon 2 of the ZFP36L1 gene sequence is represented on the right side, where the 449 base pairs sequence is amplified using primers (highlighted in pink). Guide1, guide2 and guide3 are highlighted in red, blue, and grey, respectively, and the corresponding PAM sites are highlighted in yellow. Guide 2 overlaps guide 3 (shown in bold letters in blue), targets the same site, and only differs in one base pair sequence.

Appendix B

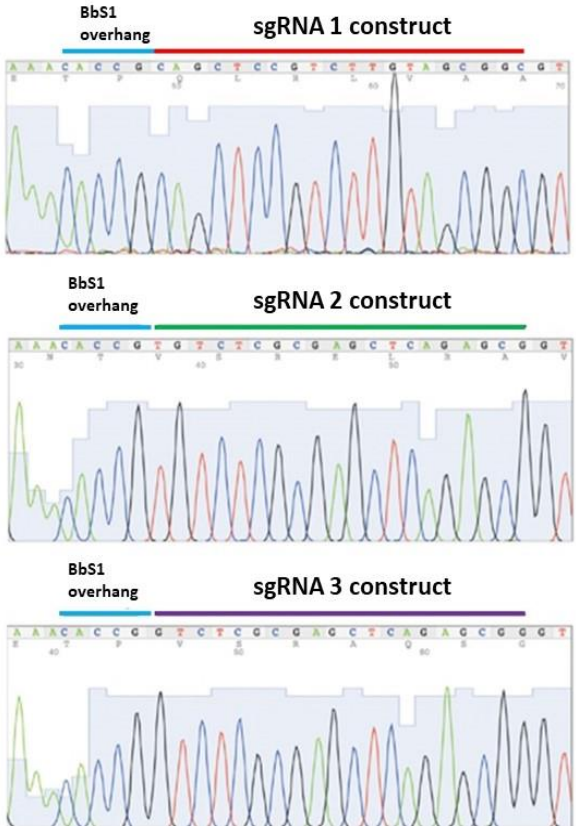

Figure B1: Sequence validation of pSpCas9(BB)-2A-Puro plasmid expressing ZFP36L1 sgRNA plasmid. Chromatograms obtained from the Sanger sequencing revealed that all the guide RNAs (sgRNA 1, sgRNA 2, and sgRNA 3) were successfully cloned separately at the BbsI restriction site in pSpCas9(BB)-2A-Puro plasmid.

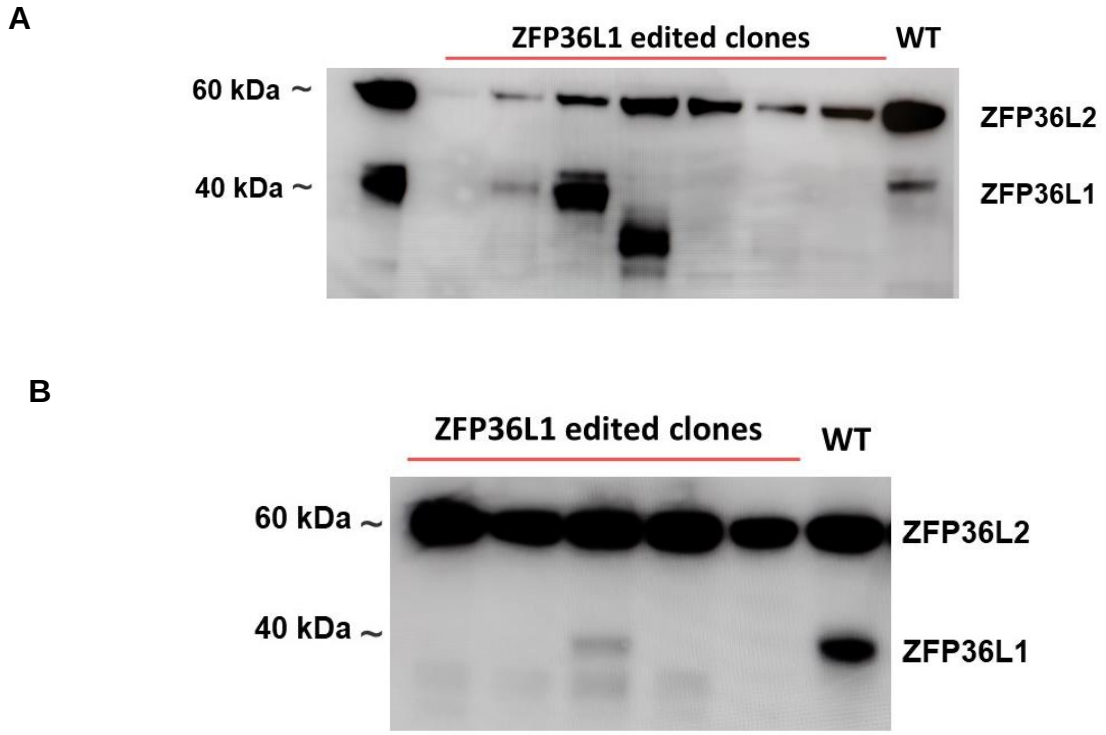

Figure B2: A and **B** represent the western blot screening by investigating the protein expression levels of ZFP36L1 and ZFP36L2 in edited monoclones in MCF-7 cells. Different types of ZFP36L1 protein expression are exhibited by the edited monoclones, including no protein expression, truncated expression (the ones running lower than WT), and heterogeneous expression (the ones expressing two bands). WT and unedited clones showed regular expression of ZFP36L1 protein. Western blot indicated no difference in the ZFP36L2 expression. 40 kDa corresponds to ZFP36L1, and 60 kDa corresponds to ZFP36L2.

A

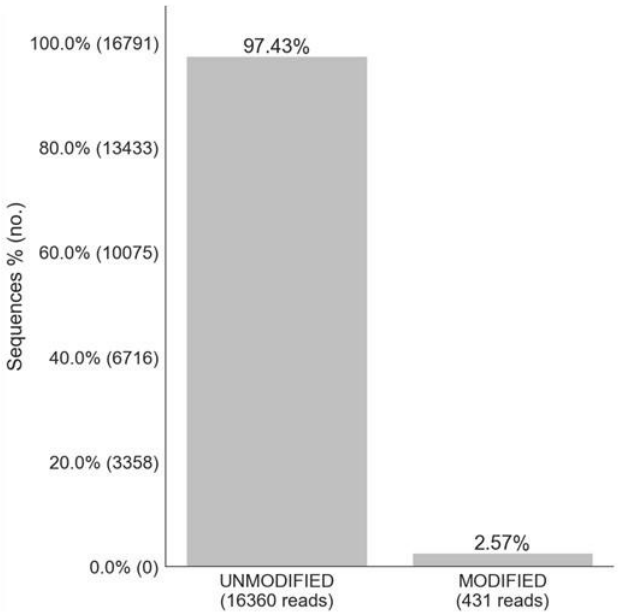

B

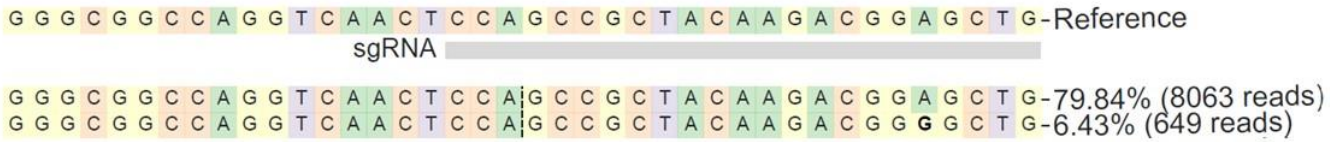

Figure B3: A and B representing NGS analysis of MCF-7 cells transfected with empty vector (EV). A represents the histogram of the percentage of the modified cell population (defined by reads) in WT MCF-7 cells. B represents the allele frequency table around the ZFP36L1 target site in WT-MCF-7 cells.

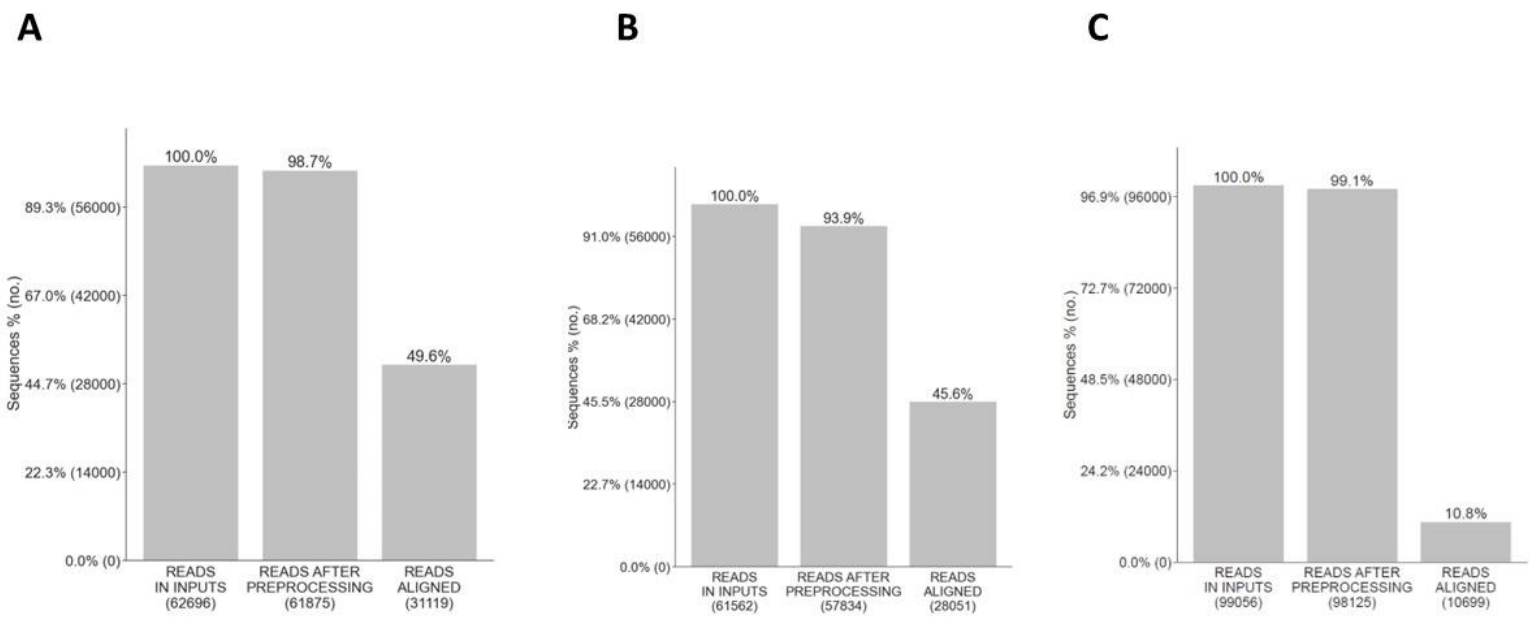

Figure B4: A, B and C represent the alignment barplot of the reads of F7, D3, and B4 clones obtained through NGS analysis. The reads obtained from edited monoclones were mapped with the reference sequence from the MCF-7 cells transfected with an empty vector. The figure was generated using the CRISSRESSO online software.

Appendix C

Table C1 Tamoxifen drug concentrations and their corresponding log values used in contructing the dose response curve (Figure 4.1).

Tamoxifen Conc. (nM)	500,000	100,000	20,000	4000	800	160	32	6.4
Tranformed log values	5.70	5.00	4.30	3.60	2.90	2.20	1.50	0.80

Table C2 Palbocilib drug concentrations and their corresponding log values used in constructing the dose response curve (Figure 5.1).

Palbociclib Conc. (nM)	500,000	250,000	125,000	62500	31200	15600	7800	3900	1950
Tranformed log values	5.70	5.40	5.09	4.79	4.50	4.20	3.90	3.60	3.30

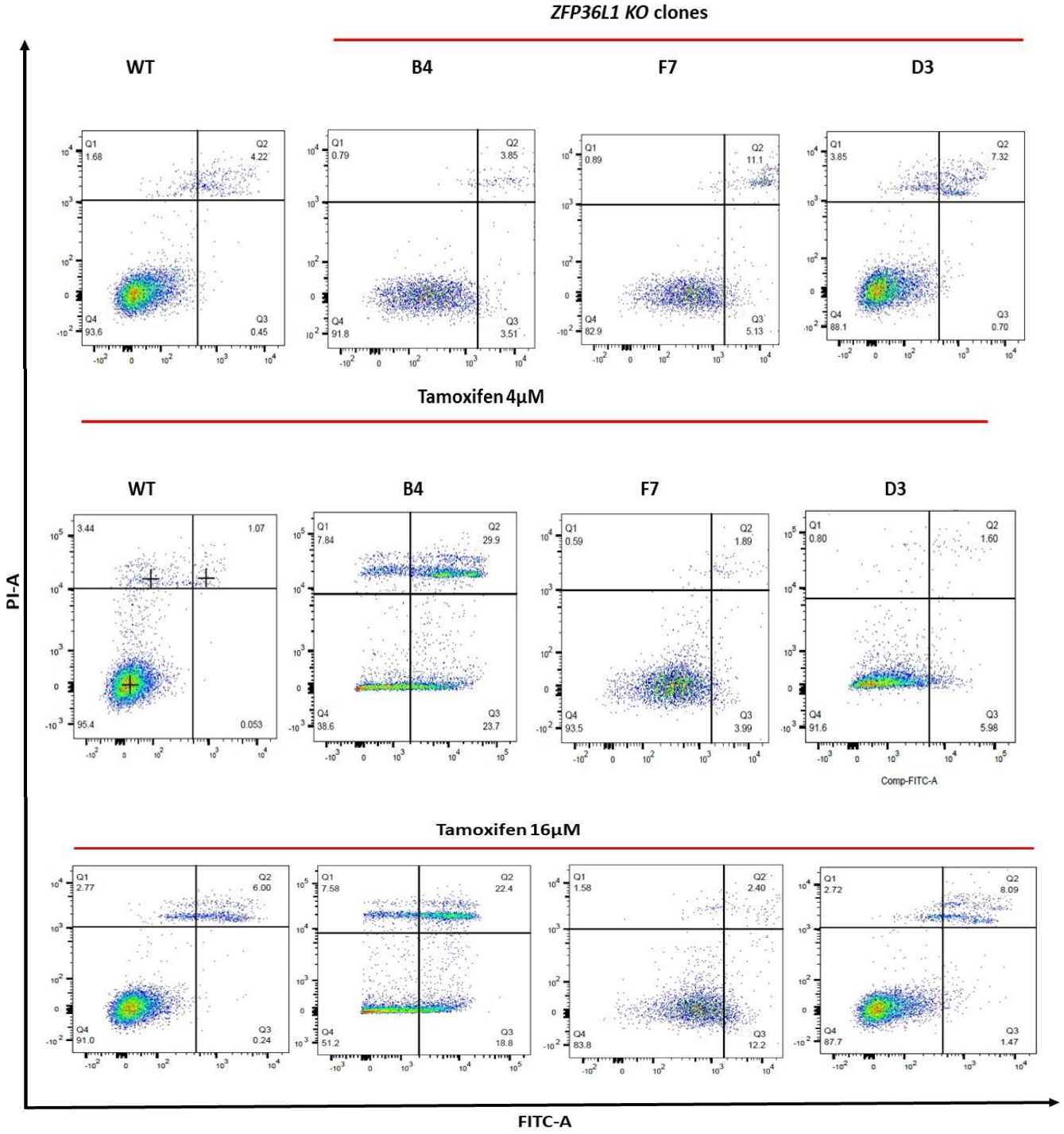

Figure C1: Representative images of PI/Annexin V apoptotic analysis stained MCF-7 cells. In the graphs, the X-axis represents Annexin V (FITC) stained cells, whereas the Y-axis represents (PI) stained cells. All the graphs are divided into four quadrants (Q), where Q1 represents late apoptotic cells, q2 represents the apoptotic cells, q3 represents the early apoptotic cells, and q4 represents the live cells, respectively. The images were generated using FlowJo software.

Appendix D

Table D1 List of upregulated AU-rich differentially expressed genes identified in the RNA-Seq data.

Gene Symbol	Ensembl Gene ID	Gene description	Log2 Fold Change	Padj-value	(%) Mutated genes frequency (cBio portal)
ABCA12	ENSG00000144452	ATP binding cassette subfamily A member 12	1.1418994	0.021495	1.6
ABCC2	ENSG00000023839	ATP binding cassette subfamily C member 2	3.0329259	1.26E-06	0.9
ABLIM1	ENSG00000099204	actin binding LIM protein 1	1.182572	9.77E-05	0.4
ADGRE2	ENSG00000127507	adhesion G protein-coupled receptor E2	1.685227	0.039346	0.9
ADGRL3	ENSG00000150471	adhesion G protein-coupled receptor L3	1.0189219	0.019898	1.1
ARHGAP42	ENSG00000165895	Rho GTPase activating protein 42	1.2414719	0.000956	0.8
ASPH	ENSG00000198363	aspartate beta-hydroxylase	1.3603476	3.44E-11	0.6
ATP1B1	ENSG00000143153	ATPase Na+/K+ transporting subunit beta 1	1.4343653	1.95E-16	0.3
ATXN1	ENSG00000124788	Ataxin 1	1.1395342	3.79E-07	1
BACH2	ENSG00000112182	BTB domain and CNC homolog 2	1.4064604	0.042068	1.3
BMPR1B	ENSG00000138696	bone morphogenetic protein receptor type 1B	1.0960075	0.016841	0.6
BTC	ENSG00000174808	betacellulin	1.7785901	0.034837	0.3
C3orf80	ENSG00000180044	chromosome 3 open reading frame 80	1.4006628	0.039493	1.2
CASK	ENSG00000147044	calcium/calmodulin-dependent serine protein kinase	1.1896429	5.18E-06	1
CASQ2	ENSG00000118729	Calsequestrin 2	1.8332988	0.005116	0.6
CD44	ENSG00000026508	CD44 molecule (Indian blood group)	1.2450146	4.50E-11	0.4
CDK6	ENSG00000105810	Cyclin dependent kinase 6	1.3266417	1.15E-10	0.2
CEMIP	ENSG00000103888	cell migration inducing hyaluronidase 1	1.4165161	1.41E-05	1
CEP126	ENSG00000110318	Centrosomal protein 126	1.1889025	0.020098	0.8
CHSY3	ENSG00000198108	chondroitin sulfate synthase 3	1.445101	0.049391	0.7
CREG2	ENSG00000175874	cellular repressor of E1A stimulated genes 2	1.1588387	2.04E-05	0.4
CSGALNACT1	ENSG00000147408	chondroitin sulfate N-acetylgalactosaminyltransferase 1	2.158275	8.71E-12	0.2

CXCR4	ENSG00000121966	C-X-C motif chemokine receptor 4	2.1120313	2.48E-16	0.3
DOCK10	ENSG00000135905	dedicator of cytokinesis 10	1.7435854	3.93E-05	1.2
DUSP4	ENSG00000120875	dual specificity phosphatase 4	1.652907	1.26E-08	0.3
EFEMP1	ENSG00000115380	EGF containing fibulin extracellular matrix protein 1	1.0967684	1.68E-08	0.6
FRK	ENSG00000111816	fyn related Src family tyrosine kinase	1.2422029	0.002102	0.2
GALNT7	ENSG00000109586	polypeptide N-acetylgalactosaminyltransferase 7	1.0785838	5.80E-06	0.6
GCNT1	ENSG00000187210	glucosaminyl (N-acetyl) transferase 1, core 2	1.7288793	1.02E-09	0.5
GPM6A	ENSG00000150625	glycoprotein M6A	2.3207232	7.09E-05	0.2
HS3ST5	ENSG00000249853	heparan sulfate-glucosamine 3-sulfotransferase 5	1.9829232	8.54E-10	0.6
IL1R1	ENSG00000115594	interleukin 1 receptor type 1	1.0510986	3.50E-07	0.3
KCND2	ENSG00000184408	potassium voltage-gated channel subfamily D member 2	3.8681203	0.001713	0.8
KDELC2	ENSG00000178202	KDEL motif containing 2	1.2874778	6.10E-08	N/A
KIAA1324	ENSG00000164659	KIAA1324	1.9602329	4.46E-11	N/A
KIAA1549	ENSG00000122778	KIAA1549	1.0354874	1.51E-06	1
MAFF	ENSG00000185022	MAF bZIP transcription factor F	1.057716	0.004638	0.1
MAOA	ENSG00000189221	monoamine oxidase A	2.5531915	2.52E-17	0.4
MEGF9	ENSG00000106780	multiple EGF like domains 9	1.002121	1.71E-07	0.4
MXD1	ENSG00000059728	MAX dimerization protein 1	1.1768692	8.53E-05	0.2
NAV3	ENSG00000067798	neuron navigator 3	3.7375489	0.008399	1.8
NOVA1	ENSG00000139910	NOVA alternative splicing regulator 1	1.056388	0.019382	0.4
NPR3	ENSG00000113389	natriuretic peptide receptor 3	1.6738986	1.33E-05	0.5
NR3C2	ENSG00000151623	nuclear receptor subfamily 3 group C member 2	1.4288702	0.037174	0.7
NTNG1	ENSG00000162631	netrin G1	2.689786	0.021065	0.5
PAQR8	ENSG00000170915	progestin and adipoQ receptor family member 8	1.0230901	7.87E-05	0.4
PARM1	ENSG00000169116	prostate androgen-regulated mucin-like protein 1	1.6942744	6.38E-09	0.2
PCDH11X	ENSG00000102290	protocadherin 11 X-linked	1.4143289	0.031122	1.5
PCDH9	ENSG00000184226	protocadherin 9	1.3410098	2.04E-07	1
PCDHB10	ENSG00000120324	protocadherin beta 10	1.3984564	0.002661	0.6
PCDHB4	ENSG00000081818	protocadherin beta 4	1.0784715	0.011763	0.6
PCLO	ENSG00000186472	piccolo presynaptic cytomatrix protein	1.0615358	0.015608	3.3

PLAT	ENSG00000104368	plasminogen activator, tissue type	1.9816151	0.030659	0.5
POF1B	ENSG00000124429	POF1B, actin binding protein	1.1009161	2.24E-06	0.6
POU3F2	ENSG00000184486	POU class 3 homeobox 2	2.083527	0.025308	0.3
PRLR	ENSG00000113494	prolactin receptor	1.1081403	2.00E-08	0.4
PTGER4	ENSG00000171522	prostaglandin E receptor 4	1.4069008	0.000149	0.2
RAB27A	ENSG00000069974	RAB27A, member RAS oncogene family	1.0630312	5.17E-10	0.2
RAB27B	ENSG00000041353	RAB27B, member RAS oncogene family	1.5698964	5.14E-17	0.2
RAET1L	ENSG00000155918	retinoic acid early transcript 1L	1.4622519	0.001183	0.6
RAPGEF5	ENSG00000136237	Rap guanine nucleotide exchange factor 5	1.5414727	1.35E-05	0.5
RASL11B	ENSG00000128045	RAS like family 11 member B	1.1379731	0.004933	0.3
SLC12A2	ENSG00000064651	solute carrier family 12 member 2	1.4001379	7.47E-12	0.5
SLC16A6	ENSG00000108932	solute carrier family 16 member 6	1.0776151	0.000146	0.3
SLC1A1	ENSG00000106688	solute carrier family 1 member 1	1.3462314	0.029051	0.3
SLC2A10	ENSG00000197496	solute carrier family 2 member 10	1.6857544	6.20E-22	0.4
SLITRK1	ENSG00000178235	SLIT and NTRK like family member 1	2.894724	0.017464	0.6
SLITRK6	ENSG00000184564	SLIT and NTRK like family member 6	1.6644706	6.97E-07	0.9
SOX2	ENSG00000181449	SRY-box 2	1.0971111	0.001385	0.4
SOX21	ENSG00000125285	SRY-box 21	2.5992075	0.006677	0.5
SYT16	ENSG00000139973	synaptotagmin 16	1.913857	0.046849	0.8
TCAF2	ENSG00000170379	TRPM8 channel associated factor 2	1.7878073	5.01E-05	0.3
TIAM1	ENSG00000156299	T cell lymphoma invasion and metastasis 1	1.1670093	1.11E-05	0.6
TMEM47	ENSG00000147027	transmembrane protein 47	1.9721807	0.000105	0.1
TNF	ENSG00000228321	tumor necrosis factor	1.550917	0.045135	0.4
TTC28	ENSG00000100154	tetratricopeptide repeat domain 28	1.0288153	0.004677	1.3
TTC9	ENSG00000133985	tetratricopeptide repeat domain 9	1.2320416	2.19E-05	0.2
UTRN	ENSG00000152818	utrophin	1.0507781	6.38E-05	3.2
VCAN	ENSG00000038427	versican	3.8298431	0.001335	2.2
VEGFC	ENSG00000150630	vascular endothelial growth factor C	1.0052323	0.00051	0.2
XK	ENSG00000047597	X-linked Kx blood group	1.0371377	0.006638	0.4
XPR1	ENSG00000143324	xenotropic and polytropic retrovirus receptor 1	1.0521314	1.37E-10	0.6
ZNF750	ENSG00000141579	zinc finger protein 750	1.7614644	0.003078	0.2

Table D2 List of significant GO-enriched terms obtained for the upregulated DEGs and AU-rich upregulated DEGs.

GO	Description	Gene Names	AU-rich gene names	(%) AU-rich genes
BP	Glycosaminoglycan biosynthetic process	CSGALNACT1/HS3ST5/CEMIP/HS3ST3A1/VCAN/UGDH/GCNT2/CHSY3	CSGALNACT1/HS3ST5/CEMIP/VCAN/CHSY3	63%
BP	Monovalent inorganic anion homeostasis	SLC12A2/XPR1/ABCC2/FGFR4	SLC12A2/XPR1/ABCC2/	75%
BP	Glycosaminoglycan metabolic process	CSGALNACT1/CD44/HS3ST5/CEMIP/HS3ST3A1/VCAN/UGDH/GCNT2/CHSY3	CSGALNACT1/CD44/HS3ST5/CEMIP/VCAN/CHSY3	67%
BP	Cell-matrix adhesion	LYPD3/CD44/CDK6/SEMA3E/CCL28/CASK/TIAM1/UTRN/VEGFC/NEXMIF	CD44/CDK6/CASK/TIAM1/UTRN/VEGFC	60%
BP	Cellular extravasation	GCNT1/CCL28/IL1R1/PTGER4/TNF	GCNT1/IL1R1/PTGER4/TNF	80%
BP	Regulation of cell-matrix adhesion	CDK6/SEMA3E/CCL28/CASK/UTRN/VEGFC/NEXMIF	CDK6/CASK/UTRN/VEGFC	58%
BP	Aminoglycan metabolic process	CSGALNACT1/CD44/HS3ST5/CEMIP/HS3ST3A1/VCAN/UGDH/GCNT2/CHSY3	CSGALNACT1/CD44/HS3ST5/CEMIP/VCAN/CHSY3	66%
BP	Leukocyte migration	CEACAM6/CEACAM5/ATP1B1/CXCR4/CD44/GCNT1/VAV3/CCL28/IL1R1/PTGER4/VEGFC/ADGRE2/TNF	ADGRE2/ATP1B1/CXCR4/CD44/GCNT1/IL1R1/PTGER4/VEGFC/TNF	61%
BP	Regulation of heterotypic cell-cell adhesion	CD44/GCNT2/TNF	CD44/TNF	66%
BP	Proteoglycan biosynthetic process	CSGALNACT1/HS3ST5/VCAN/BMPR1B/CHSY3	CSGALNACT1/HS3ST5/VCAN/BMPR1B/VCAN	100%
BP	Aminoglycan biosynthetic process	CSGALNACT1/HS3ST5/CEMIP/HS3ST3A1/VCAN/UGDH/GCNT2/CHSY3	ABCA12/MAFF/POU3F2/CSGALNACT1/HS3ST5/CEMIP/VCAN/CHSY3	100%
CC	Proteinaceous extracellular matrix	EFEMP1/KAZALD1/MEGF9/AMTN/SLITRK6/ADAMTS17/CASK/FBLN1/ZG16/VCAN/COL6A2/LRRN1/SLITRK1/TFF3/TNFRSF11B	EFEMP1/MEGF9/SLITRK6/CASK/VCAN/SLITRK1	40%

CC	Extracellular matrix	EFEMP1/KAZALD1/MEGF9/AMTN/SLITRK6/ADAMTS17/CASK/FBLN1/ZG16/VCAN/COL6A2/CDH2/LRRN1/SLITRK1/PRSS2/TFF3/TNFRSF11B	EFEMP1/MEGF9/SLITRK6/CASK/VCAN/SLITRK1	40%
CC	Synaptic membrane	CLSTN2/CHRM1/SHC4/CADPS2/CASK/ANK3/UTRN/CPE/KCND2/KCNMA1/GLRA3/CDH2/GRIK2	CASK/UTRN/KCND2	23%
CC	Postsynaptic membrane	CLSTN2/CHRM1/SHC4/CADPS2/ANK3/UTRN/KCND2/KCNMA1/GLRA3/CDH2/GRIK2	UTRN/KCND2	19%
CC	Post-synapse	CLSTN2/CHRM1/SHC4/CADPS2/TIAM1/ANK3/DOCK10/UTRN/GPM6A/KCND2/KCNMA1/NTSR1/GLRA3/CDH2/GRIK2/PCLO	TIAM1/DOCK10/UTRN/GPM6A/KCND2/PCLO	37.50%
CC	Cell-cell contact zone	ATP1B1/PCDH9/TIAM1/ANK3/FGF13/CDH2	ATP1B1/PCDH9/TIAM1/	50%
CC	Cell-cell junction	ATP1B1/PCDH9/AMTN/ABCC2/POF1B/OXTR/CASK/TIAM1/ANK3/FGF13/AKR1B1/TMEM47/FGFR4/CGNL1/CDH2/ADGRL3	ATP1B1/PCDH9/ABCC2/POF1B/CASK/TIAM1/TMEM47/ADGRL3	50%
CC	Anchored component of membrane	CEACAM6/CEACAM5/RAB27B/LYPD3/MDGA2/RAET1L/LY6G6C/NTNG1	RAB27B3/RAET1L/NTNG1	37.50%
CC	Golgi lumen	MUCL1/CGA/ZG16/VCAN/MUC5B/MUC5AC	VCAN	16.60%
CC	Apical plasma membrane	RAB27B/ATP1B1/SLC12A2/CD44/RAB27A/ABCC2/OXTR/ANO1/KCNMA1/CDH2/SLC1A1	RAB27B/ATP1B1/SLC12A2/CD44/RAB27A/ABCC2/SLC1A1	63.60%
MF	Acetylglucosaminyl transferase activity	CSGALNACT1/GALNT10/GALNT7/GALNT12/GALNT13/CHSY3	CSGALNACT1/GALNT7/CHSY3	50%
MF	Polypeptide N-acetylgalactosaminyl transferase activity	GALNT10/GALNT7/GALNT12/GALNT13	GALNT7	25%

Table D3 List of significantly enriched KEGG pathways obtained for the upregulated DEGs and AU-rich upregulated DEGs.

KEGG enriched pathways	Genes Name	AU-rich Gene Name	AU-rich genes percentage
Phenylalanine metabolism (n=4)	MAOA/ALDH3A1/ALDH3B2/MAOB	MAOA	25%
Mucin type O-glycan biosynthesis (n=5)	GCNT1/GALNT10/GALNT7/GALNT12/ GALNT13	GCNT1/GALNT7	40%
Histidine metabolism (n=4)	MAOA/ALDH3A1/ALDH3B2/MAOB	MAOA	25%
Neuroactive ligand-receptor interaction (n=10)	CHRM1/PRLR/S1PR3/OXTR/CGA/ PTGER4/NTSR1/GLRA3/GRIK2/SSTR5	PRLR/PTGER4	20%
Cytokine-cytokine receptor interaction (n=10)	CXCR4/TNFRSF19/CCL28/PRLR/IL1R1/ IL1R2/IL27RA/BMP6/ BMPR1B/TNFRSF11B	CXCR4/PRLR/IL1R1/ BMPR1B	20%
Tyrosine metabolism (n=4)	MAOA/ALDH3A1/ALDH3B2/MAOB	MAOA	25%

Table D4 List of significantly enriched GO terms obtained for the downregulated DEGs.

Category	Description	Gene Name
BP	Chondrocyte differentiation	COL27A1/CTGF/TGFBI/SULF1/SNAI2/WNT5B/MAF/SCIN/FGF18/ADAMTS7/PTHLH/SOX6/GPLD1
BP	Connective tissue development	COL27A1/CTGF/TGFBI/PLA2G16/SULF1/SNAI2/COL5A1/WNT5B/MAF/SCIN/BMP1/COL11A2/HOXC4/SELENOM/FGF18/ADAMTS7/PTHLH/SOX6/GPLD1
BP	Cartilage development	COL27A1/CTGF/TGFBI/SULF1/SNAI2/WNT5B/MAF/SCIN/BMP1/COL11A2/HOXC4/FGF18/ADAMTS7/PTHLH/SOX6/GPLD1
BP	Regulation of endopeptidase activity	DLC1/PYCARD/FYN/CST6/CTGF/SERPINA3/BIRC7/SERPINF1/TNFSF10/CPAMD8/TNFSF15/FAS/TFPI2/SERPINA1/SERPINA5/CTSH/SPINK4/PZP/WFDC2/TNFRSF10C/A2ML1/TIMP4
BP	Regulation of chondrocyte differentiation	CTGF/SNAI2/MAF/SCIN/FGF18/ADAMTS7/PTHLH/SOX6
BP	Regulation of cartilage development	CTGF/SNAI2/MAF/SCIN/BMP1/FGF18/ADAMTS7/PTHLH/SOX6
BP	Nucleosome assembly	HIST1H3G/HIST1H4H/HIST1H4E/HIST2H2BF/HIST2H3D/HIST4H4/HIST1H3B/HIST1H1D/HIST1H2BF/HIST1H1E/HIST1H2BJ/HIST2H4A/HIST1H2BO
BP	Regulation of peptidase activity	DLC1/PYCARD/FYN/CST6/CTGF/SERPINA3/BIRC7/SERPINF1/TNFSF10/CPAMD8/TNFSF15/FAS/TFPI2/SERPINA1/SERPINA5/CTSH/SPINK4/PZP/WFDC2/TNFRSF10C/A2ML1/TIMP4
BP	Chromatin silencing at rDNA	HIST1H3G/HIST1H4H/HIST1H4E/HIST2H3D/HIST4H4/HIST1H3B/HIST2H4A
BP	Skeletal system development	TGFB2/COL3A1/COL12A1/COL27A1/CTGF/TGFBI/FREM1/SULF1/SNAI2/WNT5B/MAF/SCIN/BMP1/COL11A2/HOXC4/FGF18/DHRS3/HOXC9/ADAMTS7/PTHLH/HOXC8/SOX6/TBX1/GPLD1
CC	Nucleosome	HIST1H3G/HIST1H4H/HIST1H4E/HIST2H2BF/HIST1H2AE/HIST2H3D/HIST4H4/HIST1H3B/HIST1H1D/HIST1H2BF/HIST1H1E/HIST1H2BJ/HIST2H2AA3/HIST2H4A/HIST1H2BO
CC	DNA packaging complex	HIST1H3G/HIST1H4H/HIST1H4E/HIST2H2BF/HIST1H2AE/HIST2H3D/HIST4H4/HIST1H3B/HIST1H1D/HIST1H2BF/HIST1H1E/HIST1H2BJ/HIST2H2AA3/HIST2H4A/HIST1H2BO
CC	Extracellular matrix	TGM2/TGFB2/COL3A1/COL12A1/LAMB1/COL27A1/CTGF/TGFBI/CCDC80/FREM1/SERPINF1/COL5A1/TFPI2/VWA2/WNT5B/SERPINA1/BMP1/COL11A2/LAMA3/WNT4/CSPG4/ADAMTS7/MMP11/TIMP4/A1BG/GPLD1
CC	Proteinaceous extracellular matrix	COL3A1/COL12A1/LAMB1/COL27A1/CTGF/TGFBI/CCDC80/FREM1/SERPINF1/COL5A1/TFPI2/VWA2/WNT5B/SERPINA1/BMP1/COL11A2/LAMA3/WNT4/ADAMTS7/MMP11/TIMP4/GPLD1

CC	Extracellular matrix component	COL3A1/COL12A1/LAMB1/COL27A1/TGFBI/CCDC80/FREM1/SERPINF1/COL5A1/VWA2/COL11A2/LAMA3
CC	Nuclear nucleosome	HIST1H3G/HIST1H4H/HIST1H4E/HIST4H4/HIST1H3B/HIST1H1E/HIST2H4A
CC	Protein-DNA complex	HIST1H3G/HIST1H4H/HIST1H4E/HIST2H2BF/HIST1H2AE/HIST2H3D/HIST4H4/HIST1H3B/HIST1H1D/HIST1H2BF/HIST1H1E/HIST1H2BJ/HIST2H2AA3/HIST2H4A/HIST1H2BO
CC	Fibrillar collagen trimer	COL3A1/COL27A1/COL5A1/COL11A2
MF	Serine-type endopeptidase inhibitor activity	SERPINA3/SERPINF1/CPAMD8/TFPI2/SERPINA1/SERPINA5/SPINK4/PZP/WFDC2/A2ML1
MF	Peptidase regulator activity	PYCARD/CST6/SERPINA3/BIRC7/SERPINF1/CPAMD8/TFPI2/SERPINA1/SERPINA5/CTSH/SPINK4/PZP/WFDC2/A2ML1/TIMP4
MF	Endopeptidase inhibitor activity	CST6/SERPINA3/BIRC7/SERPINF1/CPAMD8/TFPI2/SERPINA1/SERPINA5/SPINK4/PZP/WFDC2/A2ML1/TIMP4
MF	Endopeptidase regulator activity	CST6/SERPINA3/BIRC7/SERPINF1/CPAMD8/TFPI2/SERPINA1/SERPINA5/SPINK4/PZP/WFDC2/A2ML1/TIMP4
MF	Peptidase inhibitor activity	CST6/SERPINA3/BIRC7/SERPINF1/CPAMD8/TFPI2/SERPINA1/SERPINA5/SPINK4/PZP/WFDC2/A2ML1/TIMP4
MF	Immunoglobulin binding	FCGR1A/FCGRT/FCGR2B/FCGR1B
MF	Extracellular matrix structural constituent	COL3A1/COL12A1/LAMB1/COL27A1/COL5A1/TFPI2/COL11A2
MF	Cytokine activity	TGFB2/INHBA/IL24/CCL26/TNFSF10/TNFSF15/CMTM3/BMP1/CMTM7/FAM3B

Appendix E

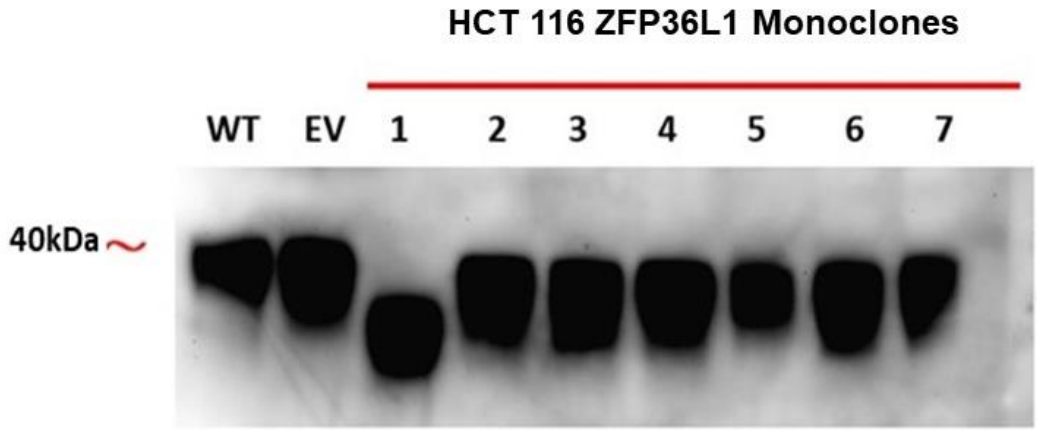

Figure E1: representing the western blot image for investigating the protein expression of ZFP36L1 in edited monoclones in the HCT-116 cell line. From left to right, wild-type (WT) and empty vector (EV) represent the expression of unedited HCT-116 cells. Samples 1-6 represent the ZFP36L1 protein expression in edited monoclones in the HCT-116 cell line, where sample 1 shows truncation in ZFP36L1 protein expression and has been used for RNA sequencing study. 40 kDa corresponds to the size of the ZFP36L1 protein.

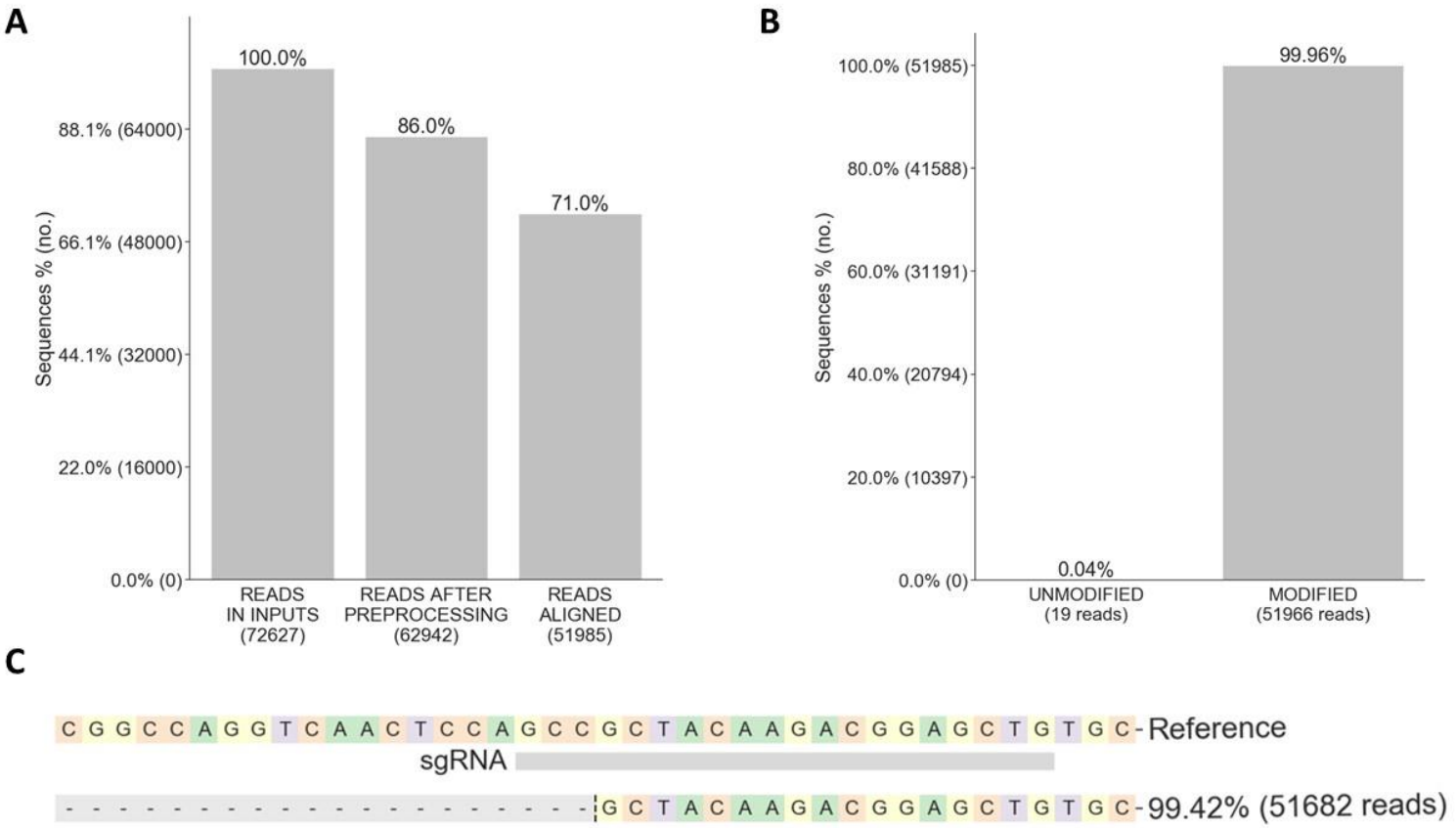

Figure E2: **A, B** and **C** represent the NGS analysis results of edited HCT116 cells generated using CRISPRESSO online software. **A** demonstrates the percentage of reads generated for edited HCT116 cells and the number of reads aligned with the reference sequence (PCR amplified ZFP36L1 gene sequence in HCT 116 cells; Figure A2). **B** demonstrates the percentage of reads modified at the targeted region in HCT 116 cells. **C** illustrates the allele frequency table around the ZFP36L1 target site in HCT 116 edited clones. Approximately 99% of reads showed 108 base pairs deletion in the edited clone.

Table E1 List of significant GO-enriched terms obtained for the upregulated DEGs and AU-rich upregulated DEGs in truncated ZFP36L1 HCT 116 cells.

Category	Description	Gene Name	AU-rich gene name
BP	Regulation of membrane potential	KCND3/SLC26A9/SCN9A/KCNQ3/WNT7A/PTN/IL1RN/SCN3B/RIMS2	SCN9A/KCNQ3/WNT7A/SCN3B
BP	Regulation of epithelial cell proliferation	TACSTD2/AKT3/WNT7A/PTN/NOG/CCL2/CEACAM1/ATOH8	WNT7A/CCL2/CEACAM1
BP	Endothelium development	PDE4D/WNT7A/PTN/CEACAM1/ATOH8	WNT7A/CEACAM1
BP	Epithelial cell proliferation	TACSTD2/AKT3/WNT7A/PTN/NOG/CCL2/CEACAM1/ATOH8	WNT7A/CCL2/CEACAM1
BP	Hindbrain development	WNT7A/PTN/MAFB/PLXNA2/NOG	WNT7A/PLXNA2
BP	Negative regulation of cell development	TACSTD2/SPOCK1/BCL11A/WNT7A/PTN/NOG/PBX1	BCL11A/WNT7A
BP	Negative regulation of cellular component movement	TACSTD2/CCL28/PTN/IL1RN/NOG/CCL2/LDLRAD4	CCL2/LDLRAD4
BP	Multicellular organismal signalling	CNTNAP2/KCND3/PDE4D/SCN9A/SCN3B	CNTNAP2/SCN9A/SCN3B
BP	Negative regulation of locomotion	TACSTD2/CCL28//NOG/CCL2/LDLRAD4	CCL2/LDLRAD4
BP	Negative regulation of cell-cell adhesion	VTCN1/LGALS9/CCL28/IL1RN/CEACAM1	CEACAM1
CC	Cation channel complex	CNTNAP2/KCND3/PDE4D/SCN9A/KCNQ3/SCN3B	KCNQ3/SCN3B/SCN9A/CNTNAP2
CC	Plasma membrane protein complex	CNTNAP2/KCND3/SNTB1/PDE4D/SCN9A/KCNQ3/ITGBL1/CEACAM1/SCN3B	CNTNAP2/SNTB1/SCN9A/KCNQ3/CEACAM1/SCN3B
CC	Ion channel complex	CNTNAP2/KCND3/PDE4D/SCN9A/KCNQ3/SCN3B	CNTNAP2/SCN9A/KCNQ3/SCN3B
CC	Transmembrane transporter complex	CNTNAP2/KCND3/PDE4D/SCN9A/KCNQ3/SCN3B	CNTNAP2/SCN9A/KCNQ3/SCN3B
CC	Transporter complex	CNTNAP2/KCND3/PDE4D/SCN9A/KCNQ3/SCN3B	CNTNAP2/SCN9A/KCNQ3/SCN3B

Glossary

AIs	Aromatase Inhibitors
ARE	Adenylate Uridylate Rich Elements
BMI	Body Mass Index
BP	Biological Process
BRCA1	Breast Cancer Gene 1
BRCA2	Breast Cancer Gene 2
BRF	Butyrate Response Factor1
CC	Cellular Component
CDK	Cyclin-dependent Kinase
cDNA	Complementary DNA
CIAP2	Cellular Inhibitor of Apoptosis Protein -2
crRNAs	CRISPR RNAs
CSCs	Cancer Stem Cells
DCCs	Disseminated Cancer Cells
DCIS	Ductal Carcinoma in situ
DEGs	Differentially Expressed Genes
DFS	Disease-free survival
DII4	Delta-Like-4
DMEM	Dulbecco Modified Eagle's Medium
DNTPs	Deoxynucleotide Triphosphates
DSBs	Double-Strand Breaks
ECM	Extracellular Matrix
ER	Oestrogen receptor
ET	Endocrine therapy
FPKM	Fragment Per kilobase of transcripts sequence per Million base pairs sequenced
GnRH	Gonadotropin-Releasing Hormone
GO	Gene ontology
HDR	Homology-Directed Repair
HER2	Human Epidermal GrowthFactor Receptor 2
HNSCC	Head and Neck Squamous Cell Carcinoma
HRP	Horseradish Peroxidase
IDFS	Invasive Disease-Free Survival
IHC	Immunohistochemistry
JNK	c-Jun N-terminal Kinases
KEGG	Kyoto Encyclopedia of Genes and Genomes
LCIS	Lobular Carcinoma in situ
MAPK2	Mitogen Activated Protein Kinase-2
MCP-1	Monocyte Chemoattractant Protein 1
MCP-1	Monocyte chemoattractant Protein 1
MF	Molecular Function
MMP1	Matrix Metalloproteinase-1
NHEJ	Non-Homologous End-Joining

OS	Overall Survival
PALB2	Partner and Localiser of BRCA2
PAM	Protospacer-adjacent motif
PARN	Poly A-specific Ribonuclease
PBS	Phosphate-buffered saline
pCR	Pathological Complete Response
PCR	Polymerase Chain Reaction
PCR	Polymerase Chain Reaction
PFS	Progression-Free Survival
PI	propidium iodide
PI3K	Phosphoinositide 3-kinase
PKA	Protein Kinase A
PKB	Protein Kinase B
PTEN	Phosphatase and Tensin Homolog
PVDF	Polyvinylidene Difluoride
RNA-Seq	RNA sequencing
SAP	Shrimp Alkaline Phosphatase
SDF-1	Stromal-derived Factor 1
SDS	Sodium Dodecyl Sulfate
SERMs	Selective Estrogen Receptor Modulators
SNPs	Single Nucleotide Polymorphisms
SOX9	Sex-determining Region Y box 9
STK11/LKB1	Serine Threonine Kinase 11
STR	Short Tandem Repeats
TALENs	Transcription Activator-like Effector Nucleases
T-ALL	T-cell acute lymphoblastic leukaemia
T-DM1	Trastuzumab Emtansine
TIMP-1	Tissue Inhibitor of Metalloprotease 1
TNBC	Triple-Negative Breast Cancer
TNF	Tumour Necrosis Factor
tracrRNA	Trans-activating RNA
TTP	Tristetraproline
uPA	Urokinase-type Plasminogen Activator
UPAR	Urokinase-type Plasminogen Activator Receptor
UTR	Untranslated Region
ZEB1	Zinc finger E-box binding homeobox 1
ZFDs	Zinc Finger Domains
ZFN	Zinc-finger nucleases

References

Agarwal, G., Pradeep, P. V., Aggarwal, V., Yip, C.H., and Cheung, P.S.Y. (2007). Spectrum of breast cancer in Asian women. World Journal of Surgery, 31 (5). Available from https://doi.org/10.1007/s00268-005-0585-9.

Alagoz, M. and Kherad, N. (2020). Advance genome editing technologies in the treatment of human diseases: CRISPR therapy (Review). International Journal of Molecular Medicine. 46 (2), 521-534.Arnold, M., Morgan, E., Rumgay, H., Mafra, A., Singh, D., Laversanne, M., Vignat, J., Gralow, J.R., Cardoso, F., Siesling, S., and Soerjomataram, I. (2022). Current and future burden of breast cancer: Global statistics for 2020 and 2040. The Breast : Official Journal of the European Society of Mastology, 66, 15. Available from https://doi.org/10.1016/J.BREAST.2022.08.010 [Accessed 12 April 2023].

Al-Souhibani, N., Al-Ahmadi, W., Hesketh, J.E., Blackshear, P.J., and Khabar, K.S.A. (2010). The RNA-binding zinc-finger protein tristetraprolin regulates AU-rich mRNAs involved in breast cancer-related processes. Oncogene, 29 (29). Available from https://doi.org/10.1038/onc.2010.168.

Arnold, M., Morgan, E., Rumgay, H., Mafra, A., Singh, D., Laversanne, M., Vignat, J., Gralow, J.R., Cardoso, F., Siesling, S., and Soerjomataram, I. (2022). Current and future burden of breast cancer: Global statistics for 2020 and 2040. The Breast : Official Journal of the European Society of Mastology, 66, 15. Available from https://doi.org/10.1016/J.BREAST.2022.08.010 [Accessed 12 April 2023].

Ashmore-Harris, C., and Fruhwirth, G.O. (2020). The clinical potential of gene editing as a tool to engineer cell-based therapeutics. Clinical and Translational Medicine 2020 9:1, 9 (1), 1–22. Available from https://doi.org/10.1186/S40169-020-0268-Z [Accessed 20 July 2023].

Baou, M., Norton, J.D., and Murphy, J.J. (2011). AU-rich RNA binding proteins in hematopoiesis and leukemogenesis. Blood, 118 (22), 5732–5740. Available from https://doi.org/10.1182/BLOOD-2011-07-347237.

Bakheet, T., Hitti, E., and Khabar, K.S.A. (2018). ARED-Plus: An updated and expanded database of AU-rich element-containing mRNAs and pre-mRNAs. Nucleic Acids Research, 46 (D1), D218–D220. Available from https://doi.org/10.1093/NAR/GKX975.

Bandera, E. V., Maskarinec, G., Romieu, I., and John, E.M. (2015). Racial and ethnic disparities in the impact of obesity on breast cancer risk and survival: a global perspective. Advances in nutrition (Bethesda, Md.), 6 (6), 803–819. Available from https://doi.org/10.3945/AN.115.009647 [Accessed 13 April 2023].

Barrios-García, T., Tecalco-Cruz, A., Gómez-Romero, V., Reyes-Carmona, S., Meneses-Morales, I., and León-Del-Río, A. (2014). Tristetraprolin represses estrogen receptor α transactivation in breast cancer cells. Journal of Biological Chemistry, 289 (22), 15554–15565. Available from https://doi.org/10.1074/jbc.M114.548552 [Accessed 6 July 2023].

Bartelink, H., Maingon, P., Poortmans, P., Weltens, C., Fourquet, A., Jager, J., Schinagl, D., Oei, B., Rodenhuis, C., Horiot, J.C., Struikmans, H., Van Limbergen,

E., Kirova, Y., Elkhuizen, P., Bongartz, R., Miralbell, R., Morgan, D., Dubois, J.B., Remouchamps, V., et al. (2015). Whole-breast irradiation with or without a boost for patients treated with breast-conserving surgery for early breast cancer: 20-year follow-up of a randomised phase 3 trial. The Lancet. Oncology, 16 (1), 47–56. Available from https://doi.org/10.1016/S1470-2045(14)71156-8 [Accessed 12 July 2023].

Behan, F.M., Iorio, F., Picco, G., Goncalves, E., Beaver, C.M., Migliardi, G., Santos, R., Rao, Y., Sassi, F., Pinnelli, M., Ansari, R., Harper, S., Jackson, D.A., McRae, R., Pooley, R., Wilkinson, P., van der Meer, D., Dow, D., Buser-Doepner, C., Bertotti, A., Trusolino, L., Stronach, E.A., Saez-Rodriguez, J., Yusa, K. and Garnett, M.J. (2019). Prioritisation of cancer therapeutic targets using CRISPR–Cas9 screens. Nature, 568, (7753), 511-516.

Benjamin, D., Schmidlin, M., Min, L., Gross, B., and Moroni, C. (2006). BRF1 Protein Turnover and mRNA Decay Activity Are Regulated by Protein Kinase B at the Same Phosphorylation Sites. Molecular and Cellular Biology, 26 (24), 9497. Available from https://doi.org/10.1128/MCB.01099-06 [Accessed 22 June 2023].

Bernard, P.S., Parker, J.S., Mullins, M., Cheung, M.C.U., Leung, S., Voduc, D., Vickery, T., Davies, S., Fauron, C., He, X., Hu, Z., Quackenhush, J.F., Stijleman, I.J., Palazzo, J., Matron, J.S., Nobel, A.B., Mardis, E., Nielsen, T.O., Ellis, M.J., et al. (2009). Supervised Risk Predictor of Breast Cancer Based on Intrinsic Subtypes. Journal of Clinical Oncology, 27 (8), 1160. Available from https://doi.org/10.1200/JCO.2008.18.1370 [Accessed 21 April 2023].

Bernier, J. (2016). Immuno-oncology: Allying forces of radio- and immuno-therapy to enhance cancer cell killing. Critical reviews in oncology/hematology, 108, 97–108. Available from https://doi.org/10.1016/J.CRITREVONC.2016.11.001 [Accessed 13 July 2023].

Blackshear, P.J. (2002). Tristetraprolin and other CCCH tandem zinc-finger proteins in the regulation of mRNA turnover. Biochemical Society transactions, 30 (Pt 6), 945–952. Available from https://doi.org/10.1042/BST0300945 [Accessed 23 June 2023].

Blackshear, P.J., Phillips, R.S., Ghosh, S., Ramos, S.V.B., Richfield, E.K., and Lai, W.S. (2005). Zfp36l3, a rodent X chromosome gene encoding a placenta-specific member of the Tristetraprolin family of CCCH tandem zinc finger proteins. Biology of reproduction, 73 (2), 297–307. Available from https://doi.org/10.1095/BIOLREPROD.105.040527 [Accessed 17 April 2024].

Bosch, A., Eroles, P., Zaragoza, R., Viña, J.R., and Lluch, A. (2010). Triple-negative breast cancer: molecular features, pathogenesis, treatment and current lines of research. Cancer treatment reviews, 36 (3), 206–215. Available from https://doi.org/10.1016/J.CTRV.2009.12.002 [Accessed 23 April 2023].

Brabetz, O., Alla, V., Angenendt, L., Schliemann, C., Berdel, W.E., Arteaga, M., Mikesch, J. (2017). RNA-Guided CRISPR-Cas9 System-Mediated Engineering of Acute Myeloid Leukemia Mutations. Molecular Therapy - Nucleic Acids. 6 243-248.

Bradley, R., Burrett, J., Clarke, M., Davies, C., Duane, F., Evans, V., Gettins, L., Godwin, J., Gray, R., Liu, H., McGale, P., MacKinnon, E., McHugh, T., James,

S., Morris, P., Pan, H., Peto, R., Read, S., Taylor, C., et al. (2015). Aromatase inhibitors versus tamoxifen in early breast cancer: Patient-level meta-analysis of the randomised trials. The Lancet, 386 (10001), 1341–1352. Available from https://doi.org/10.1016/S0140-6736(15)61074-1 [Accessed 13 July 2023].

Brennan, S.E., Kuwano, Y., Alkharouf, N., Blackshear, P.J., Gorospe, M., Wilson, G.M. (2009). The mRNA-destabilizing protein tristetraprolin is suppressed in many cancers, altering tumorigenic phenotypes and patient prognosis. Cancer Research. 69 (12), 5168-5176.

Brewer, H.R., Jones, M.E., Schoemaker, M.J., Ashworth, A., and Swerdlow, A.J. (2017). Family history and risk of breast cancer: an analysis accounting for family structure. Breast Cancer Research and Treatment, 165 (1), 193–200. Available from https://doi.org/10.1007/S10549-017-4325-2/TABLES/4 [Accessed 18 April 2023].

Brooks, S.A., and Blackshear, P.J. (2013). Tristetraprolin (TTP): Interactions with mRNA and proteins, and current thoughts on mechanisms of action. Biochimica et biophysica acta, 1829 (0), 666. Available from https://doi.org/10.1016/J.BBAGRM.2013.02.003 [Accessed 22 June 2023].

Burstein, H.J., Curigliano, G., Thürlimann, B., Weber, W.P., Poortmans, P., Regan, M.M., Senn, H.J., Winer, E.P., Gnant, M., Aebi, S., André, F., Barrios, C., Bergh, J., Bonnefoi, H., Bretel Morales, D., Brucker, S., Burstein, H., Cameron, D., Cardoso, F., et al. (2021). Customizing local and systemic therapies for women with early breast cancer: the St. Gallen International Consensus Guidelines for treatment of early breast cancer 2021. Annals of Oncology, 32 (10), 1216–1235. Available from https://doi.org/10.1016/J.ANNONC.2021.06.023.

Cai, M. and Yang, Y. (2014). Targeted genome editing tools for disease modeling and gene therapy. Current Gene Therapy. 14 (1), 2-9.

Carballo, E., Lai, W.S., and Blackshear, P.J. (1998). Feedback Inhibition of Macrophage Tumor Necrosis Factor-α Production by Tristetraprolin. Science, 281 (5379). Available from https://doi.org/10.1126/science.281.5379.1001.

Cardiff, R.D., and Borowsky, A.D. (2014). At last: classification of human mammary cells elucidates breast cancer origins. The Journal of Clinical Investigation, 124 (2), 478. Available from https://doi.org/10.1172/JCI73910 [Accessed 28 March 2024].

Cardoso, F., van't Veer, L.J., Bogaerts, J., Slaets, L., Viale, G., Delaloge, S., Pierga, J.-Y., Brain, E., Causeret, S., DeLorenzi, M., Glas, A.M., Golfinopoulos, V., Goulioti, T., Knox, S., Matos, E., Meulemans, B., Neijenhuis, P.A., Nitz, U., Passalacqua, R., et al. (2016). 70-Gene Signature as an Aid to Treatment Decisions in Early-Stage Breast Cancer. The New England journal of medicine, 375 (8), 717–729. Available from https://doi.org/10.1056/NEJMOA1602253 [Accessed 17 July 2023].

Carrick, D.M., and Blackshear, P.J. (2007). Comparative expression of tristetraprolin (TTP) family member transcripts in normal human tissues and cancer cell lines. Archives of biochemistry and biophysics, 462 (2), 278–285. Available from https://doi.org/10.1016/J.ABB.2007.04.011 [Accessed 4 May 2023].

Carvalho, S., Reis, C.A., and Pinho, S.S. (2016). Cadherins Glycans in Cancer: Sweet Players in a Bitter Process. Trends in Cancer, 2 (9), 519–531. Available from https://doi.org/10.1016/J.TRECAN.2016.08.003.

Chamboredon, S., Ciais, D., Desroches-Castan, A., Savid, P., Bono, F., Feige, J.J., and Cherradi, N. (2011). Hypoxia-inducible factor-1α mRNA: a new target for destabilization by tristetraprolin in endothelial cells. Molecular biology of the cell, 22 (18), 3366–3378. Available from https://doi.org/10.1091/MBC.E10-07-0617 [Accessed 7 July 2023].

Chen, C.Y., Gherzi, R., Ong, S.E., Chan, E.L., Raijmakers, R., Pruijn, G.J.M., Stoecklin, G., Moroni, C., Mann, M., and Karin, M. (2001). AU binding proteins recruit the exosome to degrade ARE-containing mRNAs. Cell, 107 (4), 451–464. Available from https://doi.org/10.1016/S0092-8674(01)00578-5 [Accessed 27 June 2023].

Chen, W.Y., Rosner, B., Hankinson, S.E., Colditz, G.A., and Willett, W.C. (2011). Moderate alcohol consumption during adult life, drinking patterns, and breast cancer risk. Jama, 306 (17), 1884. Available from https://doi.org/10.1001/JAMA.2011.1590 [Accessed 12 April 2023].

Chrestensen, C.A., Schroeder, M.J., Shabanowitz, J., Hunt, D.F., Pelo, J.W., Worthington, M.T., and Sturgill, T.W. (2004). MAPKAP kinase 2 phosphorylates tristetraprolin on in vivo sites including Ser178, a site required for 14-3-3 binding. The Journal of biological chemistry, 279 (11), 10176–10184. Available from https://doi.org/10.1074/JBC.M310486200 [Accessed 28 June 2023].

Chlebowski, R.T., Chen, Z., Anderson, G.L., Rohan, T., Aragaki, A., Lane, D., Dolan, N.C., Paskett, E.D., McTiernan, A., Hubbell, F.A., Adams-Campbell, L.L., and Prentice, R. (2005). Ethnicity and breast cancer: Factors influencing differences in incidence and outcome. Journal of the National Cancer Institute, 97 (6). Available from https://doi.org/10.1093/jnci/dji064.

Clark, A.R., and Dean, J.L.E. (2016). The control of inflammation via the phosphorylation and dephosphorylation of tristetraprolin: a tale of two phosphatases. Biochemical Society Transactions, 44 (5), 1321. Available from https://doi.org/10.1042/BST20160166 [Accessed 28 June 2023].

Closset, L., Gultekin, O., Salehi, S., Sarhan, D., Lehti, K., and Gonzalez-Molina, J. (2023). The extracellular matrix – immune microenvironment crosstalk in cancer therapy: Challenges and opportunities. Matrix Biology, 121, 217–228. Available from https://doi.org/10.1016/J.MATBIO.2023.07.003.

Ciais, D., Cherradi, N., and Feige, J.J. (2012). Multiple functions of tristetraprolin/TIS11 RNA-binding proteins in the regulation of mRNA biogenesis and degradation. Cellular and Molecular Life Sciences 2012 70:12, 70 (12), 2031–2044. Available from https://doi.org/10.1007/S00018-012-1150-Y [Accessed 28 September 2023].

Clement, K., Rees, H., Canver, M.C., Gehrke, J.M., Farouni, R., Hsu, J.Y., Cole, M.A., Liu, D.R., Joung, J.K., Bauer, D.E., Pinello, L. (2019). CRISPResso2 provides accurate and rapid genome editing sequence analysis. Nature Biotechnology. 37 (3), 224-226.

Conde, L., Bracci, P.M., Richardson, R., Montgomery, S.B., and Skibola, C.F. (2013). Integrating GWAS and expression data for functional characterization of disease-associated SNPs: an application to follicular lymphoma. American journal of human genetics, 92 (1), 126–130. Available from https://doi.org/10.1016/J.AJHG.2012.11.009 [Accessed 26 April 2023].

Cong, L., Ran, F.A., Cox, D., Lin, S., Barretto, R., Habib, N., Hsu, P.D., Wu, X., Jiang, W., Marraffini, L.A., Zhang, F. (2013). Multiplex Genome Engineering Using CRISPR/Cas Systems. Science.

Cortazar, P., Zhang, L., Untch, M., Mehta, K., Costantino, J.P., Wolmark, N., Bonnefoi, H., Cameron, D., Gianni, L., Valagussa, P., Swain, S.M., Prowell, T., Loibl, S., Wickerham, D.L., Bogaerts, J., Baselga, J., Perou, C., Blumenthal, G., Blohmer, J., et al. (2014). Pathological complete response and long-term clinical benefit in breast cancer: The CTNeoBC pooled analysis. The Lancet, 384 (9938), 164–172. Available from https://doi.org/10.1016/S0140-6736(13)62422-8 [Accessed 17 July 2023].

Corti, C., De Angelis, C., Bianchini, G., Malorni, L., Giuliano, M., Hamilton, E., Jeselsohn, R., Jhaveri, K., Curigliano, G., and Criscitiello, C. (2023). Novel endocrine therapies: What is next in estrogen receptor positive, HER2 negative breast cancer? Cancer Treatment Reviews, 117, 102569. Available from https://doi.org/10.1016/J.CTRV.2023.102569.

Costa, B., Amorim, I., Gärtner, F., and Vale, N. (2020). Understanding Breast cancer: from conventional therapies to repurposed drugs. European Journal of Pharmaceutical Sciences, 151. Available from https://doi.org/10.1016/j.ejps.2020.105401.

Dall, G.V., and Britt, K.L. (2017). Estrogen Effects on the Mammary Gland in Early and Late Life and Breast Cancer Risk. Frontiers in Oncology, 7 (MAY), 1. Available from https://doi.org/10.3389/FONC.2017.00110 [Accessed 12 April 2023].

Danaei, G., Vander Hoorn, S., Lopez, A.D., Murray, C.J.L., and Ezzati, M. (2005). Causes of cancer in the world: comparative risk assessment of nine behavioural and environmental risk factors. Lancet (London, England), 366 (9499), 1784–1793. Available from https://doi.org/10.1016/S0140-6736(05)67725-2 [Accessed 12 April 2023].

Dong, X., Yang, Y., Yuan, Q., Hou, J., and Wu, G. (2021). High Expression of CEMIP Correlates Poor Prognosis and the Tumur Microenvironment in Breast Cancer as a Promisingly Prognostic Biomarker. Frontiers in Genetics, 12, 2512. Available from https://doi.org/10.3389/FGENE.2021.768140/BIBTEX.

Desroches-Castan, A., Cherradi, N., Feige, J.J., and Ciais, D. (2011). A novel function of Tis11b/BRF1 as a regulator of Dll4 mRNA 3′-end processing. Molecular Biology of the Cell, 22 (19), 3625–3633. Available from https://doi.org/10.1091/MBC.E11-02-0149/ASSET/IMAGES/LARGE/3625FIG7.JPEG [Accessed 6 July 2023].

Du, W.W., Fang, L., Yang, W., Sheng, W., Zhang, Y., Seth, A., Yang, B.B., and Yee, A.J. (2012). The role of versican G3 domain in regulating breast cancer cell motility including effects on osteoblast cell growth and differentiation in vitro – evaluation towards understanding breast cancer cell bone metastasis. BMC Cancer, 12, 341. Available from https://doi.org/10.1186/1471-2407-12-341

[Accessed 2 June 2023].

Eroles, P., Bosch, A., Alejandro Pérez-Fidalgo, J., and Lluch, A. (2012). Molecular biology in breast cancer: intrinsic subtypes and signaling pathways. Cancer treatment reviews, 38 (6), 698–707. Available from https://doi.org/10.1016/J.CTRV.2011.11.005 [Accessed 22 April 2023].

Eswaran, J., Cyanam, D., Mudvari, P., Reddy, S.D.N., Pakala, S.B., Nair, S.S., Florea, L., Fuqua, S.A.W., Godbole, S., and Kumar, R. (2012). Transcriptomic landscape of breast cancers through mRNA sequencing. Scientific Reports 2012 2:1, 2 (1), 1–11. Available from https://doi.org/10.1038/srep00264 [Accessed 12 April 2022].

Fenger-Grøn, M., Fillman, C., Norrild, B., and Lykke-Andersen, J. (2005). Multiple processing body factors and the ARE binding protein TTP activate mRNA decapping. Molecular cell, 20 (6), 905–915. Available from https://doi.org/10.1016/J.MOLCEL.2005.10.031 [Accessed 27 June 2023].

Finotello, F., and Di Camillo, B. (2015). Measuring differential gene expression with RNA-seq: challenges and strategies for data analysis. Briefings in Functional Genomics, 14 (2), 130–142. Available from https://doi.org/10.1093/BFGP/ELU035 [Accessed 26 April 2023].

Francis, P.A., Pagani, O., Fleming, G.F., Walley, B.A., Colleoni, M., Láng, I., Gómez, H.L., Tondini, C., Ciruelos, E., Burstein, H.J., Bonnefoi, H.R., Bellet, M., Martino, S., Geyer, C.E., Goetz, M.P., Stearns, V., Pinotti, G., Puglisi, F., Spazzapan, S., et al. (2018). Tailoring Adjuvant Endocrine Therapy for Premenopausal Breast Cancer. New England Journal of Medicine, 379 (2), 122–137. Available from https://doi.org/10.1056/NEJMOA1803164/SUPPL_FILE/NEJMOA1803164_DISCLOSURES.PDF [Accessed 13 July 2023].

Franks, T.M., and Lykke-Andersen, J. (2007). TTP and BRF proteins nucleate processing body formation to silence mRNAs with AU-rich elements. Genes & development, 21 (6), 719–735. Available from https://doi.org/10.1101/GAD.1494707 [Accessed 27 June 2023].

Galloway, A., Saveliev, A., Łukasiak, S., Hodson, D.J., Bolland, D., Balmanno, K., Ahlfors, H., Monzón-Casanova, E., Mannurita, S.C., Bell, L.S., Andrews, S., Díaz-Muñoz, M.D., Cook, S.J., Corcoran, A., and Turner, M. (2016). RNA-binding proteins ZFP36L1 and ZFP36L2 promote cell quiescence. Science (New York, N.Y.), 352 (6284), 453–459. Available from https://doi.org/10.1126/SCIENCE.AAD5978 [Accessed 24 September 2023].

Gebauer, F., Schwarzl, T., Valcárcel, J., and Hentze, M.W. (2021). RNA-binding proteins in human genetic disease. Nature Reviews Genetics, 22 (3), 185–198. Available from https://doi.org/10.1038/S41576-020-00302-Y. [Accessed 17 July 2023]

Gianni, L., Pienkowski, T., Im, Y.H., Tseng, L.M., Liu, M.C., Lluch, A., Starosławska, E., de la Haba-Rodriguez, J., Im, S.A., Pedrini, J.L., Poirier, B., Morandi, P., Semiglazov, V., Srimuninnimit, V., Bianchi, G.V., Magazzù, D., McNally, V., Douthwaite, H., Ross, G., et al. (2016). 5-year analysis of neoadjuvant pertuzumab and trastuzumab in patients with locally advanced, inflammatory, or early-stage HER2-positive breast cancer (NeoSphere): a multicentre, open-label, phase 2 randomised trial. The Lancet. Oncology, 17 (6), 791–800. Available from

https://doi.org/10.1016/S1470-2045(16)00163-7 [Accessed 17 July 2023].

Giordano, S.H., Temin, S., Chandarlapaty, S., Crews, J.R., Esteva, F.J., Kirshner, J.J., Krop, I.E., Levinson, J., Lin, N.U., Modi, S., Patt, D.A., Perlmutter, J., Ramakrishna, N., Winer, E.P., and Davidson, N.E. (2018). Systemic Therapy for Patients With Advanced Human Epidermal Growth Factor Receptor 2-Positive Breast Cancer: ASCO Clinical Practice Guideline Update. Journal of clinical oncology : official journal of the American Society of Clinical Oncology, 36 (26), 2736–2740. Available from https://doi.org/10.1200/JCO.2018.79.2697 [Accessed 18 July 2023].

Giuliano, C.J., Lin, A., Girish, V., Sheltzer, J.M. (2019). Generating Single Cell–Derived Knockout Clones in Mammalian Cells with CRISPR/Cas9. Current Protocols in Molecular Biology. 128 (1), e100.

Goetz, M.P., Toi, M., Campone, M., Trédan, O., Bourayou, N., Sohn, J., Park, I.H., Paluch-Shimon, S., Huober, J., Chen, S.C., Manso, L., Barriga, S., Freedman, O.C., Jaliffe, G.G., Forrester, T., Frenzel, M., Smith, I.C., and Di Leo, A. (2017). MONARCH 3: Abemaciclib As Initial Therapy for Advanced Breast Cancer. Journal of clinical oncology : official journal of the American Society of Clinical Oncology, 35 (32), 3638–3646. Available from https://doi.org/10.1200/JCO.2017.75.6155 [Accessed 14 July 2023].

Gomatou, G., Trontzas, I., Ioannou, S., Drizou, M., Syrigos, N., and Kotteas, E. (2021). Mechanisms of resistance to cyclin-dependent kinase 4/6 inhibitors. Molecular Biology Reports 2021 48:1, 48 (1), 915–925. Available from https://doi.org/10.1007/S11033-020-06100-3 [Accessed 26 September 2023].

Gray, R., Bradley, R., Braybrooke, J., Liu, Z., Peto, R., Davies, L., Dodwell, D., McGale, P., Pan, H., Taylor, C., Barlow, W., Bliss, J., Bruzzi, P., Cameron, D., Fountzilas, G., Loibl, S., Mackey, J., Martin, M., Del Mastro, L., et al. (2019). Increasing the dose intensity of chemotherapy by more frequent administration or sequential scheduling: a patient-level meta-analysis of 37 298 women with early breast cancer in 26 randomised trials. Lancet (London, England), 393 (10179), 1440. Available from https://doi.org/10.1016/S0140-6736(18)33137-4 [Accessed 14 July 2023].

Gruber, A.R., Fallmann, J., Kratochvill, F., Kovarik, P., and Hofacker, I.L. (2011). AREsite: a database for the comprehensive investigation of AU-rich elements. Nucleic acids research, 39 (Database issue). Available from https://doi.org/10.1093/NAR/GKQ990 [Accessed 6 July 2023].

Hahnen, E., Lederer, B., Hauke, J., Loibl, S., Kröber, S., Schneeweiss, A., Denkert, C., Fasching, P.A., Blohmer, J.U., Jackisch, C., Paepke, S., Gerber, B., Kümmel, S., Schem, C., Neidhardt, G., Huober, J., Rhiem, K., Costa, S., Altmüller, J., et al. (2017). Germline Mutation Status, Pathological Complete Response, and Disease-Free Survival in Triple-Negative Breast Cancer: Secondary Analysis of the GeparSixto Randomized Clinical Trial. JAMA oncology, 3 (10), 1378–1385. Available from https://doi.org/10.1001/JAMAONCOL.2017.1007 [Accessed 17 July 2023].

Hanahan, D., and Weinberg, R.A. (2011). Hallmarks of cancer: The next generation. Cell. Available from https://doi.org/10.1016/j.cell.2011.02.013.

Haloua, M.H., Krekel, N.M.A., Winters, H.A.H., Rietveld, D.H.F., Meijer, S., Bloemers, F.W., and Van Den Tol, M.P. (2013). A systematic review of oncoplastic breast-conserving surgery: Current weaknesses and future prospects. Annals of Surgery, 257 (4). Available from https://doi.org/10.1097/SLA.0b013e3182888782.

Harbeck, N., Penault-Llorca, F., Cortes, J., Gnant, M., Houssami, N., Poortmans, P., Ruddy, K., Tsang, J., and Cardoso, F. (2019). Breast cancer. Nature reviews. Disease primers, 5 (1). Available from https://doi.org/10.1038/S41572-019-0111-2 [Accessed 24 April 2023].

Hau, H.H., Walsh, R.J., Ogilvie, R.L., Williams, D.A., Reilly, C.S., and Bohjanen, P.R. (2007). Tristetraprolin recruits functional mRNA decay complexes to ARE sequences. Journal of cellular biochemistry, 100 (6), 1477–1492. Available from https://doi.org/10.1002/JCB.21130 [Accessed 27 June 2023].

Herschkowitz, J.I., Simin, K., Weigman, V.J., Mikaelian, I., Usary, J., Hu, Z., Rasmussen, K.E., Jones, L.P., Assefnia, S., Chandrasekharan, S., Backlund, M.G., Yin, Y., Khramtsov, A.I., Bastein, R., Quackenbush, J., Glazer, R.I., Brown, P.H., Green, J.E., Kopelovich, L., et al. (2007). Identification of conserved gene expression features between murine mammary carcinoma models and human breast tumors. Genome biology, 8 (5). Available from https://doi.org/10.1186/GB-2007-8-5-R76 [Accessed 25 April 2023].

Hodson, D.J., Janas, M.L., Galloway, A., Bell, S.E., Andrews, S., Li, C.M., Pannell, R., Siebel, C.W., MacDonald, H.R., De Keersmaecker, K., Ferrando, A.A., Grutz, G. and Turner, M. (2010). Deletion of the RNA-binding proteins ZFP36L1 and ZFP36L2 leads to perturbed thymic development and T lymphoblastic leukemia. Nature Immunology, 11 (8), 717–724. Available from https://doi.org/10.1038/ni.1901 [Accessed 20 July 2020].

Hong, R., and Xu, B. (2022). Breast cancer: an up-to-date review and future perspectives. Cancer Communications, 42 (10), 913. Available from https://doi.org/10.1002/CAC2.12358 [Accessed 13 July 2023].

Horn, J., Åsvold, B.O., Opdahl, S., Tretli, S., and Vatten, L.J. (2013). Reproductive factors and the risk of breast cancer in old age: a Norwegian cohort study. Breast cancer research and treatment, 139 (1), 237–243. Available from https://doi.org/10.1007/S10549-013-2531-0 [Accessed 12 April 2023].

Hortobagyi, G.N., Stemmer, S.M., Burris, H.A., Yap, Y.-S., Sonke, G.S., Paluch-Shimon, S., Campone, M., Blackwell, K.L., André, F., Winer, E.P., Janni, W., Verma, S., Conte, P., Arteaga, C.L., Cameron, D.A., Petrakova, K., Hart, L.L., Villanueva, C., Chan, A., et al. (2016). Ribociclib as First-Line Therapy for HR-Positive, Advanced Breast Cancer. The New England journal of medicine, 375 (18), 1738–1748. Available from https://doi.org/10.1056/NEJMOA1609709 [Accessed 14 July 2023].

Houseley, J., LaCava, J., and Tollervey, D. (2006). RNA-quality control by the exosome. Nature reviews. Molecular cell biology, 7 (7), 529–539. Available from https://doi.org/10.1038/NRM1964 [Accessed 27 June 2023].

Hsieh-Feng, V. and Yang, Y., 2020. Efficient expression of multiple guide RNAs for CRISPR/Cas genome editing. aBIOTECH, 1(2), pp.123-134.

Huang, J., Zheng, L., Sun, Z., and Li, J. (2022). CDK4/6 inhibitor resistance mechanisms and treatment strategies (Review). International Journal of Molecular Medicine, 50 (4), 1–13. Available from https://doi.org/10.3892/IJMM.2022.5184/HTML [Accessed 26 September 2023].

Hudson, B.P., Martinez-Yamout, M.A., Dyson, H.J., and Wright, P.E. (2004). Recognition of the mRNA AU-rich element by the zinc finger domain of TIS11d. Nature Structural & Molecular Biology 2004 11:3, 11 (3), 257–264. Available from https://doi.org/10.1038/nsmb738 [Accessed 3 July 2023].

Iqbal, J., Ginsburg, O., Rochon, P.A., Sun, P., and Narod, S.A. (2015). Differences in breast cancer stage at diagnosis and cancer-specific survival by race and ethnicity in the United States. JAMA - Journal of the American Medical Association, 313 (2). Available from https://doi.org/10.1001/jama.2014.17322.

Jatoi, I., Benson, J.R., and Kunkler, I. (2018). Hypothesis: can the abscopal effect explain the impact of adjuvant radiotherapy on breast cancer mortality? npj Breast Cancer 2018 4:1, 4 (1), 1–8. Available from https://doi.org/10.1038/s41523-018-0061-y [Accessed 13 July 2023].

Jinek, M., Chylinski, K., Fonfara, I., Hauer, M., Doudna, J.A., Charpentier, E. (2012). A Programmable Dual-RNA–Guided DNA Endonuclease in Adaptive Bacterial Immunity. Science.

Joberty, G., Fälth-Savitski, M., Paulmann, M., Bösche, M., Doce, C., Cheng, A.T., Drewes, G., Grandi, P. (2020). A Tandem Guide RNA-Based Strategy for Efficient CRISPR Gene Editing of Cell Populations with Low Heterogeneity of Edited Alleles. The CRISPR Journal. 3 (2), 123-134.

Kaehler, M., Dworschak, M., Rodin, J.P., Ruemenapp, J., Vater, I., Penas, E.M.M., Liu, C., Cascorbi, I., and Nagel, I. (2021). ZFP36L1 plays an ambiguous role in the regulation of cell expansion and negatively regulates CDKN1A in chronic myeloid leukemia cells. Experimental Hematology, 99. Available from https://doi.org/10.1016/j.exphem.2021.05.006.

Kedersha, N., Stoecklin, G., Ayodele, M., Yacono, P., Lykke-Andersen, J., Fitzler, M.J., Scheuner, D., Kaufman, R.J., Golan, D.E., and Anderson, P. (2005). Stress granules and processing bodies are dynamically linked sites of mRNP remodeling. Journal of Cell Biology, 169 (6). Available from https://doi.org/10.1083/jcb.200502088.

Khabar, K.S.A. (2017). Hallmarks of cancer and AU-rich elements. Wiley Interdisciplinary Reviews: RNA, 8 (1), e1368. Available from https://doi.org/10.1002/WRNA.1368 [Accessed 6 July 2023].

Karami, F., and Mehdipour, P. (2013). A Comprehensive Focus on Global Spectrum of BRCA1 and BRCA2 Mutations in Breast Cancer. BioMed Research International, 2013. Available from https://doi.org/10.1155/2013/928562 [Accessed 18 April 2023].

Kennecke, H., Yerushalmi, R., Woods, R., Cheang, M.C.U., Voduc, D., Speers, C.H., Nielsen, T.O., and Gelmon, K. (2010). Metastatic behavior of breast cancer subtypes. Journal of Clinical Oncology, 28 (20), 3271–3277. Available from https://doi.org/10.1200/JCO.2009.25.9820.

Kim, D., Paggi, J.M., Park, C., Bennett, C., and Salzberg, S.L. (2019). Graph-based genome alignment and genotyping with HISAT2 and HISAT-genotype. Nature Biotechnology 2019 37:8, 37 (8), 907–915. Available from https://doi.org/10.1038/s41587-019-0201-4 [Accessed 27 April 2023].

Kim, T.K., Hemberg, M., Gray, J.M., Costa, A.M., Bear, D.M., Wu, J., Harmin, D.A., Laptewicz, M., Barbara-Haley, K., Kuersten, S., Markenscoff-Papadimitriou, E., Kuhl, D., Bito, H., Worley, P.F., Kreiman, G., and Greenberg, M.E. (2010). Widespread transcription at neuronal activity-regulated enhancers. Nature, 465 (7295), 182. Available from https://doi.org/10.1038/NATURE09033 [Accessed 26 April 2023].

Kölbl, A.C., Andergassen, U., and Jeschke, U. (2015). The role of glycosylation in breast cancer metastasis and cancer control. Frontiers in Oncology, 5 (OCT), 1. Available from https://doi.org/10.3389/FONC.2015.00219/PDF [Accessed 27 September 2023].

Komm, B.S., and Mirkin, S. (2014). An overview of current and emerging SERMs. The Journal of Steroid Biochemistry and Molecular Biology, 143, 207–222. Available from https://doi.org/10.1016/J.JSBMB.2014.03.003.

Kuchenbaecker, K.B., Hopper, J.L., Barnes, D.R., Phillips, K.-A., Mooij, T.M., Roos-Blom, M.-J., Jervis, S., Leeuwen, F.E. van, Milne, R.L., Andrieu, N., Goldgar, D.E., Terry, M.B., Rookus, M.A., Easton, D.F., Antoniou, A.C., Consortium, and the B. and B.C., McGuffog, L., Evans, D.G., Barrowdale, D., et al. (2017). Risks of Breast, Ovarian, and Contralateral Breast Cancer for BRCA1 and BRCA2 Mutation Carriers. JAMA, 317 (23), 2402–2416. Available from https://doi.org/10.1001/JAMA.2017.7112 [Accessed 18 April 2023].

Kuusisto, K.M., Bebel, A., Vihinen, M., Schleutker, J., and Sallinen, S.L. (2011). Screening for BRCA1, BRCA2, CHEK2, PALB2, BRIP1, RAD50, and CDH1 mutations in high-risk Finnish BRCA1/2-founder mutation-negative breast and/or ovarian cancer individuals. Breast cancer research : BCR, 13 (1). Available from https://doi.org/10.1186/BCR2832 [Accessed 18 April 2023].

Lai, W.S., Carballo, E., Thorn, J.M., Kennington, E.A., and Blackshear, P.J. (2000). Interactions of CCCH Zinc Finger Proteins with mRNA. Journal of Biological Chemistry, 275 (23), 17827–17837. Available from https://doi.org/10.1074/jbc.m001696200.

Lai, W.S., Kennington, E.A. and Blackshear, P.J. (2002). Interactions of CCCH Zinc Finger Proteins with mRNA non-binding Tristetraprolin mutants exert an inhibitory effect on degradation of au-rich element-containing mRNAs. The Journal of Biochemistry, 277 (11), 9606–9613. Available from https://doi.org/10.1074/jbc.M110395200 [Accessed 21 July 2023].

Lai, W.S., Kennington, E.A., and Blackshear, P.J. (2003). Tristetraprolin and Its Family Members Can Promote the Cell-Free Deadenylation of AU-Rich Element-Containing mRNAs by Poly(A) Ribonuclease. Molecular and Cellular Biology, 23 (11). Available from https://doi.org/10.1128/mcb.23.11.3798-3812.2003.

Lee, S.K., Kim, S.B., Kim, J.S., Moon, C.H., Han, M.S., Lee, B.J., Chung, D.K., Min, Y.J., Park, J.H., Choi, D.H., Cho, H.R., Park, S.K., and Park, J.W. (2005). Butyrate response factor 1 enhances cisplatin sensitivity in human head and neck

squamous cell carcinoma cell lines. International Journal of Cancer, 117 (1). Available from https://doi.org/10.1002/ijc.21133.

Li, C.I., Uribe, D.J., and Daling, J.R. (2005). Clinical characteristics of different histologic types of breast cancer. British journal of cancer, 93 (9), 1046–1052. Available from https://doi.org/10.1038/SJ.BJC.6602787 [Accessed 19 April 2023].

Li, Z., Liu, Q., Piao, J., Hua, F., Wang, J., Jin, G., Lin, Z., and Zhang, Y. (2016). Clinicopathological implications of Tiam1 overexpression in invasive ductal carcinoma of the breast. BMC Cancer, 16 (1). Available from https://doi.org/10.1186/s12885-016-2724-0.

Lin, Y., and Lubman, D.M. (2024). The role of N-glycosylation in cancer. Acta Pharmaceutica Sinica B, 14 (3), 1098–1110. Available from https://doi.org/10.1016/J.APSB.2023.10.014.

Litton, J.K., Rugo, H.S., Ettl, J., Hurvitz, S.A., Gonçalves, A., Lee, K.-H., Fehrenbacher, L., Yerushalmi, R., Mina, L.A., Martin, M., Roché, H., Im, Y.-H., Quek, R.G.W., Markova, D., Tudor, I.C., Hannah, A.L., Eiermann, W., and Blum, J.L. (2018). Talazoparib in Patients with Advanced Breast Cancer and a Germline BRCA Mutation . New England Journal of Medicine, 379 (8), 753–763. Available from https://doi.org/10.1056/NEJMOA1802905/SUPPL_FILE/NEJMOA1802905_DISCLOSURES.PDF [Accessed 18 July 2023].

Liu, C., Zhang, L., Liu, H., Cheng, K. (2017). Delivery strategies of the CRISPR-Cas9 gene-editing system for therapeutic applications. Journal of Controlled Release. 266 17-26.

Lida, J., Dorchak, J., Clancy, R., Slavik, J., Ellsworth, R., Katagiri, Y., Pugacheva, E.N., van Kuppevelt, T.H., Mural, R.J., Cutler, M. Lou, and Shriver, C.D. (2015). Role for chondroitin sulfate glycosaminoglycan in NEDD9-mediated breast cancer cell growth. Experimental Cell Research, 330 (2), 358–370. Available from https://doi.org/10.1016/J.YEXCR.2014.11.002.

Lloyd, M.R., Wander, S.A., Hamilton, E., Razavi, P., and Bardia, A. (2022). Next-generation selective estrogen receptor degraders and other novel endocrine therapies for management of metastatic hormone receptor-positive breast cancer: current and emerging role. Therapeutic Advances in Medical Oncology, 14. Available from https://doi.org/10.1177/17588359221113694 [Accessed 28 April 2024].

Loh, X., Sun, Q., Ding, L., Mayakonda, A., Venkatachalam, N., Yeo, M., Silva, T.C., Xiao, J., Doan, N.B., Said, J.W., Ran, X., Zhou, S., Dakle, P., Shyamsunder, P., Koh, A.P., Huang, R.Y., Berman, B.P., Tan, S., Yang, H., Lin, D., Koeffler, H.P. (2020). RNA-Binding Protein ZFP36L1 Suppresses Hypoxia and Cell-Cycle Signaling. Cancer Research. 80 (2), 219-233.

Love, M.I., Huber, W., and Anders, S. (2014). Moderated estimation of fold change and dispersion for RNA-seq data with DESeq2. Genome Biology, 15 (12), 1–21. Available from https://doi.org/10.1186/S13059-014-0550-8/FIGURES/9 [Accessed 27 April 2023].

Lykke-Andersen, J., and Wagner, E. (2005). Recruitment and activation of mRNA

decay enzymes by two ARE-mediated decay activation domains in the proteins TTP and BRF-1. Genes and Development, 19 (3). Available from https://doi.org/10.1101/gad.1282305.

MacMahon, B., Cole, P., Lin, T.M., Lowe, C.R., Mirra, A.P., Ravnihar, B., Salber, E.J., Valaoras, V.G., and Yuasa, S. (1970). Age at first birth and breast cancer risk. Bulletin of the World Health Organization, 43 (2), 209. Available from /pmc/articles/PMC2427645/?report=abstract [Accessed 12 April 2023].

Maher, C.A., Kumar-Sinha, C., Cao, X., Kalyana-Sundaram, S., Han, B., Jing, X., Sam, L., Barrette, T., Palanisamy, N., and Chinnaiyan, A.M. (2009). Transcriptome Sequencing to Detect Gene Fusions in Cancer. Nature, 458 (7234), 97. Available from https://doi.org/10.1038/NATURE07638 [Accessed 26 April 2023].

Maitra, S., Chou, C.F., Luber, C.A., Lee, K.Y., Mann, M., and Chen, C.Y. (2008). The AU-rich element mRNA decay-promoting activity of BRF1 is regulated by mitogen-activated protein kinase-activated protein kinase 2. RNA, 14 (5), 950. Available from https://doi.org/10.1261/RNA.983708 [Accessed 28 June 2023].

Makita, S., Takatori, H., and Nakajima, H. (2021). Post-Transcriptional Regulation of Immune Responses and Inflammatory Diseases by RNA-Binding ZFP36 Family Proteins. Frontiers in Immunology, 12, 711633. Available from https://doi.org/10.3389/FIMMU.2021.711633/BIBTEX [Accessed 22 April 2024].

Malhotra, G.K., Zhao, X., Band, H., and Band, V. (2010). Histological, molecular and functional subtypes of breast cancers. Cancer Biology & Therapy, 10 (10), 955. Available from https://doi.org/10.4161/CBT.10.10.13879 [Accessed 19 April 2023].

Marderosian, M., Sharma, A., Funk, A.P., Vartanian, R., Masri, J., Jo, O.D., and Gera, J.F. (2006). Tristetraprolin regulates Cyclin D1 and c-Myc mRNA stability in response to rapamycin in an Akt-dependent manner via p38 MAPK signaling. Oncogene 2006 25:47, 25 (47), 6277–6290. Available from https://doi.org/10.1038/sj.onc.1209645 [Accessed 7 July 2023].

Margenthaler, J.A., and Ollila, D.W. (2016). Breast Conservation Therapy Versus Mastectomy: Shared Decision-Making Strategies and Overcoming Decisional Conflicts in Your Patients. Annals of surgical oncology, 23 (10), 3133–3137. Available from https://doi.org/10.1245/S10434-016-5369-Y [Accessed 12 July 2023].

Marioni, J.C., Mason, C.E., Mane, S.M., Stephens, M., and Gilad, Y. (2008). RNA-seq: an assessment of technical reproducibility and comparison with gene expression arrays. Genome research, 18 (9), 1509–1517. Available from https://doi.org/10.1101/GR.079558.108 [Accessed 23 May 2023].

Martínez-Calle, N., Pascual, M., Ordoñez, R., Enériz, E.S.J., Kulis, M., Miranda, E., Guruceaga, E., Segura, V., Larráyoz, M.J., Bellosillo, B., Calasanz, M.J., Besses, C., Rifón, J., Martín-Subero, J.I., Agirre, X., and Prosper, F. (2019). Epigenomic profiling of myelofibrosis reveals widespread DNA methylation changes in enhancer elements and ZFP36L1 as a potential tumor suppressor gene that is epigenetically regulated. Haematologica, 104 (8). Available from https://doi.org/10.3324/haematol.2018.204917.

Masuda, N., Lee, S.-J., Ohtani, S., Im, Y.-H., Lee, E.-S., Yokota, I., Kuroi, K., Im, S.-A., Park, B.-W., Kim, S.-B., Yanagita, Y., Ohno, S., Takao, S., Aogi, K., Iwata, H., Jeong, J., Kim, A., Park, K.-H., Sasano, H., et al. (2017). Adjuvant Capecitabine for Breast Cancer after Preoperative Chemotherapy. New England Journal of Medicine, 376 (22), 2147–2159. Available from https://doi.org/10.1056/NEJMOA1612645/SUPPL_FILE/NEJMOA1612645_DISCLOSURES.PDF [Accessed 17 July 2023].

McCarty, N., Graham, A., Studená, L. and Ledesma-Amaro, R., 2020. Multiplexed CRISPR technologies for gene editing and transcriptional regulation. Nature Communications, 11(1).

McGale, P., Taylor, C., Correa, C., Cutter, D., Duane, F., Ewertz, M., Gray, R., Mannu, G., Peto, R., Whelan, T., Wang, Y., Wang, Z., Darby, S., Albain, K., Anderson, S., Arriagada, R., Barlow, W., Bergh, J., Bergsten Nordström, E., et al. (2014). Effect of radiotherapy after mastectomy and axillary surgery on 10-year recurrence and 20-year breast cancer mortality: Meta-analysis of individual patient data for 8135 women in 22 randomised trials. The Lancet, 383 (9935), 2127–2135. Available from https://doi.org/10.1016/S0140-6736(14)60488-8 [Accessed 13 July 2023].

McIntyre, L.M., Lopiano, K.K., Morse, A.M., Amin, V., Oberg, A.L., Young, L.J., and Nuzhdin, S. V. (2011). RNA-seq: Technical variability and sampling. BMC Genomics, 12 (1), 1–13. Available from https://doi.org/10.1186/1471-2164-12-293/COMMENTS [Accessed 23 May 2023].

Minard, M.E., Kim, L.S., Price, J.E., and Gallick, G.E. (2004). The role of the guanine nucleotide exchange factor Tiam1 in cellular migration, invasion, adhesion and tumor progression. Breast cancer research and treatment, 84 (1), 21–32. Available from https://doi.org/10.1023/B:BREA.0000018421.31632.E6 [Accessed 6 May 2024].

Minckwitz, G. von, Procter, M., Azambuja, E. de, Zardavas, D., Benyunes, M., Viale, G., Suter, T., Arahmani, A., Rouchet, N., Clark, E., Knott, A., Lang, I., Levy, C., Yardley, D.A., Bines, J., Gelber, R.D., Piccart, M., and Baselga, J. (2017). Adjuvant Pertuzumab and Trastuzumab in Early HER2-Positive Breast Cancer. The New England journal of medicine, 377 (2), 122. Available from https://doi.org/10.1056/NEJMOA1703643 [Accessed 17 July 2023].

Montorsi, L., Guizzetti, F., Alecci, C., Caporali, A., Martello, A., Atene, C.G., Parenti, S., Pizzini, S., Zanovello, P., Bortoluzzi, S., Ferrari, S., Grande, A., and Zanocco-Marani, T. (2016). Loss of zfp36 expression in colorectal cancer correlates to wnt/β-catenin activity and enhances epithelial-to-mesenchymal transition through upregulation of zeb1, sox9 and macc1. Oncotarget, 7 (37), 59144. Available from https://doi.org/10.18632/ONCOTARGET.10828 [Accessed 10 July 2023].

Morishita, H., and Yagi, T. (2007). Protocadherin family: diversity, structure, and function. Current Opinion in Cell Biology, 19 (5), 584–592. Available from https://doi.org/10.1016/J.CEB.2007.09.006.

Mukherjee, N., Jacobs, N.C., Hafner, M., Kennington, E.A., Nusbaum, J.D., Tuschl, T., Blackshear, P.J., and Ohler, U. (2014). Global target mRNA specification and regulation by the RNA-binding protein ZFP36. Genome Biology, 15 (1), 1–16. Available from https://doi.org/10.1186/GB-2014-15-1-R12/FIGURES/6 [Accessed

4 July 2023].

Munier, C.C., Ottmann, C., and Perry, M.W.D. (2021). 14-3-3 modulation of the inflammatory response. Pharmacological Research, 163, 105236. Available from https://doi.org/10.1016/J.PHRS.2020.105236 .

Murata, T., Morita, N., Hikita, K., Kiuchi, Kiyomi, Kiuchi, Kazutoshi, and Kaneda, N. (2005). Recruitment of mRNA-destabilizing protein TIS11 to stress granules is mediated by its zinc finger domain. Experimental Cell Research, 303 (2). Available from https://doi.org/10.1016/j.yexcr.2004.09.031.

Nielsen, T.O., Hsu, F.D., Jensen, K., Cheang, M., Karaca, G., Hu, Z., Hernandez-Boussard, T., Livasy, C., Cowan, D., Dressler, L., Akslen, L.A., Ragaz, J., Gown, A.M., Gilks, C.B., Van De Rijn, M., and Perou, C.M. (2004). Immunohistochemical and clinical characterization of the basal-like subtype of invasive breast carcinoma. Clinical cancer research : an official journal of the American Association for Cancer Research, 10 (16), 5367–5374. Available from https://doi.org/10.1158/1078-0432.CCR-04-0220 [Accessed 23 April 2023].

Nik-Zainal, S., Davies, H., Staaf, J., Ramakrishna, M., Glodzik, D., Zou, X., Martincorena, I., Alexandrov, L.B., Martin, S., Wedge, D.C., Van Loo, P., Ju, Y.S., Smid, M., Brinkman, A.B., Morganella, S., Aure, M.R., Lingjærde, O.C., Langerød, A., Ringnér, M., Ahn, S., Boyault, S., Brock, J.E., Broeks, A., Butler, A., Desmedt, C., Dirix, L., Dronov, S., Fatima, A., Foekens, J.A., Gerstung, M., Hooijer, G.K., Jang, S.J., Jones, D.R., Kim, H., King, T.A., Krishnamurthy, S., Lee, H.J., Lee, J., Li, Y., McLaren, S., Menzies, A., Mustonen, V., O'Meara, S., Pauporté, I., Pivot, X., Purdie, C.A., Raine, K., Ramakrishnan, K., Rodríguez-González, F.G., Romieu, G., Sieuwerts, A.M., Simpson, P.T., Shepherd, R., Stebbings, L., Stefansson, O.A., Teague, J., Tommasi, S., Treilleux, I., Van den Eynden, Gert G., Vermeulen, P., Vincent-Salomon, A., Yates, L., Caldas, C., van't Veer, L., Tutt, A., Knappskog, S., Tan, B.K.T., Jonkers, J., Borg, Å, Ueno, N.T., Sotiriou, C., Viari, A., Futreal, P.A., Campbell, P.J., Span, P.N., Van Laere, S., Lakhani, S.R., Eyfjord, J.E., Thompson, A.M., Birney, E., Stunnenberg, H.G., van de Vijver, Marc J, Martens, J.W.M., Børresen-Dale, A., Richardson, A.L., Kong, G., Thomas, G., Stratton, M.R. (2016). Landscape of somatic mutations in 560 breast cancer whole genome sequences. Nature. 534 (7605), 47-54.

Nitz, U., Gluz, O., Clemens, M., Malter, W., Reimer, T., Nuding, B., Aktas, B., Stefek, A., Pollmanns, A., Lorenz-Salehi, F., Uleer, C., Krabisch, P., Kuemmel, S., Liedtke, C., Shak, S., Wuerstlein, R., Christgen, M., Kates, R.E., Kreipe, H.H., et al. (2019). West German Study PlanB Trial: Adjuvant Four Cycles of Epirubicin and Cyclophosphamide Plus Docetaxel Versus Six Cycles of Docetaxel and Cyclophosphamide in HER2-Negative Early Breast Cancer. Journal of clinical oncology : official journal of the American Society of Clinical Oncology, 37 (10), 799–808. Available from https://doi.org/10.1200/JCO.18.00028 [Accessed 17 July 2023].

Otto, T., and Sicinski, P. (2017). Cell cycle proteins as promising targets in cancer therapy. Nature reviews. Cancer, 17 (2), 93. Available from https://doi.org/10.1038/NRC.2016.138 [Accessed 7 July 2023].

Pally, D., and Naba, A. (2024). Extracellular matrix dynamics: A key regulator of cell migration across length-scales and systems. Current Opinion in Cell Biology, 86,

102309. Available from https://doi.org/10.1016/J.CEB.2023.102309.

Pankotai-Bodó, G., Oláh-Németh, O., Sükösd, F., and Pankotai, T. (2024). Routine molecular applications and recent advances in breast cancer diagnostics. Journal of Biotechnology, 380, 20–28. Available from https://doi.org/10.1016/J.JBIOTEC.2023.12.005.

Pellagatti, A., Dolatshad, H., Valletta, S., Boultwood, J. (2015). Application of CRISPR/Cas9 genome editing to the study and treatment of disease. Archives of Toxicology. 89 (7), 1023-1034.

Perou, C.M., Sørile, T., Eisen, M.B., Van De Rijn, M., Jeffrey, S.S., Ress, C.A., Pollack, J.R., Ross, D.T., Johnsen, H., Akslen, L.A., Fluge, Ø., Pergammenschlkov, A., Williams, C., Zhu, S.X., Lønning, P.E., Børresen-Dale, A.L., Brown, P.O., and Botstein, D. (2000). Molecular portraits of human breast tumours. Nature, 406 (6797), 747–752. Available from https://doi.org/10.1038/35021093 [Accessed 14 April 2023].

Phillips, C., Jeffree, R., and Khasraw, M. (2017). Management of breast cancer brain metastases: A practical review. Breast, 31, 90–98. Available from https://doi.org/10.1016/j.breast.2016.10.006 [Accessed 13 July 2023].

Piccart, M., Hortobagyi, G.N., Campone, M., Pritchard, K.I., Lebrun, F., Ito, Y., Noguchi, S., Perez, A., Rugo, H.S., Deleu, I., Burris, H.A., Provencher, L., Neven, P., Gnant, M., Shtivelband, M., Wu, C., Fan, J., Feng, W., Taran, T., et al. (2014). Everolimus plus exemestane for hormone-receptor-positive, human epidermal growth factor receptor-2-negative advanced breast cancer: overall survival results from BOLERO-2†. Annals of oncology : official journal of the European Society for Medical Oncology, 25 (12), 2357–2362. Available from https://doi.org/10.1093/ANNONC/MDU456 [Accessed 17 July 2023].

Planel, S., Salomon, A., Jalinot, P., Feige, J.J., and Cherradi, N. (2010). A novel concept in antiangiogenic and antitumoral therapy: Multitarget destabilization of short-lived mRNAs by the zinc finger protein ZFP36L1. Oncogene, 29 (45), 5989–6003. Available from https://doi.org/10.1038/ONC.2010.341.

Platt, R.J., Chen, S., Zhou, Y., Yim, M.J., Swiech, L., Kempton, H.R., Dahlman, J.E., Parnas, O., Eisenhaure, T.M., Jovanovic, M., Graham, D.B., Jhunjhunwala, S., Heidenreich, M., Xavier, R.J., Langer, R., Anderson, D.G., Hacohen, N., Regev, A., Feng, G., Sharp, P.A., Zhang, F. (2014). CRISPR-Cas9 knockin mice for genome editing and cancer modeling. Cell. 159 (2), 440-455.

Poltavets, V., Kochetkova, M., Pitson, S.M., and Samuel, M.S. (2018). The Role of the Extracellular Matrix and Its Molecular and Cellular Regulators in Cancer Cell Plasticity. Frontiers in Oncology, 8 (OCT), 431. Available from https://doi.org/10.3389/FONC.2018.00431 [Accessed 2 June 2023].

Poortmans, P. (2014). Postmastectomy radiation in breast cancer with one to three involved lymph nodes: Ending the debate. The Lancet, 383 (9935), 2104–2106. Available from https://doi.org/10.1016/S0140-6736(14)60192-6 [Accessed 12 July 2023].

Potapenko, I.O., Lüders, T., Russnes, H.G., Helland, Å., Sørlie, T., Kristensen, V.N., Nord, S., Lingjærde, O.C., Børresen-Dale, A.L., and Haakensen, V.D. (2015).

Glycan-related gene expression signatures in breast cancer subtypes; relation to survival. Molecular Oncology, 9 (4), 861–876. Available from https://doi.org/10.1016/J.MOLONC.2014.12.013.

Prat, A., Parker, J.S., Karginova, O., Fan, C., Livasy, C., Herschkowitz, J.I., He, X., and Perou, C.M. (2010). Phenotypic and molecular characterization of the claudin-low intrinsic subtype of breast cancer. Breast cancer research : BCR, 12 (5). Available from https://doi.org/10.1186/BCR2635 [Accessed 25 April 2023].

Priestley, P., Baber, J., Lolkema, M.P., Steeghs, N., de Bruijn, E., Shale, C., Duyvesteyn, K., Haidari, S., van Hoeck, A., Onstenk, W., Roepman, P., Voda, M., Bloemendal, H.J., Tjan-Heijnen, V.C.G., van Herpen, C.M.L., Labots, M., Witteveen, P.O., Smit, E.F., Sleijfer, S., Voest, E.E. and Cuppen, E. (2019). Pan-cancer wholegenome analyses of metastatic solid tumours. Nature, 575 (7781), 210–216. Available from https://doi.org/10.1038/s41586-019-1689-y [Accessed 14 August 2023].

Raica, M., Jung, I., Cîmpean, A.M., Suciu, C., and Mureşan, A.M. (2008). From conventional pathologic diagnosis to the molecular classification of breast carcinoma: Are we ready for the change? Romanian Journal of Morphology and Embryology, 50 (1).

Ran, F.A., Hsu, P.D., Wright, J., Agarwala, V., Scott, D.A., and Zhang, F. (2013). Genome engineering using the CRISPR-Cas9 system. Nature Protocols 2013 8:11, 8 (11), 2281–2308. Available from https://doi.org/10.1038/nprot.2013.143 [Accessed 30 April 2023].

Rataj, F., Planel, S., Desroches-Castan, A., Le Douce, J., Lamribet, K., Denis, J., Feige, J.J., and Cherradi, N. (2016). The cAMP pathway regulates mRNA decay through phosphorylation of the RNA-binding protein TIS11b/BRF1. Molecular Biology of the Cell, 27 (24), 3841. Available from https://doi.org/10.1091/MBC.E16-06-0379 [Accessed 22 June 2023].

Ren, B., Yu, G., Tseng, G.C., Cieply, K., Gavel, T., Nelson, J., Michalopoulos, G., Yu, Y.P., and Luo, J.H. (2006). MCM7 amplification and overexpression are associated with prostate cancer progression. Oncogene, 25 (7), 1090–1098. Available from https://doi.org/10.1038/SJ.ONC.1209134 [Accessed 16 August 2023].

Ren, J.X., Gong, Y., Ling, H., Hu, X., and Shao, Z.M. (2019). Racial/ethnic differences in the outcomes of patients with metastatic breast cancer: contributions of demographic, socioeconomic, tumor and metastatic characteristics. Breast cancer research and treatment, 173 (1), 225–237. Available from https://doi.org/10.1007/S10549-018-4956-Y [Accessed 20 September 2023].

Richman, J., and Dowsett, M. (2018). Beyond 5 years: enduring risk of recurrence in oestrogen receptor-positive breast cancer. Nature Reviews Clinical Oncology 2018 16:5, 16 (5), 296–311. Available from https://doi.org/10.1038/s41571-018-0145-5 [Accessed 26 September 2023].

Robertson, G., Schein, J., Chiu, R., Corbett, R., Field, M., Jackman, S.D., Mungall, K., Lee, S., Okada, H.M., Qian, J.Q., Griffith, M., Raymond, A., Thiessen, N., Cezard, T., Butterfield, Y.S., Newsome, R., Chan, S.K., She, R., Varhol, R., et al. (2010). De novo assembly and analysis of RNA-seq data. Nature Methods 2010 7:11, 7

(11), 909–912. Available from https://doi.org/10.1038/nmeth.1517 [Accessed 26 April 2023].

Saini, Y., Chen, J., and Patial, S. (2020). The tristetraprolin family of RNA-binding proteins in cancer: Progress and future prospects. Cancers, 12 (6). Available from https://doi.org/10.3390/cancers12061539.

Sakurai, T. (2012). The role of NrCAM in neural development and disorders—Beyond a simple glue in the brain. Molecular and Cellular Neuroscience, 49 (3), 351–363. Available from https://doi.org/10.1016/J.MCN.2011.12.002.

Sanduja, S., Blanco, F.F., and Dixon, D.A. (2011). The roles of TTP and BRF proteins in regulated mRNA decay. Wiley Interdisciplinary Reviews: RNA, 2 (1), 42–57. Available from https://doi.org/10.1002/WRNA.28 [Accessed 29 June 2023].

Sanduja, S., Blanco, F.F., Young, L.E., Kaza, V., and Dixon, D.A. (2012). The role of tristetraprolin in cancer and inflammation. Frontiers in Bioscience, 17 (1), 174–188. Available from https://doi.org/10.2741/3920/PDF [Accessed 4 May 2023].

Saudemont, A., Jespers, L., and Clay, T. (2018). Current status of gene engineering cell therapeutics. Frontiers in Immunology, 9 (FEB), 313093. Available from https://doi.org/10.3389/FIMMU.2018.00153/BIBTEX.

Sfogliarini, C., Pepe, G., Dolce, A., Della Torre, S., Cesta, M.C., Allegretti, M., Locati, M., and Vegeto, E. (2022). Tamoxifen Twists Again: On and Off-Targets in Macrophages and Infections. Frontiers in Pharmacology, 13, 879020. Available from https://doi.org/10.3389/FPHAR.2022.879020/BIBTEX [Accessed 27 April 2024].

Sidali, A. (2023). The Adenylate-Uridylate-Rich element RNA binding protein ZFP36L1 suppresses replication stress-induced genomic instability, 201-209. Available from https://westminsterresearch.westminster.ac.uk/item/w2165/the-adenylate-uridylate-rich-element-rna-binding-protein-zfp36l1-suppresses-replication-stress-induced-genomic-instability [Accessed 26 September 2023].

Sistigu, A., Musella, M., Galassi, C., Vitale, I., and De Maria, R. (2020). Tuning Cancer Fate: Tumor Microenvironment's Role in Cancer Stem Cell Quiescence and Reawakening. Frontiers in Immunology, 11, 2166. Available from https://doi.org/10.3389/FIMMU.2020.02166/BIBTEX.

Sobhani, N., D'Angelo, A., Pittacolo, M., Roviello, G., Miccoli, A., Corona, S.P., Bernocchi, O., Generali, D., and Otto, T. (2019). Updates on the CDK4/6 Inhibitory Strategy and Combinations in Breast Cancer. Cells 2019, Vol. 8, Page 321, 8 (4), 321. Available from https://doi.org/10.3390/CELLS8040321 [Accessed 25 September 2023].

Sørlie, T., Perou, C.M., Tibshirani, R., Aas, T., Geisler, S., Johnsen, H., Hastie, T., Eisen, M.B., Van De Rijn, M., Jeffrey, S.S., Thorsen, T., Quist, H., Matese, J.C., Brown, P.O., Botstein, D., Lønning, P.E., and Børresen-Dale, A.L. (2001). Gene expression patterns of breast carcinomas distinguish tumor subclasses with clinical implications. Proceedings of the National Academy of Sciences of the United States of America, 98 (19), 10869. Available from https://doi.org/10.1073/PNAS.191367098 [Accessed 20 September 2022].

Sparano, J.A., Gray, R.J., Makower, D.F., Pritchard, K.I., Albain, K.S., Hayes, D.F.,

Charles E. Geyer, J., Dees, E.C., Goetz, M.P., John A. Olson, J., Lively, T., Badve, S.S., Saphner, T.J., Wagner, L.I., Whelan, T.J., Ellis, M.J., Paik, S., Wood, W.C., Ravdin, P.M., et al. (2018). Adjuvant Chemotherapy Guided by a 21-Gene Expression Assay in Breast Cancer. The New England journal of medicine, 379 (2), 111. Available from https://doi.org/10.1056/NEJMOA1804710 [Accessed 17 July 2023].

Sternberg, S.H., Redding, S., Jinek, M., Greene, E.C., Doudna, J.A. (2014). DNA interrogation by the CRISPR RNA-guided endonuclease Cas9. Nature. 507 (7490), 62-67.

Stoecklin, G., Stubbs, T., Kedersha, N., Wax, S., Rigby, W.F.C., Blackwell, T.K., and Anderson, P. (2004). MK2-induced tristetraprolin:14-3-3 complexes prevent stress granule association and ARE-mRNA decay. The EMBO Journal, 23 (6), 1313. Available from https://doi.org/10.1038/SJ.EMBOJ.7600163 [Accessed 28 June 2023].

Stumpo, D.J., Byrd, N.A., Phillips, R.S., Ghosh, S., Maronpot, R.R., Castranio, T., Meyers, E.N., Mishina, Y., and Blackshear, P.J. (2004). Chorioallantoic fusion defects and embryonic lethality resulting from disruption of Zfp36L1, a gene encoding a CCCH tandem zinc finger protein of the Tristetraprolin family. Molecular and cellular biology, 24 (14), 6445–6455. Available from https://doi.org/10.1128/MCB.24.14.6445-6455.2004 [Accessed 6 September 2023].

Stumpo, D.J., Broxmeyer, H.E., Ward, T., Cooper, S., Hangoc, G., Yang, J.C., Shelley, W.C., Richfield, E.K., Ray, M.K., Yoder, M.C., Aplan, P.D., and Blackshear, P.J. (2009). Targeted disruption of Zfp36l2, encoding a CCCH tandem zinc finger RNA-binding protein, results in defective hematopoiesis. Blood, 114 (12), 2401. Available from https://doi.org/10.1182/BLOOD-2009-04-214619 [Accessed 6 September 2023].

Suk, F.M., Chang, C.C., Lin, R.J., Lin, S.Y., Liu, S.C., Jau, C.F., and Liang, Y.C. (2018). ZFP36L1 and ZFP36L2 inhibit cell proliferation in a cyclin D-dependent and p53-independent manner. Scientific Reports, 8 (1). Available from https://doi.org/10.1038/s41598-018-21160-z [Accessed 27 February 2021].

Sung, H., Ferlay, J., Siegel, R.L., Laversanne, M., Soerjomataram, I., Jemal, A., and Bray, F. (2021). Global Cancer Statistics 2020: GLOBOCAN Estimates of Incidence and Mortality Worldwide for 36 Cancers in 185 Countries. CA: A Cancer Journal for Clinicians, 71 (3), 209–249. Available from https://doi.org/10.3322/CAAC.21660 [Accessed 6 April 2023].

Suzuki, Y., Tsunoda, H., Kimura, T., and Yamauchi, H. (2017). BMI change and abdominal circumference are risk factors for breast cancer, even in Asian women. Breast cancer research and treatment, 166 (3), 919–925. Available from https://doi.org/10.1007/S10549-017-4481-4 [Accessed 13 April 2023].

Tamagnone, L., and Rehman, M. (2013). To Die or Not to Die: Sema3E Rules the Game. Cancer Cell, 24 (5), 564–566. Available from https://doi.org/10.1016/J.CCR.2013.10.010.

Taylor, G.A., Lai, W.S., Oakey, R.J., Seldin, M.F., Shows, T.B., Eddy, R.L., and Blackshear, P.J. (1991). The human TTP protein: sequence, alignment with

related proteins, and chromosomal localization of the mouse and human genes. Nucleic Acids Research, 19 (12), 3454. Available from https://doi.org/10.1093/NAR/19.12.3454 [Accessed 23 June 2023].

Taylor, G.A., Carballo, E., Lee, D.M., Lai, W.S., Thompson, M.J., Patel, D.D., Schenkman, D.I., Gilkeson, G.S., Broxmeyer, H.E., Haynes, B.F., and Blackshear, P.J. (1996). A pathogenetic role for TNF alpha in the syndrome of cachexia, arthritis, and autoimmunity resulting from tristetraprolin (TTP) deficiency. Immunity, 4 (5), 445–454. Available from https://doi.org/10.1016/S1074-7613(00)80411-2 [Accessed 6 September 2023].

Thul, P.J., and Lindskog, C. (2018). The human protein atlas: A spatial map of the human proteome. Protein Science, 27 (1), 233–244. Available from https://doi.org/10.1002/pro.3307.

Tiedje, C., Ronkina, N., Tehrani, M., Dhamija, S., Laass, K., Holtmann, H., Kotlyarov, A., and Gaestel, M. (2012). The p38/MK2-Driven Exchange between Tristetraprolin and HuR Regulates AU–Rich Element–Dependent Translation. PLOS Genetics, 8 (9), e1002977. Available from https://doi.org/10.1371/JOURNAL.PGEN.1002977 [Accessed 4 July 2023].

Tjan-Heijnen, V.C.G., van Hellemond, I.E.G., Peer, P.G.M., Swinkels, A.C.P., Smorenburg, C.H., van der Sangen, M.J.C., Kroep, J.R., De Graaf, H., Honkoop, A.H., Erdkamp, F.L.G., van den Berkmortel, F.W.P.J., de Boer, M., de Roos, W.K., Linn, S.C., Imholz, A.L.T., Seynaeve, C.M., Kitzen, J.J.E.M., Strobbe, L.J.A., Kouwenhoven, E.A., et al. (2017). Extended adjuvant aromatase inhibition after sequential endocrine therapy (DATA): a randomised, phase 3 trial. The Lancet. Oncology, 18 (11), 1502–1511. Available from https://doi.org/10.1016/S1470-2045(17)30600-9 [Accessed 13 July 2023].

Toyokawa, G., Masuda, K., Daigo, Y., Cho, H.S., Yoshimatsu, M., Takawa, M., Hayami, S., Maejima, K., Chino, M., Field, H.I., Neal, D.E., Tsuchiya, E., Ponder, B.A.J., Maehara, Y., Nakamura, Y., and Hamamoto, R. (2011). Minichromosome Maintenance Protein 7 is a potential therapeutic target in human cancer and a novel prognostic marker of non-small cell lung cancer. Molecular Cancer, 10, 65. Available from https://doi.org/10.1186/1476-4598-10-65 [Accessed 16 August 2023].

Trapnell, C., Williams, B.A., Pertea, G., Mortazavi, A., Kwan, G., Van Baren, M.J., Salzberg, S.L., Wold, B.J., and Pachter, L. (2010). Transcript assembly and quantification by RNA-Seq reveals unannotated transcripts and isoform switching during cell differentiation. Nature biotechnology, 28 (5), 511–515. Available from https://doi.org/10.1038/NBT.1621 [Accessed 26 April 2023].

Turner, N.C., Slamon, D.J., Ro, J., Bondarenko, I., Im, S.-A., Masuda, N., Colleoni, M., DeMichele, A., Loi, S., Verma, S., Iwata, H., Harbeck, N., Loibl, S., André, F., Puyana Theall, K., Huang, X., Giorgetti, C., Huang Bartlett, C., and Cristofanilli, M. (2018). Overall Survival with Palbociclib and Fulvestrant in Advanced Breast Cancer. New England Journal of Medicine, 379 (20). Available from https://doi.org/10.1056/nejmoa1810527.

Qu, K., Wang, Z., Fan, H., Li, J., Liu, J., Li, P., Liang, Z., An, H., Jiang, Y., Lin, Q., Dong, X., Liu, P., and Liu, C. (2017). MCM7 promotes cancer progression through

cyclin D1-dependent signaling and serves as a prognostic marker for patients with hepatocellular carcinoma. Cell Death & Disease, 8 (2), e2603. Available from https://doi.org/10.1038/CDDIS.2016.352 [Accessed 30 August 2023].

Varnum, B.C., Ma, Q.F., Chi, T.H., Fletcher, B., and Herschman, H.R. (1991). The TIS11 primary response gene is a member of a gene family that encodes proteins with a highly conserved sequence containing an unusual Cys-His repeat. Molecular and Cellular Biology, 11 (3), 1754. Available from https://doi.org/10.1128/MCB.11.3.1754 [Accessed 26 June 2023].

Vogel, K.U., Bell, L.S., Galloway, A., Ahlfors, H., and Turner, M. (2016). The RNA-Binding Proteins Zfp36l1 and Zfp36l2 Enforce the Thymic β-Selection Checkpoint by Limiting DNA Damage Response Signaling and Cell Cycle Progression. Journal of immunology (Baltimore, Md. : 1950), 197 (7), 2673–2685. Available from https://doi.org/10.4049/JIMMUNOL.1600854 [Accessed 24 September 2023].

Wang, H., Ding, N., Guo, J., Xia, J., and Ruan, Y. (2016). Dysregulation of TTP and HuR plays an important role in cancers. Tumour biology : the journal of the International Society for Oncodevelopmental Biology and Medicine, 37 (11), 14451–14461. Available from https://doi.org/10.1007/S13277-016-5397-Z [Accessed 6 July 2023].

Wang, Z., Gerstein, M., and Snyder, M. (2009). RNA-Seq: a revolutionary tool for transcriptomics. Nature reviews. Genetics, 10 (1), 57. Available from https://doi.org/10.1038/NRG2484 [Accessed 27 April 2023].

Weigelt, B., Horlings, H.M., Kreike, B., Hayes, M.M., Hauptmann, M., Wessels, L.F.A., De Jong, D., Van De Vijver, M.J., Van't Veer, L.J., and Peterse, J.L. (2008). Refinement of breast cancer classification by molecular characterization of histological special types. The Journal of Pathology, 216 (2), 141–150. Available from https://doi.org/10.1002/PATH.2407 [Accessed 31 March 2024].

Wells, M.L., Perera, L., and Blackshear, P.J. (2017). An Ancient Family of RNA-Binding Proteins: Still Important! Trends in Biochemical Sciences, 42 (4), 285–296. Available from https://doi.org/10.1016/J.TIBS.2016.12.003.

Westcott, J.M., Prechtl, A.M., Maine, E.A., Dang, T.T., Esparza, M.A., Sun, H., Zhou, Y., Xie, Y., and Pearson, G.W. (2015). An epigenetically distinct breast cancer cell subpopulation promotes collective invasion. The Journal of clinical investigation, 125 (5), 1927–1943. Available frohttps://doi.org/10.1172/JCI77767 [Accessed 6 May 2024].

Wu, Q., and Maniatis, T. (1999). A striking organization of a large family of human neural cadherin-like cell adhesion genes. Cell, 97 (6), 779–790. Available from https://doi.org/10.1016/S0092-8674(00)80789-8 [Accessed 6 May 2024].

Wu, X., Baig, A., Kasymjanova, G., Kafi, K., Holcroft, C., Mekouar, H., Carbonneau, A., Bahoric, B., Sultanem, K., and Muanza, T. (2016). Pattern of Local Recurrence and Distant Metastasis in Breast Cancer By Molecular Subtype. Cureus, 8 (12). Available from https://doi.org/10.7759/CUREUS.924 [Accessed 24 April 2023].

Xu, L., Ning, H., Gu, L., Wang, Q., Lu, W., Peng, H., Cui, W., Ying, B., Ross, C.R., Wilson, G.M., Wei, L., Wold, W.S.M., and Liu, J. (2015). Tristetraprolin induces

cell cycle arrest in breast tumor cells through targeting AP-1/c-Jun and NF-κB pathway. Oncotarget, 6 (39), 41679. Available from https://doi.org/10.18632/ONCOTARGET.6149 [Accessed 7 July 2023].

Yersal, O., and Barutca, S. (2014). Biological subtypes of breast cancer: Prognostic and therapeutic implications. World Journal of Clinical Oncology, 5 (3), 412. Available from https://doi.org/10.5306/WJCO.V5.I3.412 [Accessed 16 April 2024].

Yoon, N.K., Maresh, E.L., Shen, D., Elshimali, Y., Apple, S., Horvath, S., Mah, V., Bose, S., Chia, D., Chang, H.R., and Goodglick, L. (2010). Higher Levels of GATA3 Predict Better Survival in Women with Breast Cancer. Human pathology, 41 (12), 1794. Available from https://doi.org/10.1016/J.HUMPATH.2010.06.010 [Accessed 21 April 2023].

Yu, G., Wang, L.G., Han, Y., and He, Q.Y. (2012). clusterProfiler: an R package for comparing biological themes among gene clusters. Omics : a journal of integrative biology, 16 (5), 284–287. Available from https://doi.org/10.1089/OMI.2011.0118 [Accessed 28 April 2022].

Yu, T.Y., Zhang, G., Chai, X.X., Ren, L., Yin, D.C., and Zhang, C.Y. (2023). Recent progress on the effect of extracellular matrix on occurrence and progression of breast cancer. Life Sciences, 332, 122084. Available from https://doi.org/10.1016/J.LFS.2023.122084.

Yuan, S., Zhai, Y., Tao, T., Zhang, X., Bashir, G., Li, G., Wang, G., and Wu, S. (2022). Conflicting Roles of ZFP36L1 in Regulating the Progression of Muscle Invasive Bladder Cancer. Frontiers in Molecular Biosciences, 9, 687786. Available from https://doi.org/10.3389/FMOLB.2022.687786/BIBTEX.

Zekavati, A., Nasir, A., Alcaraz, A., Aldrovandi, M., Marsh, P., Norton, J.D., and Murphy, J.J. (2014). Post-transcriptional regulation of BCL2 mRNA by the RNA-binding protein ZFP36L1 in malignant B cells. PloS one, 9 (7). Available from https://doi.org/10.1371/JOURNAL.PONE.0102625 [Accessed 4 May 2023].